STREAMFLOW GENERATION PROCESSES AND RESIDENCE TIMES IN A LARGE, MOUNTAINOUS WATERSHED IN THE SOUTHERN ROCKY MOUNTAINS OF COLORADO, USA

By

Marty Dale Frisbee

Submitted in Partial Fulfillment
of the Requirements for the

Doctorate of Philosophy in Earth and Environmental Science
with Dissertation in Hydrology

New Mexico Institute of Mining and Technology
Department of Earth and Environmental Science

Socorro, New Mexico

June 2010

DEDICATION

I dedicate this dissertation to my niece, Deanna Williams. In March 2006, I was doing field work in Colorado for this dissertation when I received the call that she had passed away. I miss her greatly.

I also dedicate this dissertation to my grandfather, Lester Frisbee. He taught me the value of streams and mountains.

"The mountains were his masters. They rimmed in life. They were the cup of reality, beyond growth, beyond struggle and death. They were his absolute unity in the midst of eternal change."

Thomas Wolfe Look Homeward, Angel

ABSTRACT

Streamflow generation processes in hillslopes and small catchments less than 100 km^2 have been well documented in the hydrological literature. Yet, few of these studies attempt to scale their results to larger watersheds. There are three major impediments to scaling hillslope runoff processes up to larger watershed scales. First, the characterization of streamflow generation processes in watersheds larger than 1000 km^2 remains sketchy, in part due to logistical difficulties imposed by the larger watershed size. Second, hillslope processes tend to be highly complex and heterogeneous and the scaling of these processes will result in models that are also highly complex except at a much larger scale. Finally, scaling approaches often ignore the possibility that there are processes unique to the larger scale that may not be operative at smaller scales. For watershed hydrologists, this is a complicated problem especially since there is an increasing urgency to understand streamflow generation processes at larger watershed scales due to concerns over climate change and the impacts of climate change on water resources. Addressing this fundamental gap in our knowledge is an objective in this dissertation.

One approach toward solving this problem is to identify features or processes that connect hillslope-scale processes to the response of the larger watershed. In other words, determine if there are common threads between hillslope and watershed processes. Such features or processes may provide the important link that allows us to bridge the gap in

understanding between small-scale complexity and large-scale simplicity. This approach allows watershed hydrologists to investigate the scalability of a specific feature or process without first deriving a conceptual model of runoff generation at the smaller hillslope scale. This is beneficial for two reasons: it accelerates current progress in process understanding and in the long-term, it promotes the development of new theories regarding hydrological processes at the large watershed scale. It has been suggested that travel-time distributions may be particularly useful bridging the gap between small and large-scale process understanding. However, recent studies conducted at small catchment scales indicate that there may not be a correlation between catchment area and residence times. However, contradictory evidence from recent geochemical and modeling studies indicate that chemical constituents in streamflow can be temporally persistent in watersheds. This discrepancy in streamflow residence times has much broader implications than just the reconciliation of small-scale and large-scale runoff process behavior.

This discrepancy ultimately limits our ability to predict how streamflow responses from large watersheds will be affected by climate change. Since residence times are directly linked to flowpath distributions, streamflow from watersheds exhibiting short residence times will respond rapidly to changes in meteoric forcing associated with climate change while the reverse may hold true for watersheds where long residence time waters sustain streamflow. The second objective of this dissertation is to address this discrepancy in streamflow residence times and illustrate the impact of these streamflow generation processes on the streamflow response to climate change.

ACKNOWLEDGEMENTS

During my studies at New Mexico Tech, I have received the assistance from many individuals and funding agencies. This dissertation would not have been possible without their help and support.

Funding for this research was provided primarily by SAHRA (Sustainability of semi-Arid Hydrology and Riparian Areas) Science and Technology Center of the National Science Foundation (NSF agreement EAR-9876800). Additional funding was provided from the New Mexico Water Resources Research Institute in the form of a student water research grant in 2007. Two Travel Grants provided by the New Mexico Tech Graduate Student Association allowed me to present my research at conferences.

First, I would like to thank my advisor, Fred M. Phillips, for the time and effort he spent in making me a better scientist. Fred constantly urged me to always think outside the box regardless of the possibility that I may in fact get shot by the *status quo*. I would like to thank him for his patience and good humor during this dissertation research. One of Fred's former PhD students likened him to a rose. However, I think he is more akin to the character Pai Mei in the *Kill Bill* movies. I hope he is satisfied with my progress.

My committee members were very supportive. I am grateful for the assistance and advice from Andy R. Campbell. Andy is an all-around good guy to work with and he has been a major influence on my growth and success as a PhD candidate. I am especially grateful that Andy always made time to discuss stable isotope concepts and geochemical processes and to critique my interpretations of the data despite the thousands

of waters samples that I brought in to the lab every month. While Fred was always trying to erase my engineering past, John L. Wilson was in the background urging me to keep it intact. Many students fear John's critical nature; however, not many students take the time to see his supportive side. I sought John's advice on many issues and am thankful for his insight. While John was promoting the godlike status of hydrogeologic modelers, Gary S. Weissmann was always grounding these concepts in geologic reality. Gary has been extremely supportive and he has always provided encouragement along the way wherever we met. Last but definitely not least, I would like to thank Paul D. Brooks for all his help and support. Paul constantly pushed me to think about and test alternative hypotheses and this has helped my progress tremendously.

There are professors outside my committee that have had a tremendous impact on my studies here at New Mexico Tech. I am extremely grateful for all the work that Mark Person completed on the watershed hydrogeologic model for Saguache Creek. Art F. White was instrumental in helping me develop my ideas on chemical weathering processes in watersheds. His help and suggestions greatly improved my understanding of the complexities of these processes and greatly improved the quality of my manuscript on chemical weathering processes in the Saguache Creek watershed. I would like to thank Enrique R. Vivoni for providing helpful suggestions about the scope of my research, especially regarding the surface hydrologic components and how my results mesh with current surface hydrology modeling practices. One of the reasons that I came to NMT was to get coursework and training in vadose-zone hydrology and Jan M.H. Hendrickx provided both. Without his assistance, the M-PCAPS study would not have reached fruition. In addition, Jan supported me in my quest to model the unsaturated flow along

one of the hillslope transects from my Masters research in Canada and this has been a great and frustrating learning experience. Jan has also provided lots of encouragement in my interest in hydrogeophysics and I hope that someday I can pursue these ideas.

I would like to extend a special thanks to my previous advisor at UNC Charlotte, Craig J. Allan. When I changed career paths from engineering to science, Craig took me under his wing and started my development as a watershed scientist. He gave me the opportunity to perform hydrologic field work in many different climatic conditions. The field work paid off and ultimately resulted in my decision to pursue a PhD in watershed hydrology. Craig's concern for his students is well known and I will always consider him a mentor and a friend.

Many students assisted me along the way. First and foremost, I must thank Emily Engle. When I was doing hydrologic field work with Emily in North Carolina during the tropical storm season, she surprised me with her eagerness and resilience to work in any condition although the tornado encounter was a little too close for comfort for us both. Emily has been my primary field assistant during this research as well and I am always amazed by her energy in the field. Her biggest job was in keeping me sane during this endeavor and I will be forever indebted to her (and she will likely never let me forget my indebtedness). I am especially grateful for the strong encouragement and assistance from Weon Shik Han. If it had not been for him, I would not be writing this now. I would like to thank all the field assistants that helped me during this research: Alex Rinehart, Ginny Bracht, Sung-ho Hong, Andrew Fargo, Andre Ritchie, Frank Hack, Shasta Marrero, Matt Baillie, Jane Overton, Siona Curtis-Briley, and Sam Siemens. I would also like to thank Bonnie Frey, Frederick Partey, and Dustin Baca at the New Mexico Bureau of Geology

and Mineral Resources Chemical Lab and Gabe Graf and Matt Earthman in the New Mexico Tech Stable Isotope Lab for all their hard work. I appreciate the support and friendship of many other students including Laura Rosales-Lagarde, Jesus Gomez, Alex Rinehart, Shari Houston, Megan Curry, Vyoma Nenuji, Diana Romero-Suarez, Sophia Sigstedt, Kevin Stafford, Bill Tai, Taufique Mahmood, Jason Heath, and Hugo Gutiérrez-Jurado.

There are many unsung heroes in the Department of Earth and Environmental Science. I would like to extend a special thanks to Connie Apache. She always made time for the students regardless of the situation. I would also like to thank Mary Haenichen, Pat Valentine, Leigh Davidson, Susan Delap Heath, Barbara Fazio, Lisa Majkowski, Andrew Phillips, and Pat Mills for their help.

I would like to thank the folks at the Saguache BLM/USFS Field Office for logistical support in securing sites for field installations in the Saguache Creek watershed. In particular, I would like to thank Steve Sanchez for all his assistance and suggestions along the way. Furthermore, much of my research would not have been possible without the assistance of the local ranching families in the Saguache Creek watershed by allowing me access to streams, springs, and wells located on their property. For these reasons, I would like to thank the Curtis, Gilbert, Hill, Nielsen, and Williams families.

Finally, I would like to extend a very special thanks to my parents, Dale and Linda Frisbee, and grandmother, Ellen Brittain, for all their love and support and for always encouraging me to work hard in every venture I pursue. I would also like to thank my sister, Sandra Geouge, and her family for their support. I dedicate this work to my wonderful niece, Morgan Geouge, and nephew, Thomas Geouge.

TABLE OF CONTENTS

LIST OF FIGURES

Page

LIST OF TABLES

Page

This dissertation is accepted on behalf of the
Faculty of the Institute by the following committee:

Advisor

6/03/2010
Date

I release this document to the New Mexico Institute of Mining and Technology.

Student's Signature

6/03/2010
Date

Chapter 1 Introduction

1.1 Perspectives on Streamflow Generation Processes and Residence Times

The characterization of streamflow generation processes in hillslopes and small catchments less than 100 km^2 has been well documented in the hydrological literature [see *Beven,* 2006 for reviews]. Yet, few of these studies attempt to scale their results to larger watersheds. In addition, the characterization of streamflow generation processes in watersheds larger than 1000 km^2 remains sketchy, in part due to logistical difficulties imposed by the larger watershed size [*Rodgers et al.,* 2005]. For watershed hydrologists, this is a complicated problem especially since there is an increasing urgency to understand streamflow generation processes at larger watershed scales [*Naiman et al.,* 2001]. One approach toward solving this problem is to aggregate the runoff responses from individual hillslopes and effectively upscale that aggregated response to the larger watershed. The logic behind this approach is that process understanding at smaller scales is much more complete than it is at larger scales. The problem with this approach is that hillslope processes tend to be highly complex and heterogeneous and the scaling of these processes will result in models that are also highly complex at the watershed scale [*McDonnell,* 2003; *Sivapalan,* 2003; *Uhlenbrook,* 2006]. This approach also ignores possible processes that are unique to the larger scale and may not be operative at smaller scales. An alternative approach is to identify features or processes that connect hillslope-scale processes to the response of the larger watershed, in other words, to seek common threads between hillslope and watershed processes [*Sivapalan,* 2003; *Beighley et al.,* 2005]. Such features or processes may provide the important link that allows us to bridge

the gap in understanding between small-scale complexity and large-scale simplicity [*Dooge,* 1997; *Spence*, 2007].

The second approach is particularly appealing. It allows watershed hydrologists to investigate the scalability of a specific feature or process without first deriving a conceptual model of runoff generation at the smaller hillslope scale. This is beneficial for two reasons: it accelerates current progress in process understanding and in the long-term, it promotes the development of new theories regarding hydrological processes at the large watershed scale. In fact, according to *Sivapalan* [2003], "much faster progress can be achieved, in terms of linking conceptualizations across the scales, if the hillslope and network responses can be described physically, but in terms of *travel time distributions*, to match the usual physical meaning of the unit hydrograph for the watershed as a travel time distribution" (pages 1039 and 1040). It is apparent from *Sivapalan* [2003] that scalable properties such as travel times may be the key to bridging the gap between small and large-scale process understanding. Studies have been conducted at small scales in order to quantify the relationship between catchment area and residence times [*McGlynn et al.*, 2003; *McGuire et al.*, 2005]. These studies, however, indicate that there may not be a correlation between catchment area and residence times. However, these concepts have not been thoroughly tested at larger watershed scales.

In this dissertation, I follow the suggestion of *Sivapalan* [2003] and investigate the processes that control the structuring of streamflow chemistry with increasing scale in a large watershed (drainage area greater than 1600 km^2). Several studies have documented structured trends in stream chemistry that become apparent as basin scale

increases [*Wolock et al.*, 1997; *Shaman et al.*, 2004; *Temnerud and Bishop*, 2005; *Uchida et al.*, 2005]. Since this behavior seems to be a common occurrence, streamflow chemistry may be particularly useful in linking process understanding across multiple scales. In this dissertation, I develop and test two conceptual models that could be employed to explain the structured trends in streamflow chemistry. These models represent two conceptualizations of streamflow generation at the large watershed scale. One model is essentially a 2-D conceptualization in which streamflow chemistry is controlled by the integration of runoff from surface and shallow subsurface flowpaths along hillslopes [*Sivapalan*, 2003]. The alternative model is a 3-D conceptualization in which streamflow chemistry is controlled by a distribution of flowpaths through both deep groundwater and surface and shallow subsurface routes. These conceptualizations are essentially endmembers for the range of conceptual models for streamflow generation; in reality, most streamflow generation processes probably fall somewhere between these two endmembers. One objective of this dissertation is to test the proposed conceptual models against a dataset of stream chemistry and stable isotope observations and quantify the processes responsible for streamflow generation at the large watershed scale. In particular, I quantify the overall role of groundwater in streamflow generation since the groundwater component is key to distinguishing between the two conceptual models.

I then make the connection between stream chemistry and flowpath distributions through the observation that, in both conceptual models, the underlying mechanisms of streamflow generation can be described as flowpath distributions. In the 2-D conceptual model, the flowpath distributions will be composed of short flowpaths that are capable of

rapidly transmitting water to the stream. This is not the case for the 3-D conceptual model. The flowpath distribution for the 3-D conceptual model will contain short flowpaths representative of surface and shallow subsurface runoff processes and it will also contain much longer and perhaps more tortuous flowpaths representative of large-scale groundwater flowpaths. The longer flowpaths will be characterized by much longer residence times than surface flowpaths [*Tóth,* 1963; *Cardenas,* 2007]. The chemistry observed in the stream can then be connected to a distribution of flowpaths that are responsible for streamflow generation. In general, rapid runoff processes are kinetically-limited and as a consequence, the waters in these rapid flowpaths will be geochemically unevolved when they reach the stream. In comparison, the solute release to groundwater is a function of residence time [*Lasaga,* 1984; *Bricker and Jones,* 1995]. Therefore, short-residence time groundwaters will not be as geochemically evolved as long-residence time groundwaters. From a Tóthian-flow perspective, we can envision a suite of flowpath lengths and tortuousities in any watershed, with water discharging from each flowpath having a distinct geochemical signature and residence time distribution. If components of groundwater characterized by long-residence times are being discharged to the stream, we would expect to see geochemical enrichment in the stream water even if the long-residence time groundwater mixes with younger waters in the hyporheic zone. On the other hand, if components of long-residence time groundwater are insignificant, then we may not see evidence of geochemical enrichment (i.e., the geochemical evolution of waters will be controlled by geochemical transformations only along the surface and shallow subsurface flowpaths).

Since the solute release to streamflow is a kinetically controlled process, the kinetic rates responsible for the solute release to the components of streamflow chemistry can be used to estimate apparent ages of streamflow [*Rademacher et al.,* 2001, 2005]. As mentioned previously, recent residence time studies at small catchment scales indicate that residence times in streamflow are young, on the order of days to years, and that residence times do not correlate with catchment area [*McGlynn et al.,* 2003; *McGuire et al.,* 2005]. However, contradictory evidence from geochemical and modeling studies indicate that chemical constituents in streamflow can be temporally persistent in watersheds [*Kirchner,* 2000, 2001; *Cardenas,* 2007]. This discrepancy has broader implications. This discrepancy ultimately limits our ability to predict how streamflow responses from large watersheds will be affected by climate change. Since residence times are directly linked to flowpath distributions, streamflow from watersheds exhibiting short residence times will respond rapidly to changes in meteoric forcing associated with climate change while the reverse may hold true for watersheds where long residence time waters sustain streamflow [*Tague et al.,* 2008; *Maxwell and Kollett,* 2008]. My second objective in this dissertation is to calculate apparent ages of streamflow using a geochemical kinetics approach and use those results to address this discrepancy in streamflow residence times.

1.2 Motivation and Science Questions

As illustrated in Section 1.1, there has been a historic bias in streamflow generation studies toward small scales (hillslope and small catchment scales less than 100 km^2). Few of these studies attempt to scale their findings up to the larger watershed

scale. This is not a simple process because hillslope runoff processes tend to be highly spatiotemporally heterogeneous and mechanistically complex, while the limited data available at larger scales suggests a tendency toward simplicity [*Sivapalan*, 2003]. Currently, there is an increased need to investigate and understand streamflow generation in large watersheds given the recent concerns over climate change and potential impacts of climate change on water resources (drainage areas greater than 1000 km^2). Yet, there has been little effort to investigate streamflow generation processes at these scales.

In this dissertation, I address the following questions:

1) What is the role of groundwater on streamflow generation at the large watershed scale?
2) What is role of groundwater in solute release at the large watershed scale?
3) What influence does long residence time groundwater have on streamflow residence times?

1.3 Organization of the Dissertation

Each of the following chapters in this dissertation was written as an individual manuscript for submission and publication in an appropriate journal. Footnotes are given on the first page of each chapter to provide information on the publication status for the chapter at the time of this writing. Each chapter has its own Introduction, Methods, Results, Discussion, Conclusions, and References sections. Certain sampling and analytical methods that are repetitive between chapters can be found in the Appendix. The following chapters were placed in a specific order such that smaller studies that

support the overall scientific endeavor are presented first. As such, the overarching science questions will be addressed in the final chapters. Sections 1.1 and 1.2 of this introductory chapter provide a background on the current perspectives on streamflow generation processes and residence times in large watersheds. Section 1.4 provides a brief description and motivation for the chapters included in this dissertation. Appendices will be used where needed to present detailed data tables such as chemical analyses which are not needed in the chapter itself.

1.4 Chapter Descriptions

In Chapter 2 (Modified Passive Capillary Samplers for Collecting Samples of Snowmelt Infiltration for Stable Isotope Analysis in Remote, Seasonally Inaccessible Watersheds 1: Laboratory Evaluation), the results from the laboratory evaluation of a modified passive capillary sampler (M-PCAPS) are presented. Large watersheds create logistical difficulties for field-sampling campaigns and these difficulties are compounded when access is limited due to seasonal conditions such as snowpack development in remote, rugged terrain. The San Juan Mountains in southern Colorado are a good example. During the snowbound season, very deep snowpacks develop in high-elevation regions of the San Juan Mountains and this limits our ability to successfully sample infiltrating meltwater in these regions. Therefore, the stable isotopic and geochemical composition of the soil-meltwater endmember remains poorly constrained. A robust methodology requiring little maintenance or monitoring was developed by modifying the existing passive capillary sampler design so that it could be deployed in thin, rocky alpine soils. In order to ensure that the modified design did not alter the isotopic composition of

soil water, a simple laboratory experiment was conducted to answer two important questions regarding the suitability of the M-PCAPS design. 1. Does the wicking process fractionate water? 2. How well do the M-PCAPS track the changing isotopic composition of a soil reservoir undergoing kinetic fractionation; (e.g. soil evaporation)? The results of the experiment were encouraging and indicated that the wicking process does not fractionate water and the M-PCAPS effectively tracked changes in the stable isotope composition of soil-water undergoing kinetic fractionation.

In Chapter 3 (Modified Passive Capillary Samplers for Collecting Samples of Snowmelt Infiltration for Stable Isotope Analysis in Remote, Seasonally Inaccessible Watersheds 2: Field Evaluation), the results from the field evaluation of a modified passive capillary sampler (M-PCAPS) are presented. After encouraging results from the laboratory evaluation, twelve modified passive capillary samplers (M-PCAPS) were installed in remote locations within the Saguache Creek watershed (a large, alpine watershed located in the southern Rocky Mountains of Colorado) prior to the onset of snow accumulation in October 2007 to collect samples of infiltration during the snowmelt and summer rainfall seasons. This field evaluation was designed to answer four important questions regarding the deployment of M-PCAPS to collect snowmelt for isotopic and geochemical analyses. 1. Is the isotopic composition of water collected via modified-bulk snow collectors similar to that of the actual infiltrating snowmelt? 2. Does the infiltrating meltwater undergo any isotopic and geochemical evolution in the typically shallow soils of alpine watersheds during snowmelt and what can be inferred from this data about dominant subsurface runoff processes? 3. Can M-PCAPS be used to constrain rates of meltwater infiltration in remote, seasonally inaccessible watersheds? 4. Can M-

PCAPS be used to constrain rates of infiltration during the summer rainfall season? The field deployment was successful and the results were again encouraging. The M-PCAPS collected water samples that provided data on the geochemical and stable isotopic evolution of infiltrating meltwater, shallow subsurface runoff processes, and soil-water fluxes during the snowmelt and rainfall seasons in the San Juan Mountains. More importantly, the M-PCAPS provided an opportunity to sample portions of the hydrological system that would otherwise have been difficult to quantify empirically.

In Chapter 4 (Streamflow Generation in a Large, Alpine Watershed in the Southern Rocky Mountains of Colorado, USA: Is Streamflow Generation Simply the Aggregation of Hillslope Runoff Responses?), I introduce the scientific focus of my dissertation; what is the role of groundwater in streamflow generation processes in a large watershed? In this chapter, spatial trends in streamflow chemistry in a large (1700 km^2) watershed located in the San Juan Mountains of southern Colorado, USA are used to understand mechanisms of streamflow generation processes at the large watershed scale. I introduce two conceptual models of streamflow generation at the large watershed scale and test these conceptual models against a dataset of stream chemistry observations. Endmember mixing analysis and measurements of hydraulic head gradients in streambeds are used to quantify large-scale groundwater contributions to streamflow with increasing spatial scale in the Saguache Creek watershed. I was interested in answering the following question. What is the role of groundwater in streamflow generation in the Saguache Creek watershed and do groundwater contributions in streamflow become structured with increasing scale? My results indicate that streamflow generation at the large watershed scale is not simply the aggregation of hillslope runoff responses. The

major finding of this study is that there are streamflow generation processes operable at the large watershed scale that are not always operable at the hillslope scale. The results of this study have implications for our conceptual models of hydrological behavior at the large watershed scale and broader implications for the streamflow response of large watersheds to changes in meteoric forcing associated with climate change.

In Chapter 5 (Variability in the Groundwater Component of Springflow Generation and Its Effect on Solute Weathering Release Rates in Large Watersheds), I use the geochemistry of groundwater and spring waters to understand the geochemical evolution of groundwater in the Saguache Creek watershed. I develop solute weathering release curves for groundwater based upon cation concentrations and corrected radiocarbon ages of groundwater sampled from wells terminated in bedrock. These solute weathering release curves provide an indication of the accumulated solute release from the chemical weathering of minerals in bedrock. The major finding of this study is that uncorrected spring waters will severely overpredict the solute release from bedrock as compared to wells and caution should be exercised when estimating weathering rates from spring waters due to the integrative nature of springflow generation.

In Chapter 6 (Long Residence Time Groundwater and Its Effect on Apparent Ages of Streamflow in a Large Watershed in the Southern Rocky Mountains of Colorado, USA), I discuss the broader implications of streamflow generation processes at the large watershed scale. In particular, I discuss the streamflow response to climate change and how this response is controlled by the flowpath distributions that support streamflow. Here, I couple the results from the streamflow separations performed using endmember mixing analysis in Chapter 4 with the geochemical chronometer created in Chapter 5 to

estimate streamflow ages in Saguache Creek watershed. I use the two conceptual models of streamflow generation introduced in Chapter 4 to illustrate the effect that the underlying mechanisms of these opposing conceptual models have on the residence times of streamflow and the streamflow response of large watersheds to changes in meteoric forcing associated with climate change. The major finding of this study is that contributions of long residence time groundwater have a profound effect on streamflow ages. Ages of streamflow are much older than currently published and can exceed 5000 years at the outlet of this watershed. This finding implies that streamflow sustained by long-scale, long residence time groundwater may be more resistant initially against changes in meteoric forcing associated with climate change.

In Chapter 7, I provide Conclusions and Recommendations.

1.5 References

Beighley, R.E., T. Dunne, and J.M. Melack (2005), Understanding and modeling basin hydrology: Interpreting the hydrogeological signature, *Hydrological Processes, 19,* 1333-1353.

Beven, K. (2006), *Benchmark Papers in Hydrology: Streamflow Generation Processes,* International Association of Hydrological Sciences, Oxfordshire, UK.

Bricker, O.P. and B.F. Jones (1995), Main factors affecting the composition of natural waters, in *Trace Elements in Natural Waters,* edited by B. Salbu and E. Steinnes, CRC Press, Boca Raton, FL.

Cardenas, M.B. (2007), Potential contribution of topography-driven regional groundwater flow to fractal stream chemistry: Residence time distribution analysis of Tóth flow, *Geophysical Research Letters, 34,* L05403, doi:10.1029/GL029126.

Dooge, J.C.I. (1997), Searching for simplicity in hydrology, *Surveys in Geophysics, 18,* 511-534.

Kirchner, J.W., X. Feng, and C. Neal (2000), Fractal stream chemistry and its implications for contaminant transport in catchments, *Nature, 403,* 524-527.

Kirchner, J.W., X. Feng, and C. Neal (2001), Catchment-scale advection and dispersion as a mechanism for fractal scaling in stream tracer concentrations, *Journal of Hydrology, 254,* 82-101.

Lasaga, A.C. (1984), Chemical kinetics of water-rock interactions, *Journal of Geophysical Research, 89*(B6), 4009-4025.

Maxwell, R.M., and S.J. Kollet (2008), Interdependence of groundwater dynamics and land-energy feedbacks under climate change, *Nature Geoscience, **1,*** 665-669, doi:10.1038/ngeo315.

McDonnell, J.J. (2003), Where does water go when it rains? Moving beyond the variable source area concept of rainfall-runoff response, *Hydrological Processes, 17,* 1869-1875, doi:10.1002/hyp.5132.

McGlynn, B.L., J.J. McDonnell, M. Stewart, and J. Siebert (2003), On the relationship between catchment scale and streamwater residence time, *Hydrological Processes, 17,* 175-181, doi:10.1002/hyp.5085.

McGuire, K. J., B.L. McGlynn, J.M. Welker, J. Seibert, J.J. McDonnell, M. Weiler, and C. Kendall (2005), The role of topography on catchment-scale water residence time, *Water Resources Research, 41*(5), 1-14.

Naiman, R.J., P.A. Bisson, R.G. Lee, and M.G. Turner (2001), Watershed management, in *River Ecology and Management,* edited by R.J. Naiman and R.E. Bilby, pp. 642-661, Academic Press, London.

Rademacher, L.K., J.F. Clark, G.B. Hudson, D.C. Erman, and N.A. Erman (2001), Chemical evolution of shallow groundwater as recorded by springs, Sagehen Basin; Nevada County, California, *Water Resources Research, **179,*** 37-51.

Rademacher, L. K., J.F. Clark, D.W. Clow, and G.B. Hudson (2005), Old groundwater influence on stream hydrochemistry and catchment response times in a small Sierra Nevada catchment: Sagehen Creek, California, *Water Resources Research, 41*(2), 1-10.

Rodgers, P., C. Soulsby, and S. Waldron (2005), Stable isotope tracers as diagnostic tools in upscaling flow path understanding and residence time estimates in a mountainous mesoscale catchment, *Hydrological Processes, 19,* 2291-2307, doi:10.1002/hyp.5677.

Shaman, J., M. Stieglitz, and D. Burns (2004), Are big basins just the sum of small catchments?, *Hydrological Processes, 18,* 3195-3206, doi:10.1002/hyp.5739.

Sivapalan, M. (2003), Process complexity at hillslope scale, process simplicity at the watershed scale: is there a connection?, *Hydrological Processes, 17,* 1037-1041, doi:10.1002/hyp.5109.

Spence, C. (2007), On the relation between dynamic storage and runoff: A discussion on thresholds, efficiency, and function, *Water Resources Research, 43,* W12416, doi:10.1029/2006WR005645.

Tague, C., G. Grant, M. Farrell, J. Choate, and A. Jefferson (2008), Deep groundwater mediates streamflow response to climate warming in the Oregon Cascades, *Climatic Change, **86,*** 189-210, doi:10.1007/s10584-007-9294-8.

Temnerud, J. and K. Bishop (2005), Spatial variation of streamwater chemistry in two Swedish Boreal catchments: Implications for environmental assessment, *Environmental Science and Technology, 39,* 1463-1489, doi:10.1021/es040045q.

Tóth J. (1963), A theoretical analysis of groundwater flow in small drainage basins, *Journal of Geophysical Research, 67,* 4812-4975.

Uchida, T., Y. Asano, Y. Onda, and S. Miyata (2005), Are headwaters just the sum of hillslopes?, *Hydrological Processes, 19,* 3251-3261, doi:10.1002/hyp.6004.

Uhlenbrook, S. (2006), Catchment hydrology – a science in which all processes are preferential, *Hydrological Processes, 20,* 3581-3585, doi:10.1002/hyp.6564.

Wolock, D.M., J. Fan, and G.B. Lawrence (1997), Effects of basin size on low-flow stream chemistry and subsurface contact time in the Neversink River watershed, New York, *Hydrological Processes, 11,* 1273-1286.

Chapter 2 Modified Passive Capillary Samplers for Collecting Samples of Snowmelt Infiltration for Stable Isotope Analysis in Remote, Seasonally Inaccessible Watersheds 1: Laboratory Evaluation[1]

2.1 Introduction:

Many of the river basins draining mountainous watersheds such as those in the southwestern United States depend upon snowmelt for streamflow generation [*Rango*, 2006] and recharge [*Wilson and Guan*, 2004]. Therefore, providing more accurate constraints on the redistribution of snowmelt runoff is critical for the sustainability of future agricultural, domestic, and municipal water demands in these regions. In particular, very little is known about the isotopic and geochemical evolution of infiltrating meltwater in alpine watersheds. Research into recharge and runoff generation processes has historically employed a variety of techniques including isotopic separations [*Earman et al.*, 2006; *Herrmann et al.*, 1981]. However, the snowmelt-infiltration endmember in these separations is poorly constrained due to the rugged, remote, and seasonally inaccessible nature of these mountainous watersheds. These conditions often preclude frequent sampling intervals and as a consequence, also eliminate certain vadose-zone sampling techniques. This problem is further complicated by previous research which has shown that the isotopic composition of fresh snow and/or remnant snowpack can differ greatly from the isotopic composition of the snowmelt runoff [*Herrmann et al.*, 1981; *Hooper and Shoemaker*, 1986; *Taylor et al.*, 2001]. Therefore, assuming that the isotopic composition of fresh snow and/or surface runoff from snowmelt is the same as that of the snowmelt infiltration at the end of the snowmelt season can result in errors in

[1] **Frisbee, M.D., F.M. Phillips, A.R. Campbell, and Jan. M.H. Hendrickx (2010), Modified passive capillary samplers for collecting samples of snowmelt infiltration for stable isotope analysis in remote, seasonally inaccessible watersheds 1: Laboratory evaluation, *Hydrological Processes*, 24, 825-833, doi:10.1002/hyp.7523.**

the hydrograph separation; most commonly the overestimation of pre-event water sources and underestimation of event water [*Earman et al.,* 2006; *Feng et al.,* 2002; *Taylor et al., 2002*]. Consequently, a robust method requiring little maintenance or monitoring is desirable for sampling the seasonally integrated isotopic signature(s) of snowmelt infiltration in these watersheds.

Previous researchers have employed a variety of methods to sample snowmelt infiltration and vadose-zone soil waters during snowmelt. Collecting snow cores is one common method utilized to sample snowpacks. However, the isotopic composition of the snow cores, even late season cores, does not accurately represent the isotopic composition of meltwater from the snowpack due to isotopic enrichment during the melt. Isotopic fractionation differences between the snowpack and snowmelt have been investigated in the work of *Taylor et al.*, [2001] and *Unnikrishna et al.,* [2002] at the Central Sierra Snow Laboratory in the Sierra Nevada. *Unnikrishna et al.,* [2002] for example, was able to obtain a high temporal resolution series of meltwater and snowpack isotopic composition via a combined approach using snowmelt lysimeters and snow cores. This approach may not always be practical for several reasons. For example, many of the watersheds in the southwestern United States have fractured volcanic lithologies which often imply that subsurface runoff processes are highly integrative. Therefore, high temporal resolution datasets of isotopic compositions of snowmelt endmembers may not be as useful as seasonally integrated isotopic compositions of snowmelt. Also, high-resolution sampling methodologies may not practical in many of the mountainous watersheds of the southwestern United States since backcountry access is very limited during the snowmelt season.

Obtaining the isotopic composition of meltwater via soil cores is another common methodology which has been employed in the work of *Buttle and Sami,* [1990], *Sugimoto et al.,* [2003], *Laudon et al.,* [2004], and *Robertson and Gazis,* [2006]. Although this methodology does capture the isotopic composition of the snowmelt that has infiltrated the soil, it will generally be logistically difficult in remote terrain. Snow lysimeters were used in the work of *Laudon et al.,* [2002] and *Taylor et al.,* [2001] to improve hydrograph separation techniques and better constrain the isotopic composition of meltwater. Suction lysimeters were used in the work of *Laudon et al.,* [2004] and *Murray and Buttle,* [2005] to better constrain runoff processes during snowmelt. Snow and suction lysimeters typically require more maintenance and monitoring than would be practical in most remote, snowbound landscapes. *Hoch et al.,* [1999] employed zero-tension lysimeters in the San Juan Mountains of southern Colorado to sample vadose waters. They collected these samples on a bi-annual schedule; after snowmelt and before the winter freeze. This methodology would provide an integrated signature of the snowmelt recharge; but the positive pressures required to support flow from the overlying soil column are not always experienced and may be short lived. In addition, the kinetics that control the geochemical evolution of soil-water can proceed under unsaturated conditions and these waters will not be sampled by zero-tensions lysimeters. All these methodologies have limited applicability in remote, seasonally inaccessible terrain.

Passive capillary samplers (PCAPS) may however provide a robust alternative to the aforementioned methodologies. The PCAPS concept was developed by *Brown et al.,* [1986] and was subsequently evaluated by *Holder et al.,* [1991] and *Knutson and Selker,* [1994]. PCAPS are constructed from fiberglass wicks; the length and diameter are

chosen to match the matric potential of the soil to be sampled. In the standard PCAPS design, one end of the wick is spread open and fastened to a collection surface of a known area. This end is placed in contact with the overlying, undisturbed soil. The other end of the wick is usually inserted into tubing which drains into a collection bottle (Figure 2.1). The wicks behave essentially like hanging water columns [*Boll et al.,* 1992]; thus, allowing water to be drawn from the surrounding soil with little or no maintenance, no application of external suction, and unlike the zero-tension lysimeter, no dependency upon positive pressure (Figure 2.1). PCAPS have since been used quite extensively in vadose-zone studies. These devices have also been used to generate breakthrough curves of solute transport in the porous media in the work of *Holder et al.,* [1991], *Boll et al.,* [1992], *Poletika et al.,* [1992], and *Brandi-Dohrn et al.,* [1996]. More recently, *Gee et al.,* [2002, 2003] used fiberglass wicks in the design of their modified vadose zone water fluxmeter. The strength of the modified water fluxmeter design is that is can reduce flow divergence or the lateral movement of water away from or into the wick in field soils thereby reducing the instrument dispersion coefficient. The drawback of the fluxmeter design is that in the typically shallow, rocky soils of alpine settings the installation of funnels, tipping bucket, PVC pipe, and collection bottles required for the fluxmeter may not always be feasible. *Goyne et al.,* [2000], *Brahy and Delvaux,* [2001], and *Goyne et al.,* [2001] provided a thorough discussion on proper cleaning and preparation techniques required to reduce and/or eliminate the contamination of soil water samples by weathering of the fiberglass wicking material or by the mobilization of soluble materials from within the wick. With proper preparation, PCAPS appear to be a robust, inexpensive method to sample vadose-zone waters under a variety of matric

potentials, making it a desirable alternative to the vadose-zone sampling techniques described above.

Passive capillary samplers have been deployed to collect soil water for stable isotope analysis in agricultural settings [*Landon et al.*, 1999; *Landon et al.*, 2000; *Delin and Landon*, 2002]. These studies used a standard PCAPS design (Figure 2.1) described in the work of *Brown et al.*, [1986]. The standard PCAPS design has historically been employed in agricultural settings characterized by relatively thick vadose zones containing little to no rock content. Soils in mountainous regions and in alpine settings are often very different from typical agricultural soils in valley settings. Soils in these settings are characteristically shallower and rockier. For example, soil pits installed in high elevation locations in the Saguache Creek watershed in the San Juan Mountains of the southern Rocky Mountains of Colorado indicated that these alpine soils were typically shallow (depth to weathered bedrock averaged 45 cm) and rocky. Large volcanic rocks (typically 20 cm wide by 20 cm long by 3 cm thick) often occur in discrete layers in the soil profile but the content of small stones remains high throughout the typical soil profile. Therefore, it was concluded that the standard PCAPS design was not feasible and a modified PCAPS was designed to accommodate the soils encountered in these mountainous watersheds (Figure 2.2). The modified PCAPS (M-PCAPS) collects water from a smaller contact area and can be installed in thin, rocky alpine soils. We wanted to ensure that the modified design did not alter the isotopic composition of soil water; therefore, a simple laboratory experiment was conducted to answer two important questions regarding the suitability of the M-PCAPS design. 1. Does the wicking process fractionate water? 2. How well do the M-PCAPS track the changing

isotopic composition of a soil reservoir undergoing kinetic fractionation; (e.g. soil evaporation)?

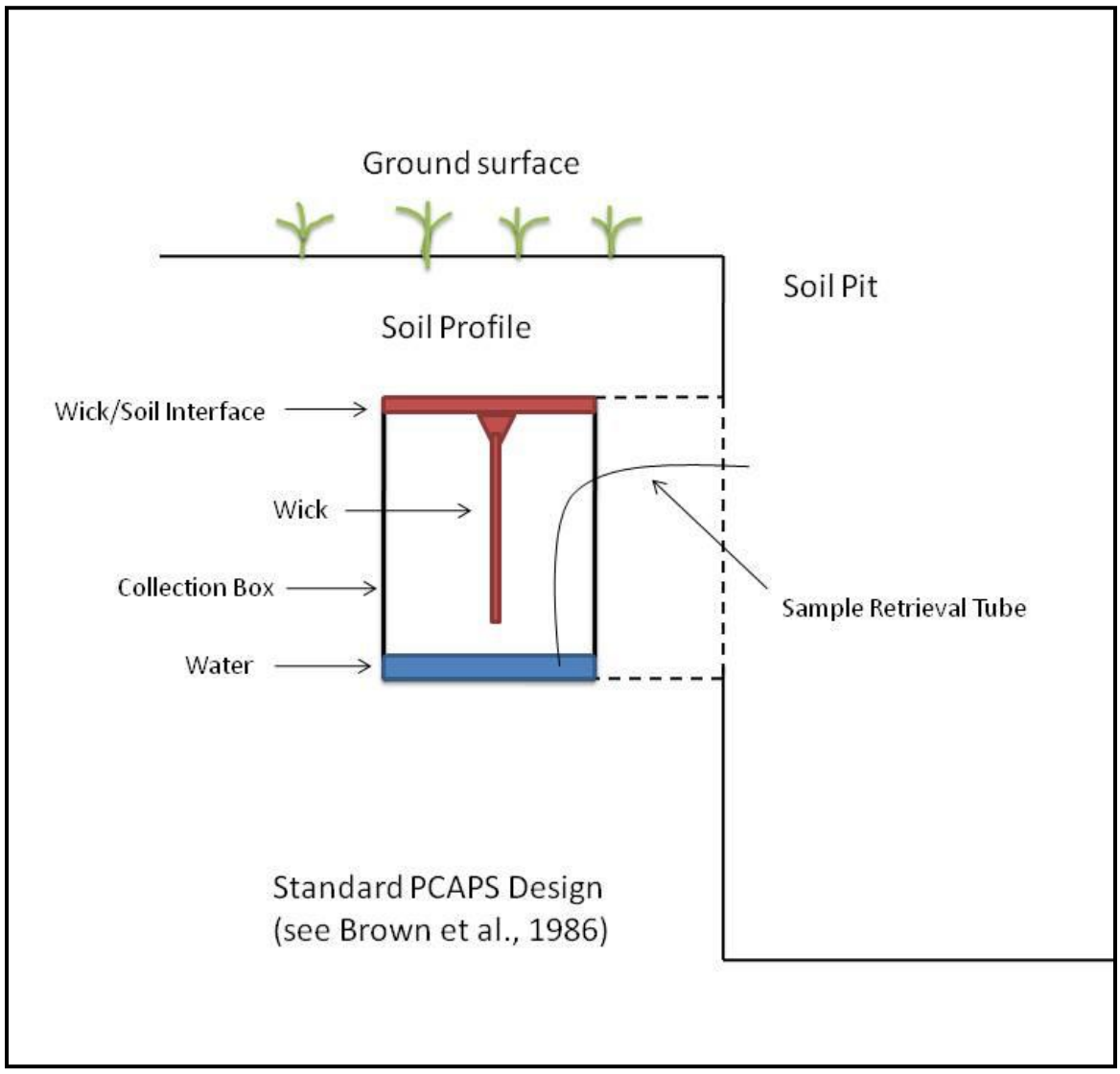

Figure 2.1: Standard PCAPS design described in the work of *Brown et al.*, (1986). PCAPS are typically inserted into the soil column as shown.

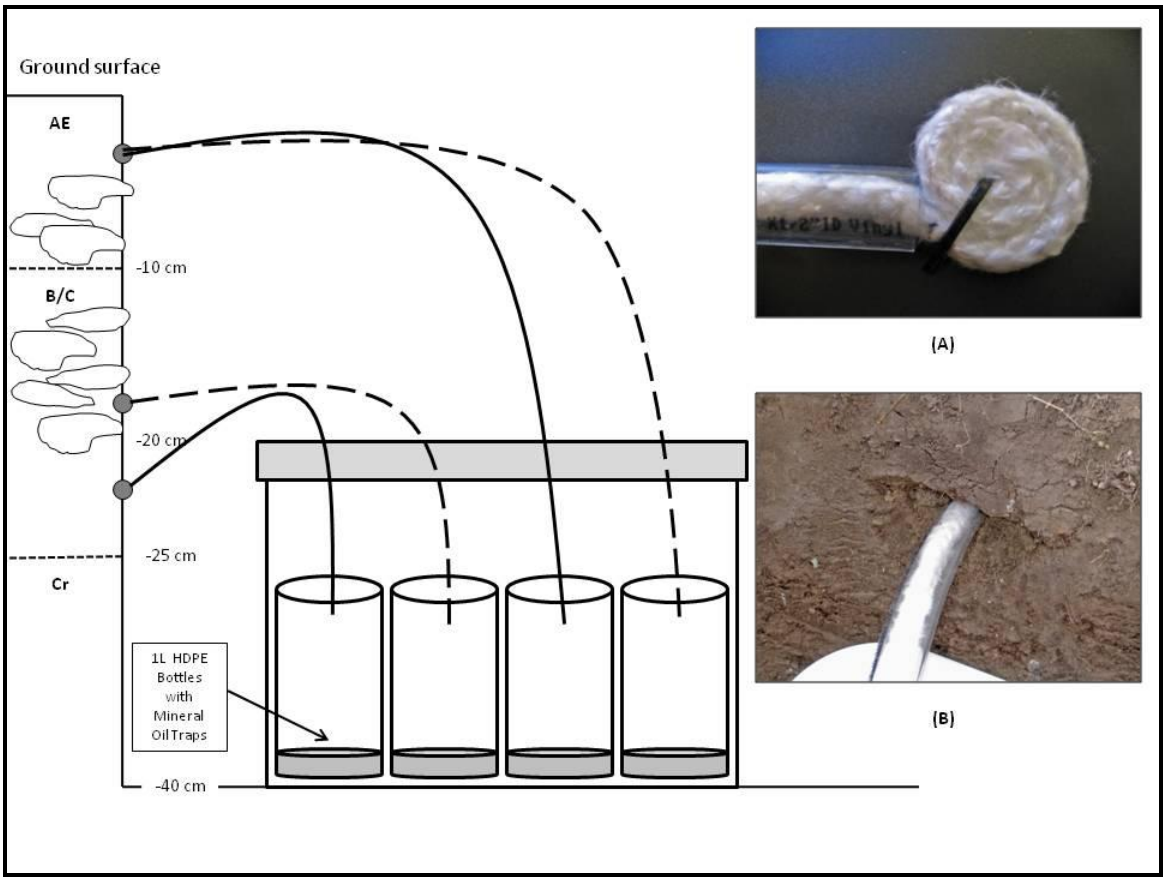

Figure 2.2: Modified PCAPS design with field applications. "Fiddleheads" shown in inset 'a' are inserted into the soil column and drain into collection bottles outside soil column. Soil disturbance is reduced since "fiddlehead" is small compared to disturbance created by insertion of standard PCAPS (inset 'b').

2.2 Methods:

Two Styrofoam boxes having dimensions of 32.4 cm long x 26.0 cm wide x 27.3 cm deep and wall thicknesses of 2.54 cm were used to create weighing lysimeters (Figure 2.3). Each side of each box had three access holes 1.59 cm (5/8 inch) in diameter for the wicks resulting in 12 total access holes per cooler. One access hole (D1) was located 4 cm below the planned surface of the sand in the box, one hole (D2) was located 14 cm below the sand surface, and the remaining hole (D3) was located 24 cm below the sand surface or at the bottom of the box. Three mini-tensiometers were installed into one side

of each box (one at each depth mentioned above). The mini-tensiometers consisted of a small porous cup approximately 2.54 cm in length, a plastic right-angle tube of approximately 5 cm in length filled with water, and a small rubber cap placed tightly over the tube.

A 50 ft. coil of fiberglass wick having a diameter of 9.5 mm (3/8 inch, Pepperell Braiding Company SKU # 1380) was used in this study. Although this study did not investigate chemical transport behavior, the wicks were soaked and rinsed in deionized water several times daily for a duration of 3 weeks to ensure that manufacturing residues were removed. The degree of cleanliness was ascertained by measuring the electrical conductivity of the rinse water after each soak. Samples of the final rinse water were also subjected to standard chemical analyses to provide chemical benchmarks for future field applications. The wicks were 30.5 cm (1 ft.) long resulting in a wick matric potential (ψ_{wick}) of -30.5 cm at soil fluxes equal to zero [*Knutson and Selker*, 1994]. One end of each wick was coiled into a "fiddlehead" shape and then securely yet loosely fastened in place using zip-ties (Figure 2.2a). The "fiddlehead" was placed in direct contact with the soil while the remainder of the wick was entirely enclosed within flexible PVC tubing (Figure 2.2b). This modification is necessary for thin, mountainous soils which cannot accommodate the assembly length associated with the standard PCAPS assembly. In comparison, passive capillary samplers (Figure 2.1) are typically comprised of a water collection plate which has wick fibers glued to the top of it and a wick draining from the center of the plate down to a collection bottle resulting in overall assembly lengths up to 100 cm [*Brown et al.*, 1986]. Using our design, the wick was pulled through flexible PVC tubing having an outer diameter of 1.59 cm (5/8 inch) and an inner diameter of 1.27

cm (1/2 inch). Each tubing/wick assembly was pushed through an access hole in the box and silicon sealant was applied at the juncture of the tubing and the box to prevent leaking and exchange between the soil and the atmospheric water vapor. The outflow end of each wick was placed in a 500 mL Nalgene® sample bottle. The mouth of each bottle was covered in Parafilm® M Barrier Film. A layer of mineral oil was poured in each bottle to prevent evaporation and atmospheric exchange.

Two scales were placed on concrete block platforms and the boxes were placed on the scales. The scales were re-zeroed. Fine uniform sand was poured into each box, filling them to approximately 3.0 cm below the top of the cooler. Column experiments were performed to determine the hydraulic parameters of the sand. These experiments indicated that the average bulk density of the sand was 1.61 g cm^{-3}, the average porosity was 0.39, and the average saturated hydraulic conductivity was $3.6*10^{-2}$ cm sec^{-1}. The dry weight of each box was recorded. One TDR probe was inserted at each of the three depths on one side of each box. Deionized water of a known stable isotopic composition was poured from a watering can onto the sand to evenly saturate the soil surface. Each box was covered with a Styrofoam lid and kept covered for 1 week. The initial wet weight of each box was recorded. By keeping the boxes covered, the effects of kinetic fractionation associated with water and soil water evaporation were minimized. Thus, the water samples obtained via wicking during week 1 should reflect the stable isotopic composition of the water added to the box. We could then determine if the water obtained by wicking during the first week was isotopically different than the water added to saturate the box. If the waters were isotopically different, then fractionation during the wicking process was a possibility (question 1).

Each individual side of the boxes represented a weekly dataset and three wicks were installed in each side of the box at each depth (D1, D2, and D3 mentioned above). The water samples obtained from these wicks were removed in weekly intervals; (i.e. box side 1 represented the week 1 sample set, box side 2 represented the week 2 sample set and so forth). The first set of weekly samples was removed at the conclusion of week 1. Then, the lids were removed from the boxes to allow evaporation from the soil. New bottles were put in place of the ones just removed to continue to collect water removed by wicking. During the next 3 weeks, the soil was allowed to evaporate. At the same time, two 250 mL bottles filled with the same water used to saturate the sand in the coolers were allowed to evaporate. The weight of each box, evaporating water sample, and water sample obtained via wicking was measured on a daily basis so that mass balances could be calculated. Soil tension measurements were conducted daily using a tensiometer and the soil moisture at each depth was calculated daily based on soil permittivity measurements made with the TDR probes and a Tektronix 1502B TDR Cable Tester (Figure 2.3).

Each water sample, including the original water, was analyzed for $\delta^{18}O$ and $\delta^{2}H$. The $\delta^{18}O$ composition was measured on 1 mL samples of water using the CO_2 / H_2O equilibration method described in *Clark and Fritz*, [1997] using a Thermo Finnigan Gasbench operated in continuous flow mode. The $\delta^{2}H$ composition was measured by gas metal reduction with powdered chromium at 850°C in an H-Device [*Nelson and Dettman*, 2001] and analyzed in dual inlet mode. Both CO_2 and H_2 were analyzed on a Thermo Finnigan Delta^{PLUS} XP Flow Stable Isotope Ratio Mass Spectrometer. All stable isotope results are reported with respect to VSMOW. At the termination of the

experiment, two soil samples were removed from each depth in Box 1. Water was vacuum distilled from the soil samples using the vacuum distillation method described in the work of *Araguás-Araguás et al.*, [1995] and later analyzed for $\delta^{18}O$ and $\delta^{2}H$. The variability in $\delta^{18}O$ was ascertained by analyzing sixteen duplicates. Variability ranged from 0.0 to 0.2 ‰ and one duplicate varied by 0.5 ‰. The overall average variability in $\delta^{18}O$ was 0.1 ‰. Sixteen duplicates of $\delta^{2}H$ were analyzed and the variability ranged from 0 to 1 ‰.

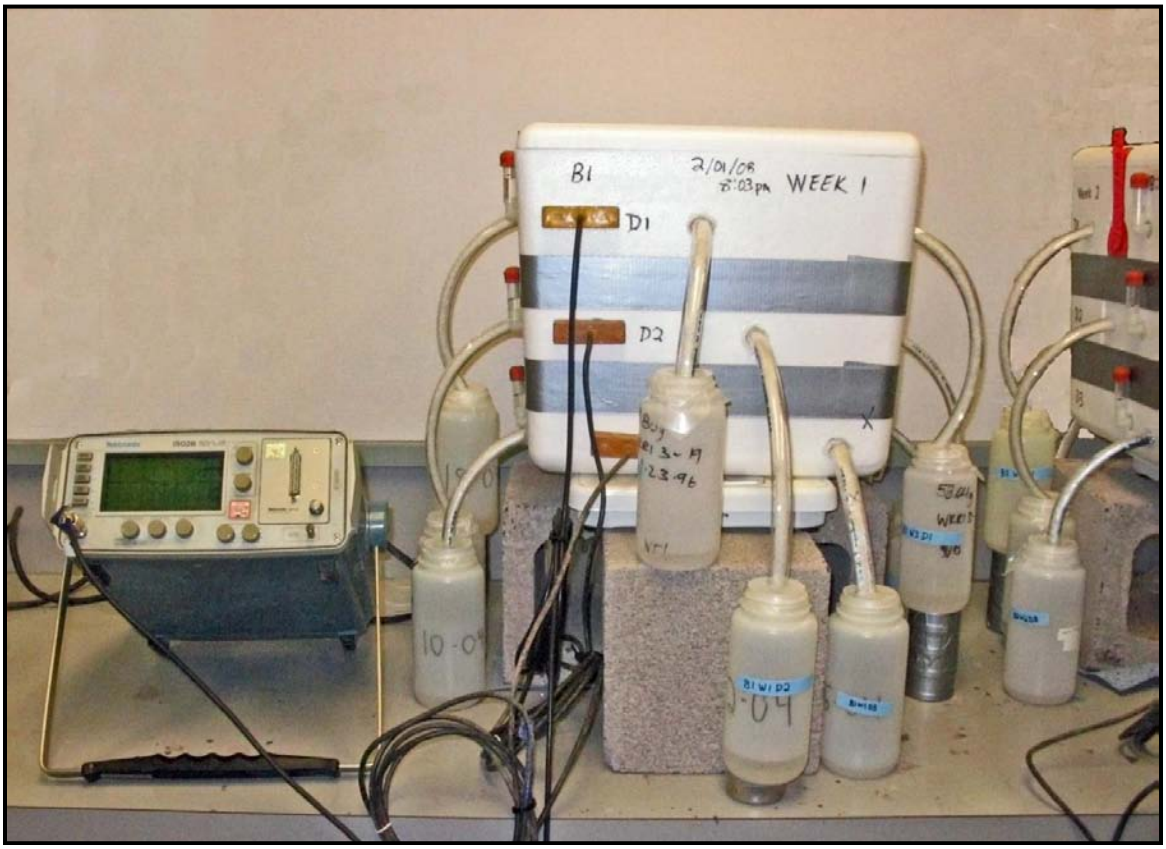

Figure 2.3: Photo of the experimental design showing PCAPS extending from Box 1, mini-tensiometers on the left side of the box, and TDR probes inserted into the box face.

2.3 Results:

Complete saturation of the boxes could not be achieved due to the occurrence of bypass flow in the wick assemblies installed at the bottom the box (D3). We observed water that bypassed the wick and moved directly from the soil into the PVC tubing at the deepest sampling locations in the box. However, soil moisture measurements indicate that saturation was achieved from -14 cm downward encompassing the D2 and D3 depths. The initial volumetric water content at -4 cm (D1) was approximately 0.14 (Table 2.1). Wicking commenced almost immediately after the coolers were saturated and relatively rapid wicking continued for the first 2 days of the experiment. Bypass flow was observed in the flexible tubing around some of the bottom wicks at D3 during the first few minutes of the experiment. These water samples were discarded. However, the weights of these samples were recorded so that the mass balances would remain accurate. The wicks at –4 and –14 cm (D1 and D2) effectively stopped conducting water at approximately 14 days into the experiment. At this point, relatively small changes in water content led to large changes in matric potential and the matric potential of the soil quickly became more negative than the matric potential of the wick (ψ_{wick} ~ -30.5 cm, Table 2.1). The wicks at the bottom of the box (D3) continued to wick for the duration of the experiment; however, wicking slowed approximately exponentially starting after the first 2 weeks.

The global meteoric water line [*Craig,* 1961] and the evaporating control water samples are shown in Figure 2.4. The original waters shown as dark blue circles in Figure 2.4 plot on the GMWL. The evaporated control samples are represented by light

blue squares, diamonds, and triangles in Figure 2.4. These evaporated waters were fit with a linear trendline resulting in: $\delta^2H = 4.7\delta^{18}O - 34$ ($R^2 = 0.99$). This slope is consistent with previously published slopes associated with evaporation from the surface of a water body at an atmospheric humidity of about twenty percent [*Craig and Gordon,* 1965; *Merlivat,* 1978]. The average humidity in the lab during the duration of the experiment was 25 percent. Figure 2.4 also shows the soil-water evaporation line obtained by fitting a linear trendline to the soil-water samples taken at the termination of the experiment. The soil-water samples are represented by the orange squares, diamonds, and triangles in Figure 2.4. The trendline for the evaporated soil-waters is given by: $\delta^2H = 2.4\delta^{18}O - 63$ ($R^2 = 0.91$). This slope is also consistent with previously published data on soil undergoing evaporation with an atmospheric humidity of twenty percent [*Allison,* 1982; *Barnes and Allison,* 1983; *Allison et al.,* 1983]. These two lines help constrain the isotopic composition of the PCAPS water samples shown in Figures 2.5, 2.6, and 2.7 (note that the x-axis has been re-sized to fit the data).

The isotopic composition of the original water for box 1 had a $\delta^{18}O$ of -13.3 ‰ and δ^2H of -96 ‰ while the original water in box 2 had a $\delta^{18}O$ of -13.6 ‰ and δ^2H of -96 ‰. These endmembers are shown as the large, dark blue circles in Figures 2.4. Water samples were collected daily for the first 2 days and at weekly intervals thereafter. The water samples obtained during the rapid wicking on day 1 had an average $\delta^{18}O$ of -13.3 ‰ and a δ^2H of -94 ‰ and the samples retrieved on day 2 had an average $\delta^{18}O$ of -13.2 ‰ and a δ^2H of -95 ‰. These values are the same, within error, to the original waters. Thus, the wicks were sampling water during the first two days which was kinetically unaltered since the boxes were covered during the first week. Data from these two days

provides an answer to question 1. The wicking process does not fractionate water. The $\delta^{18}O$ of the Week 1 samples ranges from -12.8 to -13.3 ‰ and the $\delta^{2}H$ ranges from -95 to -96 ‰. The $\delta^{2}H$ values are also very similar to the original water but the $\delta^{18}O$ values seem to indicate that very minor soil evaporation may have occurred in the boxes

Day	Depth D1		Depth D2		Depth D3	
	ψ_{tp} (cm)	θ_v	ψ_{tp} (cm)	θ_v	ψ_{tp} (cm)	θ_v
1	ND	ND	ND	ND	ND	ND
2	ND	0.14	ND	0.35	ND	0.37
3	-5.9	0.10	-9.8	0.30	-11.8	0.37
4	-6.9	0.08	-6.9	0.28	-6.9	0.37
5	-7.8	0.08	-7.8	0.28	-7.8	0.37
6	-7.8	0.08	-7.8	0.26	-7.8	0.37
7	-9.8	0.08	-8.8	0.25	-8.8	0.37
8	-9.8	0.08	-8.8	0.25	-8.8	0.37
9	-9.8	0.07	-8.8	0.21	-7.8	0.37
10	-9.8	0.07	-9.8	0.18	-8.8	0.37
11	-18.6	0.07	-13.7	0.18	-13.7	0.37
12	-43.1	0.05	-101	0.17	-14.7	0.37
13	-29.4	0.05	-155.9	0.17	-15.7	0.37
14	-127.4	0.05	-198	0.16	-16.7	0.37
15	-197	0.05	REQ	0.14	-15.7	0.37
16	-239.2	0.05	REQ	0.14	-15.7	0.37
17	-259.8	0.05	REQ	0.14	-15.7	0.37
18	-273.5	0.04	-204.9	0.14	-18.6	0.37
19	REQ	0.04	-227.4	0.12	-15.7	0.37
20	REQ	0.04	TF	0.12	-17.6	0.35
21	REQ	0.04	TF	0.12	-17.6	0.35
22	REQ	0.04	TF	0.12	-16.7	0.35
23	REQ	0.04	TF	0.11	-15.7	0.33
24	REQ	0.04	TF	0.11	-16.7	0.33
25	REQ	0.04	TF	0.11	-17.6	0.33
26	-262.7	0.04	TF	0.09	-19.6	0.32
27	-276.4	0.04	TF	0.09	-19.6	0.30
28	REQ	0.04	TF	0.09	-19.6	0.28
29	REQ	0.04	TF	0.08	-19.6	0.26

Table 2.1: The tensiometric potential (ψ_{tp}) and the volumetric water content (θ_v) measured for each depth during the experiment in Box 1. Cells which contain '**ND**' represent no data, cells which contain '**REQ**' represent re-equilibration time after re-filling the mini-tensiometer, and cells which contain '**TF**' represent tensiometer failure (days 20 to 29 at D2).

during week 1 since the media was not completely saturated. During the next 3 weeks, the soil-water continued to evaporate and the stable isotopic composition of the soil-water continued to become isotopically enriched. The remaining samples from Week 2, 3, and 4 exhibit a general trend toward isotopic enrichment following the soil-water evaporation line with an overall spread in $\delta^{18}O$ of 1.8 ‰ and 6 ‰ in $\delta^{2}H$ (Figure 2.5).

Three anomalies were encountered during the experiment (Figure 2.6). Two of the data points are associated with box 2. Box 2 was our trial run and we noticed that two of the wick installations had poor silicon seals around the flexible tubing that houses the wick. As we completed the assembly of Box 2, our method for sealing these wicking installations improved and we used this experience to make Box 1 more tightly sealed. We kept the data points in Box 2 because inspections revealed that only 2 of the silicon seals had failed. The three anomalous samples were also associated with greatly reduced wicking volume: 9.8 g in box 2 compared to 122.0 g in box 1 during week 2, 4.1 g in box 1 compared to 224.9 g in box 2, and 7.7 g in Box 2 compared to 70.3 g in Box 1. Upon inspection, it was determined that the silicon seals around the flexible tubing on the outside of the boxes had failed at these three wicks. This failure most likely enhanced evaporation of the soil immediately around the wick and possibly from the wick itself. Theoretically, the samples should plot near the soil-water evaporation line since the soil may have been evaporating in this region of the box and consequently, there was a very small vadose-zone development to enhance kinetic fractionation. This is verified by the location of the sample points near the soil-water evaporation line in Figure 2.6.

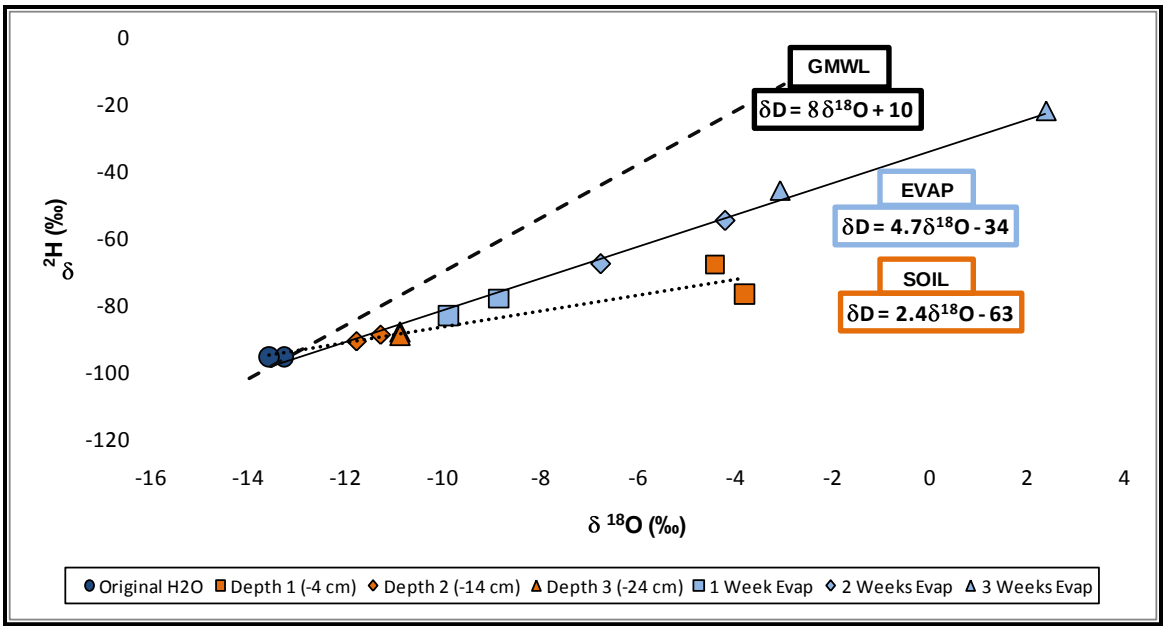

Figure 2.4: The bold, dashed line labeled 'GMWL' is the global meteoric water line given by Craig, [1961], the solid line labeled 'EVAP' is the water evaporation line, and the dotted line labeled 'SOIL' is the soil-water evaporation line. Line styles are kept the same for all subsequent plots.

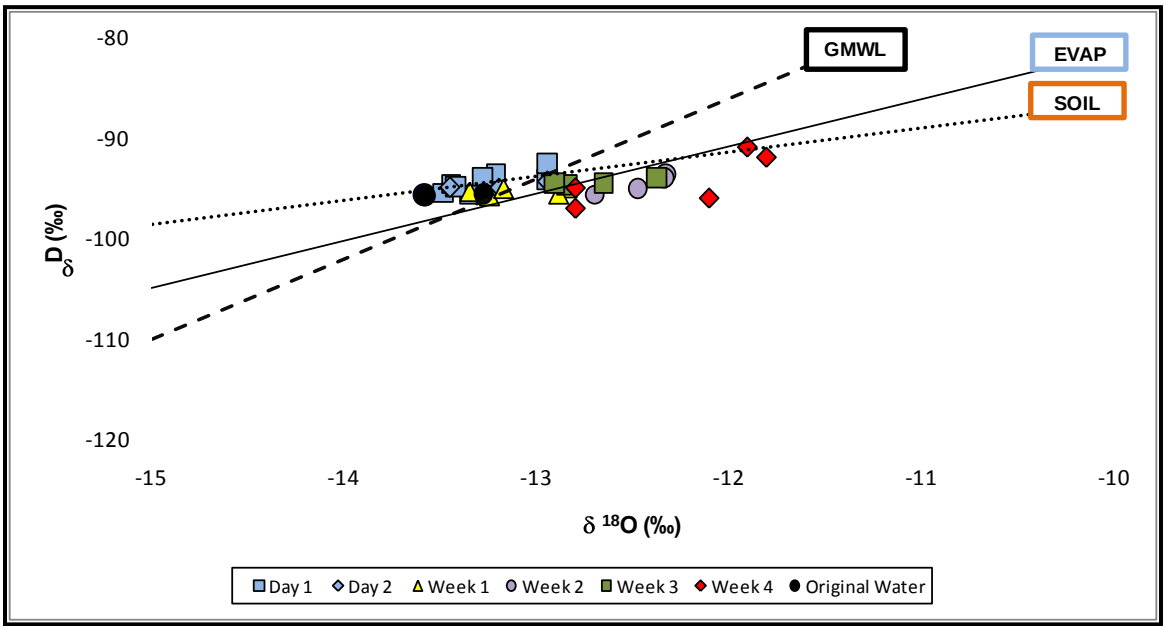

Figure 2.5: Expanded view of the data cloud representing the water samples obtained using PCAPS. Note that the water samples appear to trend along the soil-water evaporation line as the experiment progresses.

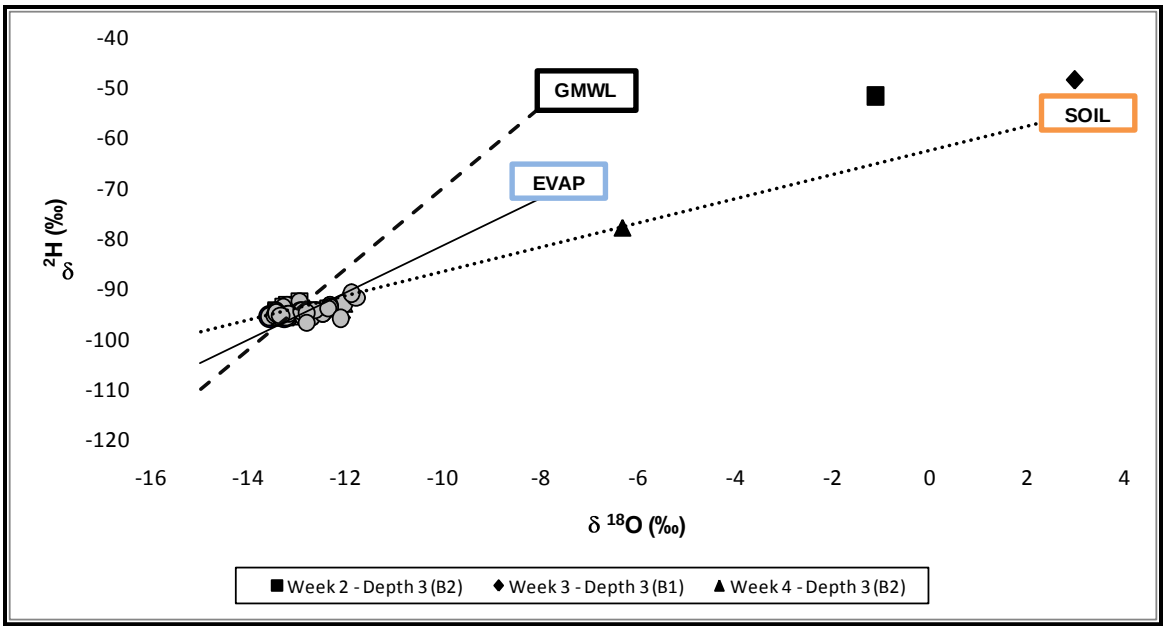

Figure 2.6: The three sample anomalies encountered during the experiment.

2.4 Discussion:

Kinetic fractionation within the soil matrix during evaporation appears to be responsible for the trends exhibited by the M-PCAPS water samples (Figure 2.5). This can be further illustrated by using data from mass balance calculations. Both boxes initially contained 8391.5 g of water. The mass balance in box 1 indicates that wicking removed 36 percent of the total water from the soil and evaporation removed 26 percent of the water contained in the soil matrix. The average evaporation rate from the soil was 0.12 cm day^{-1} while the evaporation rate from the open water bottles was 0.59 cm day^{-1}. Evaporation rates are expressed relative the volume contained in the box and in the bottle, respectively. Although the soil water evaporated at a much lower rate, kinetic fractionation was enhanced as a consequence of the deepening of the unsaturated zone. An expanding vadose zone will tend to increase tortuosity and since $H^2H^{16}O$ (mass = 19) will diffuse faster than $H_2{}^{18}O$ (mass = 20), there will be greater enrichment in $\delta^{18}O$

relative to δ^2H [*Allison*, 1982; *Clark and Fritz*, 1997; *Merlivat*, 1978]. Since the water samples, in general, trend along the soil-water evaporation line and not the water evaporation line, this indicates that the M-PCAPS samples were indeed tracking changes in the isotopic composition of the soil reservoir that were a consequence of soil-water evaporation. Figure 2.7 shows the isotopic evolution of the D3 water samples during the course of the experiment relative to the isotopic composition of the soil water obtained at the D3 depth at the termination of the experiment. Since the M-PCAPS installed at D3 continued to wick for the duration of the experiment, the water samples should theoretically trend toward the isotopic composition of the soil water. This seems to be the case. Thus, M-PCAPS appear to track the isotopic composition of the soil water.

The cessation of wicking encountered at –4 cm and –14 cm (D1 and D2) can readily be explained using a soil characteristic curve. Sandy soils exhibit a more rapid drying curve than silty or clayey soils. Thus, as evaporation continues within the soil matrix, small changes in soil moisture lead to large increases in matric potential. The matric potential of the wick ($\psi_{wick} \sim -0.5$ cm) would be theoretically exceeded once the soil moisture approached a value of 0.23. Data in Table 2.1 indicates that the soil moisture at depths of –4 cm and –14 cm (D1 and D2) was quickly reduced during the first 2 weeks of the experiment. The cessation problem is therefore a shortcoming in the design in the experiment. If for example, a silty sand had been used then wicking might have continued throughout the duration of the experiment.

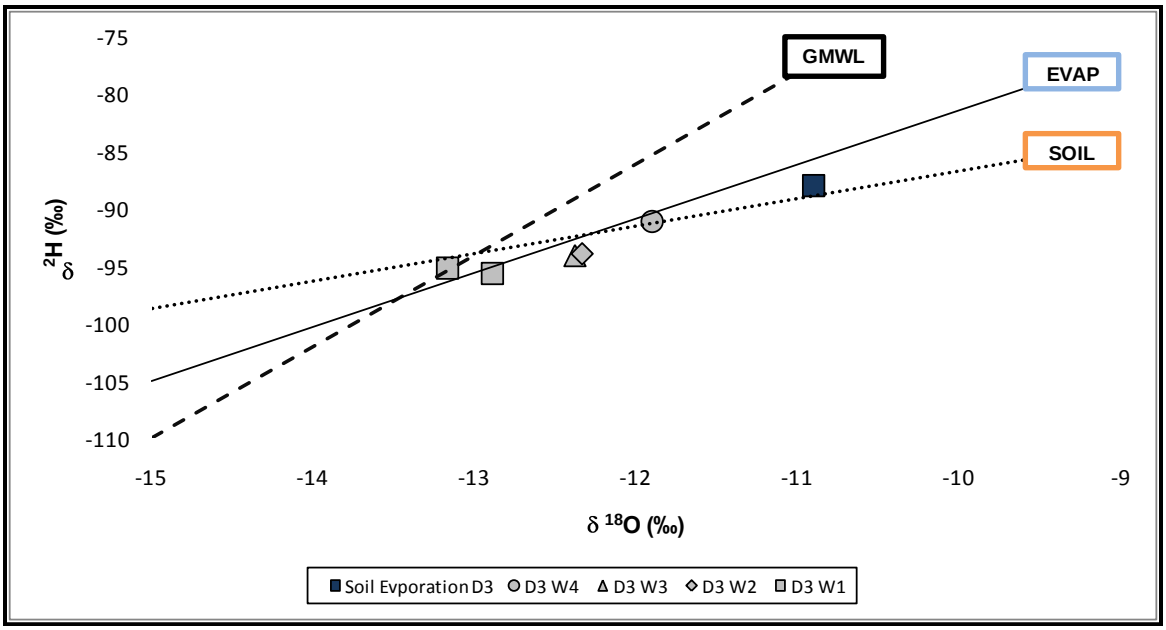

Figure 2.7: Isotopic evolution of D3 samples. W1 is week 1, W2 is week 2, etc.

We have two hypotheses for the three anomalous samples that were encountered during the experiment: failure of silicon seals and fractionation within the tubing. The wicks are essentially in a closed system as long as the flexible tubing is completely sealed off from atmospheric exchange along its length. However, if the silicon seals fail, then water vapor can exchange between the wick and the atmosphere and/or between the soil around the wick and the atmosphere. This exchange would mimic kinetic fractionation from a soil having a thin unsaturated zone. We think this is the most logical explanation since the anomalies plot between the water evaporation line and the soil-water evaporation line.

Alternatively, kinetic fractionation could occur inside the tubing surrounding the wick. Condensation was, in fact, observed in some of the tubing surrounding the deepest wicks (D3) approximately 3 weeks into the experiment. This was initially a concern since the three anomalies occurred in the D3 dataset. However, the remaining D3

samples plot consistently within the data cloud of the other M-PCAPS samples. The wick is in a closed system as long as the flexible tubing is completely sealed off from atmospheric exchange. Therefore, fractionation would not be expected if exchange resulted from re-condensation between the wick and flexible tubing surface. This process would be similar in some respects to a vacuum distillation process. In any case, we think that condensation can be minimized by using flexible tubing with a smaller inner diameter that will fit more tightly around the wick.

There are limitations to the M-PCAPS approach and to the utilization of wicks in general. The hydraulic properties of the field soils should be determined as accurately as possible under field settings. If the wick is not matched to the hydraulic properties of the field soils, then the wicks may preferentially sample different fractions of soil-water or divergent flow behavior can occur [*Gee et al.*, 2002, 2003]. If the matric potential of the wick is much more negative than the surrounding soil, then the wick may preferentially sample water residing in smaller pores. On the other hand, reverse gradients may occur if the matric potential of the soil becomes more negative than the matric potential of the wick. In this case, water may be pulled from the wick into the soil or from water stored in the collection bottles if the wick is allowed to contact the water in the collection bottles. Divergent flow can enhance the dispersive properties of the wick and create error in breakthrough curves generated during contaminant transport studies. It may also cause collection errors which affect estimates of soil-water fluxes. In fact, after the experimental design was allowed to equilibrate, we found that infiltration measured by the M-PCAPS design ranged from 84 to 127 percent of actual infiltration. *Louie et al.*, [2000] also reported collection efficiencies of 125 percent of recharge in standard PCAPS

installations. They suggested that overcollection using the standard PCAPS design could be the result of persistent saturated conditions and/or oversampling near macropores in the soil. Regardless, caution should also be exercised when reporting soil-water fluxes obtained by passive wick samplers.

This laboratory evaluation provided encouraging results and as a consequence, twelve M-PCAPS were successfully installed in the Saguache Creek watershed located in the San Juan Mountains of southwestern Colorado. These M-PCAPS were installed at elevations ranging from 9000 to 11,000 ft a.s.l in the watershed prior to the onset of snow accumulation during October 2007 and were removed at the end of the following snowmelt season during June 2008. Samples of snowmelt infiltration were successfully collected for stable isotope and geochemical analysis. These M-PCAPS samples provided information on the hydrologic system that would have otherwise been unavailable to surficial sampling methodologies. Those results are discussed in the work of *Frisbee et al.*, (2009).

2.5 Conclusions:

We designed this experiment to test the suitability of a modified passive capillary sampler design for measuring the integrated isotopic composition of snowmelt-infiltration. We were interested in determining whether the wicking process of the design modification causes fractionation. We were also interested in quantifying how accurately the wicks track the changing isotopic composition of a soil reservoir. The results are encouraging. Wicking does not appear to cause isotope fractionation, inasmuch as the samples obtained during rapid wicking of days 1 and 2 did not show any appreciable

change from the isotopic composition of the original water. Furthermore, M-PCAPS are effective in tracking the isotopic changes associated with kinetic fractionation in a soil reservoir. Certain precautions must be made to prevent atmospheric exchange along the length of the wick from soil to sample bottle. This is achieved by properly sealing the wick within flexible tubing leaving little or no head space around the wick, thereby creating a closed system for transport. If these precautions are made, M-PCAPS may be useful in other similar applications. For example, M-PCAPS may be an attractive alternative to snow lysimeters or snowmelt pans because the researcher would only need to change out sample bottles once the M-PCAPS are installed. In conclusion, this M-PCAPS design appears to be a reliable, robust method to sample the isotopic composition of snowmelt infiltration in remote, seasonally inaccessible watersheds. M-PCAPS require little to no maintenance, are not dependent on any external means of applying soil suction, and can sample vadose waters over a range of soil matric potentials.

2.6 References:

Allison, G.B. (1982), The relationship between ^{18}O and deuterium in water in sand columns undergoing evaporation, *Journal of Hydrology, 55*, 163-169.

Allison, G.B., C.J. Barnes, and M.W. Hughes (1983), The distribution of deuterium and ^{18}O in dry soils 2. Experimental, *Journal of Hydrology, 64*, 377-397.

Araguás-Araguás, L., K. Rozanski, R. Gonfiantini, and D. Louvat (1995), Isotope effects accompanying vacuum extraction of soil water for stable isotope analyses, *Journal of Hydrology, 168*, 159-171, doi:10.1016/0022-1694()94)02636-P.

Barnes, C.J. and G.B. Allison (1983), The distribution of deuterium and ^{18}O in dry soils 1. Theory, *Journal of Hydrology, 60*, 141-156.

Boll, J., T.S. Steenhuis, and J.S. Selker (1992), Fiberglass wicks for sampling of water and solutes in the vadose zone, *Soil Science Society of America Journal, 56,* 701-707.

Brahy, V. and B. Delvaux (2001), Comments on "Artifacts caused by collection of soil solution with passive capillary samplers", *Soil Science Society of America Journal, 65,* 1571-1572.

Brandi-Dohrn, F.M., R.P. Dick, M. Hess, and J.S. Selker (1996), Field evaluation of passive capillary samplers, *Soil Science Society of America Journal, 60,* 1705-1713.

Brown, K.W., J.C. Thomas, and M.W. Holder (1986), Development of a capillary wick unsaturated zone water sampler, Coop. Agreement CR812316-01-0. USEPA Environ. Monit. Sys. Lab., Las Vegas, NV.

Buttle, J.M. and K. Sami (1990), Recharge processes during snowmelt: An isotopic and hydrometric investigation, *Hydrological Processes, 4*(4), 343-360.

Clark, I., and P. Fritz (1997), *Environmental Isotopes in Hydrogeology,* Lewis, Boca Raton, Fla.

Craig, H., (1961), Isotopic variations in meteoric waters, *science, 133,* 1702-1703.

Craig, H. and L.I. Gordon (1965), Deuterium and oxygen-18 variations in the ocean and marine atmosphere, *proc. Conf. Stable Isotopes in Oceanography Studies and Paleotemperatures, Lab. Geol. Nucl.*, Pisa, 9-130.

Delin, G.N. and M.K. Landon (2002), Effects of surface run-off on the transport of agricultural chemicals to ground water in a sandplain setting, *The Science of the Total Environment, 295*, 143-155.

Earman, S., A.R. Campbell, F.M. Phillips, and B.D. Newman (2006), Isotopic exchange between snow and atmospheric water vapor: Estimation of the snowmelt component of groundwater recharge in the southwestern United States, *Journal of Geophysical Research, 111*, D09302, doi:10.1029/2005JD006470.

Feng, X., S. Taylor, and C.E. Renshaw (2002), Isotopic evolution of snowmelt 1. A physically based one-dimensional model, *Water Resources Research, 38*(10), 1217, doi:10.1029/2001WR000814.

Frisbee, M.D., F.M. Phillips, A.R. Campbell, J.M.H. Hendrickx, and E.M. Engle (2009), Modified Passive Capillary Samplers for Collecting Samples of Snowmelt Infiltration for Stable Isotope Analysis in Remote, Seasonally Inaccessible Watersheds 2: Field Evaluation, *Hydrological Processes*, DOI:10.1002/hyp.7524.

Gee, G.W., A.L. Ward, T.G. Caldwell, and J.C. Ritter (2002), A vadose zone water fluxmeter with divergence control, *Water Resources Research, 38*, doi:10.1029/2001WR000816.

Gee, G.W., Z.F. Zhang, and A.L. Ward (2003), A modified vadose zone fluxmeter with solution collection capability, *Vadose Zone Journal*, *2*, 627-632.

Goyne, K.W., R.L. Day, and J. Chorover (2000), Artifacts caused by collection of soil solution with passive capillary samplers, *Soil Science Society of America Journal, 64,* 1330-1336.

Goyne, K.W., R.L. Day, and J. Chorover (2001), Response to "Comments on 'Artifacts caused by collection of soil solution with passive capillary samplers'", *Soil Science Society of America Journal, 65,* 1572-1573.

Herrmann, A., M. Lehrer, and W. Stichler (1981), Isotope input into runoff systems from melting snow covers, *Nordic Hydrology, 12*, 309-318.

Hoch, A.R., M.M. Reddy, and J.I. Drever (1999), Importance of mechanical disaggregation in chemical weathering in a cold alpine environment, San Juan Mountains, Colorado, *GSA Bulletin, 111*(2), 304-314.

Holder, M., K.W. Brown, J.C. Thomas, D. Zabcik, and H.E. Murray (1991), Capillary-wick unsaturated zone soil pore water sampler, *Soil Science Society of America Journal, 55*(5), 1195-1202.

Hooper, R.P. and C.A. Shoemaker (1986), A comparison of chemical and isotopic hydrograph separation, *Water Resources Research, 22*, 1444-1454.

Knutson, J.H. and J.S. Selker (1994), Unsaturated hydraulic conductivities of fiberglass wicks and designing capillary wick pore-water samplers, *Soil Science Society of America Journal, 58,* 721-729.

Landon, M.K., G.N. Delin, S.C. Komor, and C.P. Regan (1999), Comparison of the stable-isotopic composition of soil water collected from suction lysimeters, wick samplers, and cores in a sandy unsaturated zone, *Journal of Hydrology, 224*, 45-54.

Landon, M.K., G.N. Delin, S.C. Komor, and C.P. Regan (2000), Relation of pathways and transit times of recharge water to nitrate concentrations using stable isotopes, *Ground Water, 38*(3), 381-395.

Laudon, H., H.F. Hemond, R. Krouse, and K.H. Bishop (2002), Oxygen 18 fractionation during snowmelt: Implications for spring flood hydrograph separation, *Water Resources Research, 38*(11), 1258, doi:10.1029/2002WR001510.

Laudon, H., J. Seibert, S. Köhler, and K.H. Bishop (2004), Hydrological flow paths during snowmelt: Congruence between hydrometric measurements and oxygen 18 in meltwater, soil water, and runoff, *Water Resources Research, 40*, W03102, doi:10.1029/2003WR002455.

Louie, M.J., P.M. Shelby, J.S. Smesrud, L.O. Gatchell, and J.S. Selker (2000), Field evaluation of passive capillary samplers for estimating groundwater recharge, *Water Resources Research, 36*(9), 2407-2416.

Merlivat, L. (1978), Molecular diffusivities of $H_2{}^{16}O$, $HD^{16}O$, and $H_2{}^{18}O$ in gases, *Journal of Chemical Physics, 69,* 2864-2871.

Murray, C.D. and J.M. Buttle (2005), Infiltration and soil water mixing on forested and harvested slopes during snowmelt, Turkey Lakes Watershed, central Ontario, *Journal of Hydrology, 306,* 1-20, doi:10.1016/j.jhydrol.2004.08.032.

Nelson, S.T., and D. Dettman (2001), Improving hydrogen isotope ratio measurements for on-line chromium reduction systems, *Rapid Communications in Mass Spectrometry. 15,* 2301-2306.

Poletika, N.N., K. Roth, and W.A. Jury (1992), Interpretation of solute transport data obtained with fiberglass wick soil solution samplers, *Soil Science Society of America Journal, 56,* 1751-1753.

Rango, A. (2006), Snow: The real water supply for the Rio Grande Basin, *New Mexico Journal of Science, 44,* 99-118.

Robertson, J.A. and C.A. Gazis (2006), An oxygen isotope study of seasonal trends in soil water fluxes at two sites along a climate gradient in Washington state (USA), *Journal of Hydrology, 328,* 375-387, doi:10.1016/j.jhydrol.2005.12.031.

Sugimoto, A., D. Naito, N. Yanagisawa, K. Ichiyanagi, N. Kurita, J. Kubota, T. Kotake, T. Ohata, T.C. Maximov, and A.N. Fedorov (2003) Characteristics of soil moisture in permafrost observed in East Siberian taiga with stable isotopes of water, *Hydrological Processes, 17,* 1073-1092, doi:10.1002/hyp.1180.

Taylor, S., X. Feng, J.W. Kirchner, R. Osterhuber, B. Klaue, and C.E. Renshaw (2001), Isotopic evolution of a seasonal snowpack and its melt, *Water Resources Research, 37*(3), 759-769.

Taylor, S., X. Feng, M. Williams, and J. McNamara (2002), How isotopic fractionation of snowmelt affects hydrograph separation, *Hydrological Processes, 16,* 3683-3690, doi:10.1002/hyp.1232.

Unnikrishna, P.V., J.J. McDonnell, and C. Kendall (2002), Isotope variations in a Sierra Nevada snowpack and their relation to meltwater, *Journal of Hydrology, 260,* 38-57.

Wilson, J.L. and H. Guan (2004), Mountain-block hydrology and mountain-front recharge, in *Groundwater Recharge in a Desert Environment: The Southwestern United States*, edited by F.M. Phillips, J. Hogan, and B. Scanlon, 23 pp., AGU, Washington, D.C.

Chapter 3 Modified Passive Capillary Samplers for Collecting Samples of Snowmelt Infiltration for Stable Isotope Analysis in Remote, Seasonally Inaccessible Watersheds 2: Field Evaluation[2]

3.1 Introduction:

Many of the river basins which drain mountainous watersheds depend upon snowmelt for streamflow generation and down-valley recharge. This is especially true in the large mountainous watersheds of the southwestern United States [*Rango,* 2006; *Winograd et al.,* 1998; *Wilson and Guan,* 2004]. Therefore, an understanding of the processes which control snowmelt runoff generation in the headwaters of these basins is critical for the sustainability of future agricultural, domestic, and municipal water demands. Research into these processes has historically employed a variety of techniques aimed at quantifying the components of recharge and runoff generation [*Earman et al.,* 2006; *Herrmann et al.,* 1981]. However, quantifying the snowmelt-infiltration endmember (soil-meltwater) is problematic due to the rugged, remote, and seasonally inaccessible nature of these mountainous watersheds. These conditions often preclude frequent sampling intervals and as a consequence, eliminate certain vadose-zone sampling techniques. Surface proxies have been used as substitutes for the actual soil-water endmember but these proxies may not be representative since previous work has shown that the isotopic composition of fresh snow and/or remnant snowpack can differ greatly from the isotopic composition of the snowmelt runoff [*Herrmann et al.,* 1981; *Hooper and Shoemaker,* 1986; *Taylor et al.,* 2001]. A robust method requiring little

[2] **Frisbee, M.D., F.M. Phillips, A.R. Campbell, Jan M.H. Hendrickx, and E.M. Engle (2010), Modified passive capillary samplers for collecting samples of snowmelt infiltration for stable isotope analysis in remote, seasonally inaccessible watersheds 2: Field evaluation, *Hydrological Processes,* 24, 834-849, doi:10.1002/hyp.7524.**

maintenance or monitoring is desirable for sampling the isotopic signature(s) of snowmelt infiltration in these watersheds.

In alpine settings, snowmelt runoff occurs during a rather narrow window when the accumulated snowpack ripens and begins to melt. During snowmelt, the snowpack also undergoes isotopic metamorphosis in which the stable isotopic composition of the snowpack changes. These changes can be due to evaporation and sublimation processes on the surface or within the snowpack. These changes may also be related to: atmospheric exchange [*Earman et al.*, 2006], mixing and exchange between water sources such as meltwater percolating through the snowpack, frozen water still sequestered in the pack itself, and shallow soil-water underneath the snowpack [*Clark and Fritz*, 1997]. Runoff from the snowpack may occur over the soil surface as Hortonian or saturation overland flow or it may infiltrate the soil and flow within the soil itself. Water flowing through the soil will encounter different sources of water and mixing can occur, it may also encounter different kinetic processes such as soil-water evaporation, and it will evolve geochemically. Therefore, the stable isotopic composition and geochemistry of soil-meltwater may be very different than snowmelt runoff occurring over the soil surface. While it is relatively easy to monitor and collect surface runoff from snowpacks, it is difficult to sample soil-meltwater in these settings often due to the presence of the snowpacks themselves and due to very limited accessibility to the backcountry during the winter and snowmelt season. Thus, the stable isotopic and geochemical composition of the soil-meltwater endmember must be accurately constrained in order to provide a unique endmember in isotopic separations.

Previous researchers have employed a variety of methods to sample snowmelt recharge and vadose-zone soil waters during snowmelt. These methods include snow cores [*Taylor et al.,* 2001; *Unnikrishna et al.,* 2002], snow lysimeters [*Laudon et al.,* 2002; *Taylor et al.,* 2001; *Unnikrishna et al.,* 2002], soil cores [*Buttle and Sami,* 1990; *Laudon et al.,* 2004; *Robertson and Gazis*, 2006; *Sugimoto et al.,* 2003], zero-tension lysimeters [*Hoch et al.,* 1999], and modified-bulk snow collectors [*Earman et al.,* 2006]. These methods may have limited applicability in remote watersheds. For example, some of these methods require more maintenance and monitoring than is typically practical in many of the mountainous watersheds of the southwestern United States since backcountry access is limited during the snowbound and snowmelt season. Another inherent problem is that some methodologies do not sample water that has been in contact with the soil. Consequently, the effects of isotopic mixing and/or kinetic fractionation in the soil will not be observed. Also, information on the geochemical evolution of infiltrating meltwater cannot be acquired through measurements made at the soil surface. This can consequently affect the "uniqueness" of the soil-meltwater endmember when it is used in endmember mixing analysis incorporating principle component analysis. For example, modified-bulk snow collectors typically contain a fine mesh screen or extended Büchner funnel that intercepts snow and allows it to exchange with atmospheric water vapor before it melts and drips into a mineral oil trap [*Friedman et al.,* 1992]. The metamorphism that occurs in the modified-bulk collector is thought to be representative of that which occurs within the snowpack before it begins to melt. Thus, it is assumed that the isotopic composition of water collected via modified-bulk collectors is similar to infiltrating meltwater [*Earman et al.,* 2006]. The disadvantage of this method is that only

the isotopic composition can be used in endmember mixing analysis since the geochemistry of the modified-bulk snow will only reflect wet and dry deposition which was collected during the winter season and not the geochemistry associated with water-soil contact. Therefore, since geochemical information is not gathered on this endmember with some of these methodologies, the soil-meltwater endmember may not be unique in endmember mixing analysis [*Liu et al.,* 2004]. Consequently, these methodologies have limited applicability in remote, seasonally inaccessible terrain.

Passive capillary samplers (PCAPS) may however provide a robust alternative to the aforementioned methodologies. The standard PCAPS concept was developed by *Brown et al.,* [1986] and was subsequently evaluated by *Holder et al.,* [1991] and *Knutson and Selker,* [1994]. PCAPS are constructed from fiberglass wicks; the length and diameter are chosen to match the matric potential of the soil to be sampled. The wicks behave essentially like hanging water columns; thus, allowing water to be drawn from the surrounding soil with little or no maintenance, no application of external suction, and unlike the zero-tension lysimeter, no dependency upon positive pressure [*Boll et al.,* 1992]. Passive capillary samplers have previously been deployed to collect soil water for stable isotope analysis in agricultural settings [*Landon et al.,* 1999; *Landon et al.,* 2000; *Delin and Landon,* 2002]. These studies used a standard PCAPS design described in the work of *Brown et al.,* [1986]. These settings can often be characterized by thick vadose zones and little rock content making them suitable for the standard PCAPS design. On the other hand, observations made from soil pits installed in high elevation locations in the Saguache Creek watershed in the San Juan Mountains indicated that alpine soils were typically shallow (average depth to weathered bedrock was 45 cm)

and rocky. Large volcanic rocks (average dimensions of 20 cm wide by 20 cm long by 3 cm thick) often occur in discrete layers in the soil profile but the content of small stones remains high throughout the typical soil profile. Therefore, a modification of the standard design was necessary to accommodate the thin, rocky soils encountered in mountainous watersheds and a simple laboratory experiment was conducted to ascertain the suitability of using M-PCAPS in these studies [*Frisbee et al.,* 2009]. The experimental results indicated that the wicking process associated with M-PCAPS does not fractionate water, but certain precautions were necessary to prevent exchange between the wick and the atmosphere, and that the M-PCAPS design effectively tracked the changing isotopic composition of a soil reservoir undergoing evaporation [*Frisbee et al.,* 2009].

In order to thoroughly field test this design modification, twelve M-PCAPS were installed in remote locations of the Saguache Creek watershed in the San Juan Mountains of southwestern Colorado prior to the onset of snow accumulation in October 2007. This field evaluation was designed to answer four important questions regarding the deployment of M-PCAPS to collect snowmelt for isotopic and geochemical analyses. 1. Is the isotopic composition of water collected via modified-bulk snow collectors similar to that of the actual infiltrating snowmelt? 2. Does the infiltrating meltwater undergo any isotopic and geochemical evolution in the typically shallow soils of alpine watersheds during snowmelt and what can be inferred from this data about dominant subsurface runoff processes? 3. Can M-PCAPS be used to constrain rates of meltwater infiltration in remote, seasonally inaccessible watersheds? 4. Can M-PCAPS be used to constrain rates of infiltration during the summer rainfall season?

3.2 Site Description:

The Saguache Creek watershed is located in the San Juan Mountains of southern Colorado (Figure 3.1). Elevation ranges from 2310 m to 4269 m. The watershed is approximately 1700 km^2 in area and is drained by a perennial stream, Saguache Creek, which recharges the northern San Luis Valley. The overall average streamflow in Saguache Creek from 1929 to 2004 is 1.78 m^3s^{-1} and this discharge is exceeded 27 percent of the time according to flow duration curves. The minimum streamflow on record is 0.20 m^3s^{-1} and the maximum streamflow on record is 19.2 m^3s^{-1}. Published streamflow data from 1910 to 2007 and provisional streamflow data from 2007 to 2008 is available at http://www.dwr.state.co.us/SurfaceWater/Default.aspx. These streamflow data are very similar to other tributary streams of the Upper Rio Grande (URG) where the URG is defined as that portion of the Rio Grande located upstream of Monte Vista, Colorado.

Most of the annual precipitation occurs as snowfall with rainfall comprising a small proportion. The overall average annual rainfall (unfrozen precipitation) is 21.2 cm, the minimum annual rainfall is 10.8 cm, and the maximum annual rainfall is 41.2 cm. Precipitation data is available at http://www.ncdc.noaa.gov/oa/ncdc.html. NRCS SNOTEL data for historical and current trends in snow depth and snow water equivalent can be found at http://www.wcc.nrcs.usda.gov/snotel/Colorado/colorado.html. The Saguache Creek watershed contains one SNOTEL site (Cochetopa Pass) with a limited history of only 4 years; however, the Porphyry Creek SNOTEL site is located to the north

of the watershed and the Slumgullion Pass SNOTEL site is located to the southwest of the watershed. The latter two sites have more extensive data histories.

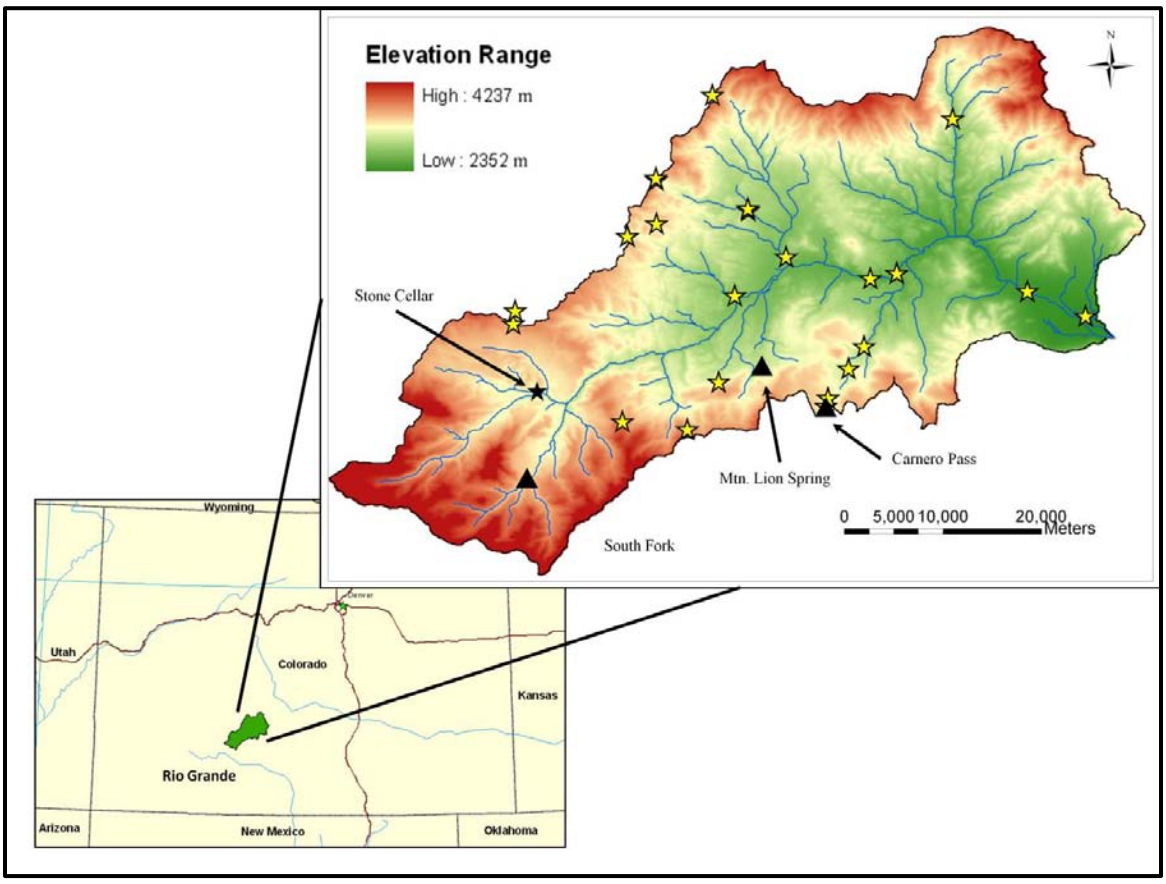

Figure 3.1: Map of sampling locations in the Saguache Creek watershed. Yellow stars indicate locations of snow and/or snowmelt runoff sampling sites, black triangles indicate locations of PCAPS installations and snow collectors, and the black star indicates the location of a stand-alone snow collector site.

The Slumgullion site may in fact be more representative of the high elevation headwaters of the Saguache Creek watershed. The average maximum snow water equivalent (SWE) for the Slumgullion SNOTEL site is 39.9 cm with a historical range of 20.6 cm to 57.7 cm. Peak SWE typically occurs on April 21 (WYD 203). Snowpacks typically begin to accumulate on October 14 (WYD 14) and are, on average, depleted by May 30 (WYD 232). The SNOTEL data for the Porphyry Creek site is very similar with an average

maximum SWE of 44.9 cm and a range from 21.6 cm to 69.6 cm. Peak SWE typically occurs on April 16 (WYD 198), snowpack accumulation typically begins on October 22 (WYD 22), and the snowpack is, on average, depleted by May 27 (WYD 239). These data imply average snowpack persistence of approximately 7 months. Mountain block recharge estimates range from 14 percent of annual precipitation in the Sangre de Cristo Mountains to 38 percent of annual precipitation for the San Juan Mountains [*Huntley,* 1979]. However, estimates of mountain block recharge and mountain front recharge in this region remain poorly constrained since many of the commonly used methodologies provide indirect measures of actual recharge and/or ignore the complexities of the regional geology which affect infiltration, percolation, and runoff [*Wilson and Guan,* 2004].

The geology of the Saguache Creek watershed is dominated by felsic volcanics resulting from the activity of the San Juan Volcanic Field (34 to 35 Mya) which overlie intermediate pre-caldera lavas including the Conejos Formation [*Steven and Lipman,* 1976; *Lipman and McIntosh,* 2008]. The soils derived from these geologic units typically contain fragments of biotite, quartz, and sodium and calcium-rich feldspars. High elevation soils have little or no organic development, loamy AE horizons, and relatively weakly developed B-horizons. These soils are broadly classified by the NRCS as very stony loams of the Bushvalley-Embargo-Bowen soil association and cobbly or gravelly loams of the Frisco-Seitz-Granile soil association. Soil descriptions for can be found at http://soils.usda.gov/survey/geography/statsgo/. Hillslope soil profiles often contain a shallow, extensive layer of platy, felsic volcanic rocks (Figure 3.2). High elevation soils are also typically thin and rocky and overlie what appears to be either a layer of saprolite

or the weathering rind of the underlying bedrock (the Cr unit in Figure 3.3). This highly weathered layer was encountered in several soil pits at depths ranging from 16 to 25 cm and persistent to depths greater than 40 cm (Figure 3.3). The saprolitic layer served as a lower boundary for our research during this field experiment since we were primarily interested in the stable isotopic and geochemical evolution of infiltrating meltwater and the amount of infiltration reaching the layer located immediately above bedrock.

Figure 3.2: Typical hillslope soil formation in low-elevation regions of watershed. Note the deposit of heavily fractured rhyolitic material in lower soil profile. Several springs emerge from similar deposits located throughout the watershed and the flow from these deposits increases considerably during snowmelt. We have also observed quickflow runoff responses in similar deposits throughout the watershed during snowmelt.

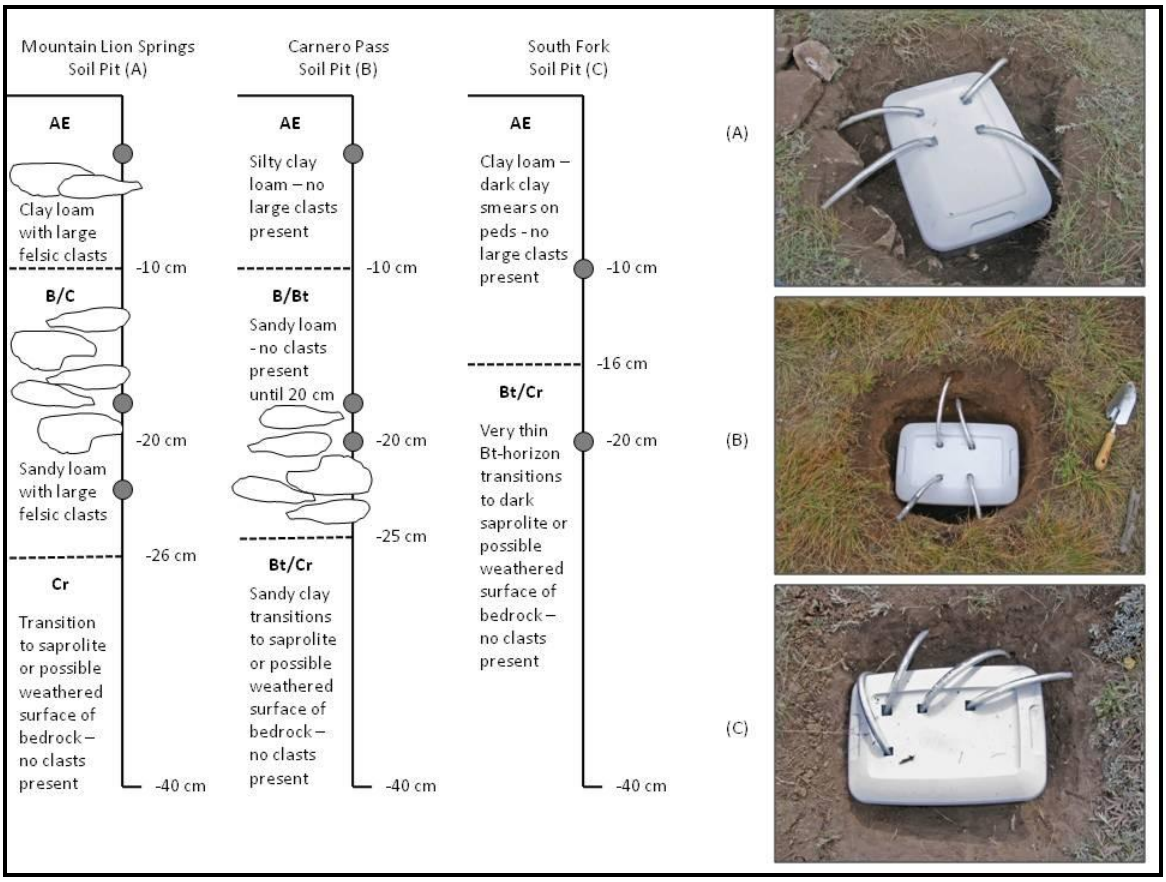

Figure 3.3: Soil descriptions and photos of individual PCAPS installations. Soil pit (A) and inset (A) illustrate the Mountain Lion Springs installation, Soil Pit (B) and inset (B) illustrate the Carnero Pass installation, and soil Pit (C) and inset (C) illustrate the South Fork installation. The dark grey circles located on the pit wall of the soil descriptions denote the locations of the M-PCAPS within the soil profile.

3.3 Methods:

A 15.2 m coil of fiberglass wick having a diameter of 9.5 mm (3/8 inch, Pepperell Braiding Company SKU # 1380) was thoroughly cleaned [*Goyne et al.*, 2000; *Brahy and Delvaux*, 2001; and *Goyne et al.*, 2001] and cut into 60.9 cm lengths resulting in wick matric potentials (ψ_{wick}) of approximately -60.9 cm [*Knutson and Selker*, 1994]. One end of each wick was coiled into a "fiddlehead" shape and then securely yet loosely fastened in place using zip-ties (Figure 3.4, Inset A). Typically a straight length of 17.8 cm could be coiled tightly to produce a collection surface of approximately 3 to 4 cm in diameter.

Additional details on cleaning and design modifications for the PCAPS are available in *Frisbee et al.,* [2009].

Soil pits were dug in three remote, high elevation locations in the watershed. The locations of these pits were based on elevation and representative snowpack accumulation (Figure 3.1). For example, all sites were located in high elevation meadows which were relatively flat and typically contain more spatially uniform soil development. The low topographic relief of these meadows should limit seepage face development resulting from lateral, downslope flow intercepting the soil pit walls. These conditions should have been conducive to snowpack accumulation and persistence. The elevations of these sites ranged from 2857 m to 3124 m a.s.l. Four lateral, horizontal holes were then dug into the walls of each soil pit using gardening spades and pocket knives to a lateral depth of approximately 12.7 to 17.8 cm. This depth was chosen to avoid the inward propagation of drying fronts from the soil pit walls. The wick assembly was pulled through flexible PVC tubing having an outer diameter of 1.59 cm and an inner diameter of 1.27 cm. The "fiddlehead" was then inserted lying horizontal to the soil surface into the hole and the hole was backfilled with native soil in an attempt to maintain soil hydraulic properties. In doing so, the wick was placed in direct contact with the soil while the remainder of the wick was entirely enclosed within flexible PVC tubing (Figure 3.4, Inset B). Standard passive capillary samplers are typically comprised of a water collection plate which has wick fibers glued to the top of it and a wick draining from the center of the plate down to a collection bottle resulting in overall assembly lengths up to 100 cm [*Brown et al.,* 1986]. Our modification reduces soil column disturbance since we are only creating a hole big enough for the "fiddlehead" not the entire PCAPS assembly

[*Frisbee et al.,* 2009]. Each soil pit contained two shallow M-PCAPS installed at depths less than 10 cm and two deep M-PCAPS installed at depths greater than 20 cm (Figure 3.3).

A plastic collection box was then assembled which contained four 1-L LDPE bottles. Each bottle contained a small reservoir of mineral oil to prevent evaporation and atmospheric exchange. The mouth of each bottle was covered with a Zip-loc sandwich bag which was securely wrapped around the bottle using zip-ties. Each tubing/wick assembly was pushed through an access hole in the lid of the plastic collection box and the open end of the wick assembly was pushed through the Zip-loc and into the mouth of the bottle (Figure 3.4). Silicon sealant was applied at the juncture of the tubing and the box to prevent leaking and flow along the outside of the tubing. Each pit was then covered with a heavy duty plastic drop cloth and wooden covers were placed over the drop cloth to prevent overburden failure.

The M-PCAPS were installed prior to the onset of snowpack accumulation during October 2007 and each installation was accompanied by a bulk and modified-bulk snow collector. The bulk collector was constructed from a 1.83 m length of 10.2 cm PVC pipe (see inset of Figure 3.9). A flat cap was cemented to the pipe and a small reservoir of mineral oil was poured into pipe. The modified-bulk snow collector was constructed from two 0.92 m lengths of 10.2 cm PVC pipe. Two 10.2 cm circular sections of fine mesh, 10 grids per 2.54 cm, were cut and placed inside a PVC coupling fitting. The two lengths of PVC were then affixed to the coupling fitting, a flat termination cap was cemented to the lower PVC, and a mineral oil reservoir was poured inside the pipe assembly. These large-scale modifications to the designs used in the work of *Earman et*

al., [2006] were necessary due to the possibility of snowpacks exceeding 1.22 to 1.52 m in the backcountry. The snow collectors were also installed prior to the onset of snowpack accumulation during October 2007 and removed in June of 2008. All M-PCAPS were left intact for the duration of the rainfall season (June to early October 2008) to quantify soil-water fluxes during the rainfall season.

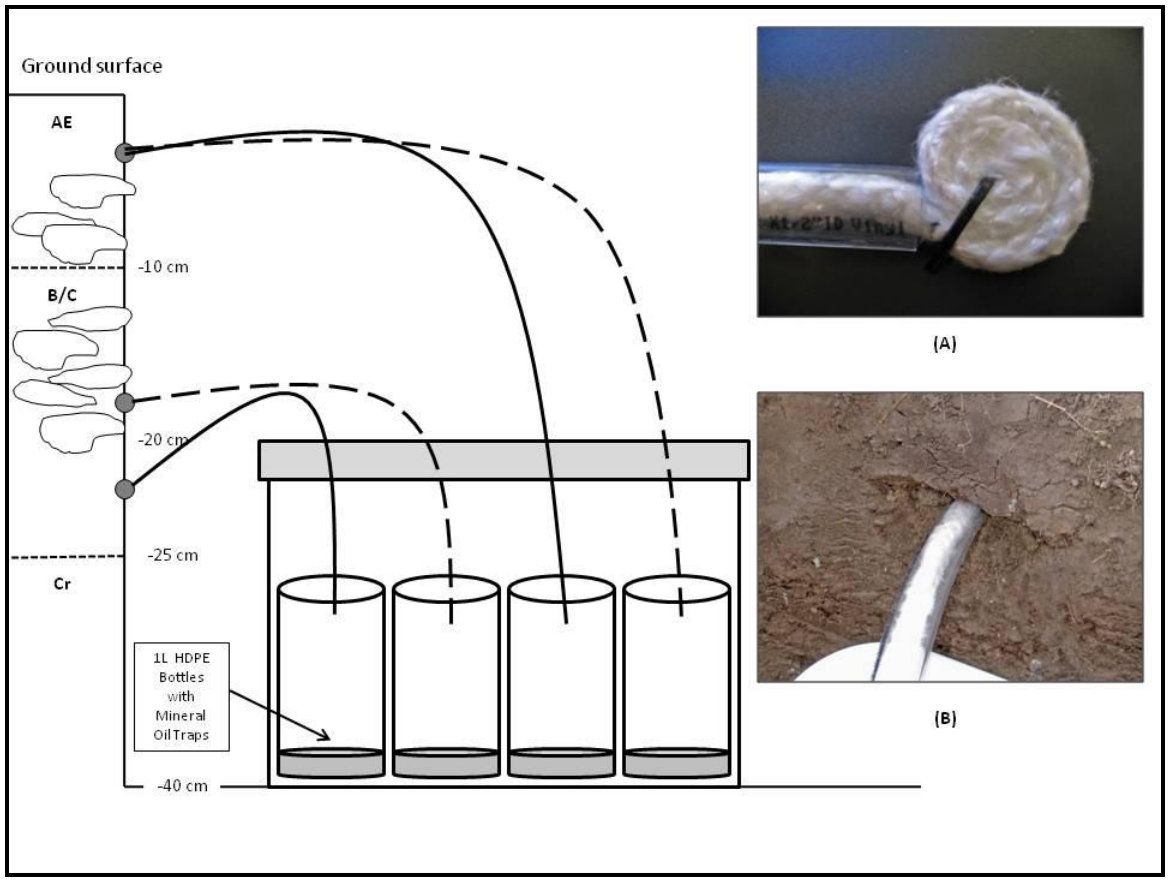

Figure 3.4: Diagram of typical M-PCAPS installation. Two M-PCAPS were installed at shallow depths and two were installed at deep depths. Dashed and solid lines represent paired PCAPS. Inset (A) is a close-up photo of "fiddlehead" and tubing assembly. Inset (B) is a close-up photo of an actual installation in a soil profile.

3.4 Analytical Methods:

All water samples including those from the snow collectors and those from obtained from the M-PCAPS were removed during the first week of June 2008. Each

water sample was analyzed for $\delta^{18}O$ and $\delta^{2}H$. The $\delta^{18}O$ composition was measured on 1 mL samples of water using the CO_2 / H_2O equilibration method described in *Clark and Fritz*, [1997] using a Thermo Finnigan Gasbench operated in continuous flow mode. The $\delta^{2}H$ hydrogen gas was generated by metal reduction with powdered chromium at 850°C in an H-Device [*Nelson and Dettman*, 2001] and analyzed in dual inlet mode. Both CO_2 and H_2 were analyzed on a Thermo Finnigan Delta^{PLUS} XP Stable Isotope Ratio Mass Spectrometer. All stable isotope results are reported with respect to VSMOW. At the time of sample retrieval, two soil samples, one shallow and one deep, were removed from the Carnero Pass installation (Figure 3.1). Water was vacuum distilled from the soil samples using the vacuum distillation method described in the work of *Araguás-Araguás et al.*, [1995] and later analyzed for $\delta^{18}O$ and $\delta^{2}H$. The variability in $\delta^{18}O$ and $\delta^{2}H$ was ascertained by analyzing twenty-one duplicates. Variability in $\delta^{18}O$ ranged from 0.0 to 0.5 ‰ (average variability was 0.1 ‰). The duplicates of $\delta^{2}H$ varied from 0 to 2 ‰ (average variability was 1 ‰).

All water samples, with the exception of the soil distillation samples, were also analyzed for standard chemistry including field measurements of pH, electrical conductivity, and TDS. Basic cations, anions, and silica were measured at the Chemistry Laboratory of the New Mexico Bureau of Geology and Mineral Resources located on the New Mexico Tech campus. Alkalinity was measured by titration methods (USEPA 310.1) and was reported as bicarbonate or carbonate. Anions were measured with a Dionex IC, DX-600 System with GS50 Gradient Pump, CD25 Conductivity Detector, AG14 Guard Column, and As14 Analytical Column per USEPA 300.0. Analyses were made with a 4-point calibration and the calibration and blanks were checked at the

beginning and end of each run and after every 10^{th} sample. Cations were measured with a PE Optima 5300 DV ICP-OES per USEPA 200.8/6020. Analyses were made with a 3-point calibration and quality control procedures were the same as for anions. The charge imbalance for all samples was acceptable and ranged from -0.98 to 3.54 percent. Duplicates were performed on water samples to assess analytical error. Duplicates were used to assess the variability in anions, cations and silica. To do this, we calculated the range in absolute variability between original samples and duplicates as well as the overall average absolute variability in the anion, cation, and silica dataset. The absolute variability of anion duplicates ranged from 0 to 0.3 mg/L (the average absolute variability was 0.03 mg/L). The absolute variability of cation duplicates ranged from 0 to 1 mg/L (the average absolute variability was 0.08 mg/L). Duplicates for silica varied from 0 to 0.01 and the average absolute variability was approximately 0.01 mg/L.

3.5 Results:

3.5.1.0 Intercomparison Between Modified-Bulk Snow Collectors and M-PCAPS:

Local meteoric water lines (LMWL) are defined by the relationship between $\delta^{18}O$ and $\delta^{2}H$ for meteoric inputs in a given watershed or locale. The LMWL for the Saguache Creek watershed defined by the stable isotopic composition of rainfall and snowfall is $\delta^{2}H = 8.3\delta^{18}O + 18$ with $R^2 = 0.99$ (Figure 3.5). The global meteoric water line (GMWL) defined by *Craig,* [1961] shown as the dash-dot line in Figure 3.5 is given by: $\delta^{2}H = 8.0\delta^{18}O + 10$. During the winter seasons from 2005 to 2008, we collected samples of early-season fresh snow, late-season fresh snow, remnant snowpack during the snowmelt season, and surface runoff from snowmelt. Here we define "early-season" as

the period from October through February and "late-season" as the period from March through May. Surface runoff samples represent primarily overland flow from remnant snowpacks and very shallow subsurface flow through forest litter and shallow talus. Using these endmembers, we then created an evolution line which describes the stable isotopic evolution from fresh snow (a meteoric input) to snowmelt runoff (a non-meteoric input). This line was labeled the Snow Evolution Line (SEL) and is shown as the red line in Figure 3.6. The SEL is given by: $\delta^2H = 7.7\delta^{18}O + 5$. It is important to note that the SEL differs from the LMWL and GMWL because it represents an evolutionary pathway (i.e. it is a directional line whose starting point is defined by early-season fresh snow and the ending point is defined by the processes which affect surface runoff during snowmelt). Thus, it is a process-oriented relationship. The slope of the SEL is close to 8 and it does not appear to be affected by kinetic fractionation since the processes of evaporation and/or sublimation typically result in slopes of 5 or 6 [*Clark and Fritz,* 1997] while soil-water evaporation typically results in slopes of 3 or 4 [*Allison,* 1982]. An expanding vadose zone will tend to increase tortuosity and since $H^2H^{16}O$ (mass = 19) will diffuse faster than $H_2{}^{18}O$ (mass = 20), there will be greater enrichment in $\delta^{18}O$ relative to δ^2H [*Allison,* 1982; *Clark and Fritz,* 1997; *Merlivat,* 1978]. We argue that the SEL provides a better benchmark through which to compare the surface and subsurface proxies for meltwater since the SEL is a process-oriented trendline as opposed to the GMWL and LMWL which only characterize the meteoric inputs themselves.

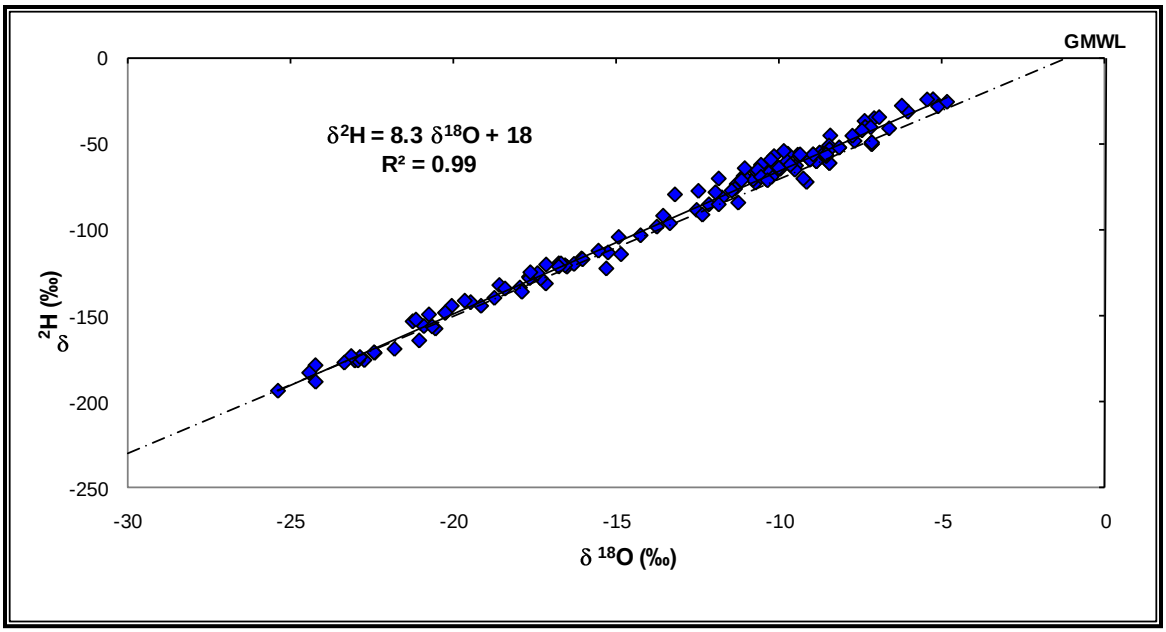

Figure 3.5: The Local Meteoric Water Line (LMWL) defined by the stable isotopic composition of rainfall and snowfall in the Saguache Creek watershed is shown as the trendline. The Global Meteoric Water Line (GMWL) defined by Craig, [1961] is shown as the dash-dot line.

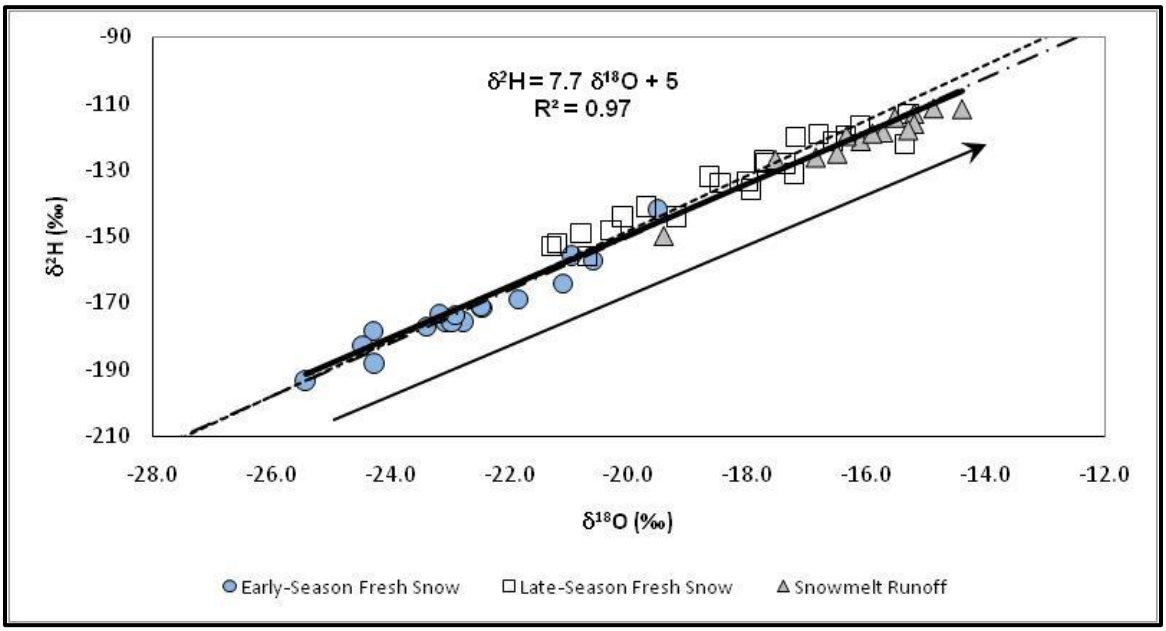

Figure 3.6: The Snow Evolution Line (SEL) is defined by the stable isotopic evolution of fresh snow (a meteoric input) to snowmelt runoff (a non-meteoric input). The SEL is represented by the bold black trendline. The dash-dot line is the GMWL and the dotted line is the LMWL. The arrow shows the direction of the stable isotopic evolution along the SEL.

SNOTEL data indicated that the San Juan Mountains received between 125 to 175 percent normal maximum SWE during the 2007-2008 winter season. This resulted in deeper than normal snowpacks in the study area and we were concerned about undercatch in the snow collectors. However, there was agreement in collection amount between the bulk and modified-bulk snow collectors. The Mountain Lion Spring site is the lowest elevation site, 2856 m, and 15.4 cm of water was collected (Table 3.1). Stone Cellar, elevation 2908 m, collected the lowest amount of water at 8.0 cm. This was not unexpected since rainfall data collected at this site is also typically lower than other rainfall gauges. This may be due to the local topography surrounding the Stone Cellar site which can be best described as a small topographic surface depression surrounded by steep mountain sides which may effectively steer moisture away from the area (Figure 3.1). The isotopic composition of the water samples from the bulk and modified-bulk snow collector at this site were the same, within error. The Carnero Pass site, elevation 3024 m, and the South Fork site, elevation 3124 m, collected 16.7 and 16.0 cm, respectively. Interestingly, however, there did not appear to be much isotopic evolution between the bulk and modified-bulk snow collector pairs (Table 3.1). In fact, most pairs show a trend opposite to that expected. The isotopic composition of the bulk collectors are slightly more enriched in heavy isotopes than the modified-bulk collectors. We speculate that this could be due to temporary burial of the snow collectors and the snow trapped in the paired collectors could have experienced kinetic processes (e.g. both snow samples experienced exchange with atmospheric water vapor). Furthermore, the isotopic values of early season snow are very similar to that of the bulk and modified-bulk snow samples and are very different than those of late season snowpack which has experienced

isotopic evolution. Thus, we can assume that the isotopic composition of the water samples collected with the bulk and modified-bulk collectors have experienced little if any isotopic evolution and either bulk or modified-bulk water sample may be used as a beginning point to quantify the evolution of infiltrating meltwater.

Sample ID	Elevation (m)	$\delta^{18}O$ (‰)	$\delta^{2}H$ (‰)	Volume (mL)	Depth (cm)
Mtn. Lion Springs - Bulk	2856	-21.3	-153	1250	15.4
Carnero Pass - Bulk	3023	-20.1	-144	650*	8.0
Carnero Pass – Modified Bulk	3023	-21.2	-152	1350	16.7
Stone Cellar – Bulk	2908	-20.8	-149	650	8.0
Stone Cellar – Modified Bulk	2908	-20.3	-148	800	9.9
South Fork – Bulk	3124	-19.7	-141	1300	16.0
South Fork – Modified Bulk	3124	-20.3	-148	1200	14.8

Table 3.1: Isotopic composition, volume, and amount (depth) of water samples retrieved from bulk and modified-bulk snow collectors. Depth was determined by dividing the collected volume by the surface area of the collector. Note: * represents accidental loss of water during sample retrieval.

The soil moisture in each soil pit was measured at the time of M-PCAPS installation in October 2007 and upon retrieval of M-PCAPS in June 2008 by collecting small soil cores and measuring the amount of water present in the samples [*Jury and Horton*, 2004]. Volumetric soil moisture ranged from 0.11 to 0.17 at the time of installation and from 0.21 to 0.24 during June 2008. Typically, the water content of the saprolite fell at the upper end of the soil moisture ranges given. When the M-PCAPS and snow collectors were retrieved during June 2008, it was discovered that the M-PCAPS installation at Mountain Lion Springs had been vandalized; therefore, no data is available for that site (see Figure 3.1). A bulk snow sample was retrieved at that site. M-PCAPS samples were obtained at the South Fork and Carnero Pass sites and bulk and modified-bulk snow samples were collected at the South Fork, Carnero Pass, and Stone Cellar

locations (Figure 3.1). The M-PCAPS collection box at the Carnero Pass location contained some overflow yet water samples were still intact. The A-Deep sample at the Carnero Pass installation had overflown and the box contained approximately 100 mL of water. The stable isotopic compositions of all M-PCAPS pairs are shown in Figure 3.7 relative to the SEL, LMWL, and GMWL. In all cases except for one pair at South Fork (Figure 3.7b), the water collected by the deep M-PCAPS is isotopically heavier than the shallow M-PCAPS. Also, note that the isotopic compositions of the M-PCAPS samples fall on the SEL and therefore, indicate that the infiltrating meltwater is not affected by kinetic fractionation processes.

The stable isotopic compositions of the shallow and deep M-PCAPS pairs were connected with trendlines to quantify the isotopic evolution of infiltrating meltwater. These trends are depicted by the arrows shown in Figure 3.8. The stable isotope composition of the shallow M-PCAPS samples plot very near the stable isotope composition of the modified-bulk collectors (open triangles in Figure 3.8). In contrast, the deep M-PCAPS samples in Figure 3.8 plot up the line toward enrichment in heavy isotopes. Three of the four M-PCAPS pairs show some degree of isotopic variation with depth. The isotopic composition of the fourth pair, South Fork – A, is the same, within error. Interestingly, the individual trendlines shown in Figure 3.8 effectively bracket the SEL shown in Figure 3.6. Carnero Pass A-Shallow and B-Shallow M-PCAPS were both installed at 5 cm below the ground surface while the Carnero Pass A-Deep was installed at 20 cm and B-Deep was installed at 18 cm (Figure 3.3). The trendline for the A-pair is given by: $\delta^2H = 7.7\ \delta^{18}O + 5$, and the trendline for the B-pair is given by: $\delta^2H = 7.4\ \delta^{18}O + 1$, both are very similar to the SEL (Figure 3.6). The South Fork A-shallow and B-

shallow M-PCAPS were both installed at 10 cm and the A-Deep and B-Deep were both installed at 20 cm (Figure 3.3). The trendline for the B-pair is given by: $\delta^2H = 8.0\ \delta^{18}O + 12$, which is similar to the GMWL and LMWL (Figure 3.5). This dataset indicates that the isotopic composition of deep snowmelt infiltration may be different than the isotopic composition of surface proxies for the snow-meltwater.

3.5.1.1 Discussion of Intercomparison:

Although no significant isotopic alteration was recorded in the modified-bulk snow collectors as compared to the bulk snow collectors, it would seem that answering question 1 would be problematic. However, it is apparent that modified-bulk collectors may not collect a stable isotopic composition similar to infiltrating meltwater (Figure 3.8). This assumption was discussed in the work of *Earman et al.*, [2006] and it does have limitations. Most importantly, this assumption ignores the degree of isotopic evolution that can occur in a relatively shallow soil profile prior to infiltration and subsequent percolation into the underlying fractured bedrock. Shallow M-PCAPS installed at depths between 5 and 10 cm do appear to preserve the isotopic composition of bulk snow in this case (Figure 3.8). However, it can be seen in Figure 3.8 that all M-PCAPS samples become enriched with respect to the isotopic composition of snow collected at the surface (i.e. the waters move up the SEL). One possible explanation for this behavior is mixing of meltwater with isotopically heavier water stored in the soil/bedrock matrix prior to snowmelt. The mechanisms responsible for the isotopic enrichment of the deep soil-water have not been investigated in this watershed but there are several possible explanations. First, the deeper soil matrix could theoretically contain water enriched in heavy isotopes due to the infiltration of late season rainfall.

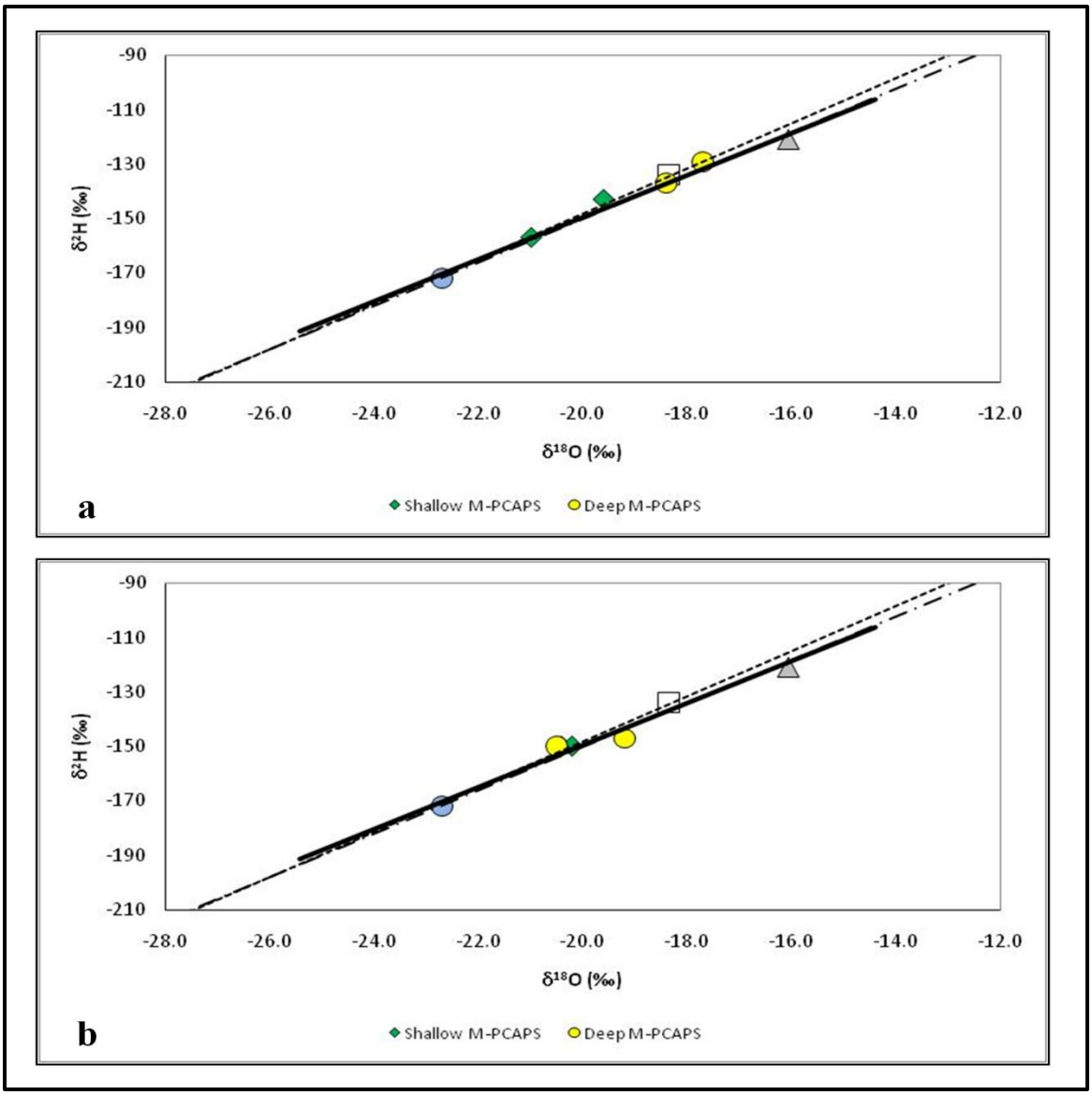

Figure 3.7: The stable isotopic composition of M-PCAPS water samples in a) Carnero Pass and b) South Fork. In both cases, shallow M-PCAPS are depicted as green-filled diamonds and deep M-PCAPS are depicted as yellow-filled circles. Note that in all cases except for one of the South Fork samples, the shallow M-PCAPS are isotopically lighter than the deep M-PCAPS. The blue-filled circle represents the average stable isotopic composition of early-season fresh snow, the open square represents the average stable isotopic composition of late-season fresh snow, and the grey-filled triangle represents the average stable isotopic composition of snowmelt runoff. The solid red line is the SEL, the dash-dot line is the GMWL, and the dotted line is the LMWL.

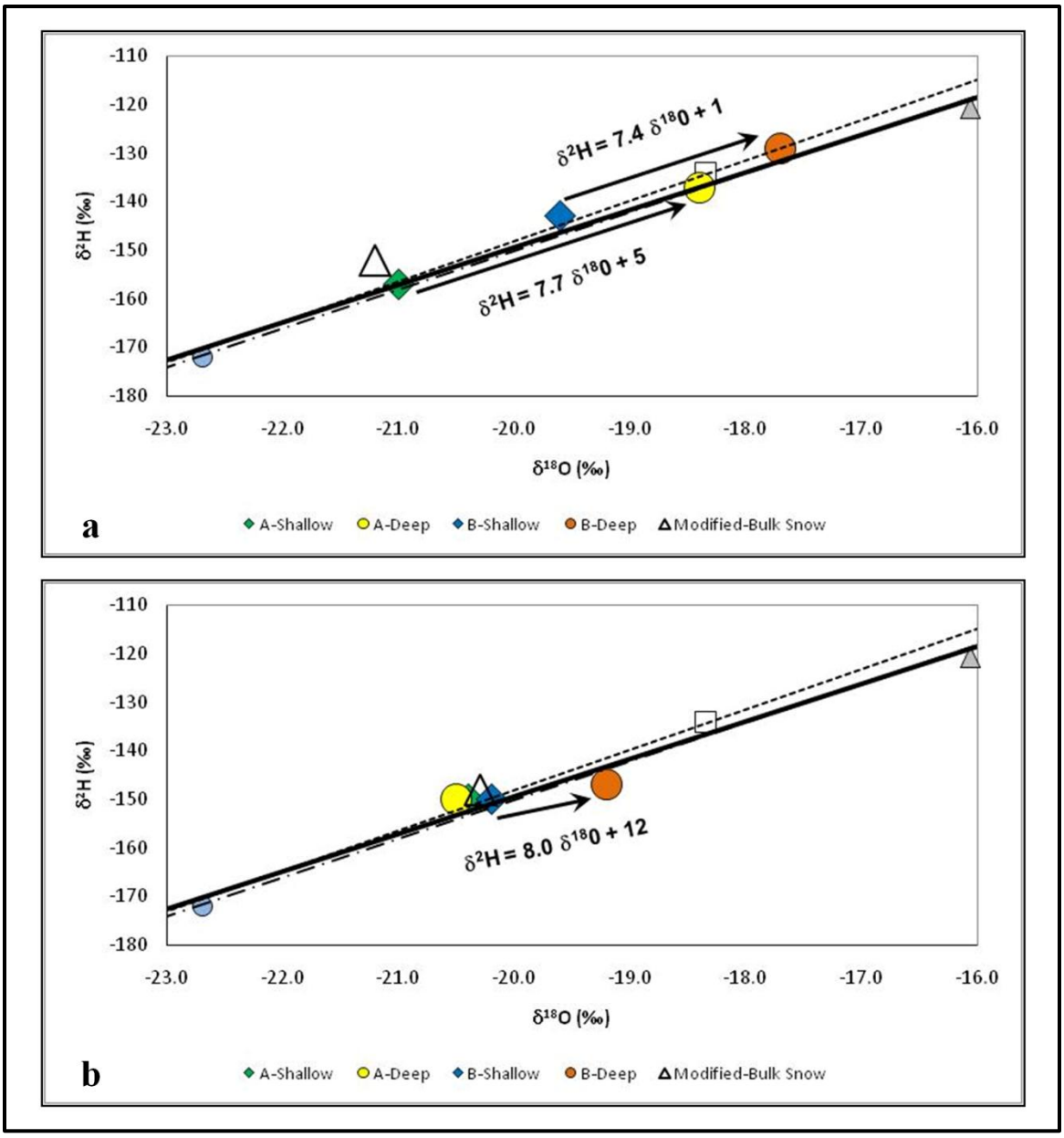

Figure 3.8: The stable isotopic evolution of paired M-PCAPS water samples in a) Carnero Pass and b) South Fork. In both cases, the shallow M-PCAPS are depicted as diamonds and deep M-PCAPS are depicted as circles. For example, A-Shallow and A-Deep are paired M-PCAPS and the arrow depicts their evolution with respect to the SEL, LMWL, and GMWL. Note that the slopes of the evolution of the paired samples effectively bracket the SEL. The open triangles represent the stable isotopic composition of the modified-bulk collectors. The bold black line is the SEL, the dash-dot line is the GMWL, and the dotted line is the LMWL.

Late season rainfall during September and early October is on average isotopically heavier, $\delta^{18}O$ = -9.6 and $\delta^{2}H$ = -62, than snow or early spring rainfall. Alternatively, the water stored at depth in the soil could be isotopically heavier due to mixing with water that has experienced some degree of soil evaporation. Water from snowmelt is probably stored in the saprolite and this water mixes with future inputs of water that may have been exposed to evaporation in the upper soil horizons during the summer. This explanation seems more plausible given the current understanding of infiltration events during the summer.

In either case, the actual isotopic composition of the infiltrating water may be very different than that of either surface or shallow subsurface measurements which have experienced little contact with the subsurface. This may be problematic especially if the stable isotope composition of water collected at the surface or shallow subsurface is used to constrain streamflow generation or recharge during the snowmelt season. If the results shown in Figure 3.6 are typical, then the contribution of snowmelt to streamflow generation and recharge may be underestimated. The M-PCAPS does provide an advantage over traditional methods since it collects samples of meltwater in the subsurface which have been in contact with soil thereby allowing the meltwater to experience both kinetic fractionation and mixing processes.

3.5.2.0 Shallow-Subsurface Runoff Processes Operative during Snowmelt:

Samples of water from the bulk collectors and paired M-PCAPS from the Carnero Pass and South Fork installations were analyzed for general chemistry and the results are shown in Figures 3.9 and 3.10, respectively. Two very different subsurface runoff mechanisms can be inferred from the geochemistry of these two installations. First,

consider the Carnero Pass installation. It would seem at first inspection that the geochemical constituents of the paired M-PCAPS are switched. The electrical conductivity and all ionic concentrations of the B-Deep M-PCAPS are lower than that of the shallow M-PCAPS. However, these trends seem logical when the geology and soil development of the Carnero Pass soil pit is considered (Figure 3.3). The A-Deep M-PCAPS was installed in the soil matrix above the layer of fractured, rhyolitic bedrock material and the B-Deep M-PCAPS was installed within the layer of fractured rhyolitic material. It appears that, during snowmelt, the rhyolitic layer promotes lateral throughflow and is capable of channeling large quantities of water downslope while the overlying soil is dominated by slow, downward matrix flow. In the field, we did observe large runoff responses through these rhyolitic soil deposits during snowmelt. In fact, several ephemeral springs emerge from these layers during large meteoric events. Perennial springs, such as JC Spring in Figure 3.2, also appear to emerge from this layer. This interpretation is supported by the lower conductivity in the B-Deep sample as opposed to the shallow samples, by the contrasting concentrations of silica, fluoride, sodium, and calcium, and by the higher EC of the A-Deep sample (Figure 3.9). Fluoride was at undetectably low concentrations in the snow sample and in the deep M-PCAPS samples. It should also be noted that cations, anions, and silica are present in the modified-bulk snow sample but in very low concentrations. The shallow M-PCAPS sample contains a small concentration of fluoride which may be representative of biotite weathering in the soil matrix. Silica was found in low concentrations in the deep sample and increased silica was observed in the shallow sample. These trends seem to indicate that soil horizons in the watershed which contain the layer of heavily fractured, platy

rhyolite can be characterized by a dual-flow regime where slow, downward matrix flow dominates the shallow soil profile and quick, lateral flow dominates the region near the rhyolitic layer. This flow regime may be important during large events such as snowmelt while, during the summer precipitation season, matrix flow may dominate and quickflow may become unimportant.

In contrast, a rhyolitic layer was not observed in the South Fork soil pit and the geochemistry seems indicative of slow, downward matrix flow (Figure 3.10). Again, cations, anions, and silica are present in the modified-bulk snow sample but in very low concentrations. Fluoride is at undetectably low concentrations in the snow. Nearly all ionic species plus silica and electrical conductivity show an increase from snow to the deep M-PCAPS sample. Fluoride concentrations in the shallow and deep samples are similar, within error because the detection limit is 0.1 mg/L. This observation may reflect the small pool of fluoride available for transport and/or the relatively slow weathering of biotite in the soil profile [*Goldich,* 1938]. Apatite could theoretically release fluoride during weathering but a coincident increase in phosphate would be expected and phosphate levels remain low or at undetectably low concentrations in these waters. It is interesting to note that the silica concentration in the South Fork shallow M-PCAPS sample (12 mg/L) was very similar to that of the shallow Carnero Pass sample (11 mg/L). The South Fork deep M-PCAPS sample exhibits further increase in silica which could suggest continued geochemical evolution in a span of only 10 cm of soil. This increase could also reflect larger amounts of silica available for transport in the weathered bedrock or saprolite layer. The South Fork dataset suggests that simple matrix flow may be the dominant subsurface runoff mechanism in some subalpine soil

associations lacking large layers of fractured bedrock. Both datasets provide more information than would otherwise be possible with a surface or shallow subsurface measurement (e.g. modified-bulk collector or snow pan).

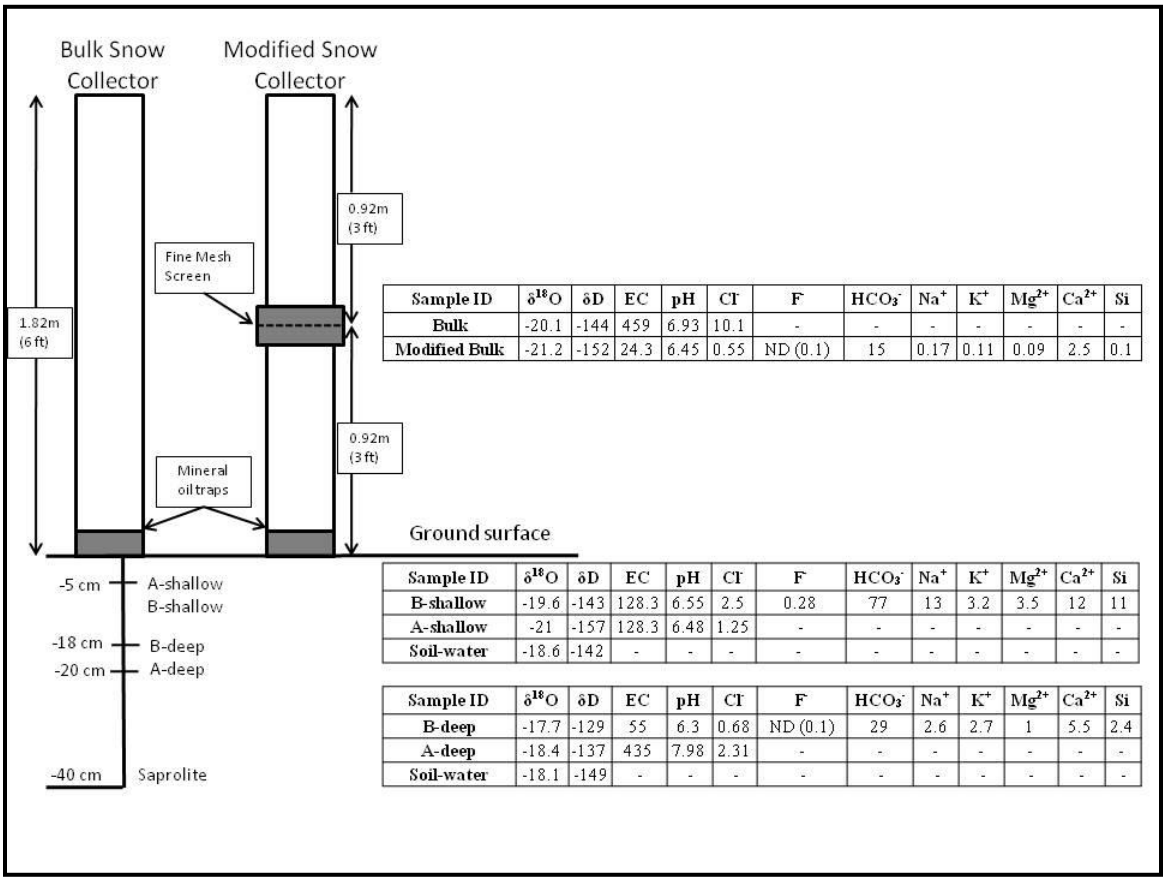

Sample ID	$\delta^{18}O$	δD	EC	pH	Cl⁻	F⁻	HCO_3^-	Na^+	K^+	Mg^{2+}	Ca^{2+}	Si
Bulk	-20.1	-144	459	6.93	10.1	-	-	-	-	-	-	-
Modified Bulk	-21.2	-152	24.3	6.45	0.55	ND (0.1)	15	0.17	0.11	0.09	2.5	0.1

Sample ID	$\delta^{18}O$	δD	EC	pH	Cl⁻	F⁻	HCO_3^-	Na^+	K^+	Mg^{2+}	Ca^{2+}	Si
B-shallow	-19.6	-143	128.3	6.55	2.5	0.28	77	13	3.2	3.5	12	11
A-shallow	-21	-157	128.3	6.48	1.25	-	-	-	-	-	-	-
Soil-water	-18.6	-142	-	-	-	-	-	-	-	-	-	-

Sample ID	$\delta^{18}O$	δD	EC	pH	Cl⁻	F⁻	HCO_3^-	Na^+	K^+	Mg^{2+}	Ca^{2+}	Si
B-deep	-17.7	-129	55	6.3	0.68	ND (0.1)	29	2.6	2.7	1	5.5	2.4
A-deep	-18.4	-137	435	7.98	2.31	-	-	-	-	-	-	-
Soil-water	-18.1	-149	-	-	-	-	-	-	-	-	-	-

Figure 3.9: Diagram of the Carnero Pass PCAPS installation. All chemical species are in units of mg/L, electrical conductivity (EC) is in units of μS cm^{-1} corrected to 25°C, and isotopic compositions are expressed as ‰. "**ND (0.1)**" denotes a non-detect at the 0.1 mg L^{-1} level. Soil samples were collected from the soil pit walls and the soil-water contained in the samples was distilled in the lab. The stable isotopic compositions of these soil-water samples were then analyzed and these are shown as "Soil-Water" in the figure.

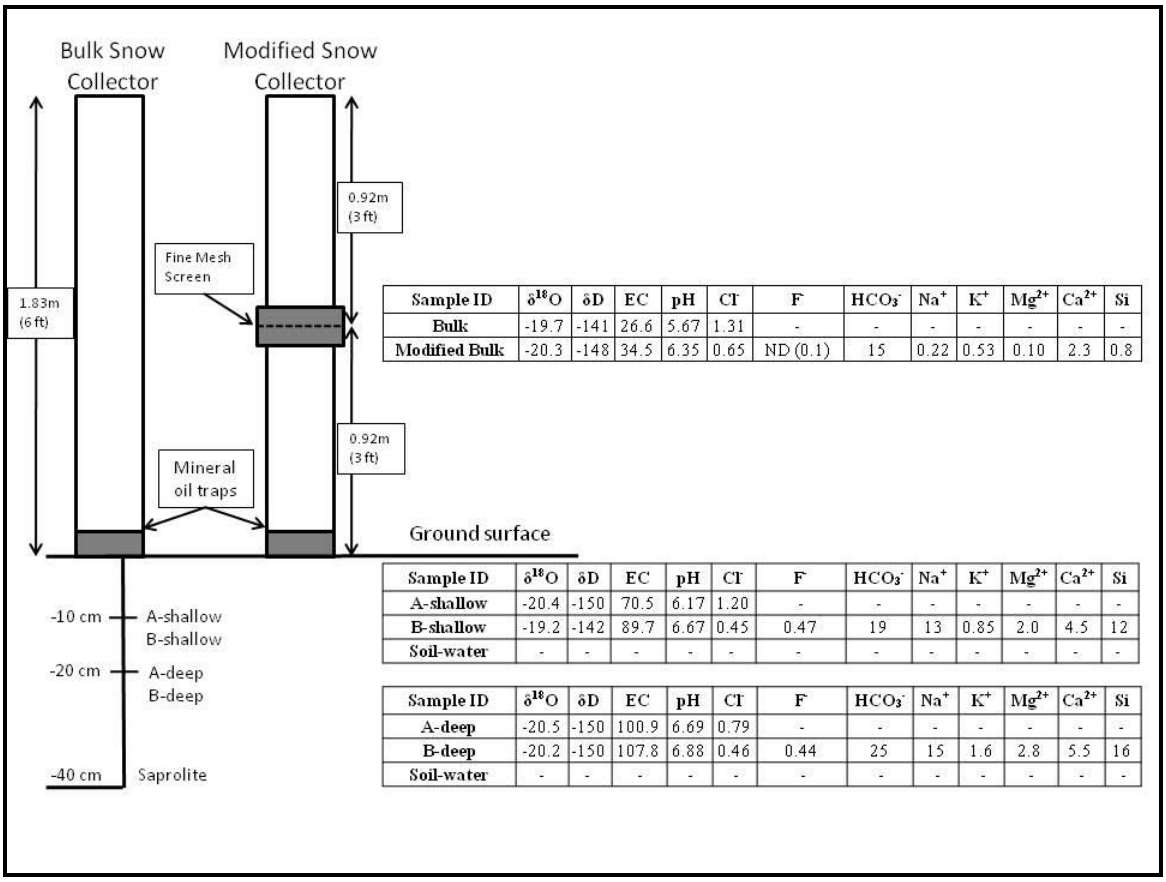

Sample ID	$\delta^{18}O$	δD	EC	pH	Cl	F	HCO_3^-	Na^+	K^+	Mg^{2+}	Ca^{2+}	Si
Bulk	-19.7	-141	26.6	5.67	1.31	-	-	-	-	-	-	-
Modified Bulk	-20.3	-148	34.5	6.35	0.65	ND (0.1)	15	0.22	0.53	0.10	2.3	0.8

Sample ID	$\delta^{18}O$	δD	EC	pH	Cl	F	HCO_3^-	Na^+	K^+	Mg^{2+}	Ca^{2+}	Si
A-shallow	-20.4	-150	70.5	6.17	1.20	-	-	-	-	-	-	-
B-shallow	-19.2	-142	89.7	6.67	0.45	0.47	19	13	0.85	2.0	4.5	12
Soil-water	-	-	-	-	-	-	-	-	-	-	-	-

Sample ID	$\delta^{18}O$	δD	EC	pH	Cl	F	HCO_3^-	Na^+	K^+	Mg^{2+}	Ca^{2+}	Si
A-deep	-20.5	-150	100.9	6.69	0.79	-	-	-	-	-	-	-
B-deep	-20.2	-150	107.8	6.88	0.46	0.44	25	15	1.6	2.8	5.5	16
Soil-water	-	-	-	-	-	-	-	-	-	-	-	-

Figure 3.10: Diagram of the South Fork PCAPS installation. All chemical species are in units of mg/L, electrical conductivity (EC) is in units of $\mu S\ cm^{-1}$ corrected to 25°C, and isotopic compositions are expressed as ‰. "**ND (0.1)**" denotes a non-detect at the 0.1 mg L^{-1} level. Soil samples were collected from the soil pit walls and the soil-water contained in the samples was distilled in the lab. The stable isotopic compositions of these soil-water samples were then analyzed and these are shown as "Soil-Water" in the figure.

3.5.2.1 Discussion of Shallow-Subsurface Runoff Interpretations:

Geochemical data obtained from the PCAPS suggests that infiltrating water can undergo extensive isotopic and geochemical alteration in a relatively shallow soil profile and this data can be very useful in quantifying subsurface runoff mechanisms and geochemical kinetics (Figures 3.7 and 3.8). Fluoride and silica concentrations proved to be particularly useful in the interpretation of these installations. Fluoride, for example, was at undetectably low concentrations in all snow samples and in one M-PCAPS

sample. Interestingly enough, the fluoride non-detect occurred in the deep Carnero Pass M-PCAPS sample while the shallow M-PCAPS sample contained a low concentration of fluoride (Figure 3.9). This observation coupled with similar silica trends led to the conclusion that fast, lateral flow could have occurred in the deep soil profile through a layer of fractured, platy rhyolite overlying the weathered bedrock layer. This type of flow may be kinetically limited implying that residence times are too short and/or flow velocities are too fast for some geochemical reactions to occur. Therefore, significant amounts of fluoride or silica cannot be mobilized.

In contrast, the shallow and deep M-PCAPS pairs at the South Fork site exhibited increases in silica and nearly equal concentrations of fluoride with depth (Figure 3.8). These observations led to the conclusion that slow, matrix flow was dominant in soil profiles lacking the platy, rhyolitic layer. It is interesting to note that the silica concentration of spring and seeps in the watershed ranges from 7.4 to 25 mg/L and the silica concentration of wells terminated in bedrock ranges from 12 to 21 mg/L. These silica trends suggest that infiltrating water can very quickly acquire silica concentrations that are nearly 50 to 75 percent of the concentrations in older, more evolved waters in the watershed. Similar behavior was reported in the work of *Davis,* [1964] and *Kennedy,* [1970]. This type of behavior seems to be transport limited and consequently, higher concentrations of fluoride and silica can be mobilized from the soil. These data suggest that relatively shallow, alpine soils can significantly modify the geochemical composition of infiltrating meltwater.

In general, similar runoff regimes have been reported in other mountainous areas of the Southwest. For example, macropore driven flow was found to be the dominant

runoff mechanism in a ponderosa pine hillslope in northern New Mexico [*Newman et al.*, 1997; *Wilcox et al.*, 1997; *Newman et al.*, 2004]. In that study, lateral subsurface flow was found to be equal to approximately 20 percent of one season's snowpack [*Wilcox et al.*, 1997]. Lateral subsurface flow at the Carnero Pass site may account for as much as 41 percent of the available SWE while the shallow PCAPS collected approximately 54 percent of the available SWE (Table 3.2). This data indicates that infiltrating meltwater in alpine settings may encounter many different runoff mechanisms prior to percolating into the underlying bedrock and these mechanisms may impart different degrees of isotopic and geochemical evolution on the meltwater that will not be captured by a surface measurement.

Recent research has shown that wick samplers may be affected by divergent flow processes whereby soil-water will move laterally away from the wick if the wick is not properly matched to the hydraulic parameters of the soil [*Gee et al.*, 2002, 2003]. In this case, the continuum of soil porosity and capillarity will be broken by the insertion of a poorly matched wick. Divergent flow processes may affect the volume and chemistry of the collected water and this has bearing on our runoff interpretations. For example, if the wick has a matric potential that is more negative than the soil, then overcollection may be a problem and vice versa. In addition, divergent flow may affect the chemistry and/or stable isotopic composition of the collected water because the poorly matched wick is sampling a different fraction of water than expected. If, for example, the matric potential of the wick is much more negative than the surrounding soil, then the wick may preferentially sample water residing in very small pores which would have a geochemical signature characteristic of long residence time and longer rock-water interaction. We

designed our M-PCAPS to match as closely as possible the average soil conditions encountered throughout the year. High-elevation soils in the watershed typically receive more meteoric inputs and soil-evaporation is much less than it is in the low-elevation regions of the watershed which can be semi-arid in nature. However, it should be noted that the thin high-elevation soils become saturated for a large portion of the snowmelt season under normal snowpack conditions. Our laboratory evaluation indicated that the M-PCAPS began wicking almost immediately after the test-soil was saturated and that wicking decreased nearly exponentially as the soil dried and consequently as the matric potential of the soil approached that of the wick [*Frisbee et al.,* 2009]. For these reasons, we believe that the M-PCAPS continued to sample during saturated conditions. While we cannot report the range of hydraulic conditions that the wicks encountered in the field, we do believe that the distinct geochemical signatures of the waters collected by the M-PCAPS in the field can be matched to both field observations of runoff during snowmelt and to the distinct properties of the soil.

3.5.3.0 Constraints on Soil-Water Fluxes during Snowmelt:

Actual constraints and measures of mountain block recharge remain elusive and most methodologies used to calculate recharge are based on water balances, chloride mass balances, or basin scale hydrogeologic models [*Wilson and Guan,* 2004]. The traditional PCAPS design described in the work of *Brown et al.,* [1986] has been employed to quantify transit times of recharging water in sand-plain corn fields of central Minnesota [*Landon et al.,* 2000] and to quantify the amount of recharge in agricultural settings in eastern Oregon [*Louie et al.,* 2000]. While we do not attempt to quantify recharge, one of our goals was to quantify rates and amounts of infiltrating meltwater

using the M-PCAPS design in hopes of better constraining deep percolation in remote, seasonally inaccessible watersheds.

Infiltration amounts and ratios were calculated. First, infiltration ratios were calculated as a percentage of SWE by dividing the volume of water collected in the individual M-PCAPS by the average volume collected in the snow collector. This provides estimates on how much snow water infiltrates the soil. Infiltration amounts were calculated as a depth of infiltration by dividing the volume of water collected in the individual M-PCAPS by the apparent collection area of the wick. We found that the apparent collection area of the wick when constructed in the M-PCAPS design could best be calculated as the surface area of a cylinder where the length of the cylinder was the total length of wick used to create the fiddlehead coil and the radius was the radius of the wick strand. *Frisbee et al.,* [2009] tested the modified PCAPS design in a controlled environment over the duration of 1 month where the actual amount of infiltration was known. After the experimental design was allowed to equilibrate, they found that infiltration measured by the M-PCAPS design ranged from 84 to 127 percent of actual infiltration. *Louie et al.,* [2000] also reported collection efficiencies of 125 percent of recharge in standard PCAPS installations. They suggested that overcollection could be the result of persistent saturated conditions and/or oversampling near macropores in the soil. Divergent flow may also be responsible for collection errors [*Gee et al.*, 2002, 2003]. Regardless, saturated conditions and the presence of macropores will both likely be encountered in any native soil during the snowmelt season. We remained hopeful that M-PCAPS could provide upper constraints on deep percolation in these environments.

Table 3.2 lists the infiltration ratios and infiltration amounts. Only two M-PCAPS samples from the Carnero Pass site were examined for this purpose. The other two samples were either full or overflowing such that the infiltration calculated from these samples may overpredict actual infiltration. The Carnero Pass site yielded higher infiltration estimates than the South Fork site. The shallow M-PCAPS collected 54 percent of the available SWE as recorded by the snow collector and the deep M-PCAPS collected 41 percent of available SWE. These result in 8.4 and 6.8 cm of infiltration, respectively. Average annual rainfall in the watershed is 21.2 cm. Therefore, these estimates account for 28 and 24 percent of total annual precipitation (rainfall plus snowfall). In contrast, the shallow South Fork M-PCAPS collected 38 percent of SWE and the deep M-PCAPS collected 39 percent of SWE. These result in 5.6 cm of infiltration during the snowmelt season. These estimates account for 21 percent of total annual precipitation. Thus, infiltration during the snowmelt season ranges from 21 to 28 percent of total annual precipitation. Interestingly, this range falls within the mountain block recharge estimates given by *Huntley et al.*, [1979] for the San Juan Mountains and for the Sangre de Cristo Mountains. While we are not measuring or attempting to measure recharge with the M-PCAPS, these data suggest that the deep percolation estimates obtained by the M-PCAPS design are similar to the estimates of recharge given in previous research. Thus, this approach may be useful in quantifying deep fluxes of snowmelt infiltration within the mountain block in these and similar landscapes.

Sample ID	V_{SNOW} (mL)	V_{PCAPS} (mL)	Infiltration Ratio (%)	A_{wick} (cm^2)	Infiltration Amount (cm)
Carnero Pass B – Shallow	1350	725	53.7	86.8	8.35
Carnero Pass B – Deep	1350	550	40.7	80.8	6.81
South Fork A – Shallow	1300	550	42.3	89.8	6.12
South Fork A – Deep	1300	600	46.2	92.8	6.47
South Fork B – Shallow	1300	450	34.6	89.8	5.01
South Fork B - Deep	1300	425	32.7	89.8	4.73

Table 3.2: Infiltration amounts for PCAPS sites. VSNOW is the volume of water collected in the bulk and/or modified-bulk collector, VPCAPS is the volume of water collected by the individual PCAPS, "Infiltration Ratio" is infiltration expressed as a percent of available snow water during the snowmelt pulse (V_{PCAPS}/V_{SNOW}), A_{wick} is the surface area of the wick in contact with the soil, and "Infiltration Amount" is the amount of infiltration during the snowmelt pulse (V_{PCAPS}/A_{wick}).

3.5.3.1 Discussion of Constraints on Soil-Water Fluxes:

Two anomalies were discovered in this dataset: 1) possible undercollection at the South Fork site and 2) possible undercollection in the layer of fractured rhyolite in the Carnero pass site. The South Fork M-PCAPS may have collected less infiltration due to increased clay content in the soil. It has been suggested that increased clay contents may promote more surface runoff than soils which contain less clay in the B-horizon [*Newman et al.,* 1997]. In fact, the shallow soil of the Carnero Pass soil pit was classified as a sandy clay loam overlying a sandy loam. It is plausible that the overlying sandy clay loam could saturate more slowly than the infiltration rate and consequently, limit the downward soil-water flux. This could also result in increased surface runoff. It is also interesting that the deep Carnero Pass M-PCAPS collected a smaller volume of water

than the shallow M-PCAPS since fast, lateral flow was thought to occur near the deep M-PCAPS. Lateral flow through the layer of fractured rhyolite may have drained more quickly than the overlying soil matrix. Consequently, the flow through the macropore channel may have stopped while the overlying shallow soil matrix continued to drain. In this case, the matric potential of the M-PCAPS was more negative than the saturated overlying soil. However, the matric potential of the M-PCAPS was less negative than the macropore channel. This is one possible explanation for the collection differences.

Divergent flow may also be a factor in the collection error [*Gee et al.*, 2002, 2003]. The wicks were cut to match the average hydraulic parameters of the field soils. If the wicks are matched to the hydraulic properties of the soil, then the wicks should sample a representative volume of soil pores and a representative volume of water flowing through these pores. These soils are broadly classified as loamy, rocky soils and typically contain large fractions of silt. Loamy soils would characteristically have a much different matric potential range than soils containing large fractions of clay. Therefore, if the wicks were in direct contact with clayey loams, then the matric potential of the wick would be less negative than that of the clay. This would theoretically result in flow away from the wick much like having a sand lens embedded in a clay soil. This is an alternative explanation for the anomalies.

3.5.4.0 Soil-Water Fluxes during the Summer Rainfall Season:

All M-PCAPS were left installed from June through early October of 2008 to quantify soil-water fluxes during the summer rainfall season. SNOTEL data suggests that, on average, snow begins to accumulate as early as October 4 in the Saguache Creek watershed and this effectively ends the summer rainfall season. M-PCAPS could be used

to quantify mixing of water stored in the soil with inputs of rainfall. However, we were interested in quantifying how much water infiltrates during the summer rainfall season. The commonly held assumption is that little if any summer rainfall percolates deeply in the soil during the summer rainfall season [*Winograd et al.*, 1998]. The M-PCAPS located at the Carnero Pass installations continued to wick during the period from late June to late July. The A-shallow M-PCAPS collected 28 mL of water, A-Deep collected a trace amount of water, B-shallow collected 19 mL, and B-Deep collected 3 mL of water. These correspond to 0.32, 0, 0.22, and 0.04 cm of infiltration intercepted by the wick. The B-shallow M-PCAPS had a $\delta^{18}O$ of -17.5 ‰ and a $\delta^{2}H$ of -132 ‰; whereas the B-Deep M-PCAPS had a $\delta^{18}O$ of -20.9 ‰ and a $\delta^{2}H$ of -133 ‰. The electrical conductivity and pH of the B-shallow sample was 34.4 μS/cm and 7.06, respectively. In contrast, the electrical conductivity and pH of the B-Deep sample was 134.2 μS/cm and 8.01. More importantly, all M-PCAPS installations either remained dry or only collected trace amounts (drops) of water for the remainder of the summer rainfall season. Monthly rainfall totals were below normal for the months of June, July, and September while August received higher than normal rainfall in 2008.

3.5.4.1 Discussion of Soil-Water Fluxes during the Summer Rainfall Season:

Like during the snowmelt season, higher soil-water fluxes were measured in the shallow soil profile of the Carnero Pass M-PCAPS installation as compared to the deeper soil profile. During the snowmelt season, the stable isotope and geochemical composition of these two regions were distinctly different and we concluded that based on the soil characteristics that a dual-flow subsurface runoff regime could be responsible for this behavior. The stable isotope composition of this site again seems to suggest a

dual-flow regime. However, when the geochemical data is evaluated, an alternative explanation seems more plausible during the rainfall season. This behavior may indicate diminished flow within the layer of fractured rhyolite located at depth and increased communication between the upper soil profile characterized by slow, downward matrix flow and the layer of fractured rhyolite. Trends in electrical conductivity, TDS, and pH seem to support this conclusion. Therefore, the layer of fractured rhyolite is a very important control on subsurface runoff generation during the snowmelt season and its importance likely diminishes during the summer rainfall season. During this period, flow in the fractured rhyolite may be supported by the interception of slow, downward matrix flow from the upper soil horizons.

The soil-water flux dataset also supports the commonly held assumption that rainfall contributions to recharge may be very small in these alpine watersheds [*Wilson et al.,* 1980; *Winograd et al.,* 1998; *Wilson and Guan,* 2004; and *Flint et al.,* 2004]. The evapotranspiration demand is typically very low during the snowmelt season at high elevations; consequently, meltwater can percolate deeply into the soil profile. However, evapotranspiration demands increase, soil matric potentials become more negative, and deep infiltration diminishes during the summer rainfall season. Our 2008 dataset plus field observations indicate that most event precipitation is captured within the very shallow soil region and wetting fronts do not appear to propagate beyond 5 to 10 cm during the summer. This behavior was observed in the M-PCAPS soil pits even during August when monthly rainfall rates were higher than normal. Diminished soil-water fluxes, such as those observed during the summer rainfall season, may have important implications for recharge in alpine watersheds when global climate change models are

considered. Many of these studies suggest an overall decrease in snowpacks and changes in rainfall rates remain inconclusive [*Mote et al.,* 2005]. If a larger proportion of the hydrologic budget in these alpine watersheds must depend on rainfall, then how will recharge be affected if deep percolation is reduced? Instrumentation is needed to better constrain and monitor soil-waters fluxes during the summer rainfall season in these watersheds and the M-PCAPS methodology may be particularly useful in this respect.

3.6 Conclusions:

We initially designed this field evaluation to test the suitability of a modified passive capillary sampler for collecting the integrated isotopic composition of soil-meltwater in remote, seasonally inaccessible watersheds. We were interested in testing the assumption that the isotopic composition of water collected by modified-bulk snow collectors is similar to that of actual snowmelt recharge. It is apparent that the assumption may not be valid in all cases since isotopic evolution of infiltrating meltwater did occur in these shallow, rocky subalpine soils to such an extent that the deep M-PCAPS samples were not similar to the isotopic composition of the waters retrieved from the snow collectors. Geochemical data supports this finding since the geochemistry of the infiltrating water evolved even more rapidly than the isotopic composition in these shallow soils. Surface proxies for snowmelt infiltration will not be geochemically evolved.

Several important findings were made during this study using M-PCAPS. The geochemical evolution of meltwater can occur quickly in a relatively shallow soil profile and the geochemical kinetics are controlled by shallow-subsurface runoff mechanisms.

One common alpine soil association contains a layer of platy, rhyolitic rocks which promotes fast, lateral flow and geochemistry that is typical of kinetically-limited conditions. In the field, we observed quick runoff responses from these rhyolitic deposits at multiple locations in the watershed and several ephemeral springs emerge from these layers during the snowmelt season. The data obtained from the M-PCAPS supports these field observations. In contrast, the other common soil association in the watershed lacks the quickflow layer and is instead conducive to slow, matrix flow and geochemistry that is typical of transport-limited conditions. When modified-snow collected at the landscape surface is used as the snowmelt-infiltration or soil-meltwater endmember, the snow has not experienced the same geochemical evolution as actual meltwater as it infiltrates the soil. Consequently, the surface proxies for infiltrating meltwater will not be geochemically distinct from snow collected in standard bulk collectors. Therefore, watershed-scale geochemical models which are based upon the surface proxy data may be in error and the soil-meltwater endmembers will not be geochemically unique in isotope separation analyses.

Soil-water fluxes were high during the snowmelt season and nearly non-existent during the summer rainfall season. Soil-water fluxes approached 38 to 54 percent of available SWE during the snowmelt season and 21 to 28 percent of total annual precipitation (rainfall plus snowfall). These findings have implications for the response of alpine watersheds to global climate change. If, for example, snowpacks decrease and rainfall increases in these watersheds, deep soil-water fluxes may be greatly reduced. Currently, there are limited in-situ observations of these processes and the M-PCAPS design may assist in providing initial benchmarks. Overall, the performance of the M-

PCAPS design was encouraging and we conclude that this design may be very useful in quantifying the isotopic composition of deep percolation in remote, seasonally inaccessible watersheds.

3.7 References:

Allison, G.B. (1982), The relationship between ^{18}O and deuterium in water in sand columns undergoing evaporation, *Journal of Hydrology, 55*, 163-169.

Araguás-Araguás, L., K. Rozanski, R. Gonfiantini, and D. Louvat (1995), Isotope effects accompanying vacuum extraction of soil water for stable isotope analyses, *Journal of Hydrology, 168*, 159-171, doi:10.1016/0022-1694()94)02636-P.

Boll, J., T.S. Steenhuis, and J.S. Selker (1992), Fiberglass wicks for sampling of water and solutes in the vadose zone, *Soil Science Society of America Journal, 56,* 701-707.

Brahy, V. and B. Delvaux (2001), Comments on "Artifacts caused by collection of soil solution with passive capillary samplers", *Soil Science Society of America Journal, 65,* 1571-1572.

Brown, K.W., J.C. Thomas, and M.W. Holder (1986), Development of a capillary wick unsaturated zone water sampler, Coop. Agreement CR812316-01-0. USEPA Environ. Monit. Sys. Lab., Las Vegas, NV.

Buttle, J.M. and K. Sami (1990), Recharge processes during snowmelt: An isotopic and hydrometric investigation, *Hydrological Processes, 4*(4), 343-360.

Clark, I., and P. Fritz (1997), *Environmental Isotopes in Hydrogeology,* Lewis, Boca Raton, Fla.

Craig, H., (1961), Isotopic variations in meteoric waters, *Science, 133*, 1702-1703.

Davis, S.N. (1964), Silica in streams and ground water, *American Journal of Science, 262,* 870-891.

Delin, G.N. and M.K. Landon (2002), Effects of surface run-off on the transport of agricultural chemicals to ground water in a sandplain setting, *The Science of the Total Environment, 295*, 143-155.

Earman, S., A.R. Campbell, F.M. Phillips, and B.D. Newman (2006), Isotopic exchange between snow and atmospheric water vapor: Estimation of the snowmelt component of groundwater recharge in the southwestern United States, *Journal of Geophysical Research, 111,* D09302, doi:10.1029/2005JD006470.

Flint, A.L. L.E. Flint, J.A. Hevesi, and J.B. Blainey (2004), Fundamental concepts of recharge in the desert Southwest: A regional modeling perspective, in *Groundwater Recharge in a Desert Environment: The Southwestern United States, Water Sci. Appl. Ser.,* Vol. 9, edited by J.F. Hogan, F.M. Phillips, and B.R. Scanlon, pp. 159-184, AGU, Washington, D.C.

Friedman, I., G.I. Smith, J.D. Gleason, A. Warden, and J.M. Harris (1992), Stable isotopic composition of waters in southeastern California: 1. Modern Precipitation, *Journal of Geophysical Research, 97,* 5795-5812.

Frisbee, M.D., F.M. Phillips, A.R. Campbell, J.M.H. Hendrickx, and E.M. Engle (2009), Modified passive capillary samplers for collecting samples of snowmelt infiltration for stable isotope analysis in remote, seasonally inaccessible watersheds 1: Laboratory Evaluation, *Hydrological Processes,* DOI:10.1002/hyp.7523.

Gee, G.W., A.L. Ward, T.G. Caldwell, and J.C. Ritter (2002), A vadose zone water fluxmeter with divergence control, *Water Resources Research, 38,* doi:10.1029/2001WR000816.

Gee, G.W., Z.F. Zhang, and A.L. Ward (2003), A modified vadose zone fluxmeter with solution collection capability, *Vadose Zone Journal, 2,* 627-632.

Goldich, S.S. (1938), A study in rock-weathering, *Journal of Geology, 46,* 17-58.

Goyne, K.W., R.L. Day, and J. Chorover (2000), Artifacts caused by collection of soil solution with passive capillary samplers, *Soil Science Society of America Journal, 64,* 1330-1336.

Goyne, K.W., R.L. Day, and J. Chorover (2001), Response to "Comments on 'Artifacts caused by collection of soil solution with passive capillary samplers'", *Soil Science Society of America Journal, 65,* 1572-1573.

Herrmann, A., M. Lehrer, and W. Stichler (1981), Isotope input into runoff systems from melting snow covers, *Nordic Hydrology, 12*, 309-318.

Hoch, A.R., M.M. Reddy, and J.I. Drever (1999), Importance of mechanical disaggregation in chemical weathering in a cold alpine environment, San Juan Mountains, Colorado, *GSA Bulletin, 111*(2), 304-314.

Holder, M., K.W. Brown, J.C. Thomas, D. Zabcik, and H.E. Murray (1991), Capillary-wick unsaturated zone soil pore water sampler, *Soil Science Society of America Journal, 55*(5), 1195-1202.

Hooper, R.P. and C.A. Shoemaker (1986), A comparison of chemical and isotopic hydrograph separation, *Water Resources Research, 22,* 1444-1454.

Huntley, D. (1979), Groundwater recharge to the aquifers of northern San Luis Valley, Colorado. *Geological Society of America Bulletin, Part II, 90,* no.8, 1196-1281.

Jury, W.A. and R. Horton (2004), *Soil Physics,* 6th Edition, 384 pp., Wiley, New York.

Kennedy, V.C. (1970), Silica variations in stream water with time and discharge, in *Nonequilibrium Systems in Natural Water Chemistry,* edited by J.D. Hem, series editor R.F. Gould, pp. 95-130, American Chemical Society, Houston, Texas.

Knutson, J.H. and J.S. Selker (1994), Unsaturated hydraulic conductivities of fiberglass wicks and designing capillary wick pore-water samplers, *Soil Science Society of America Journal, 58,* 721-729.

Landon, M.K., G.N. Delin, S.C. Komor, and C.P. Regan (1999), Comparison of the stable-isotopic composition of soil water collected from suction lysimeters, wick samplers, and cores in a sandy unsaturated zone, *Journal of Hydrology, 224,* 45-54.

Landon, M.K., G.N. Delin, S.C. Komor, and C.P. Regan (2000), Relation of pathways and transit times of recharge water to nitrate concentrations using stable isotopes, *Ground Water, 38*(3), 381-395.

Laudon, H., H.F. Hemond, R. Krouse, and K.H. Bishop (2002), Oxygen 18 fractionation during snowmelt: Implications for spring flood hydrograph separation, *Water Resources Research, 38*(11), 1258, doi:10.1029/2002WR001510.

Laudon, H., J. Seibert, S. Köhler, and K.H. Bishop (2004), Hydrological flow paths during snowmelt: Congruence between hydrometric measurements and oxygen 18 in meltwater, soil water, and runoff, *Water Resources Research, 40,* W03102, doi:10.1029/2003WR002455.

Lipman, P.W. and W.C. McIntosh (2008), Eruptive and noneruptive calderas, northeastern San Juan Mountains, Colorado: where did the ignimbrites come from?, *GSA Bulletin, 120*(7/8), 771-795, doi:10.1130/B26330.1.

Liu, F., M.W. Williams, and N. Caine (2004), Source waters and flow paths in an alpine catchment, Colorado Front Range, United States, *Water Resources Research, 40,* W09401, doi:10.1029/2004WR003076.

Louie, M.J., P.M. Shelby, J.S. Smesrud, L.O. Gatchell, and J.S. Selker (2000), Field evaluation of passive capillary samplers for estimating groundwater recharge, *Water Resources Research, 36*(9), 2407-2416.

Merlivat, L. (1978), Molecular diffusivities of $H_2{}^{16}O$, $HD^{16}O$, and $H_2{}^{18}O$ in gases, *Journal of Chemical Physics, 69,* 2864-2871.

Mote, P.W., A.F. Hamlet, M.P. Clark, and D.P. Lettenmaier (2005), Declining mountain snowpack in western North America, *American Meteorological Society,* 39-49.

Nelson, S.T., and D. Dettman (2001), Improving hydrogen isotope ratio measurements for on-line chromium reduction systems, *Rapid Communications in Mass Spectrometry. 15,* 2301-2306.

Newman, B.D., A.R. Campbell, and B.P. Wilcox (1997), Tracer-based studies of soil water movement in semi-arid forests of New Mexico, *Journal of Hydrology, 196,* 251-270.

Newman, B.D., B.P. Wilcox, and R.C. Graham (2004), Snowmelt-driven macropore flow and soil saturation in a semiarid forest, *Hydrological Processes, 18,* 1035-1042, doi:10.1002/hyp.5521.

Rango, A. (2006), Snow: The real water supply for the Rio Grande Basin, *New Mexico Journal of Science, 44,* 99-118.

Robertson, J.A. and C.A. Gazis (2006), An oxygen isotope study of seasonal trends in soil water fluxes at two sites along a climate gradient in Washington state (USA), *Journal of Hydrology, 328,* 375-387, doi:10.1016/j.jhydrol.2005.12.031.

Steven, T.A. and P.W. Lipman (1976), Calderas of the San Juan Volcanic Field, southwestern Colorado, in U.S. Dept. of the Interior, USGS Geological Survey Professional Paper 958, 35 pp.

Sugimoto, A., D. Naito, N. Yanagisawa, K. Ichiyanagi, N. Kurita, J. Kubota, T. Kotake, T. Ohata, T.C. Maximov, and A.N. Fedorov (2003) Characteristics of soil moisture in permafrost observed in East Siberian taiga with stable isotopes of water, *Hydrological Processes, 17,* 1073-1092, doi:10.1002/hyp.1180.

Taylor, S., X. Feng, J.W. Kirchner, R. Osterhuber, B. Klaue, and C.E. Renshaw (2001), Isotopic evolution of a seasonal snowpack and its melt, *Water Resources Research, 37*(3), 759-769.

Unnikrishna, P.V., J.J. McDonnell, and C. Kendall (2002), Isotope variations in a Sierra Nevada snowpack and their relation to meltwater, *Journal of Hydrology, 260,* 38-57.

Wilcox, B.P., B.D. Newman, D. Brandes, D.W. Davenport, and K. Reid (1997), Runoff from a semiarid ponderosa pine hillslope in New Mexico, *Water Resources Research, 33*(10), 2301-2314.

Wilson, L.G., K.J. DeCook, and S.P. Neuman (1980), Regional recharge research for Southwest alluvial basins, unnumbered report, Water Resour. Res. Cent., Univ. of Arizona, Tucson.

Wilson, J.L. and H. Guan (2004), Mountain-block hydrology and mountain-front recharge, in *Groundwater Recharge in a Desert Environment: The Southwestern United*

States, edited by F.M. Phillips, J. Hogan, and B. Scanlon, 23 pp., AGU, Washington, D.C.

Winograd, I.J., A.C. Riggs, and T.B. Coplen (1998), The relative contributions of summer and cool-season precipitation to groundwater recharge, Spring Mountains, Nevada, USA, *Hydrogeology Journal, 6*, 77-93.

Chapter 4 Streamflow Generation in a Large, Alpine Watershed in the Southern Rocky Mountains of Colorado, USA: Is Streamflow Generation Simply the Aggregation of Hillslope Runoff?[3]

4.1 Introduction:

The characterization of streamflow generation processes in hillslopes and small catchments less than 100 km^2 has been well documented in the hydrological literature [see *Beven,* 2006 for reviews]. Yet, few of these studies attempt to scale their results to larger watersheds. In addition, the characterization of streamflow generation processes in watersheds larger than 1000 km^2 remains sketchy, in part due to logistical difficulties imposed by the larger watershed size [*Rodgers et al.,* 2005]. For watershed hydrologists, this is a complicated problem especially since there is an increasing urgency to understand streamflow generation processes at larger watershed scales [*Naiman et al.,* 2001]. One approach toward solving this problem is to aggregate the runoff responses from individual hillslopes and effectively upscale that aggregated response to the larger watershed. The logic behind this approach is that process understanding at smaller scales is much more complete than it is at larger scales. The problem with this approach is that hillslope processes tend to be highly complex and heterogeneous and the scaling of these processes will result in models that are also highly complex at the watershed scale [*McDonnell,* 2003; *Sivapalan,* 2003; *Uhlenbrook,* 2006]. This approach also ignores possible processes that are unique to the larger scale and may not be operative at smaller scales. An alternative approach is to identify features or processes that connect hillslope-scale processes to the response of the larger watershed, in other words, to seek common

[3] **Frisbee, M.D., F.M. Phillips, A.R. Campbell, F. Liu, and S.A. Sanchez (2010), Streamflow generation in a large, alpine watershed in the southern Rocky Mountains of Colorado, USA: Is streamflow generation simply the aggregation of hillslope runoff responses?, *Water Resources Research,* submitted – April 2, 2010.**

threads between hillslope and watershed processes [*Sivapalan*, 2003; *Beighley et al.*, 2005]. Such features or processes may provide the important link that allows us to bridge the gap in understanding between small-scale complexity and large-scale simplicity [*Dooge*, 1997; *Spence*, 2007].

The second approach is particularly appealing. It allows watershed hydrologists to investigate the scalability of a specific feature or process without first deriving a conceptual model of runoff generation at the smaller hillslope scale. This is beneficial for two reasons: it accelerates current progress in process understanding and in the long term, it promotes the development of new theories regarding hydrological processes at the large watershed scale. In fact, according to *Sivapalan* [2003], "much faster progress can be achieved, in terms of linking conceptualizations across the scales, if the hillslope and network responses can be described physically, but in terms of *travel time distributions*, to match the usual physical meaning of the unit hydrograph for the watershed as a travel time distribution" (pages 1039 and 1040). It is apparent from *Sivapalan* [2003] that scalable properties such as travel times may be the key to bridging the gap between small and large-scale process understanding. Studies have been conducted at small scales in order to quantify the relationship between catchment area and residence times [*McGlynn et al.*, 2003; *McGuire et al.*, 2005]. These studies, however, indicate that there may not be a correlation between catchment area and residence times. However, these concepts have not been thoroughly tested at larger watershed scales.

In this paper, we follow the suggestion of *Sivapalan* [2003] and investigate the processes that control the structuring of streamflow chemistry with increasing scale in a

large watershed (drainage area greater than 1600 km^2). Several studies have documented structured trends in stream chemistry that become apparent as basin scale increases [*Wolock et al.,* 1997; *Shaman et al.,* 2004; *Temnerud and Bishop,* 2005; *Uchida et al.,* 2005]. Since this behavior seems to be a common occurrence, streamflow chemistry may be particularly useful in linking process understanding across multiple scales. In the following paragraphs, we develop two conceptual models that could be employed to explain the structured trends in streamflow chemistry. These models represent two conceptualizations of streamflow generation at the large watershed scale. One model is essentially a 2-D conceptualization in which streamflow chemistry is controlled by the integration of runoff from surface and shallow subsurface flowpaths along hillslopes (Figure 4.1a). The alternative model is a 3-D conceptualization in which streamflow chemistry is controlled by a distribution of flowpaths through both deep groundwater and surface and shallow subsurface routes (Figure 4.1e). These conceptualizations are essentially endmembers in the range of conceptual models for streamflow generation; in reality, most streamflow generation processes probably fall somewhere between these two endmembers.

We use the results of *Wolock et al.* [1997], *Shaman et al.* [2004], *Temnerud and Bishop* [2005], and *Uchida et al.* [2005] to define and illustrate the 2-D conceptual model of streamflow generation processes at the large watershed scale. *Shaman et al.* [2004] and *Wolock et al.* [1997] found that low-flow stream chemistry in the Neversink River watershed was quite spatially variable in sub-basins of less than 8 km^2 and above this basin threshold, stream chemistry became scale invariant. *Shaman et al.* [2004] attributed this behavior to the integration of contributions from shallow subsurface

macropores and bedrock fractures and by the effective damping of the chemical signature by mixing processes with water stored in the riparian soil matrix. *Uchida et al.* [2005] also found that low-flow stream chemistry was quite spatiotemporally variable in very small sub-basins and hillslopes (areas < 0.1 km^2) in Japan. This variability was inferred to be controlled by spotty contributions of subsurface water from the bedrock to the soil-water and to the stream itself. They concluded, however, that the chemical signatures from these hillslopes were damped by mixing in the stream and not in the riparian zone, since streams in their study were not always bounded by laterally extensive riparian areas. *Temnerud and Bishop* [2005] observed similar behavior in two Swedish boreal catchments but found that stream chemistry became stable beyond a critical basin size of 15 km^2. The common theme among these studies is that concentrations of chemical constituents in streamflow approached an asymptotic concentration as basin scale increased (Figure 4.1d). This is an important characteristic of the 2-D conceptual model which provides the framework for the network-mixing conceptual model.

These studies suggest that streamflow chemistry is primarily controlled by contributions from surface and shallow subsurface flowpaths that become mixed in the stream or riparian zone. These authors do not propose that contributions from basin-scale groundwater are spatially continuous or significant components of streamflow chemistry. As a consequence, any structure in stream chemistry that becomes apparent with scale will be controlled by mixing processes within the stream network and/or mixing in the riparian zone [*Shaman et al.,* 2004; *Uchida et al.,* 2005]. These findings fit within the conceptual framework of "hillslope aggregation" described in the work of *Sivapalan* [2003] and we term this behavior the "network-mixing conceptual model". This is

essentially a 2-D conceptual model with limited storage and runoff is generated primarily by surface and shallow subsurface flowpaths along hillslopes (Figure 4.1a). As a consequence, network-mixing will produce a rapid runoff response (Figure 4.1b). This conceptual model also implies short travel times when the basin is subjected to a tracer pulse (Figure 4.1c). In this conceptual model, inputs from surface and shallow subsurface flowpaths become increasingly mixed as scale increases and this leads to the convergence of streamflow chemistry toward asymptotic concentrations of chemical constituents in streamflow (Figure 4.1d). This conceptual model provides an explanation for the asymptotic trends in streamflow chemistry described in the work of *Shaman et al.* [2004] and *Uchida et al.* [2005].

Alternatively, we can use the topography-driven flow concepts originated by *Tóth* [1963, 1995, 1999] and results from the work of *Kirchner et al.* [2000, 2001], *Lindgren et al.* [2004], and *Cardenas* [2007] to illustrate and define the 3-D conceptual model for streamflow generation at the large watershed scale. In this conceptual model, streamflow will be mainly generated by runoff from surface and shallow subsurface flowpaths at the hillslope scales and also by basin-scale groundwater flowpaths that increase in importance as the scale of the basin increases. The significance of the basin-scale groundwater conceptualization is based upon the topographically-driven flow model proposed by József Tóth, in which local, intermediate, and regional groundwater flowpaths develop in basins as a consequence of the distribution of topographic features and energy gradients [*Tóth,* 1963, 1995]. These flowpaths have different distributions of residence times associated with them and consequently, the amounts of water, heat, and solutes that they transport to surface drainages are controlled by varying residence time in

the subsurface [*Tóth,* 1999; *Cardenas,* 2007]. For example, low-order streams might receive groundwater contributions that have sampled primarily shorter flowpaths and the residence time distribution of the groundwater discharged to the stream will be dominantly young. On the other hand, high-order streams might receive groundwater discharge originating from flowpaths of a variety of lengths and tortuousities and the residence time distribution discharged to the stream will have a tail of much older age. Unfortunately, very little is known about the role of basin-scale groundwater contributions in streamflow generation from large watersheds. Yet, from a Tóthian-flow perspective, it seems logical to infer that contributions to streamflow from basin-scale groundwater flowpaths will become increasingly more important as watershed scale increases.

The 3D catchment-mixing conceptual model is shown in Figure 4.1e. This is a 3-D conceptualization and the salient difference between this conceptual model and the network-mixing model is that there is much more storage and much more variability in flowpath length. This conceptualization contains a distribution of surface, shallow subsurface, and basin-scale groundwater flowpaths. The runoff response from this model will be similar to that of the network-mixing model (Figure 4.1f). However, the travel time distribution will be much different (Figure 4.1g). The increased storage and variability in flowpath lengths and tortuousities will result in longer residence times in the subsurface. Components of this long-residence time groundwater that are discharged to the stream will create tailing in the travel-time distribution for the watershed. This behavior has been reported in the work of *Kirchner et al.* [2000], *Lindgren et al.* [2004], and *Cardenas* [2007]. Longer residence times also enhance rock/water interactions

[*Lasaga*, 1984]. Basin-scale groundwater that has a long residence time will therefore be more geochemically evolved than runoff flowing along short flowpaths. From a Tóthian-flow perspective, contributions of this long-residence time groundwater to streamflow should increase as scale increases. Since these groundwater components also have evolved geochemical signatures, concentrations of chemical constituents in streamflow should likewise increase with increasing scale (Figure 4.1h) and should not asymptotically approach some median concentration.

Ultimately, one of the distinguishing characteristics between these two conceptual models is the magnitude and structuring of groundwater contributions in streamflow chemistry with basin scale. We use this characteristic to test these two conceptual models. For example, *Shaman et al.* [2004] argue that although there is some flowpath heterogeneity in natural systems, there is nevertheless open exchange and mixing between deeper, older groundwaters and shallower, younger surficial waters. This mixing effectively masks or damps the signature of older groundwaters and instead, integrated chemical signatures emerge as scale increases. Therefore, if the network-mixing conceptual model holds, we would expect to see only small groundwater contributions to streamflow and evidence of asymptotic behavior in streamflow chemistry with increasing scale indicative of those mixing processes. Since this conceptual model explains runoff generation by means of surface and shallow subsurface runoff flowpaths, we should also expect that contributions from endmembers such as meteoric inputs (direct inputs to streamflow), surface runoff, and soil-moisture are present and dominant in streamflow. Alternatively, *Shaman et al.* [2004] state that if residence time in the subsurface continues to increase with increasing scale and if these flowpaths are

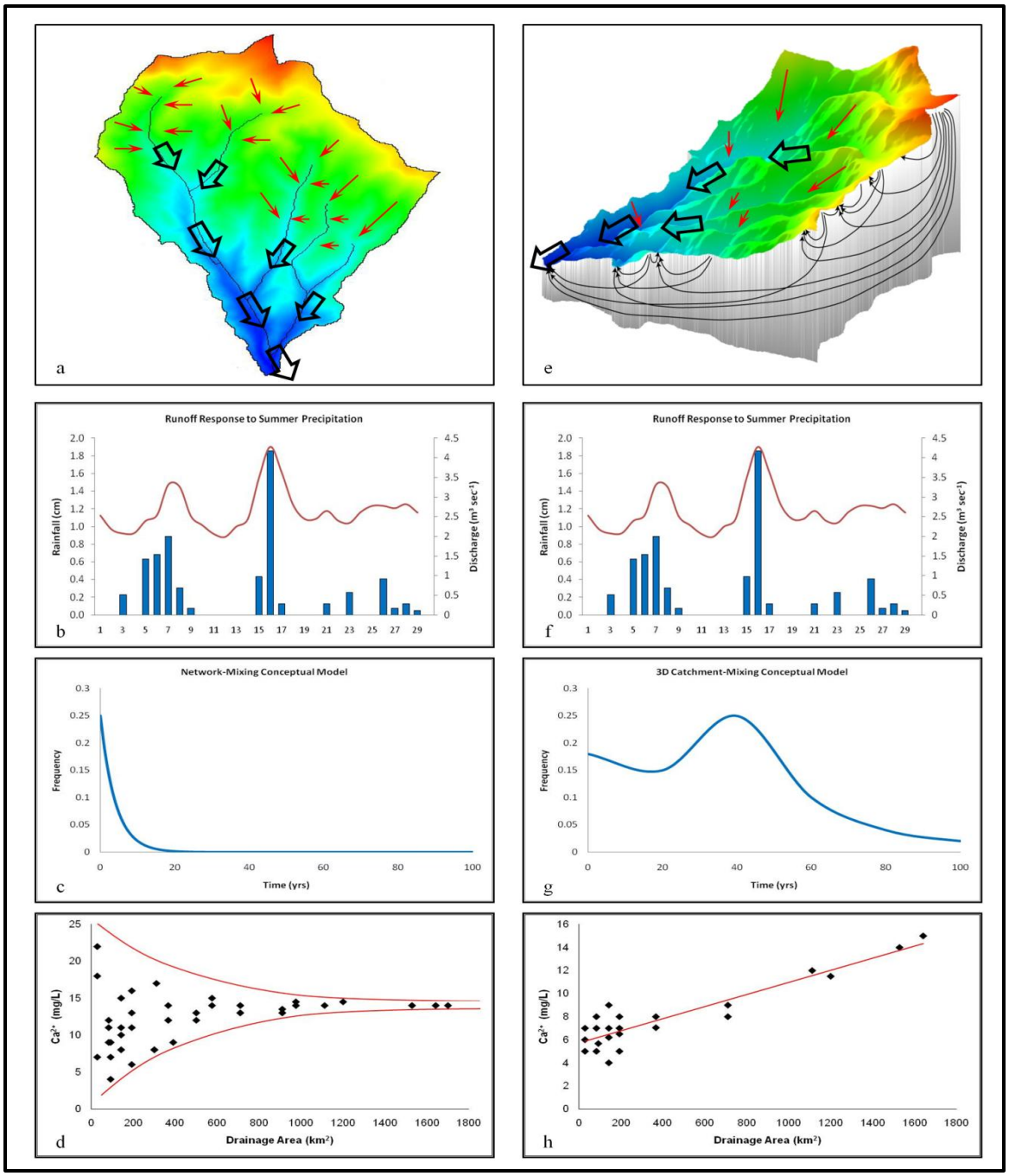

Figure 4.1: Conceptual models for streamflow generation at large watershed scales. The conceptual model for the network-mixing conceptual model is on the left including: a) schematic representation, b) runoff response, c) tracer travel time distribution, and d) t trends in streamflow chemistry with increasing watershed scale. The conceptual model for the 3D catchment-mixing conceptual model is on the right including: e) schematic representation (please note that crossing flowlines are an artifact of 3D representation), f) runoff response, g) tracer travel time distribution, and h) trends in streamflow chemistry with increasing watershed scale.

discharged to the stream, then we would expect concentrations of chemical constituents in streamflow to continue to increase with increasing scale as opposed to asymptotic behavior. Empirical evidence of such behavior has remained elusive.

In this paper, we use endmember mixing analysis (EMMA) on 4 years of stream chemistry and stable isotope data to quantify the components of streamflow generation in the Saguache Creek watershed, a large (1670 km^2) mountainous watershed located in the San Juan Mountains of southwestern Colorado (38° 5' 14" N and 106° 8' 29" W). We analyzed the chemistry and stable isotopic composition of streamflow from nested headwater and tributary subwatersheds and at increments in accumulated watershed area working longitudinally down the main channel of Saguache Creek. This nested approach allowed us to monitor streamflow generation processes in scales ranging from 56 km^2 to 1447 km^2. We also measured vertical hydraulic gradients in mini-piezometers installed in streambeds distributed throughout the watershed to quantify the spatial patterns of groundwater discharge to streamflow. The EMMA results and measurements of vertical hydraulic gradient were used to test the two proposed conceptual models. Since contributions from basin-scale groundwater are so critical in distinguishing between these two conceptual models, we were interested in answering the following question. What is the role of groundwater in streamflow generation in the Saguache Creek watershed and do groundwater contributions in streamflow become structured with increasing scale? We used the results from EMMA and measurements of vertical hydraulic gradients to quantify the role of groundwater in streamflow across multiple scales in the Saguache Creek watershed. If we see evidence of structured contributions of groundwater in streamflow, then our dataset would support the 3D catchment-mixing conceptual model.

On the other hand, evidence of insignificant groundwater contributions in streamflow and/or evidence of asymptotic behavior in streamflow chemistry with increasing scale would support the network-mixing conceptual model.

4.2 Site Description:

The Saguache Creek watershed is located in the San Juan Mountains of southern Colorado (Figure 4.2). The elevations in the watershed range from 2352 m to 4237 m. The watershed is approximately 1670 km^2 in area and is drained by a perennial stream, Saguache Creek, which flows into the northern San Luis Valley. The overall average daily streamflow in Saguache Creek from 1929 to 2004 is 1.78 $m^3 sec^{-1}$ (62.6 cfs) and this discharge is exceeded 27 percent of the time according to flow duration curves. The minimum average daily streamflow on record is 0.20 $m^3 sec^{-1}$ (7.0 cfs) and the maximum average daily streamflow on record is 19.2 $m^3 sec^{-1}$ (678.0 cfs). Published historical streamflow data from 1910 to 2008 and provisional recent streamflow data is available at http://www.dwr.state.co.us/SurfaceWater/Default.aspx. These streamflow data are very comparable to other tributary streams of the Upper Rio Grande (URG) where the URG is defined as that portion of the Rio Grande located upstream of the border between Colorado and New Mexico.

In low-elevation regions of the watershed, snowfall accounts for 70 percent of the basin-wide average annual precipitation and rain comprises the remainder. In comparison, snowfall accounts for 88 percent of the basin-wide average annual precipitation in high-elevation regions of the watershed. The overall average annual rainfall recorded at the Saguache Creek Colorado Division of Water Resources (DWR)

station located at an elevation of 2470 m is 21.2 cm, the minimum annual rainfall is 10.8 cm, and the maximum annual rainfall is 41.2 cm. Precipitation data is available at http://www.ncdc.noaa.gov/oa/ncdc.html. Our analyses indicate that the majority of rainfall typically falls during the months of July, August, and September and that June and October are typically dry months. May and October are both transitional months where rainfall and snowfall are both encountered. NRCS SNOTEL data is available for the Saguache Creek watershed. Data for snow depth and snow water equivalent can be found http://www.wcc.nrcs.usda.gov/snotel/Colorado/colorado.html. The Saguache Creek watershed contains one SNOTEL site (Cochetopa Pass) with a limited history of only 5 years; however, more extensive datasets area available from the Porphyry Creek SNOTEL site located to the north of the watershed and the Slumgullion Pass SNOTEL site located to the southwest of the watershed. The Slumgullion site may actually be more representative of the high elevation headwaters of the Saguache Creek watershed. The average maximum snow water equivalent (SWE) for the Slumgullion SNOTEL site is 39.9 cm with a historical range of 20.6 cm to 57.7 cm. Peak SWE typically occurs on April 21 (WYD 203). Snowpacks typically begin to accumulate on October 14 (WYD 14) and are, on average, depleted by May 30 (WYD 232). These data yield average annual snowpack persistence of approximately 7 months.

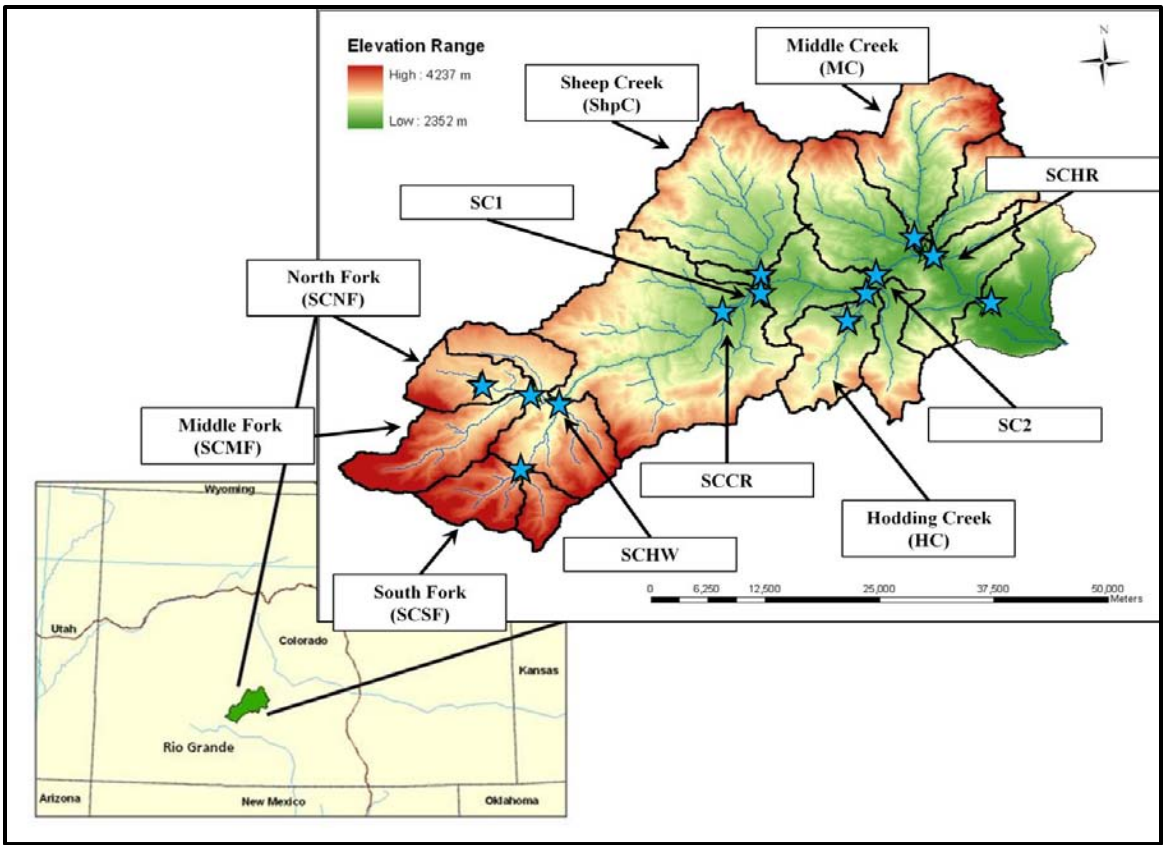

Figure 4.2: Map of Saguache Creek watershed. Blue stars indicate locations of stream sampling sites.

4.2.1: Geology of Saguache Creek:

A geologic map for Saguache Creek is shown in Figure 4.3. The geology of the Saguache Creek watershed is dominated by felsic volcanic tuffs resulting from the activity of the San Juan Volcanic Field (see Taf units in Figure 4.3) that overlie intermediate composition pre-caldera lavas and breccias (see Tpl units in Figure 4.3) from the Conejos/Rawley Formations [*Steven and Lipman*, 1976; *Lipman and McIntosh*, 2008]. The extent of the volcanic rim of the La Garita Caldera is indentified in Figure 4.3 by the dotted line. This caldera is massive and the presence of the caldera wall in the headwaters has likely played some role in the readjustment and development of local and intermediate groundwater flowpaths in the watershed. Rock glaciers and expansive talus-

covered regions are present in the steep headwater subwatersheds (see Ql units in Figure 4.3). Streams are not always bounded by extensive riparian zones except in the lower reaches of the watershed and these riparian zones are developed in the gravels and alluvium of the Pinedale and Bull Lake glaciations (see Qg units in Figure 4.3).

Soils in remote watersheds are not often classified beyond the soil association level since there is little agricultural or economic urgency to classify these soils at a finer resolution [*Engle,* 2009]. Therefore, we classified soils in the field using soil pits. These classifications indicated that the thin, high-elevation soils have little or no organic development, loamy AE horizons, and relatively weakly developed B-horizons. The soils typically contain fragments of biotite, quartz, and sodium and calcium-rich feldspars and often overlie fractured bedrock (Figure 4.4a). These soils are broadly classified by the NRCS as very stony loams of the Bushvalley-Embargo-Bowen soil association and cobbly or gravelly loams of the Frisco-Seitz-Granile soil association. Soil descriptions can be found at http://soils.usda.gov/survey/geography/statsgo/. Hillslope and low-elevation soils often contain a shallow, extensive layer of platy, felsic volcanic rocks which most likely promotes rapid infiltration and throughflow (Figure 4.4b). Saprolite was encountered in both high-elevation and low-elevation soil pits at depths ranging from 16 to 25 cm and persistent to depths greater than 40 cm. This layer serves as a translatory unit during snowmelt events that saturates from above and then slowly transmits water to the underlying fractured bedrock. Consequently, this layer may be an important control on recharge to bedrock aquifers within the mountain block.

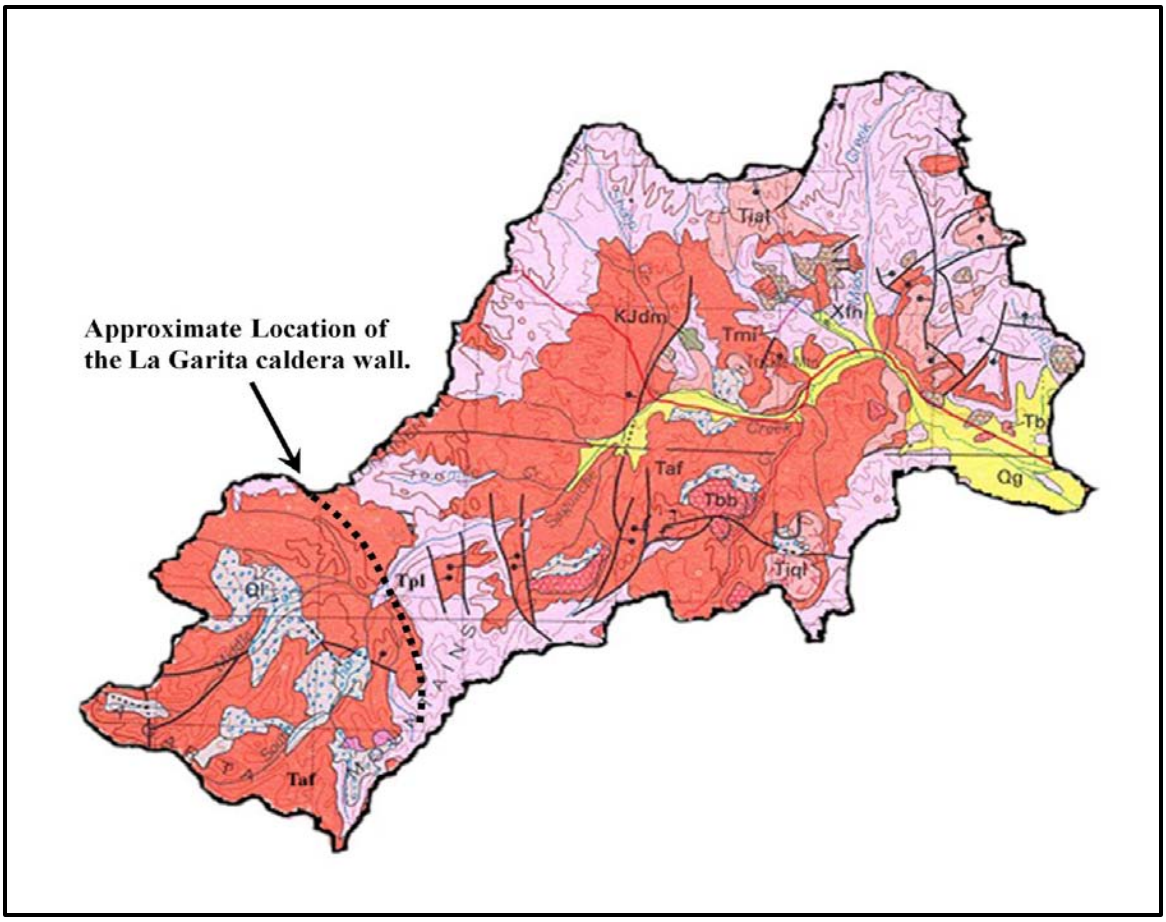

Figure 4.3: Geologic map of Saguache Creek watershed. Geological designations are as follows: Qg: gravels and alluvium from the Pinedale and Bull Lake glaciations, Ql: landslide deposits including thin talus, rock-glaciers, and thick colluvial deposits, Taf: ash-flow tuff of main volcanic sequence (26-30 Mya), Tpl: pre-ash-flow andesitic lavas, breccias, tuffs, and conglomerates (30-35 Mya), Tbb: basalt flows and associated tuffs, breccias, and conglomerates (3.5-26 Mya), Tial: intra-ash-flow andesitic lavas, and Tiql: intra-ash-flow quartz latitic lavas.
(http://geology.about.com/library/bl/maps/blcoloradomap.htm)

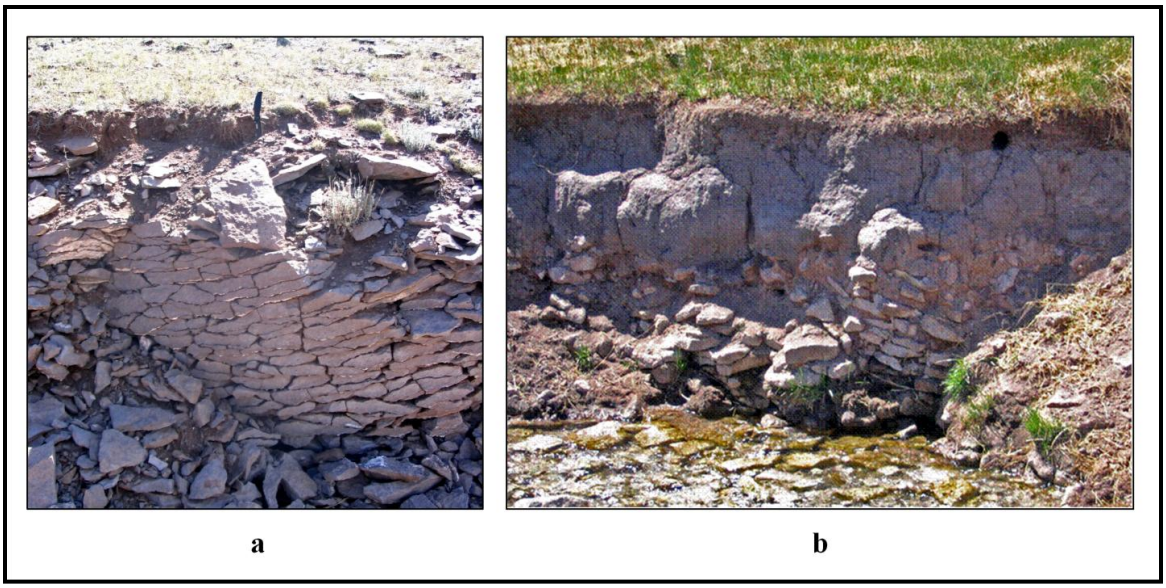

Figure 4.4: a) Soil development and underlying fractured bedrock at an elevation of 3139 m above sea-level. Note pocket knife for scale (length 19.5 cm). b) Typical hillslope soil development at an elevation of 2621 m above sea-level. Note the deposit of heavily fractured rhyolitic material near lower soil profile and the seep expansion following snowmelt that appears to originate from this layer.

4.3: Methods:

Streamflow samples were collected monthly during the ice-free season from 2005 to 2009 in nested headwater and tributary subwatersheds and longitudinally down the main channel of Saguache Creek. The results from 10 of those sampling sites will be presented in this paper (Figure 4.2). Samples were analyzed for pH, electrical conductivity (EC), total dissolved solids (TDS), and temperature while in the field. Field acidification was not performed on water samples since the samples were analyzed quickly after collection for chloride (Cl^-), calcium (Ca^{2+}), and sodium (Na^+) using ion-selective electrodes. Some samples were also subjected to a full general chemistry analysis of all basic cations and anions in the Chemistry Laboratory of the New Mexico Bureau of Geology and Mineral Resources located on the New Mexico Tech campus.

Analytical methods for chemical analyses and stable isotope analyses are included in the Appendix. The geochemical evolution of waters in the Saguache Creek watershed is shown in Figure 4.5 for reference.

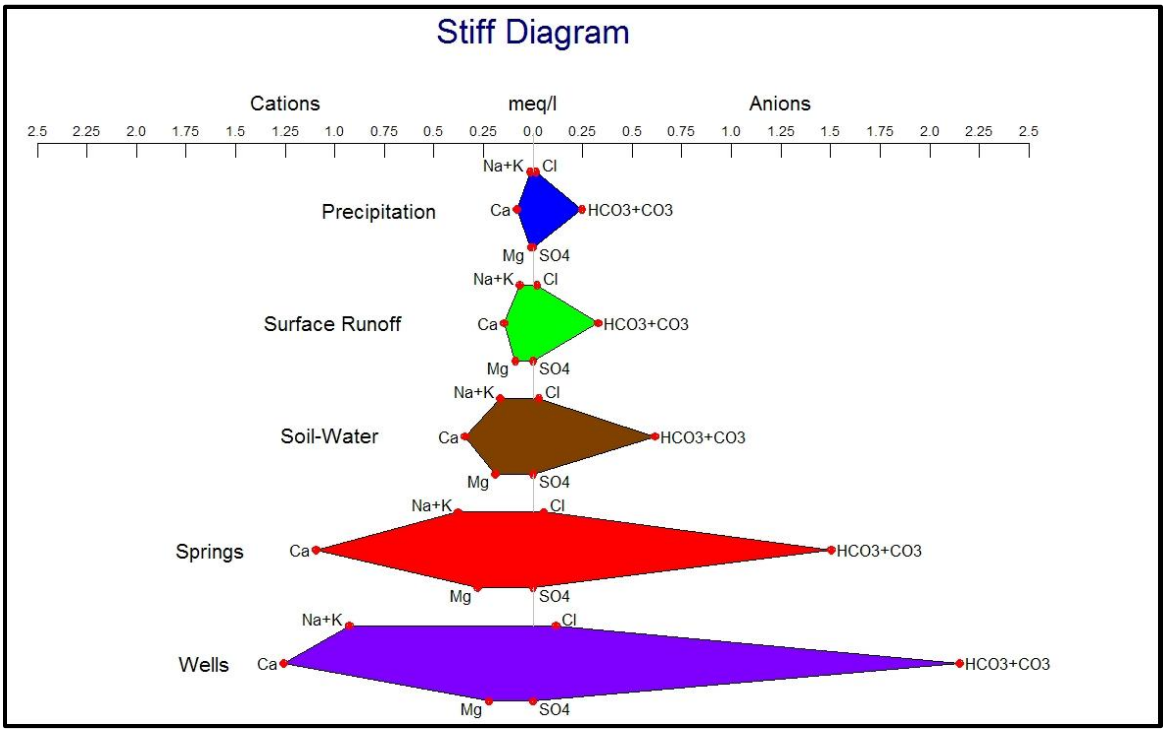

Figure 4.5: Stiff diagram showing the evolution of waters in the watershed. Overall average values for each endmember are shown.

In order to obtain water samples representative of longer residence times, springs and wells were sampled in the watershed. Seventeen perennial springs were sampled from 2005 to 2009. These springs span an elevation range from 2500 to 3400 m above sea level. Wells are sparse in the watershed and consequently only six wells were sampled. Most of these wells are located below an elevation of 2600 m above sea level. However, two wells were located in the backcountry at elevations of 2900 and 3100 m above sea level. All wells appear to terminate in the local bedrock. All well and spring samples were analyzed using the same procedures as streamflow samples.

Modified passive capillary samplers (M-PCAPS) were installed at remote, high elevation locations in the watershed to obtain samples of infiltrating meltwater during snowmelt and infiltrating rainwater during the summer precipitation season [*Frisbee et al.*, 2010a, 2010b]. At each installation, two M-PCAPS were installed at depths less than 10 cm and two were installed at depths greater than 20 cm, often within the saprolite layer located between 20 and 40 cm deep. The M-PCAPS were installed prior to the onset of snowpack accumulation during October 2007 and snowmelt infiltration samples were removed in June 2008. All M-PCAPS were left intact during the remainder of the 2008 summer season to sample soil-water during the summer precipitation season. Soil samples were collected near the M-PCAPS to compare with the data obtained via the M-PCAPS. Water collected from the M-PCAPS samples were subjected to the same analyses as stream water [*Frisbee et al.*, 2010b].

Mini-piezometers were installed in 11 streams in order to sample the chemical and stable isotopic composition of groundwater discharging to the stream through the streambed and to measure the vertical hydraulic gradient in the streambed [*Baxter et al.*, 2003; *Cey et al.*, 1998; *Pretty et al.*, 2006]. Our mini-piezometers were constructed from 1.5 m lengths of 2.2 cm CPVC pipe. A 20.3 cm ported interval was created in each pipe by drilling 0.16 cm holes at 2.54 cm intervals. A rubber stopper was plugged into the ported interval end of the pipe to be installed in the streambed and two small holes were drilled in the opposite end of the pipe beneath the cap to allow for pressure exchange within the pipe. The mini-piezometers were installed at depths ranging from 0.80 m to approximately 1.10 m according to the methodology presented in *Baxter et al.* [2003]. Mini-piezometers were pumped and allowed to refill prior to sampling. Samples were

retrieved on a monthly basis from installation in June 2008 to removal in October 2008. These samples were subjected to the same analyses as stream water.

Rainfall was collected during the months of April through September of 2007 and 2008 from 11 precipitation collectors installed at elevations ranging from 2530 to 3220 m above sea level. These collectors were constructed following the work of *Earman et al.* [2006]. Fresh early-season snow (October through February) and fresh late-season snow (March through late May) were collected from 2006 through 2008. Remnant snowpack and snowmelt surface runoff (often encountered in May) were collected during the snowmelt seasons of 2006 through 2009. Bulk and modified snowfall collectors were constructed by modifying the designs presented in *Earman et al.* [2006]. These collectors were installed in October 2007 at remote, high-elevation sites in the watershed prior to the onset of snowpack accumulation during October 2007 and removed in June of 2008 [*Frisbee et al.,* 2010b]. Rainfall, snowfall, and snowmelt runoff samples were subject to the same analyses as stream water.

Our hydrochemical dataset reveals that concentrations in stream chemistry are structured and increase in a linear fashion with increasing accumulated watershed area with the exception of North Fork (Figure 4.6). The North Fork is chemically very different than nearby Middle Fork or South Fork because it drains a subwatershed characterized by lower elevations (maximum elevation is 3110 m above sea level) and streamflow receives inputs from a conveyance ditch in the upper reaches of this stream. The geochemical evolution of waters in the Saguache Creek watershed appears to be controlled by relatively rapid geochemical transformations in the soil [*Frisbee et al.,* 2010b] and much slower geochemical transformations in the bedrock aquifer [*Frisbee et*

al., 2010c]. Results from our weathering study in the watershed indicate that chemical weathering of bedrock minerals, namely sodium and calcium-rich feldspars, potassium feldspar, biotite, quartz, and hornblende, is the primary source of solute release to groundwater, streamflow, and springflow. Other studies have also indicated that chemical weathering is the dominant process responsible for solute and mass release in alpine environments [*Dixon and Thorn,* 2005]. The chemical weathering of bedrock is a kinetically controlled process and the release of solutes from bedrock due to weathering is directly related to the residence time of the water in the bedrock. Therefore, short-residence time groundwaters will not be as geochemically evolved as long-residence time groundwaters. From a Tóthian-flow perspective, we can envision a suite of flowpath lengths and tortuousities in the watershed, with water discharging from each flowpath having a distinct geochemical signature and residence time distribution. If components of groundwater characterized by long-residence times are being discharged to the stream, we would expect to see geochemical enrichment in the stream water even if the long-residence time groundwater mixes with younger waters in the hyporheic zone (Figure 4.1e, h). On the other hand, if components of long-residence time groundwater are insignificant, then we may not see evidence of geochemical enrichment with increasing scale (i.e., the geochemical evolution of waters will be controlled by geochemical transformations only along the surface and shallow subsurface flowpaths indicated in Figures 4.1a, d).

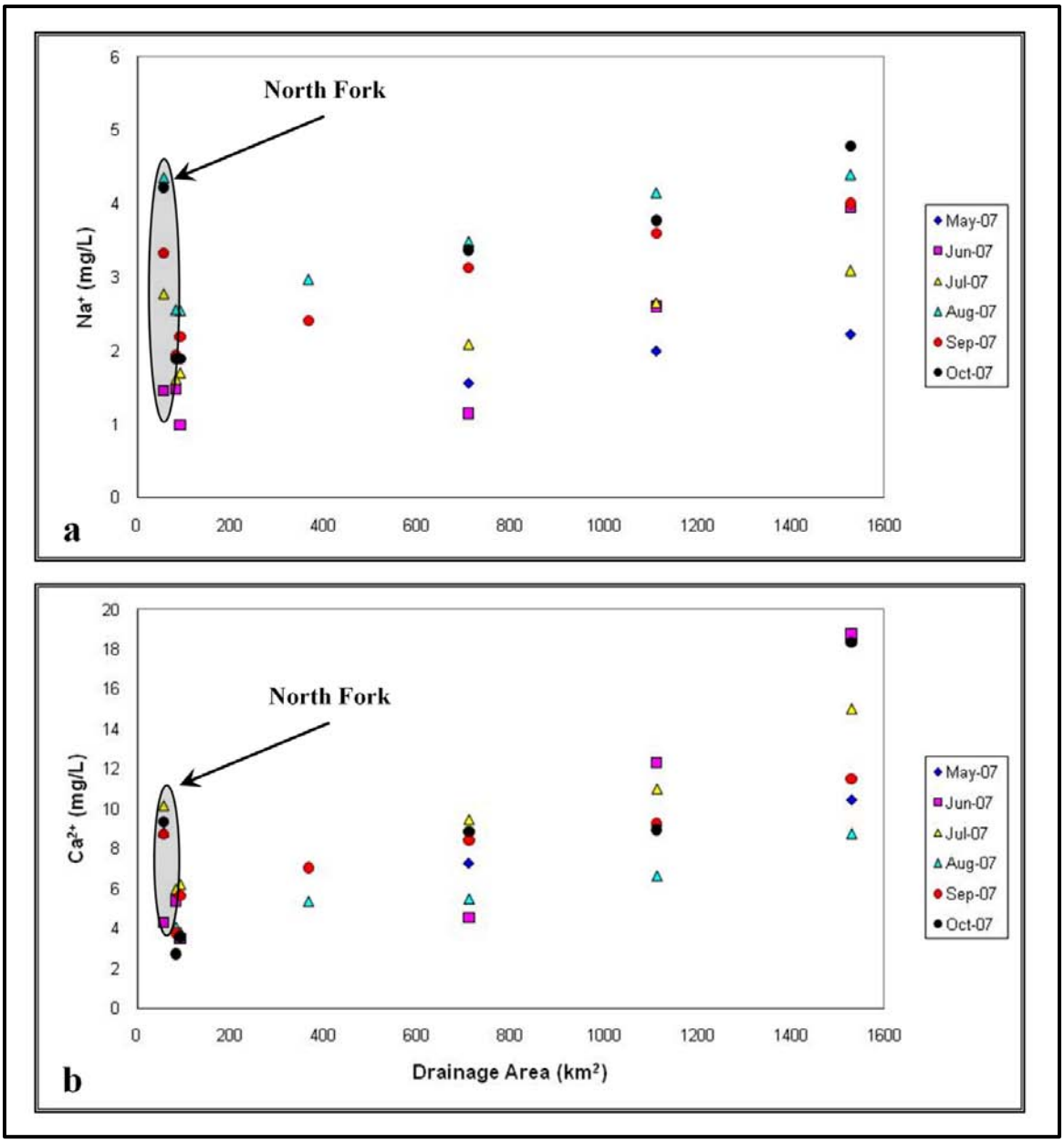

Figure 4.6: Trends in Na^+ and Ca^{2+} with accumulated subwatershed area. Note the development of linear trends in stream chemistry as drainage area increases.

4.3.1: End-Member Mixing Analysis:

End-member mixing analysis utilizes principal component analysis techniques in order to reduce datasets of streamflow chemistry so that chemical constituents and endmembers are identified that explain the greatest amount of variability in the chemical dataset. No *a priori* information about the endmember population is needed. This is a well-established methodology that has been used to identify endmembers responsible for runoff generation in hillslopes, small catchments, and large watersheds spanning a range of geographic, geologic, climatic, and environmental conditions [*Christophersen and Hooper,* 1992; *Hooper,* 2003; *Liu et al.,* 2004, 2008]. Diagnostic tools of mixing are first applied to select conservative tracers and to determine the dimension of the mixing subspace. In our sample collection, EC, Ca^{2+}, Na^{+}, Cl^{-}, $\delta^{18}O$, and $\delta^{2}H$ were continuously monitored over the period of study so these were the tracers tested for conservative behavior in EMMA. End-member mixing analysis is then used to identify endmembers and to calculate the proportions of endmembers in the stream samples [*Christophersen and Hooper,* 1992]. A principal component analysis is performed on the conservative tracers of the endmember matrix. Eigenvectors are extracted from the correlation matrix of conservative tracers and these eigenvectors are used to re-project both streamflow samples and endmember samples into a mixing subspace [*Liu et al.,* 2008]. The orthogonal projections of the streamflow samples and endmembers are then used to calculate the mixing proportions of each endmember. The re-projected concentrations of each individual constituent are then plotted against actual concentrations to ascertain how well the model recreated stream chemistry. A well-posed model produces high R^2 ($R^2 > 0.70$) when the two concentrations are fit with a linear trendline; in other words, the re-

projected chemistry is very similar to the actual measured chemistry [see *Liu et al.,* 2008].

4.3.2: Diagnostic Tools of Mixing Models:

In our EMMA analyses, diagnostic tools of mixing models were first applied to streamflow samples in order to ascertain the conservative behavior of tracers and to determine the number of end-members to be retained in further analyses [*Christophersen and Hooper,* 1992; *Hooper,* 2003; *Liu et al.,* 2004, 2008]. In our study, we follow the work of *Liu et al.* [2008]. Streamflow chemistry was re-projected using eigenvectors extracted from the correlation matrix of the streamflow chemistry dataset. Residuals calculated from the re-projected streamflow chemistry and original chemistry dataset were used to ascertain the "fit" or appropriateness of the tracers. Random distributions ($p > 0.05$ and $R^2 < 0.2$) in the plot of residuals versus actual chemical concentration of chemical constituent indicated a well-posed model while structure in the plot indicated a poorly constrained model [*Hooper,* 2003; *Liu et al.,* 2008]. The relative root-mean square error (RRMSE) was also used to ascertain model "fit". In a well-posed model, the RRMSE typically decreased for any given constituent from one lower dimensional mixing subspace to the next lower dimensional subspace (e.g. from 1-D to 2-D subspace). This behavior provided an indication of the rank of X which is equal to the number of endmembers to be retained minus one (X = EM -1).

4.3.3: Selection of Endmembers:

The selection of endmembers is a critical process in any study employing endmember mixing analyses and streamflow separation in general because the endmembers must be unique. In order for this condition to be true, the endmembers must

obtain their unique geochemical and isotopic compositions through different evolutionary pathways. In other words, different runoff processes will be affected by and will reflect different geochemical transformations. For example, in order for rapid surface runoff from snowmelt to be distinguished from deep, subsurface runoff, the two types of runoff must be geochemically and isotopically distinct. The deep, subsurface runoff will characteristically have a longer residence time, consequently rock/water interactions will be enhanced leading to different geochemistry.

We attempted to sample all of the significant geochemical endmembers in our study area. We monitored water samples from wells, springs, streams, soil (subsurface runoff), surface runoff (during snowmelt and rainfall events), late-season snowpack, fresh snowfall, and rainfall. Rainfall and fresh snowfall were monitored because they represent beginning points in the geochemical evolution of water in a watershed. In general, rainfall and fresh snowfall are both chemically dilute and show little chemical variation with elevation. Furthermore, we discovered that late-season fresh snow from March through May was geochemically and isotopically distinct from early-season fresh snow from October through February. We, therefore, specified two endmembers to represent fresh snowfall: early-season and late-season. A volume-weighted average of the chemical and isotopic composition of rainfall was used for the rainfall endmember. Rainfall amounts vary monthly during the growing season and in general, most of the summer precipitation falls during July, August, and September. Significant monthly variability in the chemical composition of rainfall was not observed. However, the stable isotope composition becomes isotopically heavier as the season progresses from May to October.

In this study, surface runoff from late-season snowpacks and surface runoff from rainfall were lumped into one endmember for two reasons. First, the geochemical composition of surface runoff from remnant snowpacks was not distinctly different than surface runoff collected during rainfall events. Snowpacks develop as fresh snowfall begins to accumulate during the winter season and this snowpack will acquire minerals and nutrients, primarily from aeolian deposition [*Clow et al.,* 2002; *Frisbee et al.,* 2010b]. As the snowpack begins to melt, these accumulated minerals and nutrients are dissolved or entrained in the direct runoff from the snowpacks. The runoff from these snowpacks will therefore be chemically enriched relative to fresh snow, but since the contact time with soil is limited, further geochemical evolution cannot be achieved. Rainfall is also very dilute and surface runoff from rainfall will be chemically enriched relative to the composition of rainfall itself. Runoff from snowpacks and runoff from rainfall are similar geochemically. Second, the majority of surface runoff is generated during the snowmelt season when conditions are conducive to the generation of surface runoff. In comparison, conditions are not always conducive to the generation of surface runoff during the summer rainfall season and surface runoff was not frequently observed during field campaigns. Therefore, we used one surface runoff endmember.

Further geochemical evolution is achieved when runoff, or direct inputs from rainfall, snowfall, or snowmelt, infiltrate the soil and create subsurface runoff. We monitored soilwater to constrain the shallow subsurface runoff component. Geochemical transformations can be quite rapid in soil and lengthy residence times are not always needed to obtain significant geochemical evolution in the soil [*Davis,* 1964; *Kennedy,* 1970; *Campbell et al.,* 1995; *Frisbee et al.,* 2010b]. Fresh meteoric inputs are the

beginning points in the geochemical evolution of water in a watershed and surface runoff and shallow subsurface runoff are intermediate stages of geochemical evolution. Subsurface runoff will be more geochemically evolved than surface runoff. The importance of these components may vary considerably within a given watershed. As a consequence, in a simple mixing diagram where meteoric inputs are beginning points in the geochemical evolution of water and groundwater is an endpoint in the geochemical evolution of water, surface runoff and subsurface runoff components are usually located as intermediate stages between the meteoric inputs and older, more geochemically evolved endpoints.

Inputs of rainfall, snowfall, snowmelt, or subsurface runoff that percolate into the underlying fractured bedrock may ultimately recharge the bedrock aquifer. This groundwater may become the source of water for springs and wells and may discharge to streams to support streamflow. We monitored water samples from wells and springs since they are potential points of access to the groundwater flowing in the local bedrock aquifer. Geochemical transformations in the saturated bedrock are controlled by flow velocities, residence times, rates of kinetic weathering of minerals, and supply of weatherable material in the bedrock [*Goldich,* 1938]. Deep basin-scale groundwater has longer residence times than water from shallow, fast runoff processes and this enhances rock-water interactions [*Lasaga,* 1984; *Bricker and Jones,* 1995]. Water from the bedrock aquifer should thus represent an approximate endpoint in chemical evolution within a watershed. In order to characterize the groundwater discharge to the streams, we analyzed water samples from mini-piezometers installed in streambeds [*Baxter et al.,* 2003]. Each stage of runoff represents a distinct progression in the geochemical

evolution of waters within a watershed as indicated in Figure 4.5 for the Saguache Creek watershed.

4.3.4: Measurement of Vertical Hydraulic Gradients:

We measured the vertical hydraulic gradient (VHG) in each mini-piezometer according to the methodology presented in *Baxter et al.* [2003]. VHG is equal to $\Delta h/\Delta L$; where Δh is the difference in head between the water level at the stream surface and the water level in the mini-piezometer and ΔL is the length of the mini-piezometer from the streambed surface to the top of the ported interval of the mini-piezometer installed below the streambed surface. The water levels were measured relative to the top of the mini-piezometer. Groundwater discharge to the stream is indicated by a positive value for Δh (i.e. the water level in the mini-piezometer is higher than the water level at the stream surface) whereas, downward infiltration from the stream is indicated by a negative value for Δh.

4.3.5: Analytical Methods:

Each water sample was analyzed for $\delta^{18}O$ and $\delta^{2}H$. The $\delta^{18}O$ composition was measured on 1 mL samples of water using the CO_2 / H_2O equilibration method described in *Clark and Fritz* [1997] using a Thermo Finnigan Gasbench operated in continuous flow mode. The $\delta^{2}H$ hydrogen gas was generated by metal reduction with powdered chromium at 850°C in an H-Device [*Nelson and Dettman,* 2001] and analyzed in dual inlet mode. Both CO_2 and H_2 were analyzed on a Thermo Finnigan Delta^{PLUS} XP Stable Isotope Ratio Mass Spectrometer. Water was vacuum distilled from the soil samples using the vacuum distillation method described in the work of *Araguás-Araguás et al.* [1995] and analyzed for $\delta^{18}O$ and $\delta^{2}H$. The variability in $\delta^{18}O$ and $\delta^{2}H$ was ascertained

by analyzing sixty-seven $\delta^{18}O$ duplicates and seventy-four $\delta^{2}H$ duplicates. Variability in $\delta^{18}O$ ranged from 0.0 to 1.0 ‰ (average variability was 0.2 ‰). The duplicates of $\delta^{2}H$ varied from 0 to 2 ‰ (average variability was 1 ‰).

All water samples, with the exception of the soil distillation samples, were also analyzed for standard chemistry including field measurements of pH, EC, and TDS. Ion-selective electrodes were used to measure chloride (Cl^{-}), calcium (Ca^{2+}), and sodium (Na^{+}) and these constituents were also analyzed in the Chemical Laboratory of the New Mexico Bureau of Geology and Mineral Resources located on the New Mexico Tech campus in order to corroborate the ion-selective measurements. Basic cations, anions, and silica were measured at the Chemistry Laboratory. Anions were measured with a Dionex IC, DX-600 System with GS50 Gradient Pump, CD25 Conductivity Detector, AG14 Guard Column, and As14 Analytical Column per USEPA 300.0. Analyses were made with a 4-point calibration and the calibration and blanks were checked at the beginning and end of each run and after every 10^{th} sample. Cations were measured with a PE Optima 5300 DV ICP-OES per USEPA 200.8/6020. Analyses were made with a 3-point calibration and quality control procedures were the same as for anions. The charge imbalance for all samples was acceptable and ranged from -0.98 to 3.54 percent. Duplicates were performed on water samples to assess analytical error (i.e. to assess the variability in anions, cations and silica between original and duplicate). To do this, we calculated the range in absolute variability between original samples and duplicates as well as the overall average absolute variability in the anion, cation, and silica dataset. The absolute variability of anion duplicates ranged from 0 to 0.3 mg/L (the average absolute variability was 0.03 mg/L). The absolute variability of cation duplicates ranged

from 0 to 1 mg/L (the average absolute variability was 0.08 mg/L). Duplicates for silica varied from 0 to 0.01 and the average absolute variability was approximately 0.01 mg/L.

4.4: Results:

4.4.1: Endmember Contributions in Headwater Subwatersheds:

The Saguache Creek watershed has three headwater subwatersheds: the North Fork (SCNF), Middle Fork (SCMF), and South Fork (SCSF) of Saguache Creek (Figure 4.2). These have areas of 56.2, 91.6, and 82.3 km^2, respectively. The North Fork is chemically very different than nearby Middle Fork or South Fork because it drains a subwatershed characterized by lower elevations (maximum elevation is 3110 m above sea level) and streamflow receives inputs from a conveyance ditch in the upper reaches of this stream. Streamflow chemistry in North Fork varies little seasonally and instead retains an evolved groundwater signature year-round in comparison to Middle and South Fork, both of which have seasonally variable stream chemistry. The Middle Fork drains a high-elevation (maximum elevation is 4237 m above sea level) subwatershed and the South Fork also drains a high-elevation (maximum elevation is 3900 m above sea level) subwatershed that is geologically similar to Middle Fork. Stream samples from all three headwater subwatersheds could be plotted in 2-D mixing subspaces requiring 3 endmembers. To conserve space, the data from the correlations between the re-projected stream chemistry and actual stream chemistry for all stream sampling sites are compiled in Table 4.1. This data includes the R^2 correlation coefficient, the p-value that indicates how different the slope of the correlation line is from a slope equal to zero, and the dimension (D) of the mixing subspace where the endmembers to be retained are equal to

D + 1. The *U*-space projections for North Fork and Middle Fork are shown in Figure 4.7 and the *U*-space projection for South Fork is shown in Figure 4.9a. The separated streamflows for North and Middle Fork are shown in Figure 4.8 and the separated streamflow for South Fork is shown in Figure 4.10a.

Stream ID	EC (μS/cm)			Ca^{2+} (mg/L)			Na^{+} (mg/L)			Cl^{-} (mg/L)			$\delta^{18}O$ (‰)			$\delta^{2}H$ (‰)		
	R^2	p	D	R^2	p	D	R^2	p	D	R^2	p	D	R^2	p	D	R^2	p	D
SCNF	0.11	0.36	2	0.14	0.29	2	0.08	0.44	2	0.11	0.35	3	0.24	0.15	2	0.07	0.47	2
SCMF	0.16	0.25	2	0.13	0.30	2	0.09	0.40	2	0.04	0.58	3	0.09	0.40	2	0.01	0.77	2
SCSF	0.08	0.41	2	0.16	0.22	2	0.32	0.09	2	0.10	0.37	3	0.07	0.42	3	0.04	0.53	2
HC	0.13	0.25	3	0.32	0.05	2	0.14	0.24	2	0.13	0.25	3	0.10	0.32	2	0.12	0.28	2
ShpC	0.07	0.41	2	0.19	0.16	2	0.07	0.46	2	0.23	0.12	2	0.16	0.20	2	0.003	0.87	3
MC	0.29	0.06	2	0.17	0.16	2	0.06	0.43	2	0.08	0.36	3	0.15	0.19	2	0.32	0.05	2
SCCR	0.18	0.57	2	0.39	0.38	2	0.39	0.37	2	0.44	0.34	2	0.46	0.32	2	0.75	0.13	2
SC1	0.17	0.12	2	0.05	0.41	3	0.13	0.18	2	0.26	0.05	2	0.16	0.14	2	0.19	0.11	2
SC2	0.16	0.12	2	0.12	0.19	3	0.01	0.69	4	0.08	0.30	3	0.11	0.22	2	0.25	0.05	2
SCHR*	0.10	0.80	1	0.08	0.82	1	0.08	0.82	1	0.24	0.67	1	0.71	0.36	1	0.08	0.82	1

Table 4.1: Data from the correlations between residuals of re-projected stream chemistry and original stream chemistry for each sampling site. Random distributions in the plots, indicated by $p > 0.05$ and $R^2 < 0.2$, indicate well-posed models while structure in the plot indicates poorly constrained models. R^2 is the correlation coefficient, p-value describes how significantly different the slope of the correlation line is from a value of zero for $p > 0.05$, and D is the dimension of the mixing subspace where the required number of endmembers is equal to D + 1. The degrees of freedom are low for SCHR due to limited sampling. Please see Figure 4.2 for locations of stream sampling sites.

All three headwater subwatersheds have drainage areas less than the critical area of 300 km^2 (Figure 4.1). The steep topography and climatology of these subwatersheds is conducive to small-scale runoff processes such as overland flow or shallow subsurface flow. In fact, the EMMA results indicated that late season snow and rainfall were strong endmembers for all three headwater subwatersheds. As mentioned above, runoff generated over the soil will typically have a different chemistry than runoff flowing through the soil since the extent of chemical evolution is directly related to the residence

time of water in the soil or bedrock. In this case, the late season snow and rainfall endmembers are both relatively dilute and chemically distinct from soil-water and groundwater (Figure 4.5). In order for these dilute chemical signatures to constitute a significant component of streamflow, geochemical transformations during the runoff process must be minimal. These results confirm that rapid runoff processes are important in streamflow generation in the headwater subwatersheds.

The groundwater components represented by the water samples from the mini-piezometers were selected as the third endmember for each headwater stream. The chemistries of all the mini-piezometer water samples plotted very close to the chemistry of the water from Stone Cellar well (Figures 4.7 and 4.9a). Streamflow generation in South Fork and Middle Fork was controlled mostly by event contributions from rainfall and late season snow in 2007 and early 2008 and primarily by groundwater and late season snow in late 2008 (Figures 4.8b and 4.10a). The velocity-area method described in *Dingman,* [2002] was used to measure discharge in all the streams presented in this paper. Stream discharge was measured at each sampling site on a monthly basis in 2007 and 2008. In comparison, streamflow generation in North Fork relies less upon event water and more upon groundwater (Figure 4.8a). Overall, groundwater accounts for 14 to 44 percent of streamflow generation during the peak of the snowmelt freshet and it accounts for 19 to 78 percent of baseflow generation. The strength of the groundwater endmember during the peak of snowmelt is surprising given the large volume of event water that these small, high-elevation subwatersheds convey during the snowmelt season. This is an important finding that indicates groundwater flowpaths are well-developed in the headwater subwatersheds and in drainage areas smaller than the critical area of 300

km^2. This finding also indicates that we should not ignore the contribution of groundwater in small, high-elevation drainages. In summary, streamflow generation in the headwater subwatersheds appears to be a combination of contributions from rapid runoff mechanisms and relatively consistent contributions from deeper groundwater from the local groundwater flow system.

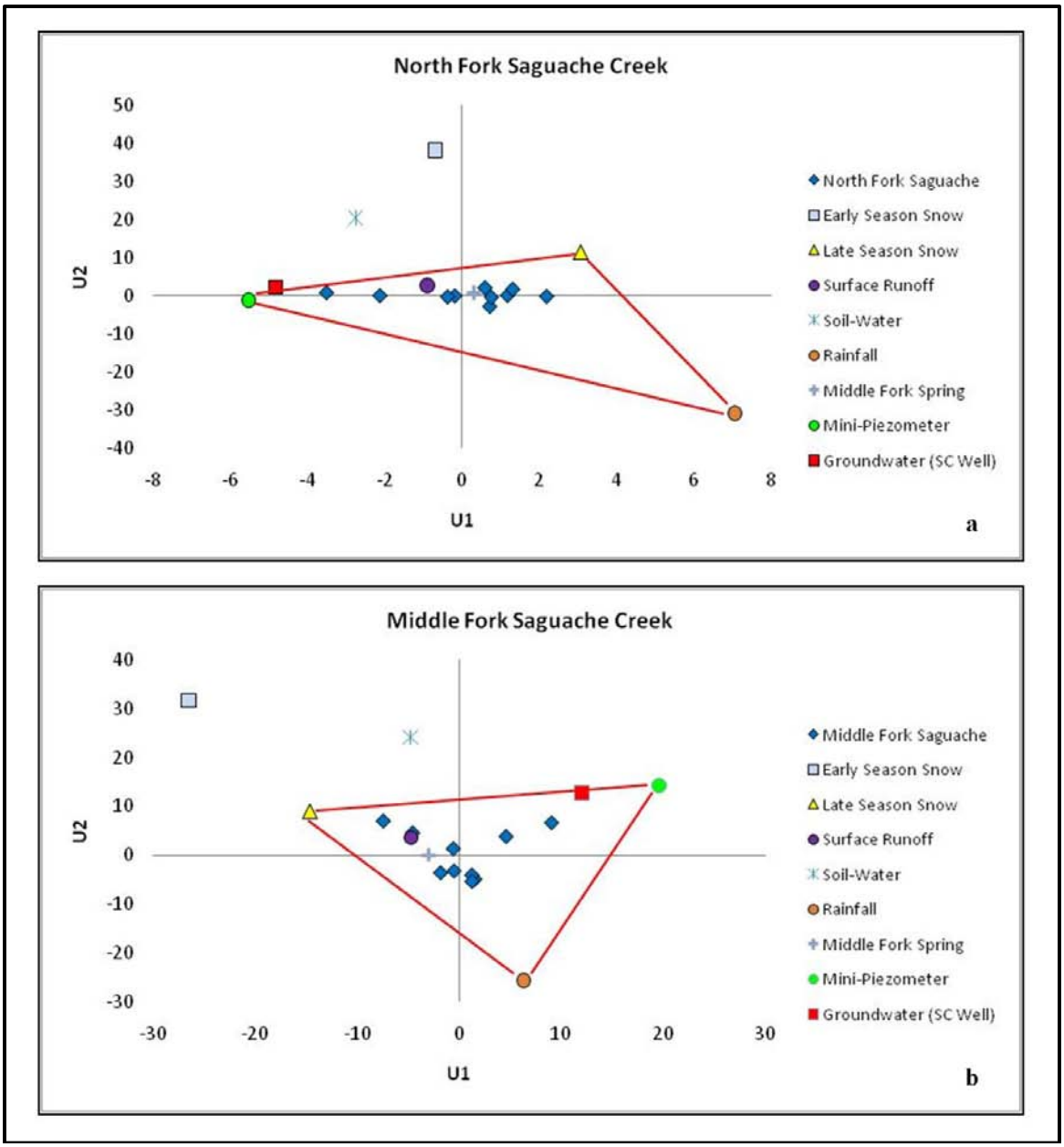

Figure 4.7: U-space mixing diagram for a) North Fork and b) Middle Fork. North Fork drains an area of 56.2 km^2 and Middle Fork drains an area of 91.6 km^2.

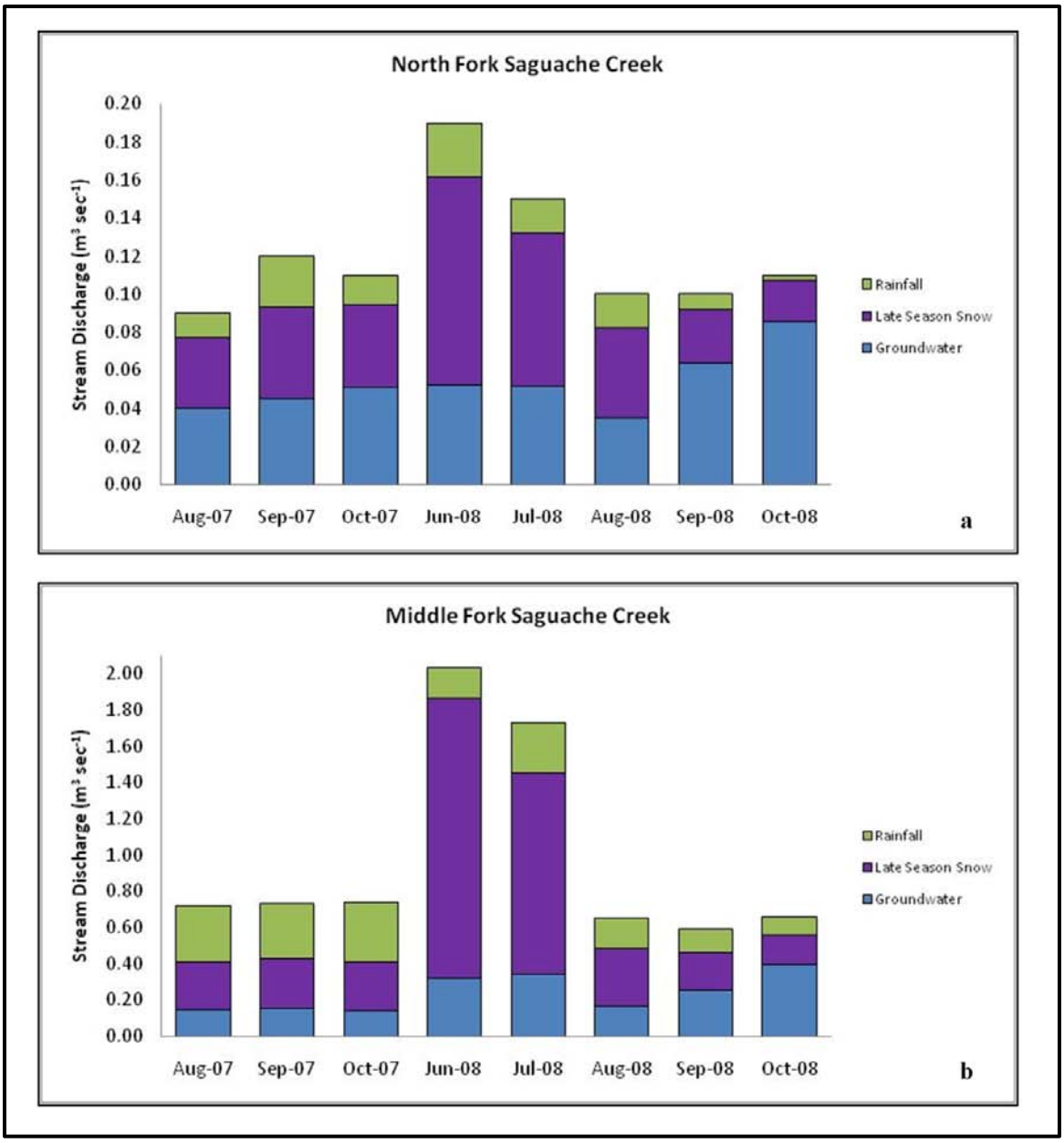

Figure 4.8: Streamflow separations for a) North Fork and b) Middle Fork. The y-axis is flow from individual components expressed in units of m^3 sec^{-1}.

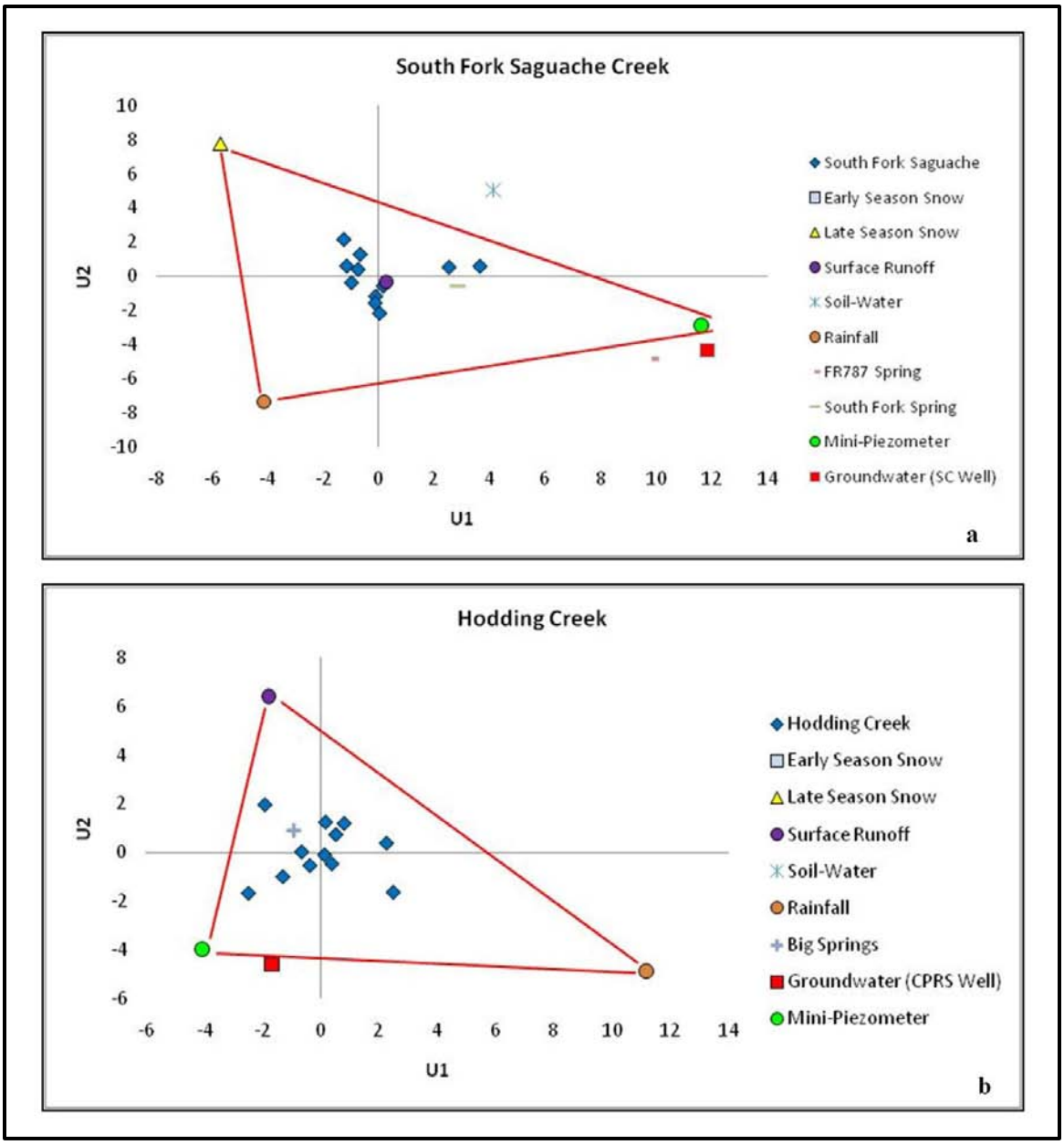

Figure 4.9: U-space mixing diagram for a) South Fork and b) Hodding Creek. South Fork drains an area of 82.3 km^2 and Hodding Creek drains an area of 80.7 km^2.

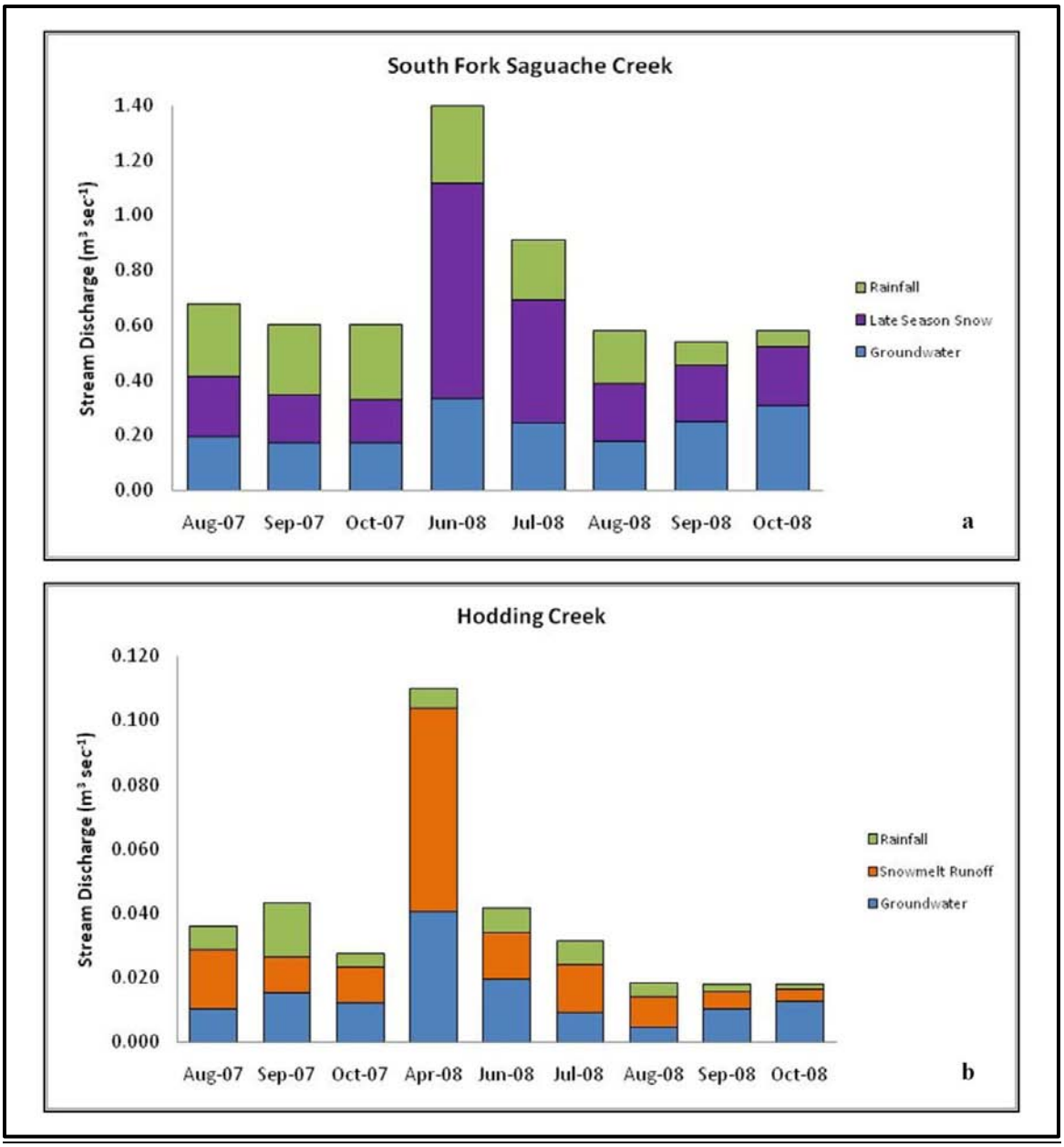

Figure 4.10: Streamflow separations for a) South Fork and b) Hodding Creek. The y-axis is flow from individual components expressed in units of m^3 sec^{-1}.

4.4.2: Endmember Contributions in Tributary Subwatersheds:

The Saguache Creek watershed has four primary tributary subwatersheds: Hodding Creek, Sheep Creek, Middle Creek and Ford Creek (Figure 4.2). Ford Creek, located near Middle Creek, was not sampled regularly due to an ongoing stream restoration project in the headwaters of its drainage. These first subwatersheds have areas of 80.7, 192.2, and 141.6 km^2, respectively but they do not have elevation gradients as high as those encountered in the headwater subwatersheds. The average elevation at the watershed divide in all three tributary subwatersheds ranges from 3110 m to 3410 m. The topography is not as steep as it is in the headwater subwatersheds and as a consequence, soils thicken as elevation and slope decrease (Figures 4.2 and 4.4). Snowfall, snowpack development, and temperature are strongly correlated with elevation in the San Juan Mountains. Therefore, thinner snowpacks and differences in the timing and amount of snowmelt runoff are expected in the tributary subwatersheds which drain lower elevations. Snowmelt in the headwater subwatersheds may occur gradually over the course of 3 or 4 months and snowmelt runoff may persist for a similar length of time. At some point during the snowmelt season, the characteristically thin alpine soils become saturated and saturation-excess overland runoff is common. In comparison, the lower elevation subwatersheds have deeper soil development and the snowmelt season starts earlier and does not last as long. Field observations indicated that low-elevation snowpacks are typically depleted by early April. In comparison, snowpacks can be persistent through early June at mid-elevation sites and early August at high-elevation sites. The snowmelt season in these tributary subwatersheds may only last 2 or 3 months. As a consequence, saturated soils may not always be encountered and instead, these

conditions may promote enhanced infiltration of snowmelt runoff and replenishment of soil-water storage [*Wilson and Guan,* 2004]. These physical factors have a direct influence on runoff generation in the tributary subwatersheds and on changes in dominant runoff mechanisms between headwater and tributary subwatersheds.

One difference in endmember contributions was observed between the tributary and the headwater subwatersheds and this difference reflects an important change in dominant runoff mechanisms. EMMA results indicated that the late season snow endmember is replaced with the snowmelt runoff endmember in Hodding Creek (Figure 4.9b) and with the soil-water endmember in Sheep Creek and Middle Creek (Figure 4.11). Again, it is important to note that snowmelt runoff is more chemically evolved than late season snow and soil-water is more chemically evolved than snowmelt runoff. The chemical distinction between these endmembers is due to the differences in runoff generation and the media through which runoff is flowing. The snowmelt runoff and soil-water endmembers are large contributors to streamflow generation in the tributary subwatersheds. In our study, we defined snowmelt surface runoff as overland flow and very shallow subsurface flow through forest litter and thin talus. Snowmelt runoff is a rapid runoff mechanism that accounts for between 35 to 52 percent of streamflow generation during the snowmelt freshet (Figure 4.10b). Soil-water is a major contributor to streamflow generation in Sheep Creek and Middle Creek. Soil-water accounts for 44 to 55 percent of streamflow generation during the snowmelt freshet in Sheep Creek and for 44 to 64 percent of streamflow generation in Middle Creek. During baseflow, soil-water accounts for 23 to 66 percent of streamflow generation in Sheep Creek and for 34 to 55 percent of streamflow generation in Middle Creek (Figure 4.12). These three

tributary subwatersheds have drainage areas less than the critical area of 300 km^2 and the shift in dominant endmembers represents a coincident shift in runoff generation processes in drainages smaller than the critical area. Rapid runoff processes are important in the headwater subwatersheds but these processes diminish in importance as scale increases to the tributary subwatersheds.

Groundwater was also a significant contributor to streamflow generation in all three tributary subwatersheds. In Hodding Creek (Figure 4.9b) and Middle Creek (Figure 4.11b), the water samples from the mini-piezometers plotted as distinct endmembers. The mini-piezometer in Hodding Creek plotted near the CPRS Well in the *U*-space mixing diagram providing support that it was sampling waters that were geochemically similar to local groundwater. However, the mini-piezometer in Middle Creek did not plot near a local well and could not be correlated with a groundwater well in the subwatershed. The chemistry of the water sampled by this mini-piezometer is, however, similar to other groundwater sources in the Saguache Creek watershed. In Sheep Creek (Figure 4.11a), the mini-piezometer plotted within the mixing subspace indicating that it was sampling water that had a mixed chemical signature representing the integration of water sources. A groundwater well (EN Well) located near the stream sampling site provided the groundwater endmember in this case. During the snowmelt freshet, groundwater accounted for 20 to 46 percent of streamflow generation in Hodding Creek, 2 to 15 percent of streamflow generation in Sheep Creek, and 2 to 21 percent of streamflow generation in Middle Creek. Groundwater contributions to baseflow were higher. During baseflow, groundwater accounted for 35 to 71 percent of streamflow generation in Hodding Creek, 16 to 54 percent of streamflow generation in Sheep Creek,

and 21 to 35 percent of streamflow generation in Middle Creek (Figures 4.10b and 4.12). In summary, streamflow generation in the tributary subwatersheds appears to be a combination of minor contributions from fast runoff mechanisms, large contributions from slow runoff mechanisms, and consistent contributions from deep groundwater.

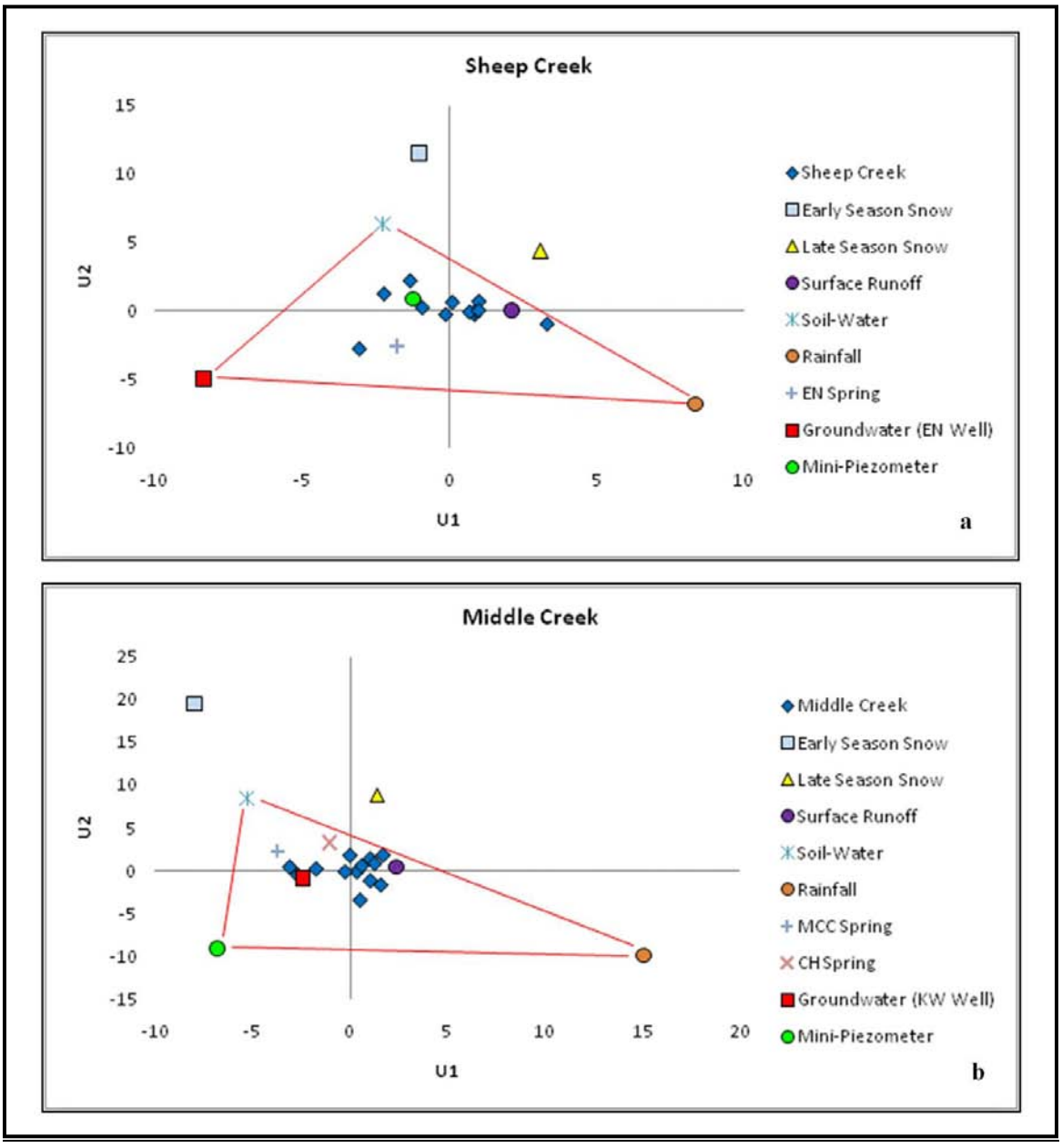

Figure 4.11: U-space mixing diagram for a) Sheep Creek and b) Middle Creek. Sheep Creek drains an area of 192.2 km^2 and Middle Creek drains an area of 141.6 km^2.

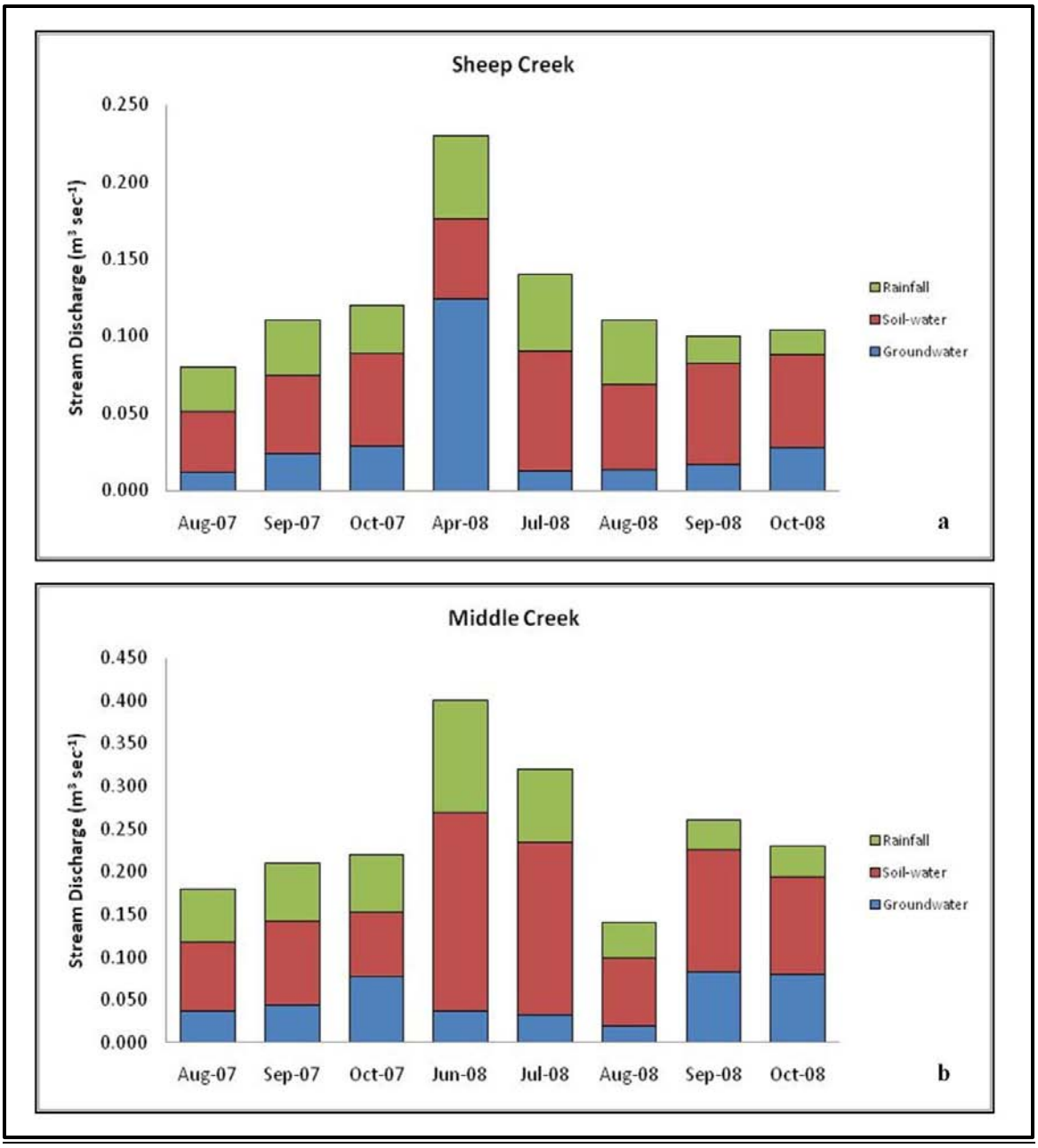

Figure 4.12: Streamflow separations for a) Sheep Creek and b) Middle Creek. The y-axis is flow from individual components expressed in units of m^3 sec^{-1}.

4.4.3: Endmember Contributions in Saguache Creek:

Saguache Creek was sampled longitudinally downstream from the confluence of the headwater streams (SCHW) to the sampling site near the outlet on the Hill Ranch (SCHR, Figure 4.2). Saguache Creek is a gaining stream upstream of SCHR but changes to a losing stream downstream of SCHR due to groundwater pumping for irrigation in the northern San Luis Valley and diversions for the town of Saguache, CO. Mini-piezometers were maintained at all locations with the exception of the site located at the confluence of the headwater streams. The mini-piezometers at SCHW were repeatedly vandalized or stolen; therefore, no mini-piezometer data is available at this site. The SCHW, SCCR, SC1, SC2, and SCHR sampling sites represent accumulated watershed areas of 366, 543, 710, 1112, and 1447 km^2, respectively. In the low-elevation reaches of Saguache Creek, the stream is bounded by a narrow riparian corridor and floodplain (Figure 4.3). The floodplain is itself bounded by cliffs of volcanic bedrock in much of the downstream reach and this land is used for grazing and non-irrigated hay fields.

Rainfall, soil-water, and groundwater were selected as the three endmembers for sampling sites SCHW and SCCR that are located in the upper reach of the main channel of Saguache Creek. In the lower reach of Saguache Creek, rainfall, late season snow, and groundwater were selected as the three endmembers at sampling sites SC1, SC2, and SCHR (Figures 4.13, and 4.15). The strength of the rainfall endmember indicates that rapid runoff must contribute to streamflow at these sampling sites. Field observations indicated that surface runoff in these portions of the watershed occurs primarily during the peak of snowmelt when the floodplain sediments become saturated. Surface runoff was also observed during intense summer thunderstorms and we think this is related to

the semiarid environment of the low-elevation portions of the watershed. Rainfall was a stronger endmember in SCHW and SCCR and accounted for 8 to 48 percent of streamflow generation (Figure 4.14a). Rainfall was a relatively minor contributor to streamflow in SC1, SC2, and SCHR and accounted for 6 to 37 percent of streamflow generation (Figures 4.14b and 4.16). The appearance of rainfall as a minor endmember in streamflow generation in Saguache Creek indicates that fast runoff processes do occur in this region of the watershed although they are not dominant (Figures 4.13 and 4.15).

The strength of the late-season snow endmember is unlikely to be due to local rapid runoff generation. Snowpacks are relatively thin in the lower reaches of Saguache Creek, these snowpacks melt early in the snowmelt season, and snowmelt runoff is not temporally persistent. Instead, the strength of the late-season snow endmember is presumable derived from the integration of snowmelt runoff from the tributary and headwater subwatersheds into the main channel of Saguache Creek. The late-season snow endmember becomes important at SC1, remains important at SC2, and is also important at the final sampling site SCHR. Within this span, Saguache Creek receives flow from confluences with Hodding Creek, Sheep Creek, Middle Creek, and Ford Creek. This confirms that channel routing and connectivity between the main channel of Saguache Creek and its tributaries are important in the overall runoff response from Saguache Creek. This in-stream integration of tributary solute loads increases the solute load of the main channel of Saguache Creek in a structured fashion similar to that proposed by the network-mixing conceptual model [*Uchida et al.*, 2005]. One way to test the dependence of the stream chemistry on integration of contributions at successively larger scales is to calculate the increment in solute load in Saguache Creek

as a function of accumulated watershed area and calculate the solute loads from each of the tributary subwatersheds. Solute loads [kg day^{-1}] were calculated by multiplying stream discharge [m^3 day^{-1}] by solute concentration [kg m^{-3}]. For example, the increment in solute load between SC1 and SC2 would simply be equal to the solute load at SC2 minus the solute load at SC1 (see Figure 4.2). If the increment in solute load between sampling sites in Saguache Creek is equal to the sum of the solute additions from the tributaries that enter Saguache Creek between the sampling sites, then this would indicate that in-stream integration processes are responsible for the observed structured trends in stream chemistry. Table 4.2 gives the results of this mass-balance calculation. The increments in stream chemistry do not equal the sum of the solute additions from the tributaries. Instead, a considerable amount of solute is missing. Given the mini-piezometer chemistry data, the most plausible source of this missing solute is groundwater discharge. In summary, these observations suggest that rapid runoff processes are operative across scales; however, these processes become less important as scale increases beyond 300 km^2. These findings also suggest that while in-stream integration of tributary runoff may be an important process in the overall runoff response from Saguache Creek, it does not explain the structured trends in stream chemistry in drainages greater than 300 km^2.

Sampling Location	Na^+ Load (kg day^{-1})	ΔNa^+ Load (kg day^{-1})	Calculation Method
SCCR	384.1		
SC1	407.8	23.7	**SC1 – SCCR**
Tributary Input 1	44.1		
SC2	516.5	108.7	**SC2 – SC1** (SC2-SC1) > Input 1
Tributary Input 2	55.6		
SCHR	584.1	67.6	**SCHR – SC2** (SCHR-SC2) > Input 2

Sampling Location	Ca^{2+} Load (kg day^{-1})	ΔCa^{2+} Load (kg day^{-1})	Calculation Method
SCCR	1091.8		
SC1	1121.5	29.7	**SC1 – SCCR**
Tributary Input 1	112.3		
SC2	1370.3	248.8	**SC2 – SC1** (SC2-SC1) > Input 1
Tributary Input 2	193.5		
SCHR	1572.5	202.2	**SCHR – SC2** (SCHR-SC2) > Input 2

Table 4.2: Data showing the increments in Na^+ and Ca^{2+} between stream sampling locations during September 2008. Column 1 contains the sampling location name which can be referenced in Figure 4.2. Column 2 has the Na^+ and Ca^{2+} load at each sampling location in kg day^{-1}. Column 3 has the difference in Na^+ and Ca^{2+} between successive sampling locations. For example, the increment in Na^+ between SC1 and SC2 is 108.7 kg day^{-1}. Column 3 also shows the comparison between solute increment between successive sampling locations and the solute load addition to the main stream by tributary inputs. There are no tributary inputs between SCCR and SC1. "Tributary Input 1" is the combined tributary input from Sheep Creek and Hodding Creek that occurs between SC1 and SC2. "Tributary Input 2" is the combined tributary input from Middle Creek and Ford Creek that occurs between SC2 and SCHR. Column 4 contains comments on how the differences in solute load were calculated.

Groundwater was a strong endmember at all sampling sites in Saguache Creek (Figures 4.14 and 4.16). Groundwater accounts for 49 to 59 percent of baseflow at SCHW and 31 to 56 percent of baseflow at SCCR (Figure 4.14a). In comparison, groundwater accounts for 6 to 12 percent of streamflow generation at SCCR during the snowmelt freshet (Figure 4.14a). More extensive sampling histories are available at SC1 and SC2. During the snowmelt freshet, groundwater remains a relatively consistent

contributor to streamflow and accounts for 15 to 26 percent of streamflow generation at these sites (Figures 4.14b and 4.16a). Groundwater contributions account for as much as 48 to 64 percent of baseflow at these sites. This range also seems reasonable for the final sampling site, SCHR, which represents the largest accumulated drainage area in our study. Although the sampling history is limited, groundwater accounted for 26 to 61 percent of streamflow generation at this site. Therefore, it appears that groundwater contributions are very important in streamflow generation across all scales.

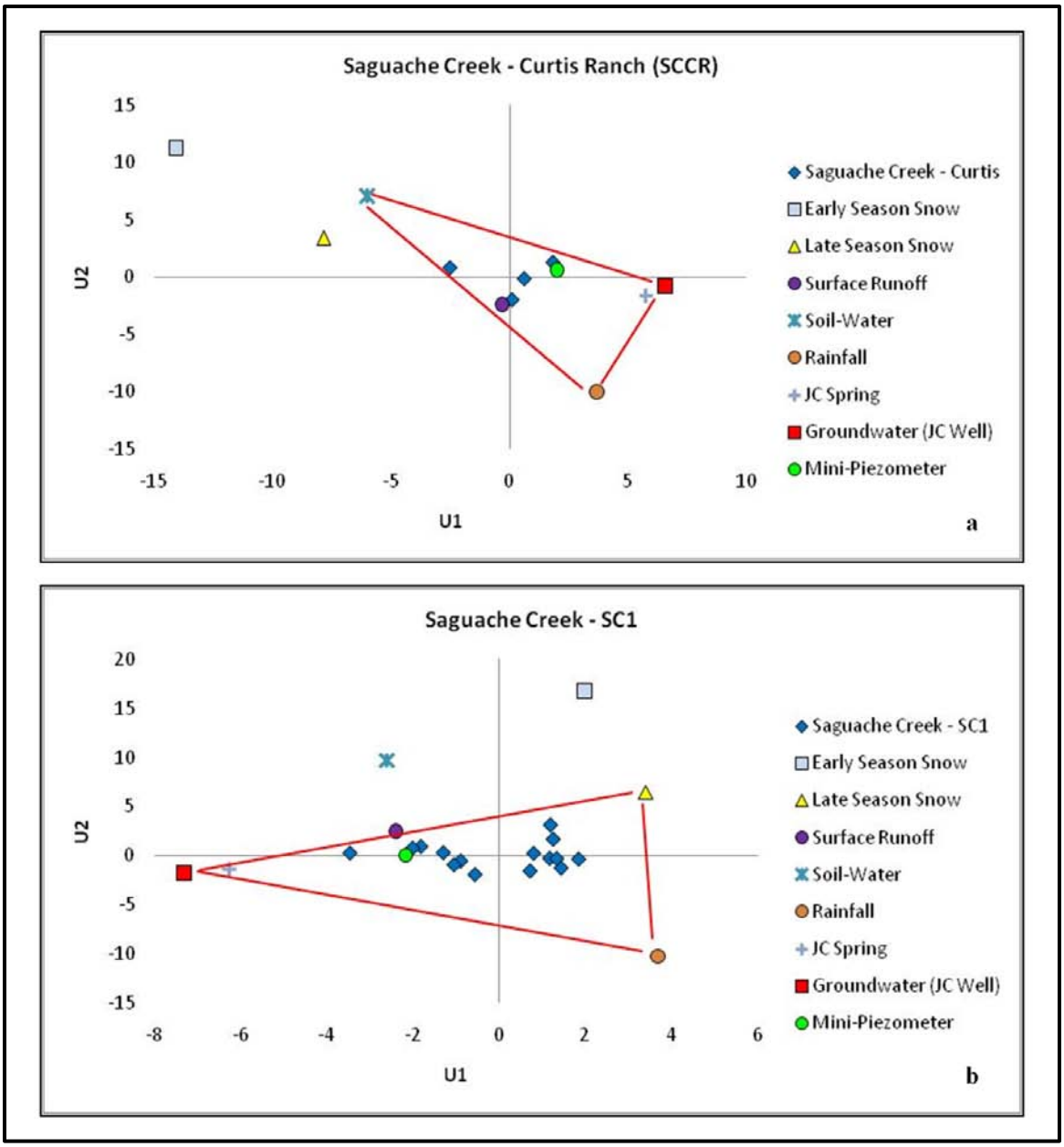

Figure 4.13: U-space mixing diagram for a) Saguache Creek – Curtis Ranch (SCCR) and b) Saguache Creek – SC1. The accumulated watershed area at SCCR is 542.6 km^2 and the accumulated watershed area at SC1 is 709.7 km^2.

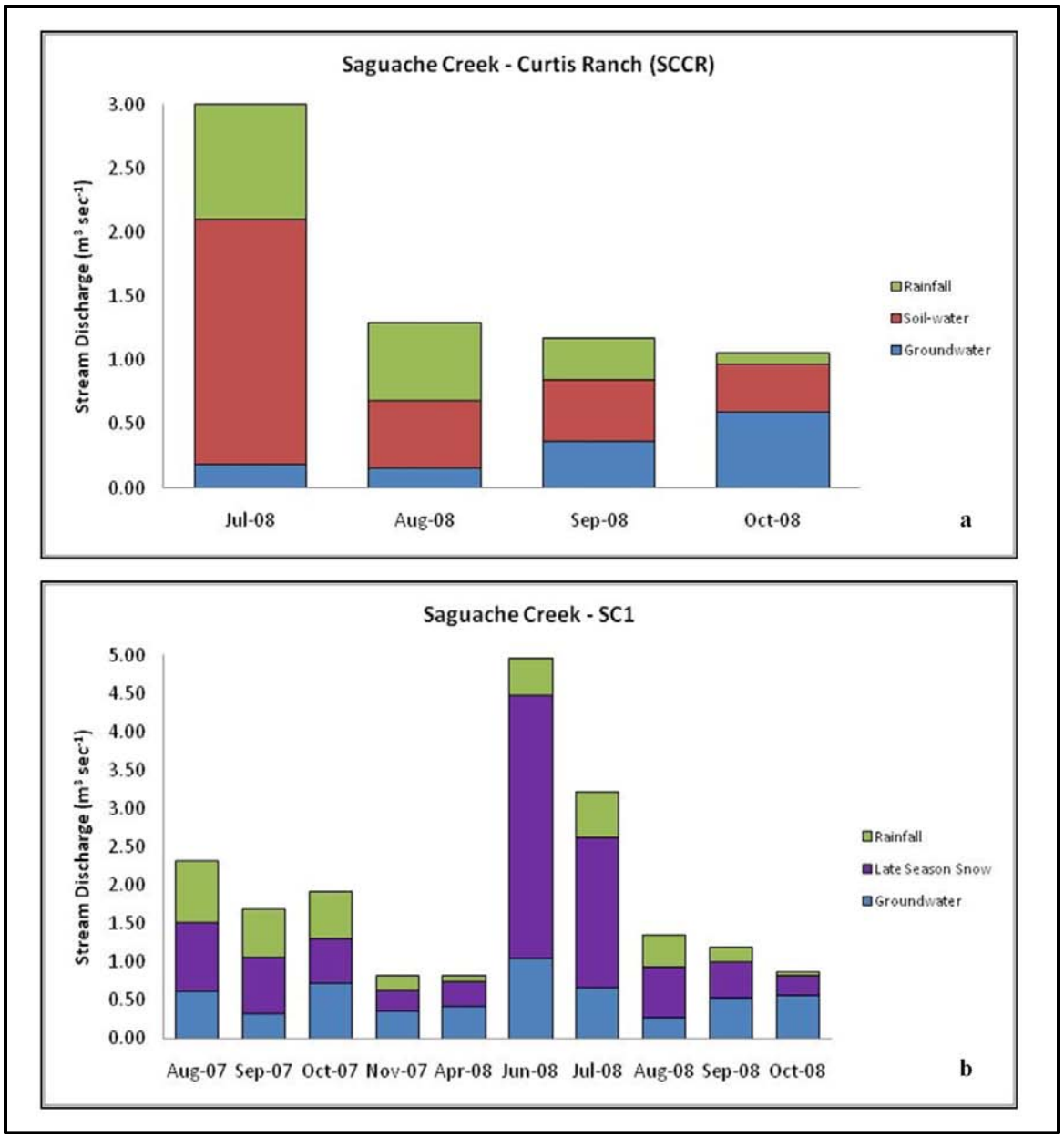

Figure 4.14: Streamflow separations for a) Saguache Creek – Curtis Ranch (SCCR) and b) Saguache Creek – SC1. The y-axis is flow from individual components expressed in units of m^3 sec^{-1}.

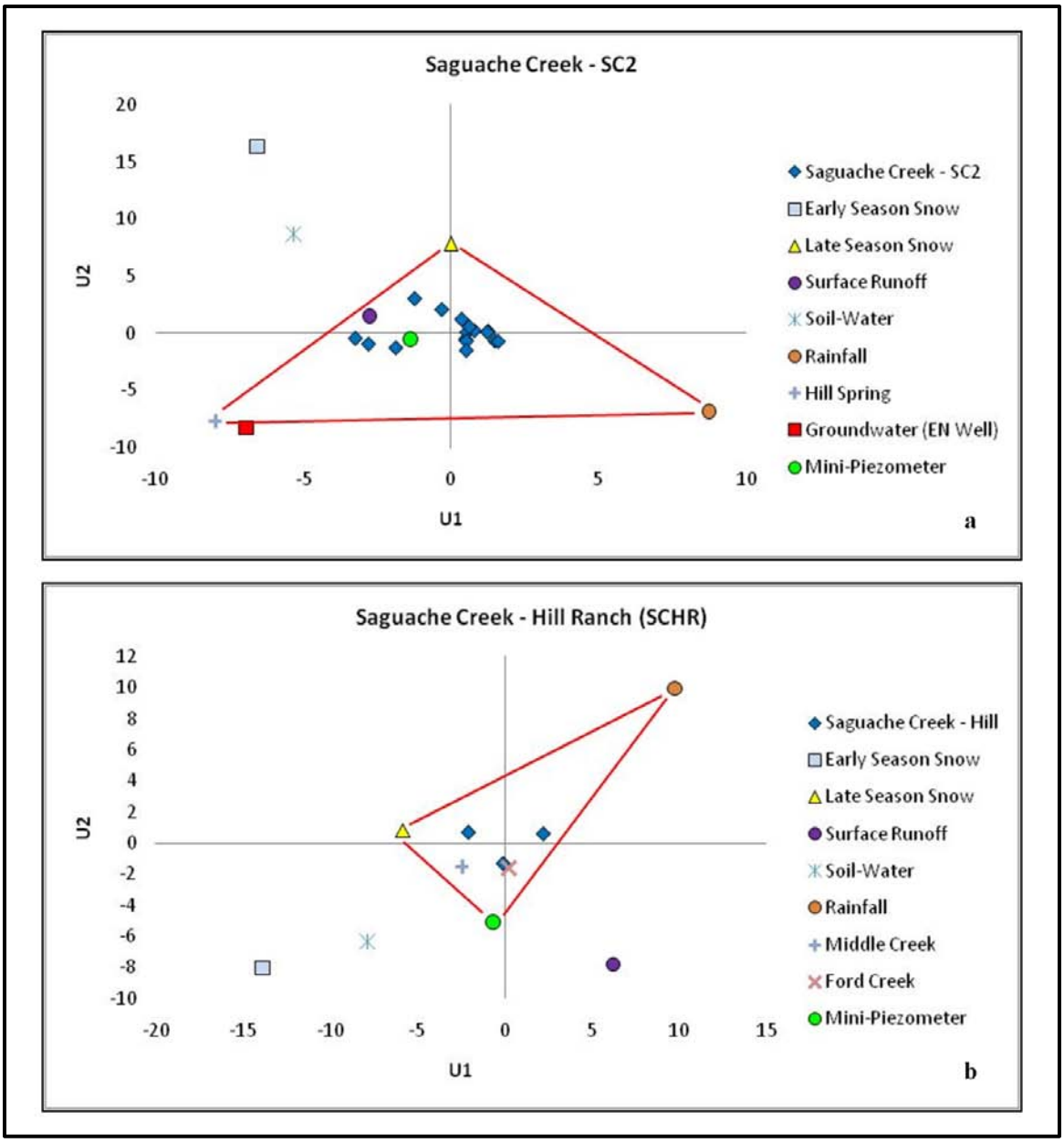

Figure 4.15: U-space mixing diagram for a) Saguache Creek – SC2 and b) Saguache Creek – Hill Ranch (SCHR). The accumulated watershed area at SC2 is 1111.9 km^2 and the accumulated watershed area at SCHR is 1447.2 km^2.

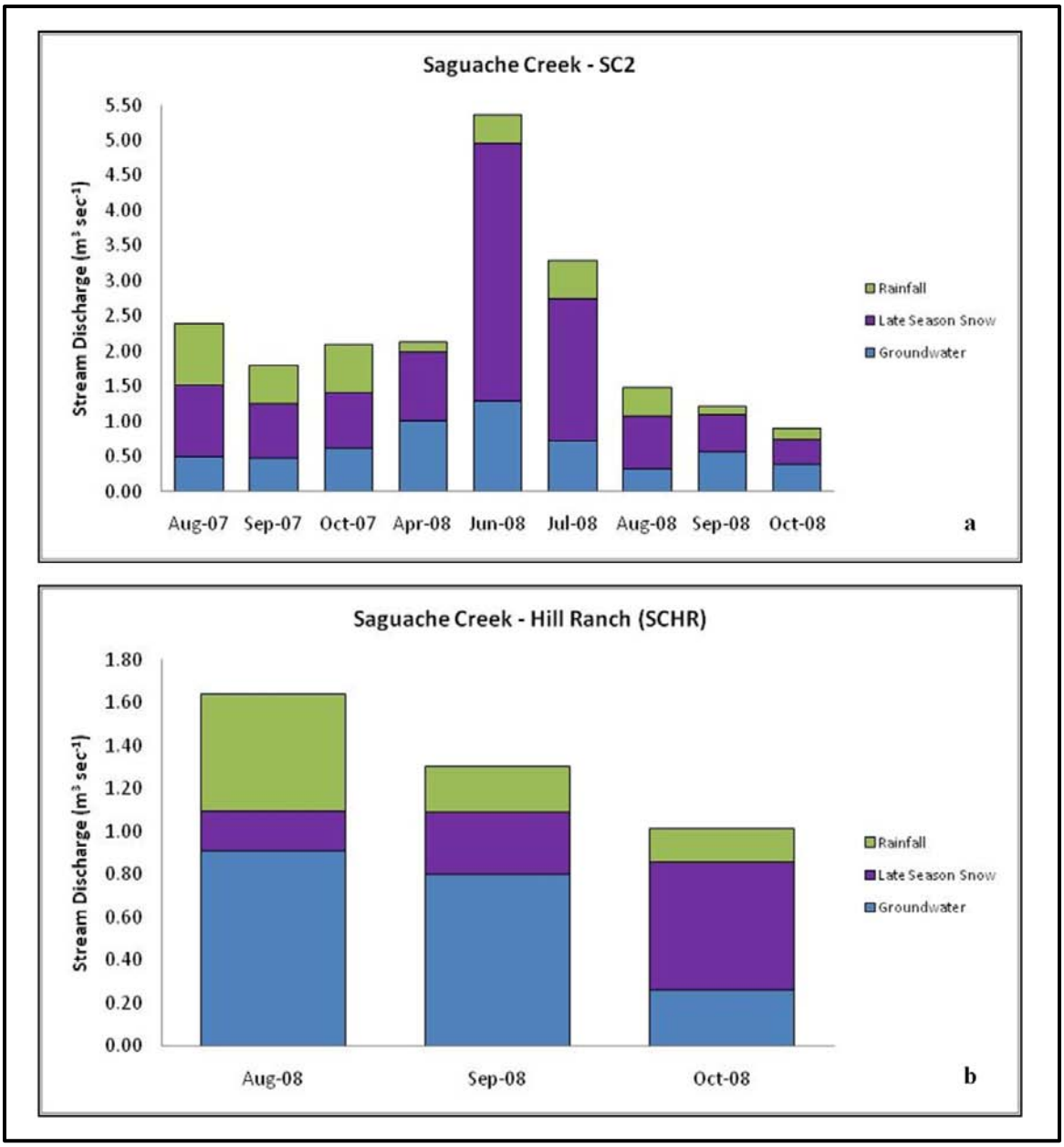

Figure 4.16: Streamflow separations for a) Saguache Creek – SC2 and b) Saguache Creek – Hill Ranch (SCHR). The y-axis is flow from individual components expressed in units of m^3 sec^{-1}.

4.4.4: Structure of Groundwater Contributions and Vertical Hydraulic Gradients:

Ultimately, the key distinguishing feature between the two proposed conceptual models is the magnitude and more importantly, the structure of groundwater contributions to streamflow. In order to determine if structure was present in groundwater contributions to streamflow, we plotted individual monthly groundwater contributions against drainage area. In Figure 4.17, we plot groundwater contributions during baseflow (September 2008 – Figure 4.17a) and prior to baseflow (August 2008 – Figure 4.17b). During baseflow conditions, the groundwater contributions are very structured in drainage areas greater than 300 km^2 and in drainage areas less than 300 km^2. Perhaps the most important observation is that groundwater contributions do in fact increase with increasing scale beyond 300 km^2 during baseflow (Figure 4.17a). We did not observe asymptotic behavior in the plots of stream chemistry and we do not observe asymptotic behavior in Figure 4.17a. Therefore, this finding provides support for the 3D catchment-mixing conceptual model and does not support the network-mixing conceptual model.

The trends in groundwater contributions at scales larger than 300 km^2 prior to baseflow in August 2008 suggest that groundwater contributions are becoming structured (Figure 4.17b). During early August, the recession of the snowmelt pulse was still working through the stream network. This snowmelt input to the stream network coupled with inputs from rainfall probably accounts for the variability observed in Figure 4.17b. This effect is very strong near the confluence of the headwater streams (see SCHW at ~ 350 km^2 in Figure 4.17b). Otherwise, we observe some structure in groundwater contributions beyond 300 km^2.

In comparison, groundwater contributions are structured very differently in drainages less than 300 km^2 during August and September (Figure 4.17a,b). In fact, groundwater contributions decrease with increasing scale in drainages less than 300 km^2 during baseflow. It is also important to note that groundwater contributions during baseflow in these small drainages are quite large illustrating the importance of groundwater across multiple scales. The physical processes responsible for these variations in groundwater contributions at small drainage scales are not known at this time but are being investigated using environmental tracers and hydrogeologic modeling efforts. In addition, there are two distinct trends in Figure 4.17: a trend for small drainages less than 300 km^2 and a trend for drainages larger than 300 km^2. We provide an explanation for the structure of these trends in Section 5.0.

Vertical hydraulic gradients were positive in all mini-piezometers during the period of observation. Although the mini-piezometers provide only point sources of data, this behavior indicates that the contributions from groundwater were relatively consistent during the period of observation. The vertical hydraulic gradients were also plotted against drainage area to investigate the role of groundwater contributions with increasing scale during August and September of 2008 (Figure 4.18). During baseflow, it is apparent that vertical hydraulic gradients do increase with increasing scale at drainages greater than 300 km^2 (Figure 4.18a). This behavior supports our EMMA results that indicate that groundwater contributions increase with increasing scale beyond the critical area (Figure 4.17a). Data was limited during August 2008 due to vandalism at several mini-piezometer installations and a relationship with increasing scale cannot be accurately inferred (Figure 4.18b). The data presented in Figures 4.17a and 4.18a

provide strong support for the 3D catchment-mixing conceptual model. At scales larger than the critical area, it is apparent that the structured trends in stream chemistry are related to increases in groundwater contributions as watershed scale increases.

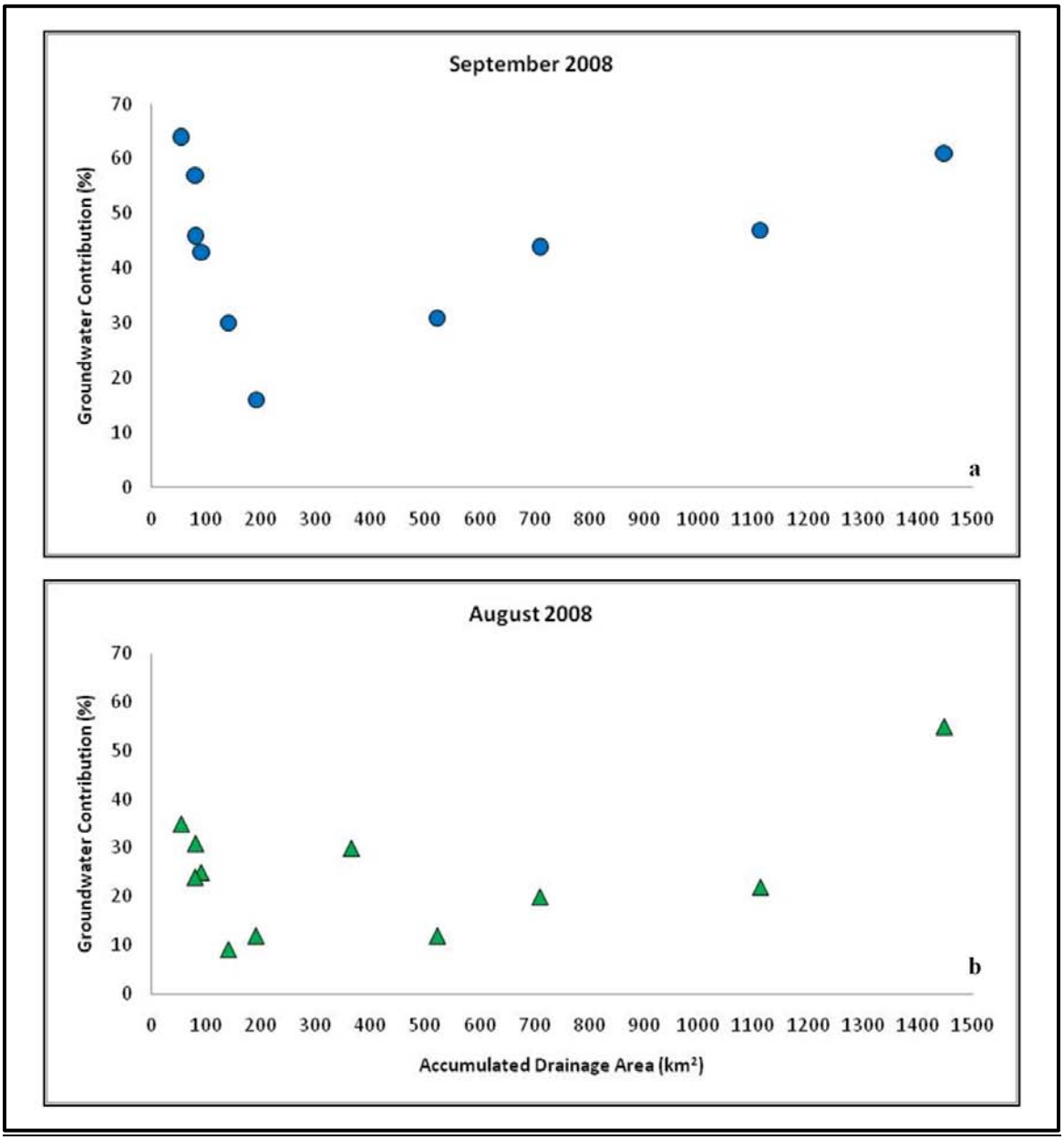

Figure 4.17: Fractional groundwater contribution to streamflow during a) September 2008 and b) August 2008.

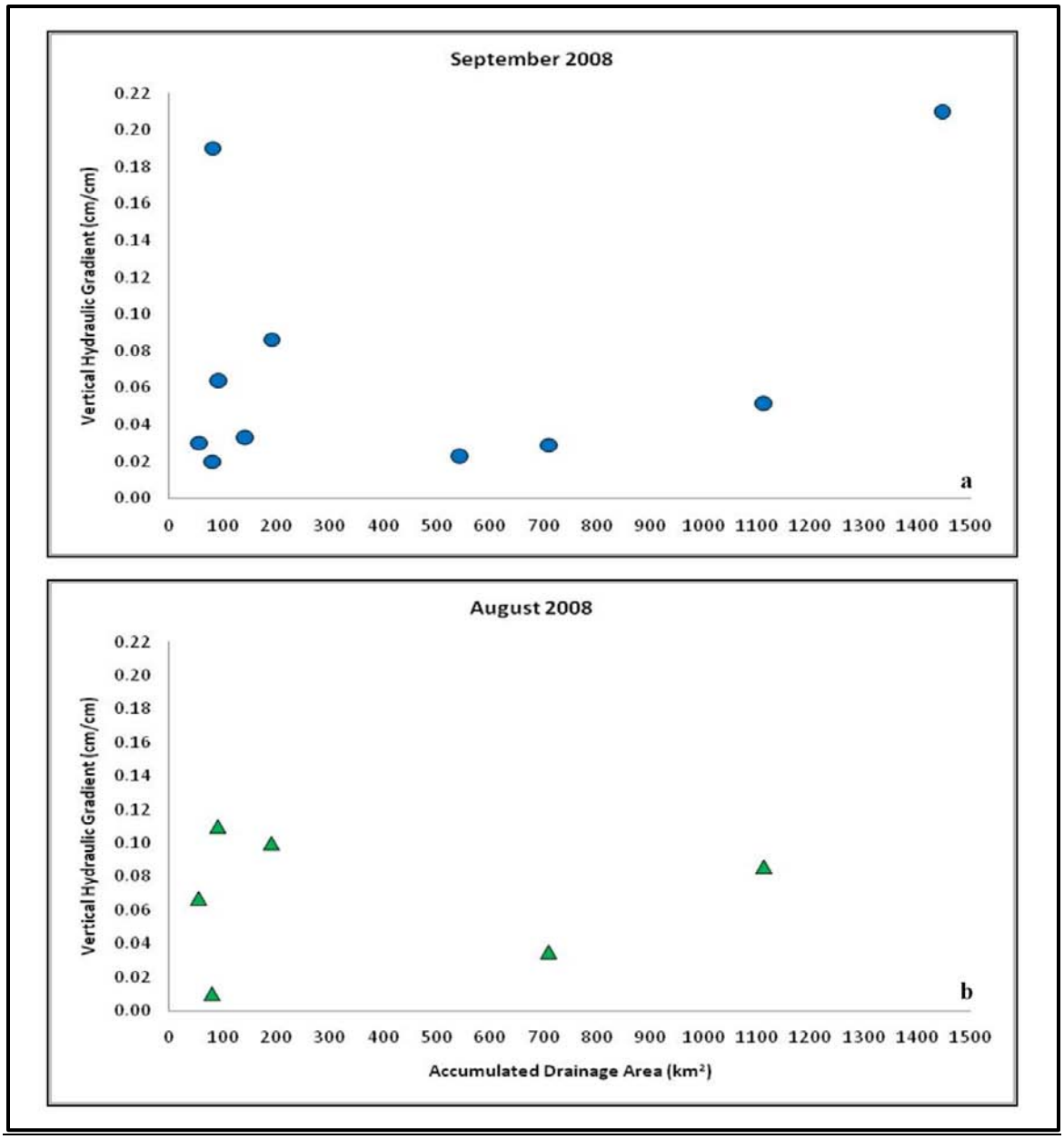

Figure 4.18: Vertical hydraulic gradients measured in mini-piezometers installed in streambeds during a) September 2008 and b) August 2008. Note the similarity between Figure 4.15b and Figure 4.16b.

4.4.5: Geologic Impacts to Basin-Scale Groundwater Flowpath Development:

Small drainages less than 300 km^2 exhibit significant variability in streamflow chemistry, but drainages greater than 300 km^2 show structured linear increases in streamflow chemistry with increasing scale (Figure 4.6). An area of 300 km^2 seems to be significant and suggests that the basin-scale groundwater flowfield may not be continuous in the Saguache Creek watershed. In fact, the critical area coincides with the geographical location of the La Garita caldera wall (Figures 4.2 and 4.3). The La Garita caldera wall is a remnant of the largest documented volcanic eruption in Earth's history [*Mason et al.*, 2004] and certainly the largest eruption in the San Juan Volcanic Field [*Bachmann et al.*, 2002]. The La Garita Caldera Wall and the ring fractures associated with caldera subsidence [*Lipman*, 1997] are likely to strongly influence the development and connectivity of groundwater flowpaths in the watershed. As a consequence, groundwater flowpaths in the headwater subwatersheds might penetrate more deeply than they would in the absence of this barrier. In addition, the groundwater flowfields of the headwater subwatersheds might be disconnected from the groundwater flowpaths in the high-order, low-elevation regions of the watershed because of this barrier.

As mentioned previously, there are two distinct trends in Figures 4.6, 4.17, and 4.18: a trend for small drainages less than 300 km^2 and a trend for drainages larger than 300 km^2. The influence of the La Garita caldera wall on groundwater flowpath development is one possible explanation for these two trends. If, for example, the subsurface is a homogeneous media and contributions from Tóthian groundwater flowfields are the only sources of water and solutes to streamflow, then we would expect to see a relatively smooth increase in streamflow chemistry with increasing watershed

scale [*Cardenas*, 2007]. However, natural media are almost never homogeneous. As a consequence, geologic features in other watersheds may disrupt the development and connectivity of basin-scale flowfields and this, in turn, may mask trends in streamflow chemistry and age distributions if the geologic history of the watershed is not considered.

4.4.6: Assessment of EMMA Source Partitioning Using Known Mixtures:

In order to assess the validity of the source partitioning based on the EMMA analysis, a hypothetical stream-water was created using known components (endmembers) from our dataset. The EMMA source partitioning was tested two separate ways. First, twenty water samples were created for the hypothetical stream-water using known, measured components and random mixtures of these components for each sample. This test was designed to determine if the EMMA code could successfully identify the components responsible for streamflow generation and to determine if the EMMA code could successfully predict the contributions of the components in each sample. Three components were selected (one well water, rainfall, and soil-water) and each sample was composed of a mixture of these three components. The EMMA code was then used to identify the endmembers of the samples and the component contributions of the endmembers in each sample. The EMMA code successfully identified the three components of streamflow for the hypothetical stream-water and successfully predicted the contributions of each component in each sample. There was no variability between the actual contributions and the predicted contributions. Second, the rainfall component was eliminated and replaced with late season snow in two samples and replaced with surface runoff in two other samples. This test was designed to generate four outliers and determine if these outliers were spatially correct in the *U*-space mixing

diagram. The outliers were successfully generated and the placement of these outliers was spatially correct. Two of the outliers trended outside the mixing diagram toward the late season snow component and two outliers trended outside the mixing diagram toward the surface runoff component. These tests provided confidence that the source partitioning provided by the results of the EMMA code was correct.

4.5: Conclusions:

We designed our study to test two conceptual models for streamflow generation at large watershed scales. The network-mixing conceptual model consists of surface and shallow subsurface runoff responses from individual hillslopes that mix in the stream network until, as scale increases, an integrated runoff response emerges. The aggregation of all hillslope runoff responses can therefore be used to approximate streamflow generation processes at larger watershed scales. In this conceptual model, mixing processes lead to the convergence of streamflow chemistry on median concentrations of chemical constituents in streamflow as scale increases. Alternatively, the 3D catchment-mixing conceptual model explains streamflow generation at large watershed scales as a system response that consists of rapid surface and shallow subsurface flowpaths as well as large-scale groundwater flowpaths that are structured within individual hillslopes and within the larger watershed itself. The watershed is more than just an aggregation of hillslopes. Contributions to streamflow from these large-scale groundwater flowpaths will also be structured with scale. In this conceptual model, we envision groundwater contributions increasing with increasing scale and this leads to increases in concentrations of chemical constituents in streamflow with increasing scale. The amount

and structure of basin-scale groundwater contributions with increasing scale are critical in distinguishing between these two conceptual models. Therefore, we were particularly interested in determining whether or not groundwater contributions in streamflow were structured with scale in a large, alpine watershed in the southern Rocky Mountains of Colorado.

Streamflow chemistry data indicated that two trends were apparent in the plots of chemical constituents in streamflow as a function of accumulated drainage area. Significant variability was observed in concentrations of chemical constituents from small drainages less than 300 km^2 and those same concentrations became structured and increased linearly with increasing scale from drainage areas greater than 300 km^2. We used endmember-mixing analyses (EMMA) and measurements of vertical hydraulic gradients (VHG) in streambeds to quantify the role of deep, large-scale groundwater in streamflow generation. EMMA results indicate that groundwater contributions were highly variable in drainages less than 300 km^2. This finding was supported by measurements of VHG which also indicated significant variability in groundwater discharge to the streams. EMMA results also, more importantly, indicated that groundwater contributions did increase with increasing scale from accumulated drainage areas greater than 300 km^2. This finding was also supported by measurements of VHG which indicated that VHG increased with increasing scale from accumulated drainage areas greater than 300 km^2. When considered together, these findings support the 3D catchment-mixing conceptual model over the network-mixing conceptual model in this large, alpine watershed.

What are the implications of these findings? These results indicate that large-scale groundwater contributions are dominant controls on streamflow generation and on trends in streamflow chemistry across multiple scales in the Saguache Creek watershed. The structure of groundwater contributions in streamflow (Figures 4.17 and 4.18) has important implications for our perception of apparent ages in streamflow. Contributions to streamflow range from direct inputs during meteoric events to very old, long-lived contributions from basin-scale groundwater flowpaths. These old, persistent contributions from groundwater are likely responsible for the tailing observed in residence time distributions in watersheds. For example, the 3D catchment-mixing conceptual model that we propose in this paper may provide an explanation for the fractal scaling of residence times reported in the work of *Kirchner et al.* [2000, 2001]. Previous modeling efforts have indicated that the topography-driven flowfield concepts proposed by *Tóth* [1963] can generate fractal behavior in residence time distributions [*Cardenas*, 2007]. In fact, *Lindgren et al.* [2004] proposed that in watersheds where residence time distributions are fractal, most of the solute mass in streamflow must be contributed by groundwater flowpaths as opposed to rapid runoff processes. We assert that in the Saguache Creek watershed, groundwater contributions are the framework for the geochemical signal observed in streamflow across multiple scales and that hillslope-scale runoff processes superimpose noise on that signal. Our findings cast doubt on the hillslope aggregation concepts for scaling runoff processes to larger watershed scales at least in the Saguache Creek watershed. Large watersheds are more than simply the aggregation of hillslope runoff responses.

4.6: References:

Araguás-Araguás, L., K. Rozanski, R. Gonfiantini, and D. Louvat (1995), Isotope effects accompanying vacuum extraction of soil water for stable isotope analyses, *Journal of Hydrology, 168*, 159-171, doi:10.1016/0022-1694(94)02636-P.

Bachmann, O., M.A. Dungan, and P.W. Lipman (2002), The Fish Canyon Magma Body, San Juan Volcanic Field, Colorado: Rejuvenation and eruption of an upper-crustal batholiths, *Journal of Petrology, 43*(8), 1469-1503.

Baxter, C., F.R. Hauer, and W.W. Woessner (2003), Measuring groundwater-stream water exchange: New techniques for installing minipiezometers and estimating hydraulic conductivity, *Transactions of the American Fisheries Society, 132,* 493-502.

Beighley, R.E., T. Dunne, and J.M. Melack (2005), Understanding and modeling basin hydrology: Interpreting the hydrogeological signature, *Hydrological Processes, 19,* 1333-1353.

Beven, K. (2006), *Benchmark Papers in Hydrology: Streamflow Generation Processes,* International Association of Hydrological Sciences, Oxfordshire, UK.

Bricker, O.P. and B.F. Jones (1995), Main factors affecting the composition of natural waters, in *Trace Elements in Natural Waters,* edited by B. Salbu and E. Steinnes, CRC Press, Boca Raton, FL.

Campbell, D.H., D.W. Clow, G.P. Ingersoll, M.A. Mast, N.E. Spahr, and J.T. Turk (1995), Processes controlling the chemistry of two snowmelt-dominated streams in the Rocky Mountains, *Water Resources Research, 31* (11), 2811-2821.

Cardenas, M.B. (2007), Potential contribution of topography-driven regional groundwater flow to fractal stream chemistry: Residence time distribution analysis of Tóth flow, *Geophysical Research Letters, 34,* L05403, doi:10.1029/GL029126.

Cey, E.E., D.L. Rudolph, G.W. Parkin, and R. Aravena (1998), Quantifying groundwater discharge to a small perennial stream in southern Ontario, Canada, *Journal of Hydrology, 210,* 21-37.

Christophersen, N., and R.P. Hooper (1992), Multivariate analysis of stream water chemical data: The use of principal components analysis for the end-member mixing problem, *Water Resources Research, 28* (1), 99-107.

Clark, I., and P. Fritz (1997), *Environmental Isotopes in Hydrogeology,* Lewis, Boca Raton, Fla.

Clow, D.W., G.P. Ingersoll, M.A. Mast, J.T. Turk, and D.H. Campbell (2002), Comparison of snowpack and winter wet-deposition chemistry in the Rocky Mountains, USA: Implications for winter dry deposition, *Atmospheric Environment, 36,* 2337-2348.

Davis, S.N., L.D. Cecil, M. Zreda, and S. Moysey (2001), Chlorine-36, bromide, and the origin of spring water, *Chemical Geology, 179,* 3-16.

Dingman, S.L. (2002), *Physical Hydrology, 2nd Edition,* Prentice-Hall, Upper Saddle River, New Jersey.

Dixon , J.C. and C.E. Thorn (2005), Chemical weathering and landscape development in mid-latitude alpine environments, *Geomorphology, 67,* 127-145, doi:10.106/j.geomorph.2004.07.009.

Dooge, J.C.I. (1997), Searching for simplicity in hydrology, *Surveys in Geophysics, 18,* 511-534.

Earman, S., A.R. Campbell, F.M. Phillips, and B.D. Newman (2006), Isotopic exchange between snow and atmospheric water vapor: Estimation of the snowmelt component of groundwater recharge in the southwestern United States, *Journal of Geophysical Research, 111,* D09302, doi:10.1029/2005JD006470.

Engle, E.M. (2009), Digital soil boundary detection using quantitative hydrologic remote sensing, M.S. Thesis, Department of Earth and Environmental Science, New Mexico Tech, Socorro, NM, USA.

Frisbee, M.D., F.M. Phillips, A.R. Campbell, J.M.H. Hendrickx, (2010a), Modified passive capillary samplers for collecting samples of snowmelt infiltration for stable isotope analysis in remote, seasonally inaccessible watersheds 1: Laboratory evaluation, *Hydrological Processes, 24,* 825-833, DOI:10.1002/hyp.7523.

Frisbee, M.D., F.M. Phillips, A.R. Campbell, J.M.H. Hendrickx, and E.M. Engle (2010b), Modified passive capillary samplers for collecting samples of snowmelt infiltration for stable isotope analysis in remote, seasonally inaccessible watersheds 2: Field evaluation, *Hydrological Processes*, 24, 834-849, DOI:10.1002/hyp.7524.

Frisbee, M.D. F.M. Phillips, A.F. White, A.R. Campbell, F. Liu (2010c), Variability of the groundwater component in springflow generation and its affect on calculated bedrock weathering rates in a large, alpine watershed in the southern Rocky Mountains of Colorado, in preparation for submission.

Goldich, S.S. (1938), A study in rock-weathering, *Journal of Geology, 46,* 17-58.

Hooper, R.P. (2003), Diagnostic tools for mixing models of stream water chemistry, *Water Resources Research, 39* (3), 1055, doi:10.1029/2002WR001528.

Kennedy, V.C. (1970), Silica variations in stream water with time and discharge, in *Nonequilibrium Systems in Natural Water Chemistry,* edited by J.D. Hem, series editor R.F. Gould, pp. 95-130, American Chemical Society, Houston, Texas.

Kirchner, J.W., X. Feng, and C. Neal (2000), Fractal stream chemistry and its implications for contaminant transport in catchments, *Nature, 403,* 524-527.

Kirchner, J.W., X. Feng, and C. Neal (2001), Catchment-scale advection and dispersion as a mechanism for fractal scaling in stream tracer concentrations, *Journal of Hydrology, 254,* 82-101.

Lasaga, A.C. (1984), Chemical kinetics of water-rock interactions, *Journal of Geophysical Research, 89*(B6), 4009-4025.

Lindgren, G.A., G. Destouni, and A.V. Miller (2004), Solute transport through the integrated groundwater-stream system of a catchment, *Water Resources Research, 40,* W03511, doi:10.1029/2003WR002765.

Lipman, P.W. (1997), Subsidence of ash-flow calderas: Relation to caldera size and magma-chamber geometry, *Bulletin of Volcanology, 59,* 198-218.

Lipman, P.W. and W.C. McIntosh (2008), Eruptive and noneruptive calderas, northeastern San Juan Mountains, Colorado: where did the ignimbrites come from?, *Geological Society of America Bulletin, 120* (7/8), 771-795, doi:10.1130/B26330.1.

Liu, F., M.W. Williams, and N. Caine (2004), Source waters and flow paths in an alpine catchment, Colorado Front Range, United States, *Water Resources Research, 40,* W09401, doi:10.1029/2004WR003076.

Liu, F., R.C. Bales, M.H. Conklin, and M.E. Conrad (2008), Streamflow generation from snowmelt in semi-arid, seasonally snow-covered, forested catchments, Valles Caldera, New Mexico, *Water Resources Research, 44,* W12443, doi:10.1029/2007WR006728.

Mason, B.G., D.M. Pyle, and C. Oppenheimer (2004), The size and frequency of the largest explosive eruptions on Earth, *Bulletin of Volcanology, 66,* 735-748.

McDonnell, J.J. (2003), Where does water go when it rains? Moving beyond the variable source area concept of rainfall-runoff response, *Hydrological Processes, 17,* 1869-1875, doi:10.1002/hyp.5132.

McGlynn, B.L., J.J. McDonnell, M. Stewart, and J. Siebert (2003), On the relationship between catchment scale and streamwater residence time, *Hydrological Processes, 17,* 175-181, doi:10.1002/hyp.5085.

McGuire, K.J., J.J. McDonnell, M. Weiler, C. Kendall, B.L. McGlynn, J.M. Welker, and J. Siebert (2005), The role of topography on catchment-scale water residence time, *Water Resources Research, 41,* W05002, doi:10.1029/2004WR003657.

Naiman, R.J., P.A. Bisson, R.G. Lee, and M.G. Turner (2001), Watershed management, in *River Ecology and Management,* edited by R.J. Naiman and R.E. Bilby, pp. 642-661, Academic Press, London.

Nelson, S.T., and D. Dettman (2001), Improving hydrogen isotope ratio measurements for on-line chromium reduction systems, *Rapid Communications in Mass Spectrometry. 15,* 2301-2306.

Pretty, J.L., A.G. Hildrew, and M. Trimmer (2006), Nutrient dynamics in relation to surface-subsurface hydrological exchange in a groundwater fed chalk stream, *Journal of Hydrology, 330,* 84-100, doi:10.1016/j.jhyrol.2006.04.013.

Rodgers, P., C. Soulsby, and S. Waldron (2005), Stable isotope tracers as diagnostic tools in upscaling flow path understanding and residence time estimates in a mountainous mesoscale catchment, *Hydrological Processes, 19,* 2291-2307, doi:10.1002/hyp.5677.

Shaman, J., M. Stieglitz, and D. Burns (2004), Are big basins just the sum of small catchments?, *Hydrological Processes, 18,* 3195-3206, doi:10.1002/hyp.5739.

Sivapalan, M. (2003), Process complexity at hillslope scale, process simplicity at the watershed scale: is there a connection?, *Hydrological Processes, 17,* 1037-1041, doi:10.1002/hyp.5109.

Spence, C. (2007), On the relation between dynamic storage and runoff: A discussion on thresholds, efficiency, and function, *Water Resources Research, 43,* W12416, doi:10.1029/2006WR005645.

Steven, T.A. and P.W. Lipman (1976), Calderas of the San Juan Volcanic Field, southwestern Colorado, in U.S. Dept. of the Interior, USGS Geological Survey Professional Paper 958, 35 pp.

Temnerud, J. and K. Bishop (2005), Spatial variation of streamwater chemistry in two Swedish Boreal catchments: Implications for environmental assessment, *Environmental Science and Technology, 39,* 1463-1489, doi:10.1021/es040045q.

Tóth J. (1963), A theoretical analysis of groundwater flow in small drainage basins, *Journal of Geophysical Research, 67,* 4812-4975.

Tóth, J. (1995), Hydraulic continuity in large sedimentary basins, *Hydrogeology Journal, 3*(4), 4-16.

Tóth, J. (1999), Groundwater as a geologic agent: An overview of the causes, processes, and manifestations, *Hydrogeology Journal, 7,* 1-14.

Uchida, T., Y. Asano, Y. Onda, and S. Miyata (2005), Are headwaters just the sum of hillslopes?, *Hydrological Processes, 19*, 3251-3261, doi:10.1002/hyp.6004.

Uhlenbrook, S. (2006), Catchment hydrology – a science in which all processes are preferential, *Hydrological Processes, 20*, 3581-3585, doi:10.1002/hyp.6564.

Wilson, J.L. and H. Guan (2004), Mountain-block hydrology and mountain-front recharge, in *Groundwater Recharge in a Desert Environment: The Southwestern United States*, edited by J. Hogan, F.M. Phillips, and B. Scanlon, 23 pp., AGU, Washington, D.C.

Wolock, D.M., J. Fan, and G.B. Lawrence (1997), Effects of basin size on low-flow stream chemistry and subsurface contact time in the Neversink River watershed, New York, *Hydrological Processes, 11*, 1273-1286.

Chapter 5 Variability in the Groundwater Component of Springflow Generation and Its Effect on Solute Weathering Release Rates in Large Watersheds[4]

5.1: Introduction:

The chemical weathering of bedrock is a fundamental component of geochemical and geomorphological systems, but it is difficult to quantify the individual contribution of bedrock weathering to the overall weathering release from large watersheds. Bedrock weathering processes provide minerals, nutrients, and matrix products for soil development [*Gabet et al.,* 2006] and solutes to streamflow, springflow, and groundwater [*Garrels and Mackenzie,* 1967; *Bricker and Jones,* 1995; *Dixon and Thorn,* 2005]. Chemical weathering of bedrock is not scale dependent; consequently, it is an important source of solutes at scales ranging from hillslopes and small headwater catchments [*West et al.,* 2002; *Kosugi et al.,* 2006; *Likens and Buso,* 2006] to watersheds [*Bassett,* 1997; *Velbel and Price,* 2007], islands [*Rad et al.,* 2007], and even continents [*Millot et al.,* 2002]. Yet, despite the ubiquitous nature and importance of chemical weathering, bedrock weathering rates in large watersheds remain poorly constrained.

In many bedrock weathering studies performed at the watershed scale, mass-balance approaches based on the chemical composition of streamflow or springflow are used to determine solute release from the watershed [*Drever,* 2002]. The mass-balance method essentially lumps all weathering reactions operative in the watershed into a single weathering rate usually described by the removal of a mass of solute from a watershed measured in streamflow at the watershed outlet. This ultimately limits our ability to quantify individual solute release mechanisms. *Tóth* [1999] described the importance of

[4] **Frisbee, M.D., F.M. Phillips, A.F. White, A.R. Campbell, and F. Liu (2010), Variability in the groundwater component of springflow generation and its effect on solute weathering release rates in large watersheds, formatted for submission to *Water Resources Research,* not submitted as of this writing.**

groundwater as a geologic agent and recent evidence indicates that the solute release from groundwater flow systems may be especially important in volcanic bedrock [*Rad et al.,* 2007]. In large watersheds where groundwater may be a dominant component of streamflow generation, the mechanisms responsible for solute release are poorly understood and consequently, solute release cannot be accurately partitioned between surficial weathering processes and weathering processes in the groundwater flow system [*Frisbee et al.,* 2010b].

In this paper, we expand on the work of *Rad et al.* [2007] and constrain our focus to the weathering release of solutes from groundwater flow systems in large inland watersheds. Here, we define *bedrock weathering* as the chemical transformation of minerals found within bedrock by interactions occurring between rock and groundwater. More specifically, we focus on the dissolution of common bedrock minerals such as quartz, feldspars, amphiboles, and micas found within the bedrock aquifer system and the subsequent release of silica and cations such as calcium, sodium, potassium, and magnesium from those minerals. We do not include surficial weathering processes such as the development of weathering rinds, regolith weathering, or eluviation processes in soil. Furthermore, we define *groundwater* according to *Freeze and Cherry* [1979] as subsurface water flowing beneath the water table in fully saturated geologic formations. We make this distinction to avoid confusion because *springs* are classically defined as points where "groundwater" intersects and flows over the Earth's surface [*Freeze and Cherry,* 1979]. Therefore, springs are considered, by definition, a surficial expression of groundwater. However, springflow generation is an integrative process and springs will consequently be a mixture of contributions of water from many different sources in a

watershed including groundwater (as previously defined), unsaturated flow in the soil (termed *soil-water* in this paper), preferential flow in the soil or near the spring emergence, and meteoric inputs [*Manga,* 2001]. These different sources of water become *components* of springflow if they contribute to springflow generation. In this paper, the term groundwater will refer only to water flowing beneath the water table in fully saturated media not preferential flow in the soil zone or unsaturated flow in the soil zone.

Bedrock weathering rates (mol m^{-2} s^{-1}) provide an indication of the mass of an individual solute (mol) released from the contributing area (m^2) responsible for springflow generation as a function of time [*White,* 2005]. Solute weathering release curves, on the other hand, provide an indication of the total accumulated solute release from bedrock as a function of time and are not adjusted to the contributing area of the spring. The contributing area of a spring is typically very difficult to determine because there may not be a surficial expression of the contributing area analogous to a watershed in the landscape. Solute weathering release curves can be used to create geochemical chronometers that describe evolutionary pathways for individual chemical constituents (Figure 5.1). For example, the approximate geochemical age of any spring or well sample can be estimated by plotting its chemical composition on the solute weathering release curve. Bedrock weathering rates and solute weathering release curves can be estimated using different approaches including: monitoring the solute release from fresh rock under laboratory controlled conditions [*Hoch et al.,* 1999; *White and Brantley,* 2003], monitoring the solute release from *in-situ* rocks in the field [*Hoch et al.,* 1999], monitoring mass loss from sample rocks placed at the soil surface [*Caine,* 1979], quantifying chemical changes along groundwater flowpaths [*Zhu,* 2005], applying

watershed mass-balance approaches [*Finley and Drever*, 1997; *Drever*, 2002; *White*, 2008]; and by measuring solutes in springflow [*Rademacher et al.*, 2001; *Pacheco and Van der Weijden*, 2002; *Pacheco and Alencoão*, 2006]. The latter two approaches are most commonly applied in watershed-scale studies. However, both approaches have disadvantages. The watershed mass-balance approach, for example, may be most applicable in bare rock watersheds as opposed to forested watersheds due to the difficulty in removing the biologic cycling term from the mass balance equation [*Velbel*, 1995; *Bassett*, 1997]. In addition, the watershed mass-balance methods provide only indirect estimates of bedrock weathering due to the integrative nature of streamflow and springflow since it lumps all weathering processes into a single weathering rate measured at the watershed outlet. The mass-balance approach does not account for the integrative nature of streamflow.

In the absence of wells, springflow is often used as a means of sampling groundwater in order to avoid the integrative problems associated with streamflow. In many cases, spring chemistry appears to be dominated by contributions from deep, basin-scale groundwater [*Hoch and Reddy*, 2001; *Manga*, 2001; *Rademacher et al.*, 2001]. The geochemistry of springs therefore provides insight into bedrock weathering rates and solute release in watersheds. This approach has been recently used to quantify weathering rates in the Sierra Nevada [*Rademacher et al.*, 2001] and in the Trás-os-Montes province of northern Portugal [*Pacheco and Van der Weijden*, 2002; *Pacheco and Alencoão*, 2006]. However, very little effort has been spent in quantifying the variability of the groundwater component in springflow generation. Consequently, direct estimates of the weathering release from groundwater based on springflow data may be

hindered by the same problems as streamflow although possibly to a lesser extent [*Manga*, 2001]. The principal components responsible for springflow generation must be separated and the groundwater component must be isolated in order to accurately quantify the weathering release of solutes from only bedrock/groundwater interactions. This step should help improve the calibration of watershed geochemical models [*Bassett*, 1997] and quantify the bias associated with mass-balance approaches [*Velbel and Price*, 2007].

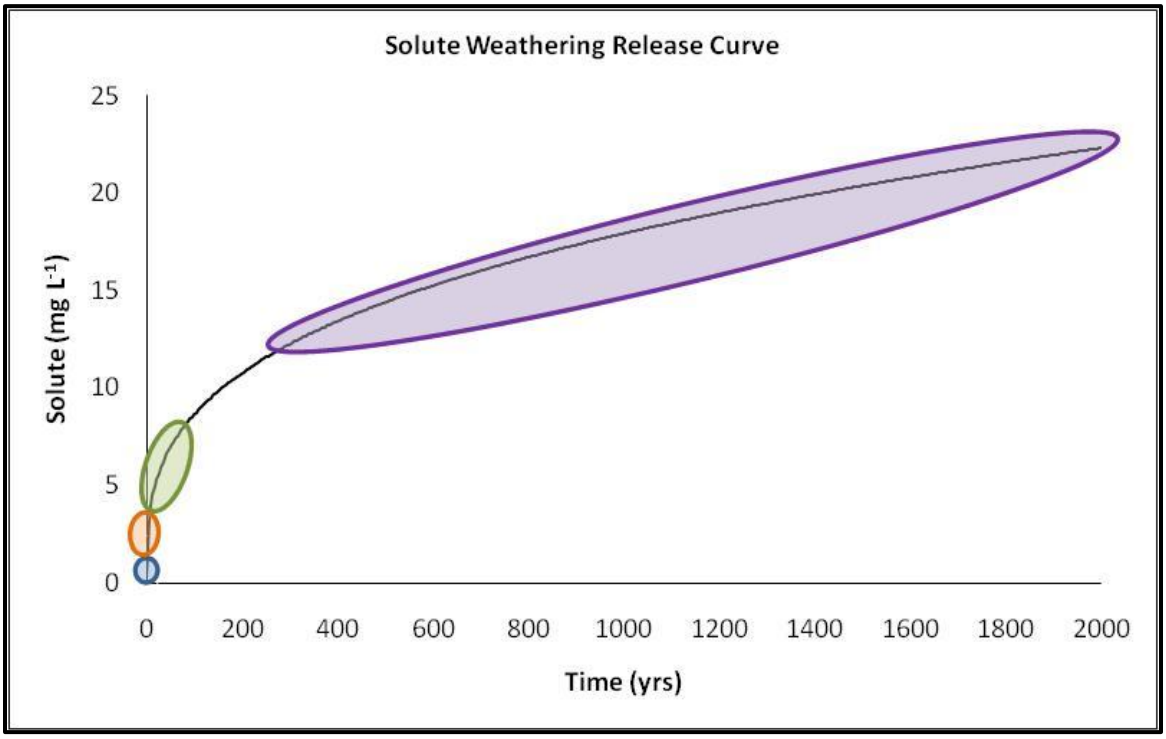

Figure 5.1: Schematic representation of solute weathering release curve. These curves represent a geochemical evolutionary pathway from meteoric inputs (blue oval) to groundwater (purple oval). Intermediate stages of this geochemical pathway are constrained by runoff processes (orange oval) and unsaturated flow in the soil (green oval).

In this paper, we investigate how temporal variability in the groundwater component of springflow generation affects solute weathering release curves by testing two conceptual models of springflow generation against our spring chemistry

observations. In one conceptual model, springflow is generated only by groundwater and as a consequence, the chemistry observed in springflow will represent only the solutes released by chemical weathering reactions involving groundwater flow (Figure 5.2a). Alternatively, in the second conceptual model, springflow is integrative and is composed of different components representing different water sources (Figure 5.2b). Consequently, the groundwater component in springflow may not be temporally consistent and the chemistry observed in springflow will represent solutes released by possibly many different chemical weathering reactions. We use this characteristic to test these two conceptual models. In order to quantify the temporal variability of the groundwater component in springflow, we employ endmember mixing analysis (EMMA) using 4 years of springflow chemistry and stable isotope data from the Saguache Creek watershed, a large (1670 km^2), mountainous watershed in the San Juan Mountains of southwestern Colorado (38° 5' 14" N and 106° 8' 29" W). We analyzed the chemistry and stable isotopic composition of seven perennial springs and five wells spanning a range in elevations. Our goal in conducting this research was to answer the following questions. Is the groundwater component in springflow generation temporally variable and if so, how does this variability affect solute weathering release curves? If we see evidence that the groundwater component in springflow is temporally variable, then our dataset would support the conceptual model for integrative springflow. As a consequence, solute weathering release curves and bedrock weathering rates based on the geochemical composition of springflow may be in error. Alternatively, if we see evidence that the groundwater component in springflow is not variable, then our dataset supports the conceptual model indicating springflow is only composed of groundwater.

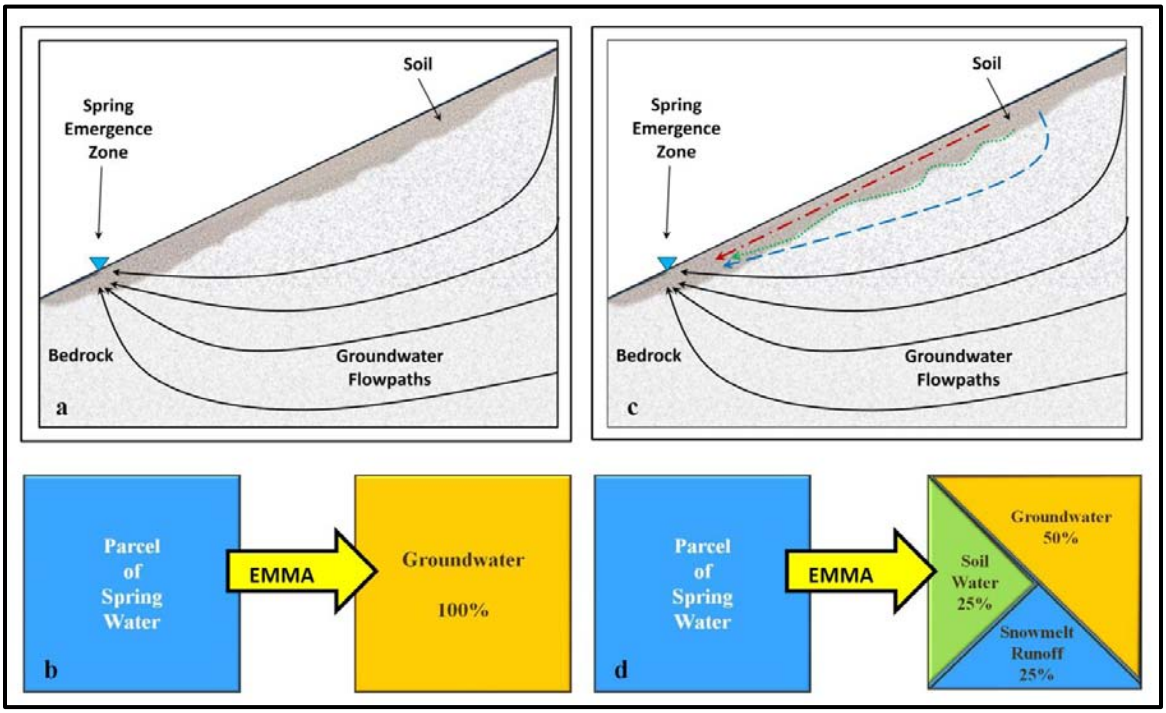

Figure 5.2: Conceptual models of springflow generation. a) The conceptual model where springflow is only generated by groundwater, b) the chemistry of springflow in this conceptual model will only represent the solute release from weathering processes associated with groundwater/bedrock interactions, c) the conceptual model where springflow is a integrative mix of water sources (soil-water is represented by the red dash-dot line, preferential flow in the soil is represented by the green dotted line, and shallow bedrock flow is represented by the blue dashed line), and d) the chemistry of springflow in this conceptual model will represent the solute release from an combination of water sources (groundwater, soil-water, and snowmelt runoff are shown in this example).

5.2: Site Description:

The Saguache Creek watershed is located in the San Juan Mountains of southern Colorado (Figure 5.3). The elevations in the watershed range from 2352 m to 4237 m. The watershed is approximately 1670 km^2 in area and is drained by a perennial stream, Saguache Creek, which flows into the northern San Luis Valley. The overall average daily streamflow in Saguache Creek from 1929 to 2004 is 1.78 $m^3 sec^{-1}$ (62.6 cfs) and this

discharge is exceeded 27 percent of the time according to flow duration curves. The minimum average daily streamflow on record is 0.20 $m^3 sec^{-1}$ (7.0 cfs) and the maximum average daily streamflow on record is 19.2 $m^3 sec^{-1}$ (678.0 cfs). Published historical streamflow data from 1910 to 2008 and provisional recent streamflow data is available at http://www.dwr.state.co.us/SurfaceWater/Default.aspx. These streamflow data are very comparable to other tributary streams of the Upper Rio Grande (URG) where the URG is defined as that portion of the Rio Grande located upstream of the border between Colorado and New Mexico.

In low-elevation regions of the watershed, snowfall accounts for 70 percent of the basin-wide average annual precipitation and rain comprises the remainder. In comparison, snowfall accounts for 88 percent of the basin-wide average annual precipitation in high-elevation regions of the watershed. The overall average annual rainfall recorded at the Saguache Creek Colorado Division of Water Resources (DWR) station located at an elevation of 2470 m is 21.2 cm, the minimum annual rainfall is 10.8 cm, and the maximum annual rainfall is 41.2 cm. Precipitation data is available at http://www.ncdc.noaa.gov/oa/ncdc.html. Our analyses indicate that the majority of rainfall typically falls during the months of July, August, and September and that June and October are typically dry months. May and October are both transitional months where rainfall and snowfall are both encountered. NRCS SNOTEL data is available for the Saguache Creek watershed. Data for snow depth and snow water equivalent can be found http://www.wcc.nrcs.usda.gov/snotel/Colorado/colorado.html. The Saguache Creek watershed contains one SNOTEL site (Cochetopa Pass) with a limited history of only 5 years; however, more extensive datasets area available from the Porphyry Creek

SNOTEL site located to the north of the watershed and the Slumgullion Pass SNOTEL site located to the southwest of the watershed. The Slumgullion site may actually be more representative of the high elevation headwaters of the Saguache Creek watershed. The average maximum snow water equivalent (SWE) for the Slumgullion SNOTEL site is 39.9 cm with a historical range of 20.6 cm to 57.7 cm. Peak SWE typically occurs on April 21 (WYD 203). Snowpacks typically begin to accumulate on October 14 (WYD 14) and are, on average, depleted by May 30 (WYD 232). These data yield average annual snowpack persistence of approximately 7 months.

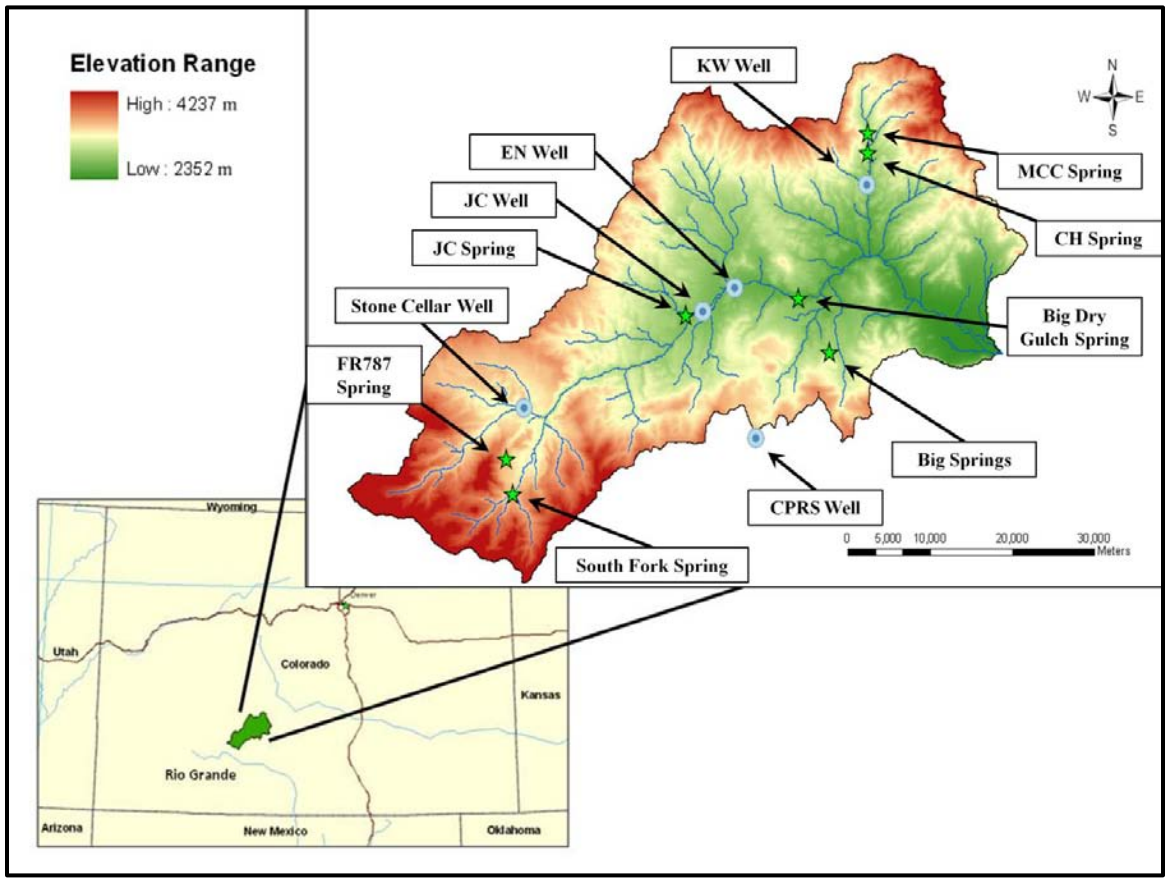

Figure 5.3: Map of Saguache Creek watershed. Green stars indicate spring sampling locations. Blue circles represent well sampling locations.

5.3: Geology of Saguache Creek:

A geologic map for Saguache Creek is shown in Figure 5.4. The geology of the Saguache Creek watershed is dominated by felsic volcanic tuffs resulting from the activity of the San Juan Volcanic Field (see Taf units in Figure 5.4) that overlie intermediate composition pre-caldera lavas and breccias (see Tpl units in Figure 5.4) from the Conejos/Rawley Formations [*Steven and Lipman,* 1976; *Lipman and McIntosh,* 2008]. Rock glaciers and expansive talus-covered regions are present in the steep headwater subwatersheds (see Ql units in Figure 5.4). Streams are not always bounded by extensive riparian zones except in the lower reaches of the watershed and these riparian zones are developed in the gravels and alluvium of the Pinedale and Bull Lake glaciations (see Qg units in Figure 5.4).

Soils in remote watersheds are not often classified beyond the soil association level since there is little agricultural or economic urgency to classify these soils at a finer resolution [*Engle,* 2009]. Therefore, we classified soils in the field using soil pits. These classifications indicated that the thin, high-elevation soils have little or no organic development, loamy AE horizons, and relatively weakly developed B-horizons. The soils typically contain fragments of biotite, quartz, and sodium and calcium-rich feldspars and often overlie fractured bedrock (Figure 5.5a). These soils are broadly classified by the NRCS as very stony loams of the Bushvalley-Embargo-Bowen soil association and cobbly or gravelly loams of the Frisco-Seitz-Granile soil association. Soil descriptions can be found at http://soils.usda.gov/survey/geography/statsgo/. Hillslope and low-elevation soils often contain a shallow, extensive layer of platy, felsic volcanic rocks which most likely promotes rapid infiltration and throughflow (Figure 5.5b). Field

observations indicated that many springs emerged from this type of layer in the watershed (Figure 5.5b). Saprolite was encountered in both high-elevation and low-elevation soil pits at depths ranging from 16 to 25 cm and persistent to depths greater than 40 cm. This layer serves as a translatory unit during snowmelt events that saturates from above and then slowly transmits water to the underlying fractured bedrock. Consequently, this layer may be an important control on recharge to bedrock aquifers within the mountain block.

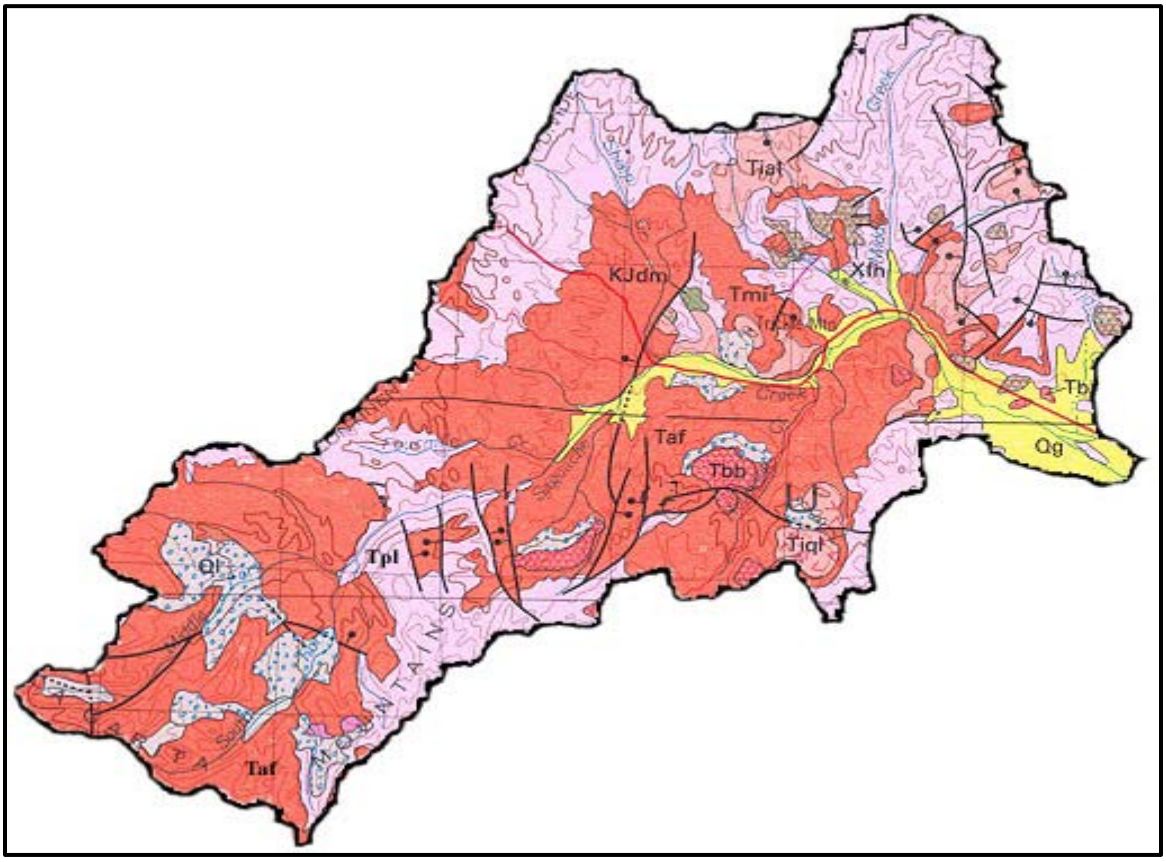

Figure 5.4: Geologic map of Saguache Creek watershed. Geological designations are as follows: Qg: gravels and alluvium from the Pinedale and Bull Lake glaciations, Ql: landslide deposits including thin talus, rock-glaciers, and thick colluvial deposits, Taf: ash-flow tuff of main volcanic sequence (26-30 Mya), Tpl: pre-ash-flow andesitic lavas, breccias, tuffs, and conglomerates (30-35 Mya), Tbb: basalt flows and associated tuffs, breccias, and conglomerates (3.5-26 Mya), Tial: intra-ash-flow andesitic lavas, and Tiql: intra-ash-flow quartz latitic lavas. (http://geology.about.com/library/bl/maps/blcoloradomap.htm).

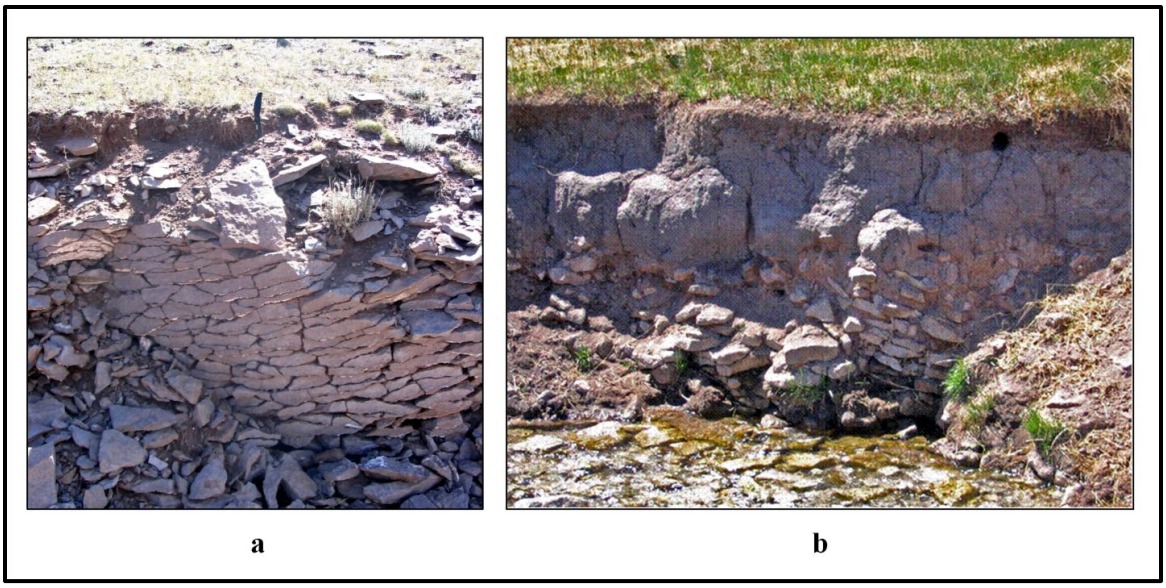

Figure 5.5: a) Soil development and underlying fractured bedrock at an elevation of 3139 m above sea-level. Note pocket knife for scale (length 19.5 cm). b) Typical hillslope soil development at an elevation of 2621 m above sea-level. Note the deposit of heavily fractured rhyolitic material near lower soil profile and the seep expansion following snowmelt that appears to originate from this layer.

5.4: Methods:

Springflow samples were collected from 2005 to early 2009. Seven springs were targeted during this study (Figure 5.3). Samples were analyzed for pH, electrical conductivity (EC), total dissolved solids (TDS), and temperature while in the field. Field acidification was not performed on water samples since the samples were analyzed quickly after collection for chloride (Cl^-), calcium (Ca^{2+}), and sodium (Na^+) using ion-selective electrodes. Some samples were also subjected to a full general chemistry analysis of all basic cations and anions in the Chemistry Laboratory of the New Mexico Bureau of Geology and Mineral Resources located on the New Mexico Tech campus. Analytical methods for chemical analyses and stable isotope analyses are included in the Appendix. The geochemical evolution of waters in the Saguache Creek watershed is shown in Figure 5.6 for reference.

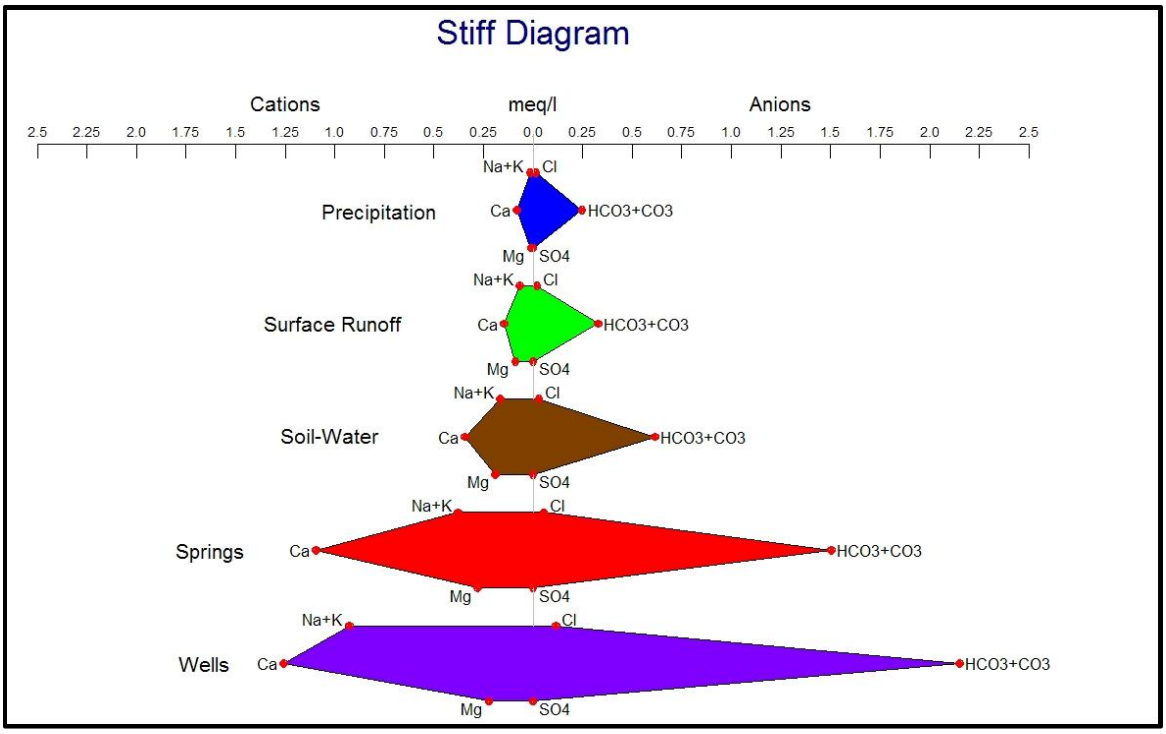

Figure 5.6: Stiff diagram depicting the geochemical evolution of relatively dilute precipitation to more geochemically evolved well waters in the watershed. Note that spring waters (red polygon) are not as geochemically evolved as well waters (navy blue polygon). This is an indication of the integrative nature of springs.

Wells were sampled in the watershed in order to obtain groundwater samples representative of longer residence times and enhanced geochemical evolution. Wells are sparse in the watershed and consequently only six wells were sampled (Figure 5.3). Most of these wells are located below an elevation of 2600 m above sea level. However, two wells were located in the backcountry at elevations of 2900 and 3100 m above sea level. All wells appear to terminate in the local bedrock. All well samples were analyzed using the same procedures for spring water samples. Two wells had very distinct geochemistry and plotted outside the grouping of the other wells in the watershed (Figure 5.7). These two wells had anomalous concentrations of sulfate and iron and were omitted from further analyses.

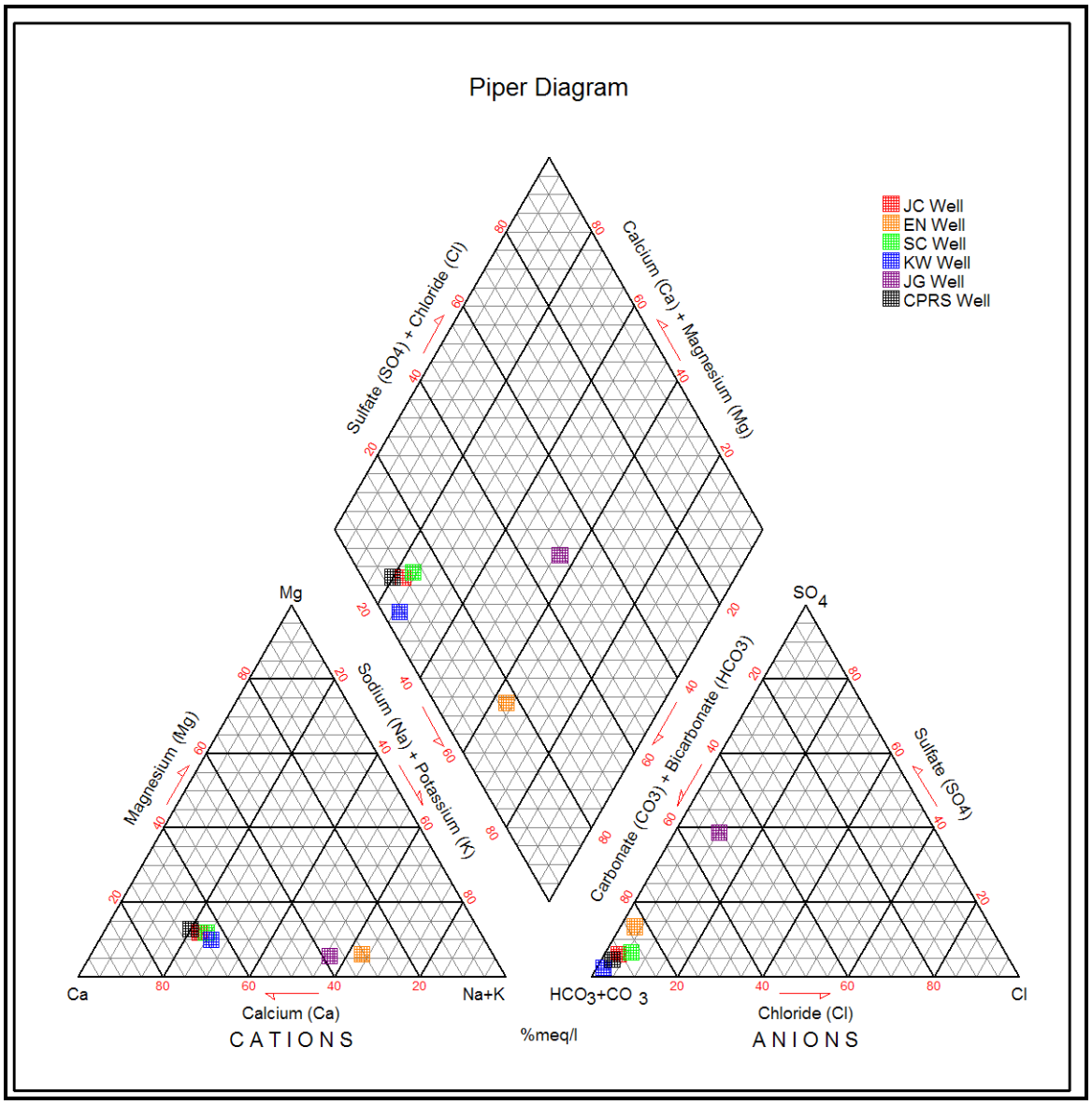

Figure 5.7: Piper diagram for groundwater wells in the watershed. All wells plot together except for JG Well (purple square) and EN Well (orange square). These two wells were not used in this study.

5.4.1: Analytical Methods:

Analytical methods are described in Chapter 4, Section 4.3.5.

5.4.2: Radiocarbon Sampling Methods and Corrections:

One 1-L sample of water from each spring and well were collected for radiocarbon dating. Springs were plumbed whenever possible with flexible 1.27 cm ID

PVC tubing. The tubing was inserted into flowing fractures when present or into the spring orifice and pushed as deeply as possible into the bedrock to eliminate contamination by modern atmospheric carbon (Figure 5.8). Well water was collected from spigots located near the well casings. The spigots were allowed to flow freely for a short duration in order to purge water that was retained in pipes or tanks and in order to sample fresh water from the bedrock aquifer. In all cases, water was collected to fill a 1-L LDPE bottle leaving only a very small headspace. The cap for the bottle was then securely tightened and wrapped with duct tape. Radiocarbon dating was performed on these samples by Beta Analytic, INC. of Miami, FL.

Figure 5.8: Plumbing methodology used to sample springflow from within the fractured bedrock.

We used radiocarbon analyses to estimate groundwater ages for well and spring waters. The initial ^{14}C activity, A_0, [*Fontes and Garnier,* 1979] in each well and spring sample was determined using the geochemical code NETPATH [*Plummer et al.,* 1994] and the method described in the work of *Fontes and Garnier,* (1979). The results from the Fontes and Garnier method were comparable to those of the Vogel method where A_0 is assumed to be 85 pmC [*Vogel and Ehhalt,* 1963; *Vogel,* 1967, 1970]. The Pearson method was also used for comparison [*Pearson,* 1965; *Pearson and Henshaw,* 1970]. In the Pearson method, A_0 is determined by a correction based on the concentrations of $\delta^{13}C$ in the individual water sample, in carbonate rock sources, and in recharging waters. The $\delta^{13}C$ of the individual spring samples was provided by Beta Analytic, INC. and by analysis conducted in the New Mexico Tech Stable Isotope Lab using DIC precipitation [*Szynkiewicz et al.,* 2006]. We measured the $\delta^{13}C$ of recharging water using water samples that were obtained from passive capillary samplers installed deep in soil horizons throughout the watershed in 2007 and 2008 [*Frisbee et al.,* 2010a]. The average $\delta^{13}C$ of deep percolating waters in the watershed was -16.5‰. There are no obvious sources of carbonate minerals in the watershed because the underlying bedrock is almost entirely volcanic [*Steven and Lipman,* 1976]. Any carbonate minerals with which the infiltrating precipitation may react are therefore probably primarily exogenic.

In order to improve our radiocarbon corrections, we attempted to identify exogenic carbonate sources by sampling dust, soil, organic litter, and calcite fracture fillings. The $\delta^{13}C$ of solid carbonates such as those present in dust, soil, and calcite fracture fillings was measured in the New Mexico Tech Stable Isotope Lab according the method described in *McCrea* [1950]. Aeolian deposition of carbonate was monitored

using dust collectors described in the work of *Reheis and Kihl* [1995] and *Reheis et al.* [2002]. Dust deposition rates ranged from 0.63 to 1.59 g m^{-2} y^{-1} during 2007. The average $\delta^{13}C$ of carbonate in dust was -9.7‰. We collected soil samples from soil pits used for soils classification and M-PCAPS installations. We analyzed greater than 20 soil samples over a range in sample masses from 25 mg to 55 mg and sufficient CO_2 for $\delta^{13}C$ analysis could not be generated from any soil sample. This does not seem to be a methodological problem since only 25 mg of dust or less than 1 mg of solid calcite is typically required for this procedure [*McCrea,* 1950]. Such low carbonate concentrations indicate that carbon found in dust is probably flushed from soils during large precipitation events or is being rapidly removed by biological processes, corresponding to the fast-cycling carbon reservoir described in *Blumhagen and Clark* [2008]. To further quantify potential sources of carbon in the soil, we analyzed pine needle duff from the organic horizons of high-elevation soils in the watershed. The pine needle duff was modern (pmC = 116.5) indicating that little if any old carbon is stored in the organic layer. Calcite fracture fillings were found in some of the exposed bedrock outcroppings and roadcuts. These calcite fillings had an average $\delta^{13}C$ of 3.1‰ and the $\delta^{13}C$ ranged from -4.1 to 8.5‰. The samples at the upper end of this range were isotopically heavier than those reported in the Bandelier Tuff near Los Alamos, NM ($\delta^{13}C$ ranged from -4.1 to -5.2 ‰) [*Newman et al.,* 1997] and in the Snowshoe Mountain area near Creede, CO ($\delta^{13}C$ ranged from -3.5 to -8.7 ‰) [*Hoch et al.,* 2000]. The ^{14}C ages of the calcite fracture fillings at Snowshoe Mountain ranged from 30.1 to 46.4 ka [*Hoch et al.,* 2000] and we think these ages may also be appropriate for the fracture fillings found in the

Saguache Creek watershed based on the close proximity between Snowshoe Mountain and the headwaters of the Saguache Creek watershed.

When these data were included in the radiocarbon corrections, the corrected ages found using the Pearson method were not always in agreement with the other two approaches. The Vogel corrected ages and the Fontes and Garnier corrected ages were in close agreement in most cases; however, the results from the Fontes and Garnier method were chosen because this method couples a geochemical mass-balance of all carbon sources with an isotopic mass-balance to account for fractionation between gas, liquid, and mineral carbon phases [*Fontes and Garnier,* 1979]. The corrected ages of wells ranged from modern (50 years) to 2300 years. Spring water ages ranged from modern (50 years) to 3200 years. Radiocarbon ages did not correlate with either spring elevation or the contributing areas for springs.

5.4.3: End-Member Mixing Analysis:

A description of end-member mixing analysis can be found in Chapter 4, Section 4.3.1.

5.4.4: Diagnostic Tools of Mixing Models:

Diagnostic tools for mixing models are described in Chapter 4, Section 4.3.2.

5.4.5: Selection of Endmembers:

The selection of endmembers is described in Chapter 4, Section 4.3.3.

5.4.6: Calculation of Weathering Release Curves:

Weathering release curves provide an indication of total accumulated solute release from bedrock as a function of time. These curves were created by plotting concentrations of silica (Si), calcium (Ca^{2+}), magnesium (Mg^{2+}), and sodium(Na^{+}) against

the corrected radiocarbon age for each individual spring. We created weathering release curves for uncorrected spring samples and for spring samples which had been corrected for groundwater contribution. Springflow can be broken down into its individual components:

$$Q_{spr} = \sum_i Q_i \quad (1)$$

Where Q_{spr} is the total springflow measured at the time of sampling and Q_i represents the potential components. For example, Q_{gw}, Q_{ro}, and Q_{sw} are the contributions to springflow from groundwater (gw), runoff (ro), and soil-water (sw), respectively. Using the EMMA results, we can quantify the contributions of each component that contribute flow to the spring:

$$Q_i = X_i\, Q_{spr} \quad (2)$$

Where Q_{spr} is the total springflow measured at the time of sampling and X_i represents the fractions of the components that contribute to springflow. For example, X_{gw}, X_{ro}, and X_{sw} are the fractions of the components that contribute to springflow from groundwater, runoff, and soil-water, respectively. Based on these relationships, we can then define the chemical composition of springflow as the sum of the chemical compositions of its components:

$$C_{spr} = \boldsymbol{X_{gw}\, C_{gw}} + X_{ro}\, C_{ro} + X_{sw}\, C_{sw} \quad (3)$$

Where C_{spr} is the concentration of a specific chemical constituent in total springflow measured at the time of sampling, C_{gw}, C_{ro}, and C_{sw} are the concentrations of the same specific chemical constituent in the contributions to springflow from groundwater, runoff, and soil-water, respectively. The groundwater component, indicated by the bold, italicized letters in equation 3, is the component of interest in this study. Finally, we can

define the weighted mean age of springflow as the sum of the ages of the components which contribute to springflow:

$$t_{spr} = \boldsymbol{X_{gw}\, t_{gw}} + X_{ro}\, t_{ro} + X_{sw}\, t_{sw} \qquad (4)$$

where, t_{spr} is the apparent age of the spring sample (i.e., the corrected radiocarbon age), t_{gw}, t_{ro}, and t_{sw} are the apparent ages of the contributions to springflow from groundwater, runoff, and soil-water, respectively. The corrected radiocarbon age of the runoff component, t_{ro}, was assumed to be modern and on the order of days. We collected samples of infiltrating meltwater using M-PCAPS [*Frisbee et al.*, 2010a] to quantify the geochemistry and isotopic composition of soil-meltwater. These M-PCAPS were left intact over the course of a complete snow accumulation and subsequent snowmelt cycle (a duration of 7 months). Therefore, the corrected radiocarbon age of soil-water, t_{sw}, was assumed to represent the geochemical and isotopic evolution of infiltrating water occurring during that 7-month time interval. The corrected radiocarbon age of the groundwater component, t_{gw}, was estimated using the corrected radiocarbon ages of groundwater wells that were located in close proximity to the springs.

Weathering release curves for the original, uncorrected spring water samples were created by plotting chemical concentrations in total springflow (C_{spr} in Equation 3) against the apparent of ages of the spring samples (t_{spr} in Equation 4) for each chemical constituent. For comparison, we also created weathering release curves for corrected springflow in which the groundwater component had been isolated. To do this, we plotted the groundwater contribution of spring chemistry (C_{gw} in Equation 3) against the groundwater contribution of spring age (t_{gw} in Equation 4). Solute weathering release curves were created for Si, Ca^{2+}, Mg^{2+}, Na^{+}, and K^{+}.

5.5: Results:

5.5.1: Variability of the Groundwater Component in Springflow:

All spring waters in this study plot together in a piper diagram (Figure 5.9). Spring waters are generally characterized by Ca^{2+} and Mg^{2+} which are balanced by HCO_3^-. Seven springs shown in Figure 5.3 were chosen for this study: Big Dry Gulch Spring (BDGS – elevation 2525 m), Big Springs (BGS – elevation 2761 m), JC Spring (elevation 2620 m), FR787 Spring (elevation 3148 m), CH Spring (elevation 2651 m), Middle Creek Campground Spring (MCC – elevation 2723 m), and South Fork Spring (SFS – elevation 3095 m). Residuals calculated from the re-projected springflow chemistry and original chemistry dataset were plotted for each spring to ascertain the conservative nature or appropriateness of the tracers. Table 5.1 includes the R^2 and p-value for each correlation between the re-projected chemistry and original chemistry of each chemical constituent for an individual spring. Table 5.1 also includes the dimension of the mixing subspace (D) which indicates the number of endmembers to be retained (# endmembers = D + 1). A 2-endmember mixing subspace is a line and a 3-endmember mixing subspace is a triangle. Random distributions in the plots where $p > 0.05$ and $R^2 < 0.2$ indicate well-posed models while structure in the plots indicates poorly constrained models. As can be inferred from Table 5.1, CH Spring and MCC Spring required 2 endmembers and all other springs required 3 endmembers in the mixing subspace. The two-endmember mixing model is most likely due to the limited number of samples from these two springs. Infrequent sampling limits the degrees of freedom in the diagnostic

analysis. Therefore, we are unable to re-project the spring chemistry beyond a 2-endmember mixing subspace.

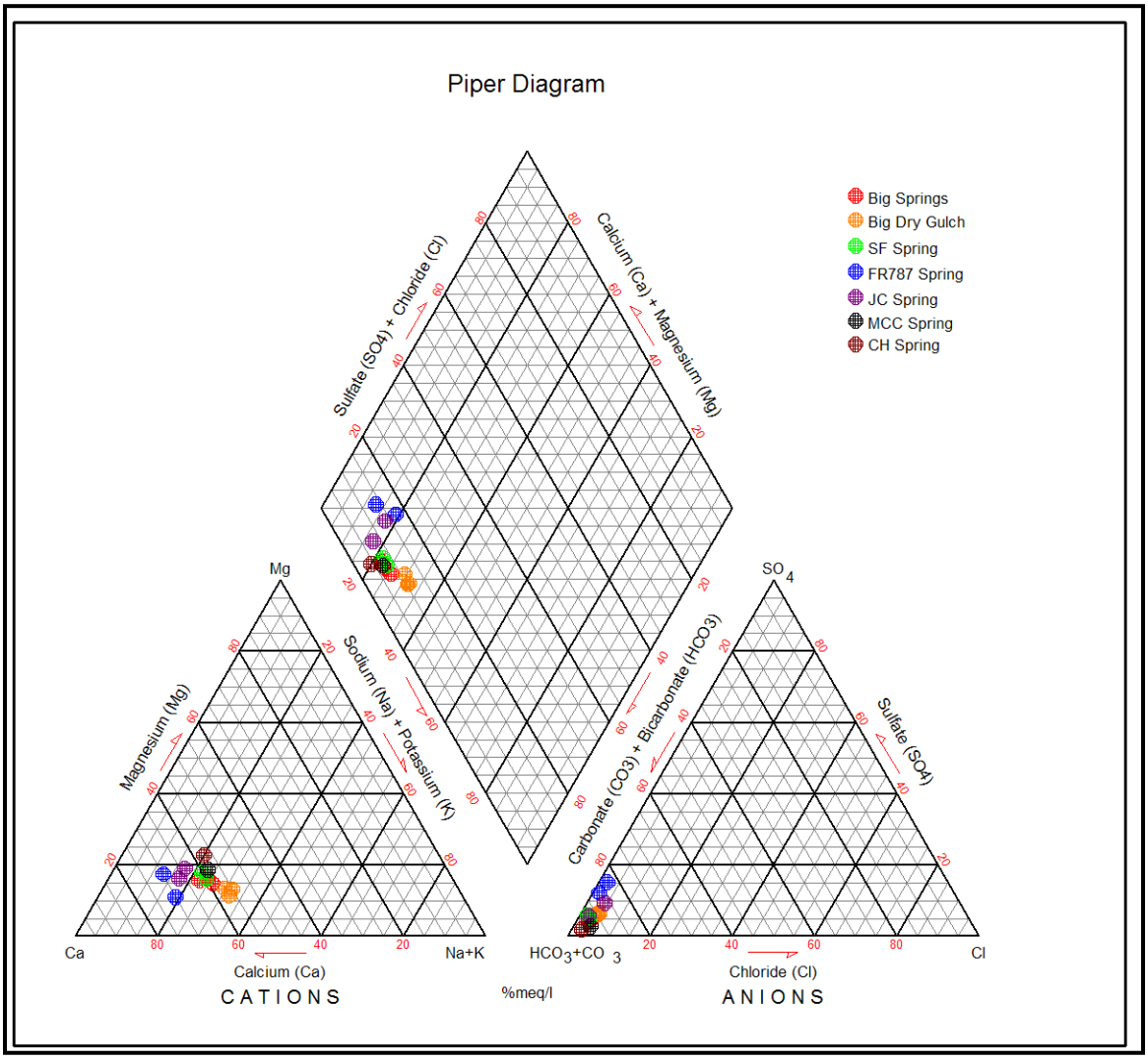

Figure 5.9: Piper diagram for springs sampled during this study. FR787 Spring (blue circle) is the highest elevation spring and Big Dry Gulch Spring (orange circle) is the lowest elevation spring. Note that there is a slight evolution toward increasing sodium and potassium with decreasing elevation.

Spring ID	EC (μS/cm)			Ca^{2+} (mg/L)			Na^{+} (mg/L)			Cl^{-} (mg/L)			$\delta^{18}O$ (‰)			$\delta^{2}H$ (‰)		
	R^2	p	D	R^2	p	D	R^2	p	D	R^2	p	D	R^2	p	D	R^2	p	D
BDGS	0.14	0.19	3	0.21	0.10	3	0.05	0.43	2	0.22	0.09	2	0.23	0.09	3	0.25	0.07	2
BGS	0.14	0.19	3	0.21	0.10	1	0.23	0.08	1	0.30	0.05	3	0.13	0.20	3	0.19	0.12	4
JC	0.14	0.47	1	0.09	0.57	1	0.20	0.38	1	0.24	0.32	1	0.05	0.67	2	0.14	0.46	2
FR787	0.14	0.29	1	0.13	0.31	2	0.08	0.44	2	0.41	0.05	1	0.21	0.18	1	0.04	0.57	2
CH*	0.43	0.54	1	0.11	0.78	1	0.07	0.83	1	0.06	0.85	1	0.61	0.43	1	0.87	0.07	1
MCC	0.57	0.14	2	0.10	0.61	1	0.12	0.57	1	0.12	0.56	2	0.52	0.17	1	0.56	0.15	1
SFS	0.37	0.06	2	0.18	0.22	1	0.15	0.27	2	0.20	0.20	2	0.20	0.19	2	0.01	0.78	3

Table 5.1: Data from the correlations between residuals of re-projected spring chemistry and original spring chemistry. Random distributions in the plots, indicated by $p > 0.05$ and $R^2 < 0.2$, indicate well-posed models while structure in the plot indicates poorly constrained models. R^2 is the correlation coefficient, p-value describes how significantly different the slope of the correlation line is from a value of zero, and D is the dimension of the mixing subspace where the required number of endmembers is equal to D + 1.

Since endmember mixing analysis and separations are not common in springflow studies, we provide an example of a mixing subspace, in particular the mixing subspace for Big Springs, in Figure 5.10. The x-axis, *U1*, is the first PCA reprojection for the spring and the y-axis, *U2*, is the second reprojection for the spring. The *U*-space is determined by the first and second eigenvectors extracted from the correlation matrix of conservative tracers [*Liu et al.,* 2008]. In Figure 5.10, there are four possible endmembers that encompass the Big Springs data cloud (purple diamonds). These endmembers are CPRS Well (groundwater – orange circle), rainfall (blue triangle), soil-water (yellow circle), and surface runoff (green triangle). The groundwater, soil-water, and snowmelt runoff components were chosen because they exhibited the smallest distance between original chemistry and re-projected chemistry (see *Hooper,* 2003 and *Liu et al.,* 2008]. It can be seen in Figure 5.10 that the groundwater endmember is the dominant endmember since all the samples for Big Springs plot near the groundwater endmember in the mixing subspace. However, it also appears that the contributions from

the groundwater are variable since the spring samples are spread out in the mixing subspace. Outliers are indicated in Figure 5.10 and these are solved using the geometrical approach described in the work of *Liu et al.*, [2008]. Similar *U*-space mixing diagrams were created for all springs but will not be shown in this paper to conserve space.

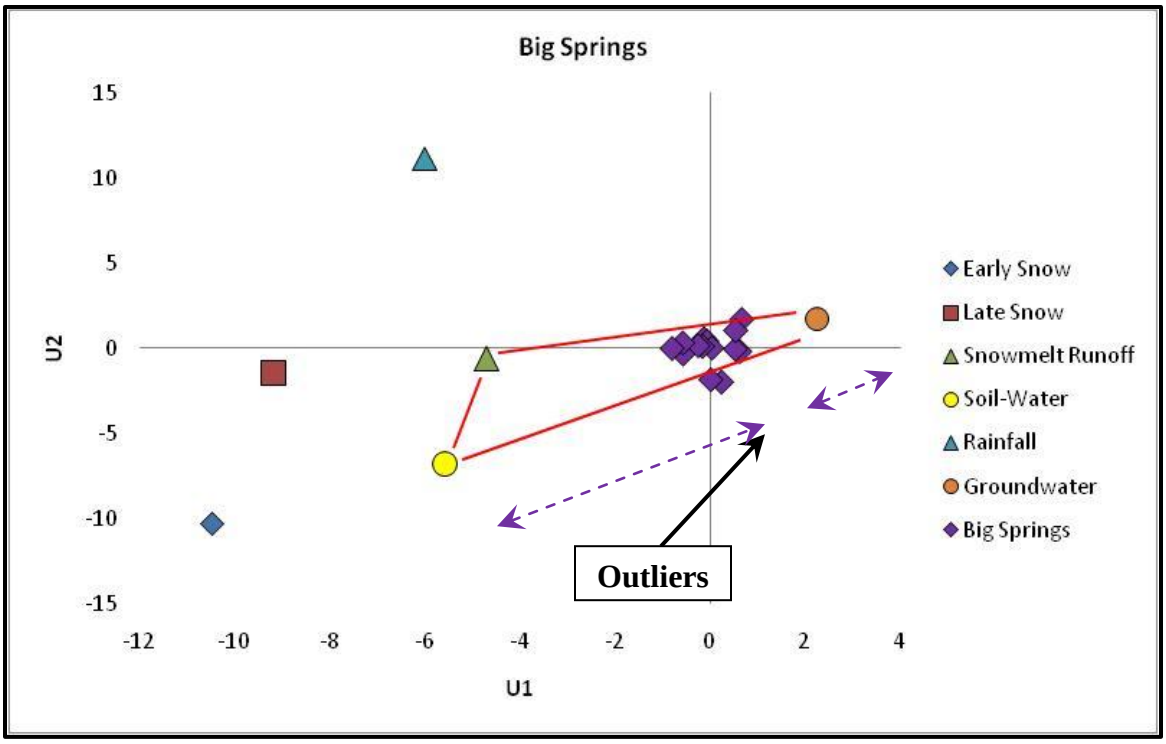

Figure 5.10: Example of the U-space mixing subspace used to illustrate the relationship between samples for an individual spring (purple diamonds indicate samples for Big Springs) and potential sources of springflow. In this example, the springflow appears to be composed of groundwater (orange circle), soil-water (yellow circle), and snowmelt runoff (green triangle). The outliers are indicated by the black arrow. The composition of an outlier is typically determined as a combination of two closest lying endmembers indicated by the purple dashed lines. In this case, groundwater and soil-water are components of springflow and snowmelt runoff does not make a contribution to springflow.

As mentioned previously, the key between distinguishing these conceptual models is whether or not the groundwater component in springflow is variable. Our EMMA results indicate that the groundwater component in springflow is very variable. In fact,

no spring in the Saguache Creek watershed is composed of 100 percent groundwater. This is readily apparent if the overall minimum and overall maximum groundwater contributions of all the in this dataset are examined (Figure 5.11). Minimum groundwater contributions range from 8 to 61 percent of springflow while maximum groundwater contributions range from 70 to 98 percent of springflow (Figure 5.11). Springs were sampled on monthly intervals and springflow was influenced by local fluctuations in the water table created by seasonal meteoric events. It is also apparent from Figure 5.11 that groundwater contributions are not strongly correlated with spring elevation. Therefore, it cannot be assumed that low-elevation springs will always have larger groundwater contributions than high-elevation springs. As a consequence of these findings, solutes in uncorrected springflow will be acquired from multiple solute sources and the groundwater contributions will be variable at all elevations. These results illustrate the integrative springflow conceptual model and suggest that the variability in the groundwater component will create bias in solute weathering release curves based solely on uncorrected springflow chemistry.

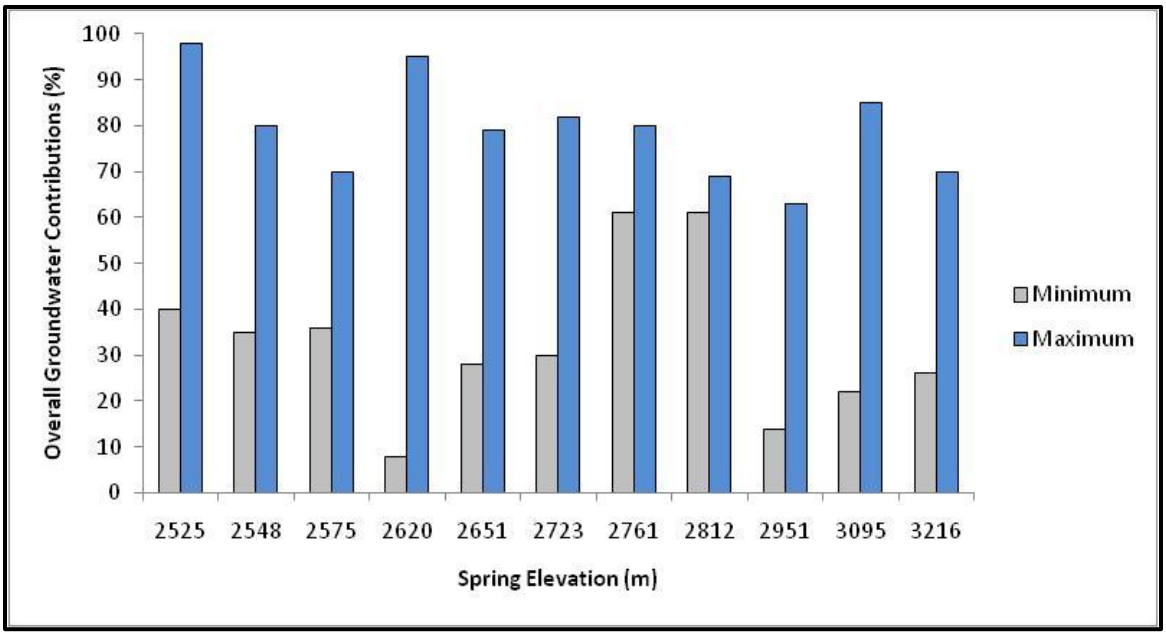

Figure 5.11: Overall minimum (grey) and overall maximum (blue) groundwater contributions to springflow. All available data was considered in this range.

5.5.2: Comparison of Solute Weathering Release Curves:

Solute weathering release curves provide an indication of the accumulated solute release from bedrock as a function of time. The weathering release curves for silica, calcium, magnesium, sodium, and potassium are shown in Figures 5.12, 5.13, 5.14, 5.15, and 5.16, respectively. For each chemical constituent, we show the solute weathering release curve determined using the chemistry of groundwater sampled from wells in the top plot of the figure and we plot the solute weathering release curves for the uncorrected springflow (represented by squares) and corrected springflow (represented by diamonds) in the bottom plot of the figure. The similarity in the solute weathering release curves between wells and uncorrected springflow is striking. Despite the variability observed in the groundwater component of springflow, there appears to be little difference between these two solute weathering release curves (refer to plots 'a' and dashed-line curve in plot

'b' in each figure). However, when the groundwater component in springflow is isolated and solute weathering release curves are based only on the ages and chemical compositions of the groundwater components in springflow, we see a definite decrease in the solute weathering release (refer to dotted-line curve in plot 'b' in each figure).

We calculated the weathering release of Si, Ca^{2+}, Mg^{2+}, Na^{+}, and K^{+} over the course of 4000 years since this time interval seemed to bracket the range of water ages in the watershed. In all cases, the weathering release curves for uncorrected springflow overpredicted the solute release as compared to corrected springflow. In fact, the weathering release curves for uncorrected springflow overpredicted Si by 50 percent, Ca^{2+} by 10 percent, Mg^{2+} by 51 percent, Na^{+} by 7 percent, and K^{+} by 32 percent. This bias is significant. As a consequence, estimates of the solute release from bedrock weathering based on uncorrected springflow will be too large. These trends illustrate the complex integrative nature of springflow.

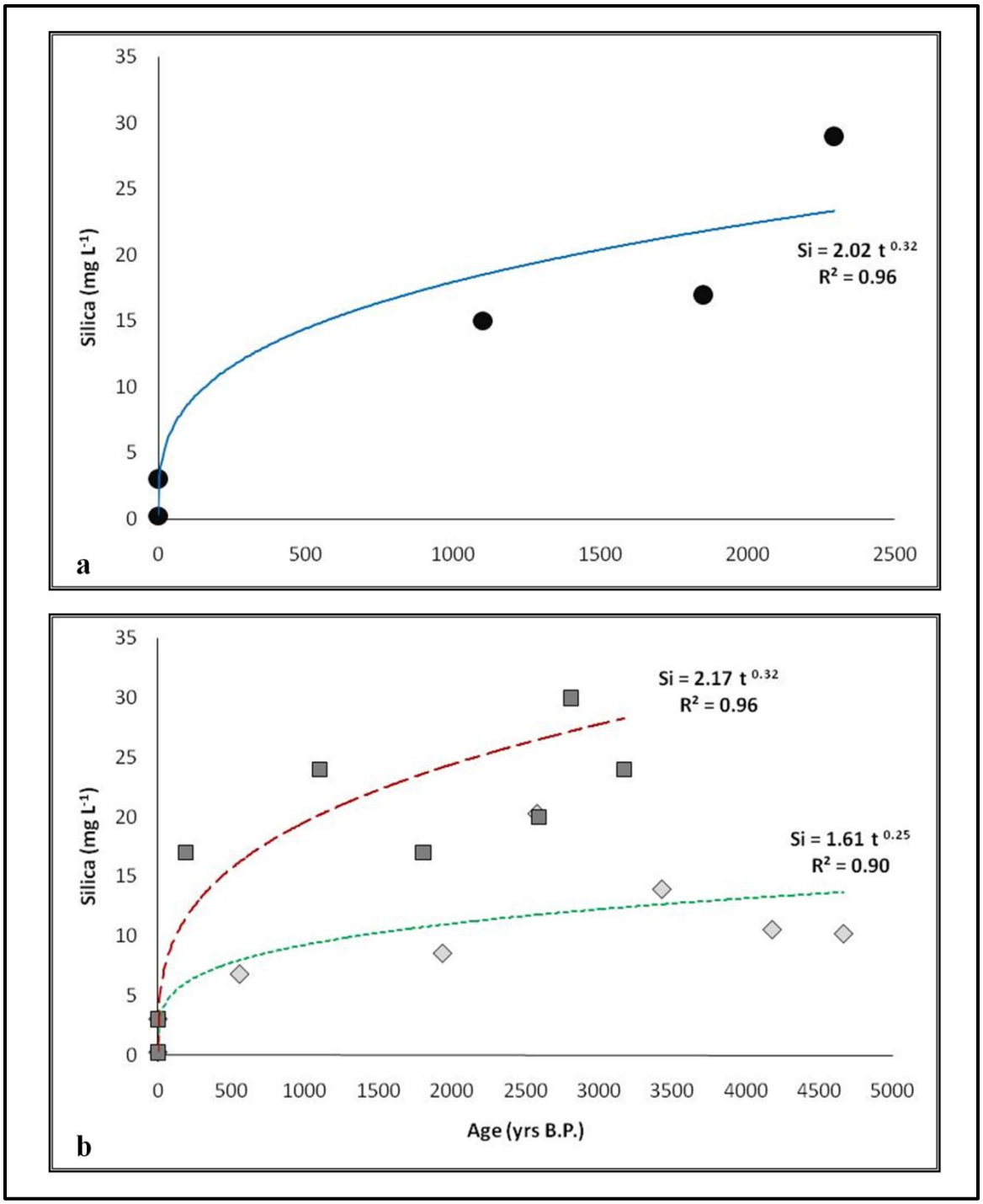

Figure 5.12: Weathering release curves for silica. a) The solid blue line in represents the silica release calculated for groundwater wells. b) The red dashed line represents the silica release calculated for uncorrected springflow and the green dotted line represents the silica release calculated for the corrected springflow. These color and style patterns are held consistent in each of the weathering release curve plots.

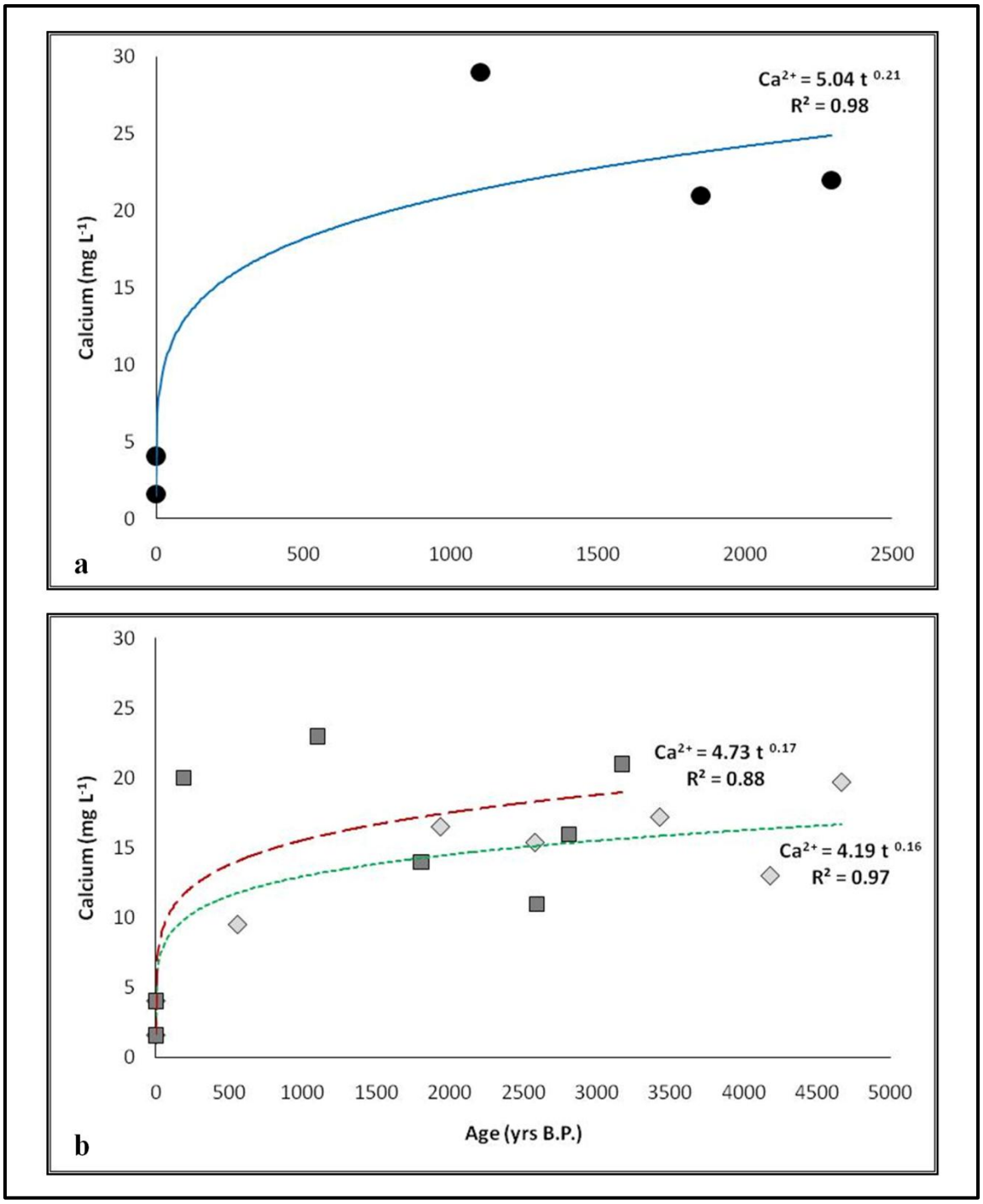

Figure 5.13: Weathering release curves for calcium.

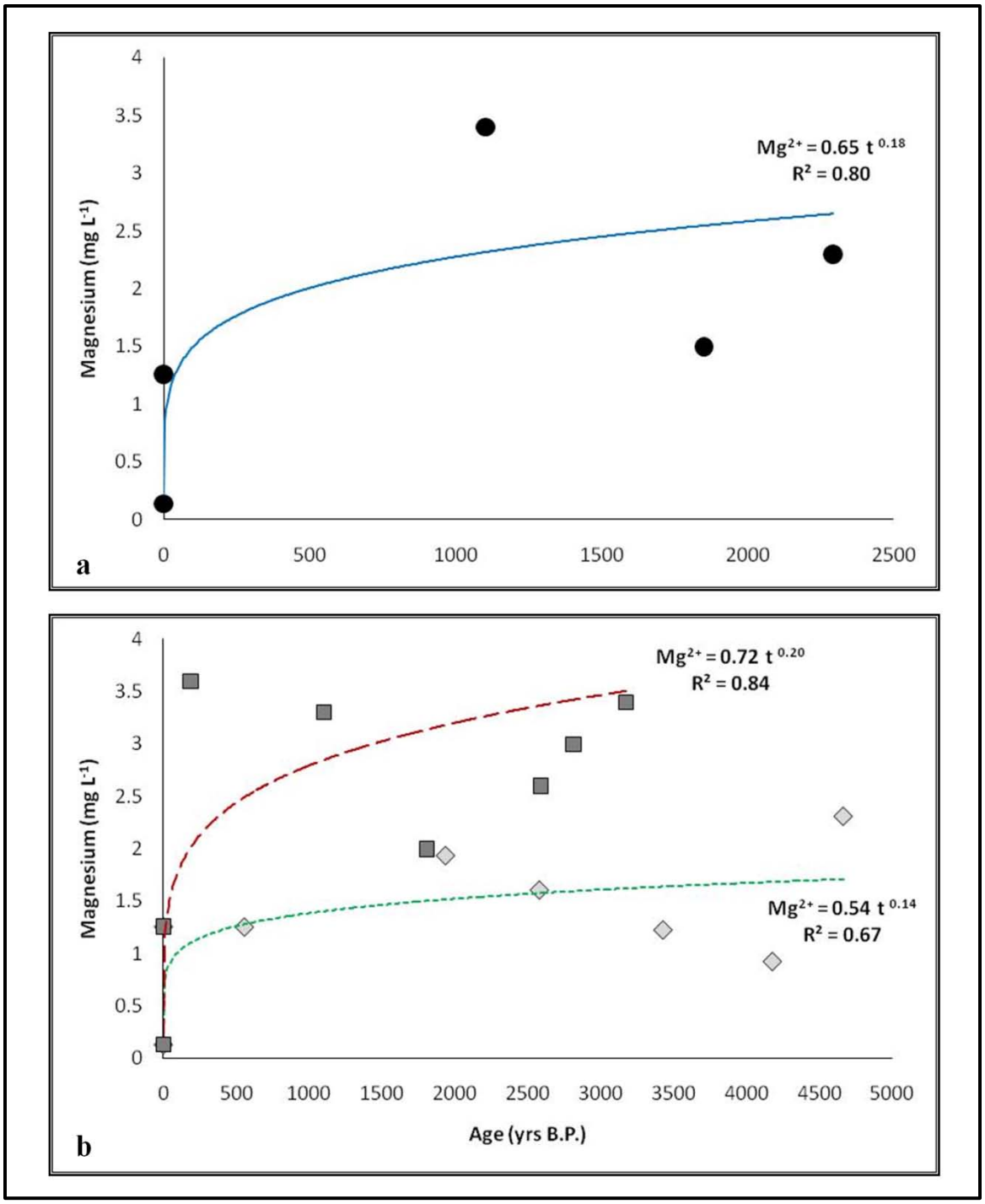

Figure 5.14: Weathering release curves for magnesium.

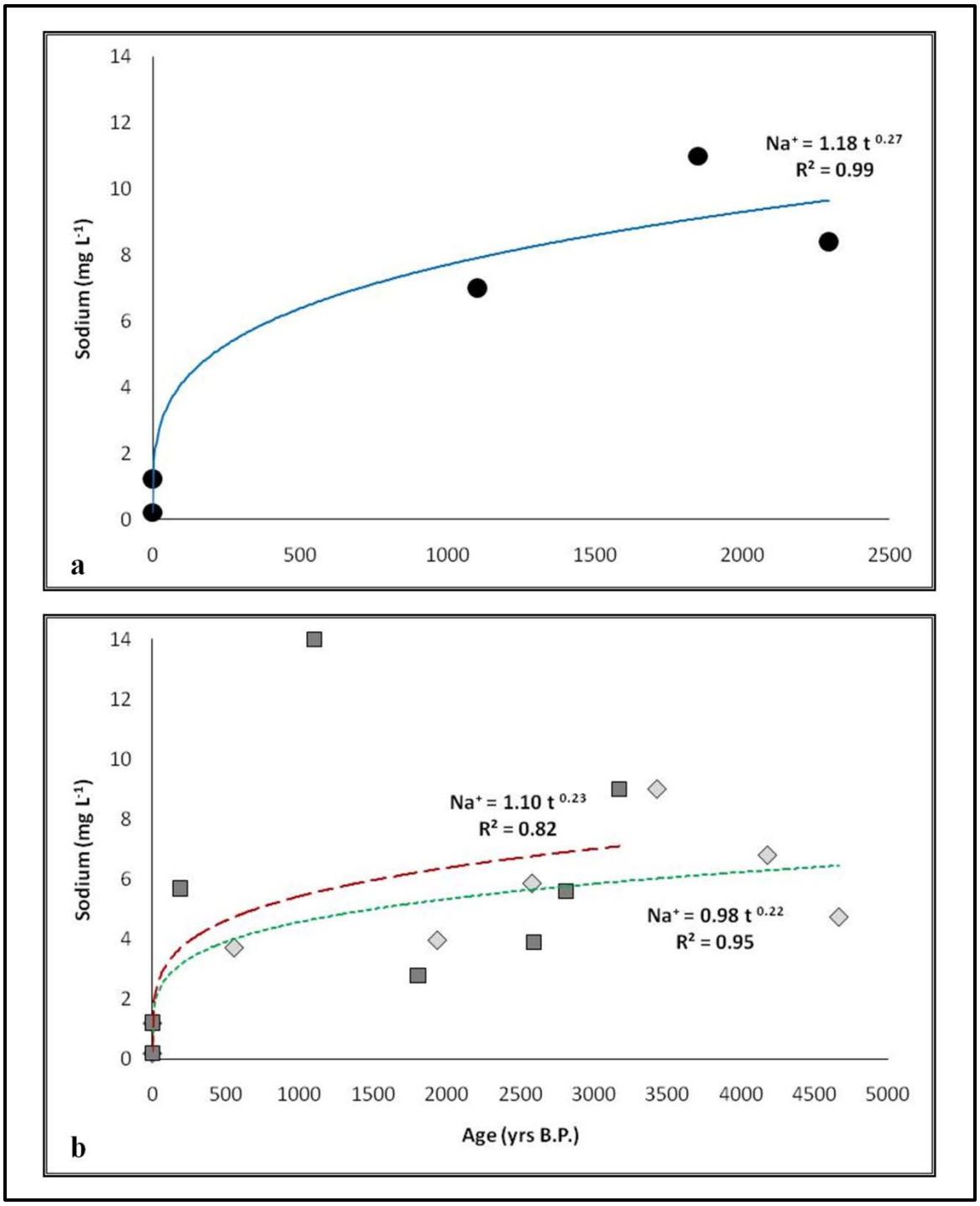

Figure 5.15: Weathering release curves for sodium.

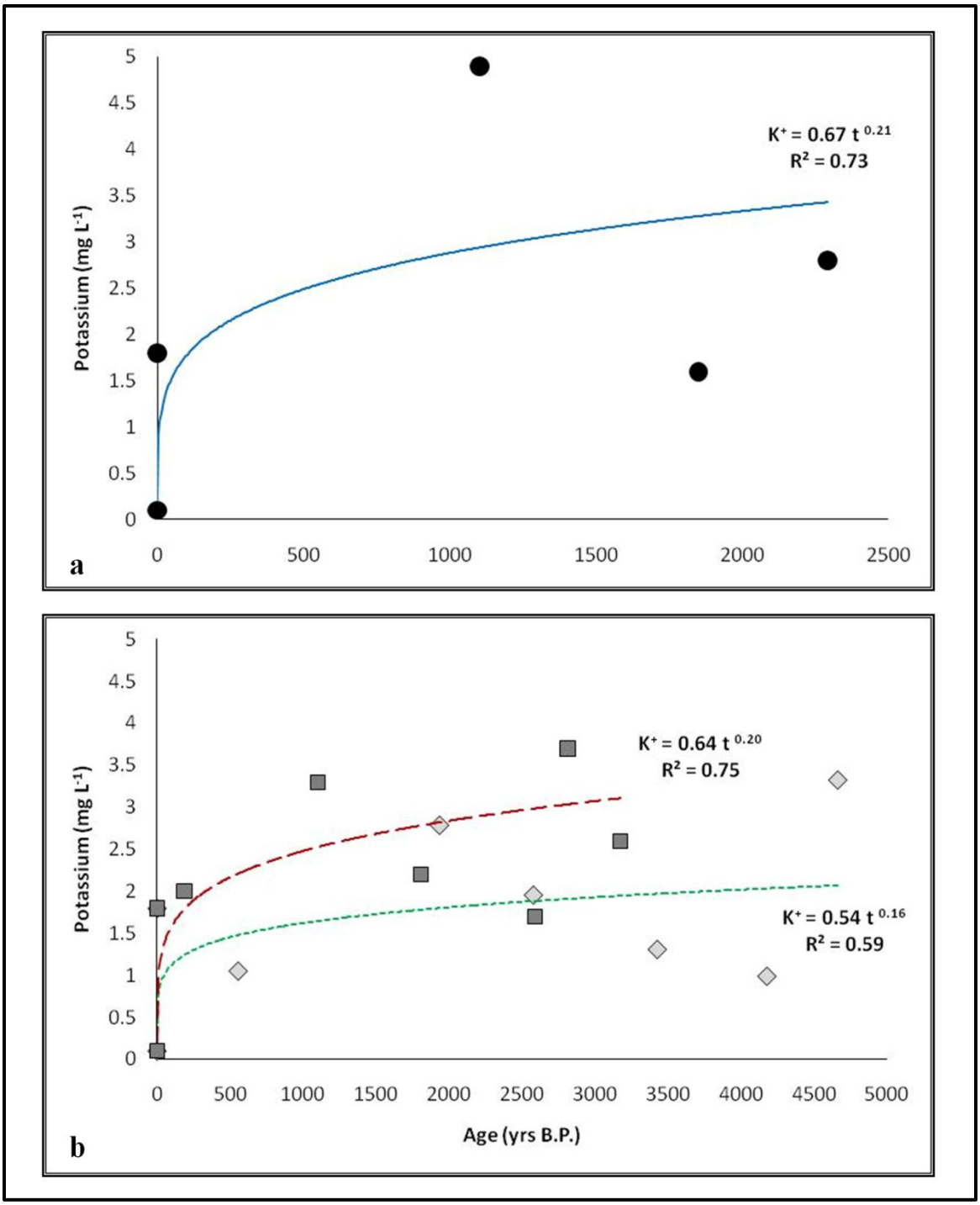

Figure 5.16: Weathering release curve for potassium.

5.5.3: Discussion of Solute Weathering Release Curves:

Our dataset shows that there are similarities between the solute weathering release curves for wells and uncorrected springs that seem to support the conceptual model in which springflow is generated only by groundwater. This finding would, therefore, imply that the chemistry from uncorrected springs can be used to determine the solute release from weathering processes in groundwater. However, EMMA results are contradictory and indicate that these springs are integrated mixtures of different sources of water. One possible explanation for the similarities between the solute weathering release curves created for wells and uncorrected springflow is that the EMMA results are not correct, i.e., that springs are in fact not integrated mixtures. We believe that the EMMA results are correct for two reasons. First, we observed that the PCA values for several springs plotted within the *U*-space mixing subspace when these springs were projected as potential components of streamflow generation during a previous study (See Figure 4.9 in Chapter 4). In this study, springs were used as proxies for groundwater; however, not all springs plotted outside the mixing subspace. This indicated that springflow, like streamflow, was integrating different water sources. Second, we assessed the source partitioning provided by the EMMA results using an "artificial" stream-water composed of known components and known contributions of each component (See Chapter 4, Section 4.4.6). This test verified that the EMMA approach was capable of correctly identifying components responsible for streamflow generation and identifying the contributions of each component in each individual, "artificial" sample. Therefore, the evidence supports the EMMA results and strongly suggests that the solute weathering release curves for uncorrected springflow and wells do not have the

same physical meaning. As a consequence, solute weathering release curves from uncorrected springflow will generate erroneous estimates of solute release.

The EMMA results indicated that the groundwater component in these springs ranged from 34 to 82 percent; yet, the solute weathering release curves for the corrected springflow are much lower than the curves for the groundwater wells. This is surprising since the groundwater components in springflow add substantial solute mass and almost all the age to the springs while the other sources of water add additional solute mass but little if any age (Figure 5.17). Thus, we would expect to observe somewhat similar solute weathering release curves between wells and corrected springflow. One explanation for this behavior is that the wells are sampling relatively stable distributions of groundwater flowpaths within the bedrock aquifer while the springs are possibly sampling discrete portions of the groundwater flow system with highly variable flowpath distributions. Springflow generation is a complex process and there are often subsurface geologic features present that enhance spring development. For example, springflow can be generated: along the contact between two geologic units having different permeabilities or structures, along faults and joints, along fractured zones, at surface depressions, and along preferential-flow zones in the soil (See Figure 5.5b) [*Manga,* 2001]. These subsurface features may intercept water from many different flowpaths or only portions of the groundwater flow system. As a consequence, the contributing areas for the springs may be highly variable or very confined. These factors ultimately influence the age and solute load of individual springs and these influences become readily apparent when the groundwater component is isolated in springflow. Some springs may be sourcing relatively young groundwater which is far from equilibrium with the minerals in the

bedrock, some springs may be sourcing very old groundwater which may be in approximate equilibrium with the minerals in the bedrock, and some springs may be sourcing a mixture of groundwater flowpaths [*West et al.*, 2005]. If our explanation is true, then there will not be a correlation between spring age and saturation index in our dataset.

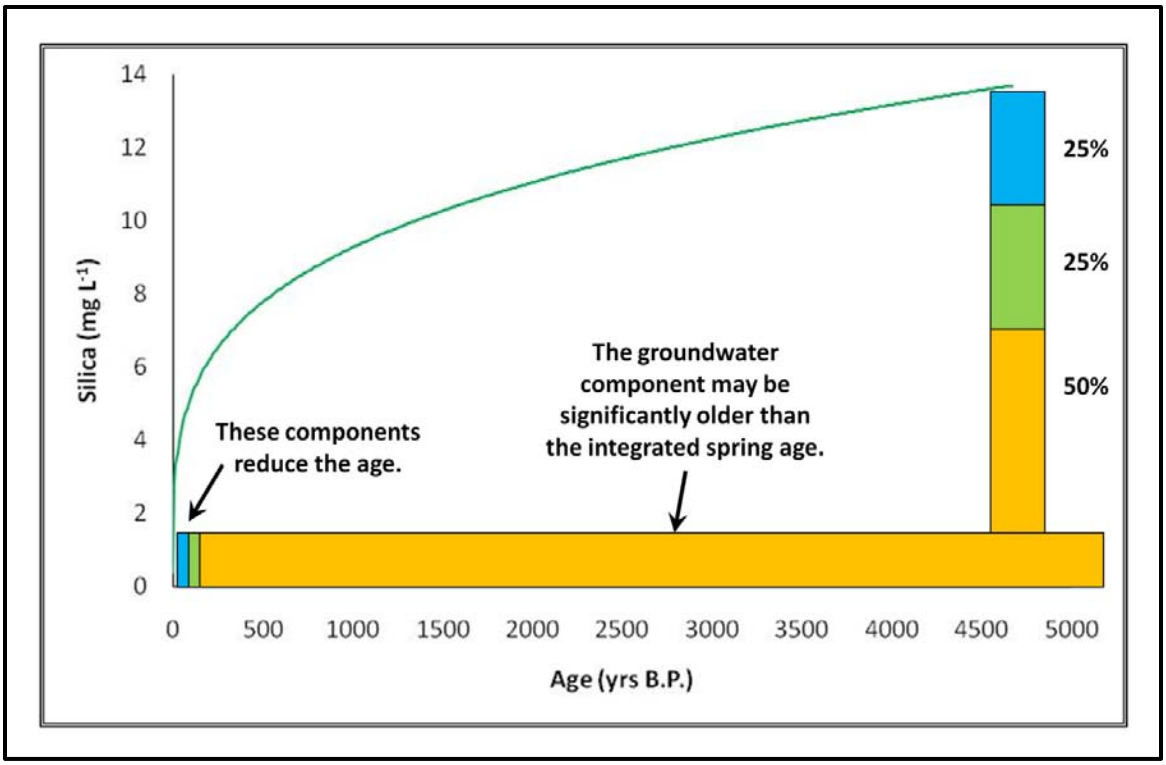

Figure 5.17: Schematic illustrating how solute weathering release curves are affected by contributions of age and solute mass from the groundwater endmember.

We calculated saturation indices for the spring and well waters using the SpecE8 program in The Geochemist's Workbench Standard Version 8.0 and the thermo_phreeqc.dat thermodynamic database. Aluminum concentrations were not measured in the spring waters but were instead calculated based on the dissolution of crystalline gibbsite [*White et al.*, 2009]. Since the Fish Canyon Tuff is so areally extensive in the Saguache Creek watershed [*Lipman and McIntosh*, 2008], we used the

modal abundances of minerals in the Fish Canyon Tuff [*Bachmann et al.,* 2002] in the geochemical modeling efforts. In particular, *Bachmann et al.* [2002] indicated that plagioclase, K-feldspar, quartz, and biotite were the most abundant minerals in the Fish Canyon Tuff. The saturation indices for albite, phlogopite, K-feldspar, and quartz are shown in Figure 18. We used albite to constrain the plagioclase endmember since published data indicate that the plagioclase minerals in the Fish Canyon Tuff ranged from An_{25} to An_{35} [*Bachmann et al.,* 2002]. In general, all well waters are saturated with respect to K-feldspar and quartz (Figure 5.18a). The well waters show a weak trend toward increasing saturation with respect to albite with increasing residence time (Figure 5.18a). *White et al.* [2009] found that pore waters and groundwater in a marine terrace became increasingly saturated with respect to albite and that this behavior was the result of longer residence times in the soil and a transition from kinetically-limited to transport-limited conditions in the terrace. The saturation indices for spring waters are shown in Figure 5.18b. In general, all spring waters are saturated with respect to K-feldspar and quartz. More importantly, there is no discernable trend toward albite saturation with increasing spring age (Figure 5.18b). This supports our inference that springs do not sample sequential portions or similar volumes of the groundwater flow system; therefore, springs are sampling different portions of the geochemical evolutionary pathway of the groundwater flow system. As a consequence, the solute weathering release curves will be lower than those created for wells and will not provide the same information as wells.

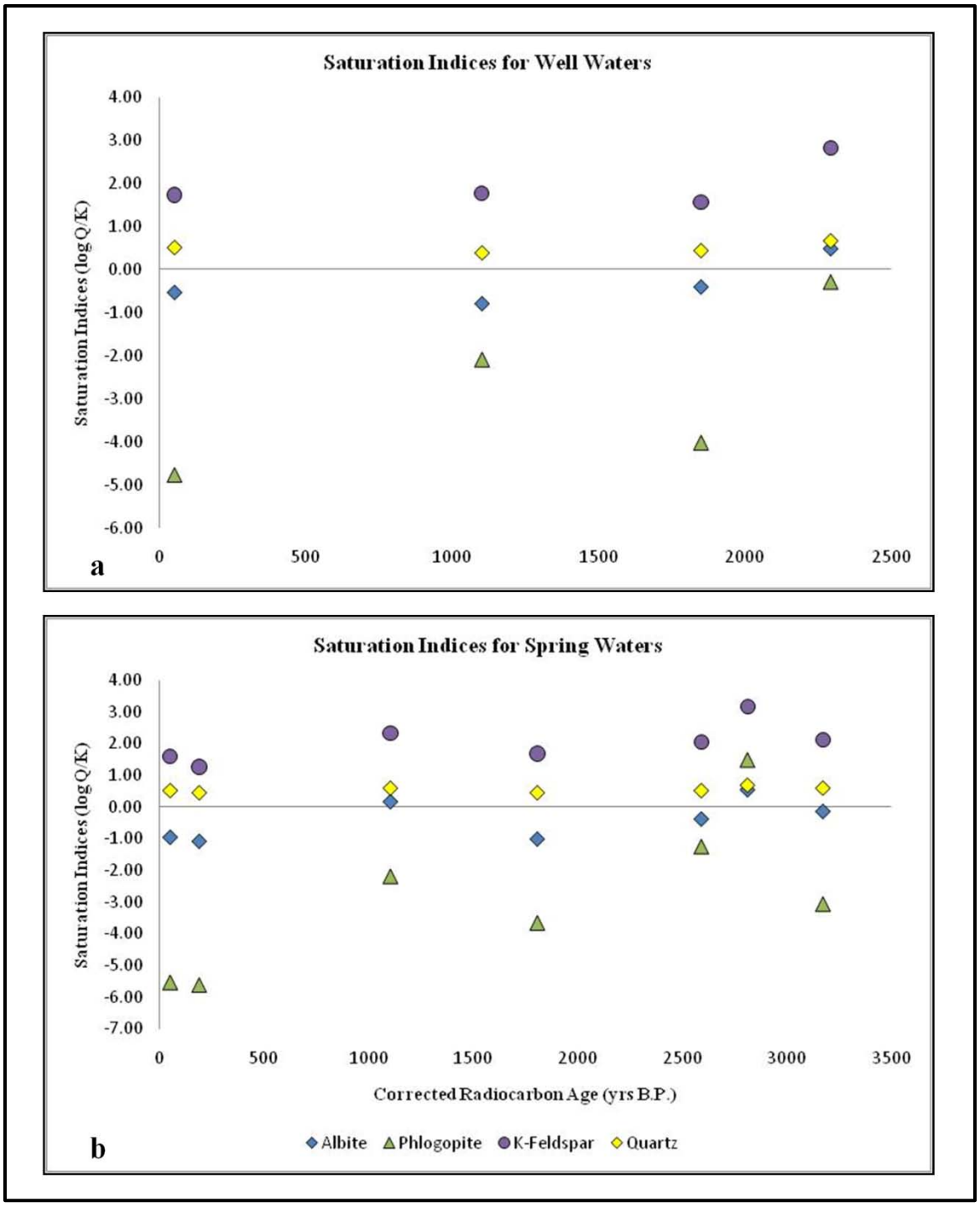

Figure 5.18: (a) Saturation indices for the well waters and common minerals found in the volcanic bedrock aquifer. Note the gradual trend toward albite saturation as the age of the well water increases. (b) Saturation indices for the spring waters and common minerals found in the volcanic bedrock aquifer. There is no strong, discernable trend toward albite saturation.

5.6: Conclusions:

We designed this study to investigate how temporal variability in the groundwater component of springflow generation affects solute weathering release curves by testing two conceptual models of springflow generation against our spring chemistry observations. In one conceptual model, springflow is generated only by groundwater and as a consequence, the chemistry observed in springflow will represent only the solutes released by chemical weathering reactions involving groundwater flow. Alternatively, in the second conceptual model, springflow is integrative and is composed of different components representing different water sources. Consequently, the groundwater component in springflow may not be temporally consistent and the chemistry observed in springflow will represent solutes released by possibly many different chemical weathering reactions. Ultimately, the distinguishing characteristic between these two conceptual models is whether or not the groundwater component in springflow is temporally variable. Therefore, our goal in conducting this research was to answer the following questions. Is the groundwater component in springflow generation temporally variable and if so, how does this variability affect solute weathering release curves?

Groundwater was a significant component of springflow generation in all springs analyzed in this study; yet, no spring was composed of 100 percent groundwater. The groundwater component ranged from 8 to 98 percent of springflow overall. These factors illustrate the integrative nature of springflow even those springs that emerge from local bedrock. It also illustrates the need for caution in the analysis of springflow chemistry especially when it is assumed to be representative of local groundwater.

The weathering release curves for corrected spring waters did not have similar powers as those curves generated for well waters. In all cases, the calculated weathering release from corrected springflow was lower than that from the wells. This is due to the observation that springflow is not composed of 100 percent groundwater, springs do not sample similar geochemical evolutionary pathways, and the contributing areas of springs may be sampling different portions of the groundwater flow system. We calculated the weathering release of Si, Ca^{2+}, Mg^{2+}, Na^{+}, and K^{+} over the course of 4000 years since this time interval seemed to bracket the range of water ages in the watershed. In all cases, the weathering release curves for uncorrected springflow overpredicts the solute release from bedrock as compared to corrected springflow. In fact, the weathering release curves for uncorrected springflow overpredicts Si by 50 percent, Ca^{2+} by 10 percent, Mg^{2+} by 51 percent, Na^{+} by 7 percent, and K^{+} by 32 percent. As a consequence, estimates of solute release from bedrock weathering based on uncorrected springflow will be too large.

These findings illustrate the complex integrative nature of springs. Further quantification on the variability of the groundwater endmember in springflow generation from other watersheds with different lithologies and climatic forcings is needed in order to provide more accurate constraints on bedrock weathering rates in groundwater flow systems. We recommend that the chemistry of wells should be used to investigate bedrock weathering processes in groundwater flowfields and that springs should only be used if wells are not available. Furthermore, springflow data should be used cautiously in these efforts especially if no *a priori* information is available on the age of spring waters or on the relative groundwater contributions in springflow.

5.7: References:

Araguás-Araguás, L., K. Rozanski, R. Gonfiantini, and D. Louvat (1995), Isotope effects accompanying vacuum extraction of soil water for stable isotope analyses, *Journal of Hydrology, 168*, 159-171, doi:10.1016/0022-1694(94)02636-P.

Bachmann, O., M.A. Dungan, and P.W. Lipman (2002), The Fish Canyon Magma Body, San Juan Volcanic Field, Colorado: Rejuvenation and eruption of an upper-crustal batholith, *Journal of Petrology, 43*(8), 1469-1503.

Bassett, R.L. (1997), Chemical modelling on the bare rock or forested watershed scale, *Hydrological Processes, 11*, 695-717.

Berkowitz, B. (2002), Characterizing flow and transport in fractured geological media: A review, *Advances in Water Resources, 25*, 861-884.

Blumhagen, E.D., and J.F. Clark (2008), Carbon sources and signal through time in an alpine groundwater basin, Sagehen, California, *Applied Geochemistry, **23,*** 2284-2291, doi:10.1016/j.apgeochem.2008.03.010.

Bricker, O.P. and B.F. Jones (1995), Main factors affecting the composition of natural waters, in *Trace Elements in Natural Waters*, edited by B. Salbu and E. Steinnes, CRC Press, Boca Raton, FL.

Caine, N. (1979), Rock weathering at the soil surface in an alpine environment, *Catena, 6*, 131-144.

Campbell, D.H., D.W. Clow, G.P. Ingersoll, M.A. Mast, N.E. Spahr, and J.T. Turk (1995), Processes controlling the chemistry of two snowmelt-dominated streams in the Rocky Mountains, *Water Resources Research, 31* (11), 2811-2821.

Christophersen, N., and R.P. Hooper (1992), Multivariate analysis of stream water chemical data: The use of principal components analysis for the end-member mixing problem, *Water Resources Research, 28* (1), 99-107.

Clark, I., and P. Fritz (1997), *Environmental Isotopes in Hydrogeology,* Lewis, Boca Raton, FL.

Clow, D.W., G.P. Ingersoll, M.A. Mast, J.T. Turk, and D.H. Campbell, (2002), Comparison of snowpack and winter wet-deposition chemistry in the Rocky Mountains, USA: Implications for winter dry deposition, *Atmospheric Environment, 36,* 2337-2348.

Davis, S.N. (1964), Silica in streams and ground water, *American Journal of Science, 262,* 870-891.

Dixon , J.C. and C.E. Thorn (2005), Chemical weathering and landscape development in mid-latitude alpine environments, *Geomorphology, 67,* 127-145, doi:10.106/j.geomorph.2004.07.009.

Drever, J.I. (2002), *The Geochemistry of Natural Waters: Surface and Groundwater Environments, 3rd Edition,* Prentice Hall, Upper Saddle River, NJ.

Earman, S., A.R. Campbell, F.M. Phillips, and B.D. Newman (2006), Isotopic exchange between snow and atmospheric water vapor: Estimation of the snowmelt component of groundwater recharge in the southwestern United States, *Journal of Geophysical Research, 111,* D09302, doi:10.1029/2005JD006470.

Engle, E.M. (2009), Digital soil boundary detection using quantitative hydrologic remote sensing, M.S. Thesis, Department of Earth and Environmental Science, New Mexico Tech, Socorro, NM, USA.

Finley, J.B. and J.I. Drever (1997), Chemical mass balance and rates of mineral weathering in a high-elevation catchment, West Glacier Lake, Wyoming, *Hydrological Processes, 11,* 745-764.

Fontes, J.C., and J.M. Garnier (1979), Determination of the initial ^{14}C activity of the total dissolved carbon: A review of the existing models and a new approach, *Water Resources Research, 15*(2), 399-413.

Freeze, A.R., and J.A. Cherry (1979), *Groundwater*, Prentice Hall, Upper Saddle River, NJ.

Frisbee, M.D., F.M. Phillips, A.R. Campbell, J.M.H. Hendrickx, and E.M. Engle (2010a), Modified passive capillary samplers for collecting samples of snowmelt infiltration for stable isotope analysis in remote, seasonally inaccessible watersheds 2: Field evaluation, *Hydrological Processes, **24,*** 834-849, DOI:10.1002/hyp.7524.

Frisbee, M.D., F.M. Phillips, A.R. Campbell, F. Liu, and S.A. Sanchez (2010b), Streamflow generation in a large, alpine watershed in the southern Rocky Mountains of Colorado, USA: Is streamflow generation simply the aggregation of hillslope runoff responses?, *Water Resources Research,* submitted.

Gabet, E.J., R. Edelman, and H. Langner (2006), Hydrological controls on chemical weathering rates at the soil-bedrock interface, *Geology, 34*(12), 1065-1068, doi:10.1130/G23085A.1.

Garrels, R.M. and F.T. Mackenzie (1967), Origin of the chemical compositions of some springs and lakes, in *Equilibrium Concepts in Natural Water Systems,* 344 pp., American Chemical Society, Washington, DC.

Goldich, S.S. (1938), A study in rock-weathering, *Journal of Geology, 46,* 17-58.

Hoch, A.R., M.M. Reddy, and J.I. Drever (1999), Importance of mechanical disaggregation in chemical weathering in a cold alpine environment, San Juan Mountains, Colorado, *GSA Bulletin, 111*(2), 304-314.

Hoch, A.R., M.M. Reddy, and M.J. Heymans (2000), Transient calcite fracture fillings in a welded tuff, Snowshoe Mountain, Colorado, *Applied Geochemistry, 15,* 1495-1504.

Hoch, A.R. and M.M. Reddy (2001), The water chemistry at Snowshoe Mountain, Colorado: Mixed processes in a common bedrock, in *Water-Rock Interaction, Volume 1,* edited by Rosa Cidu, Swets and Zeitlinger, Lisse, 533-536.

Hooper, R.P. (2003), Diagnostic tools for mixing models of stream water chemistry, *Water Resources Research, 39* (3), 1055, doi:10.1029/2002WR001528.

Kennedy, V.C. (1970), Silica variations in stream water with time and discharge, in *Nonequilibrium Systems in Natural Water Chemistry,* edited by J.D. Hem, series editor R.F. Gould, pp. 95-130, American Chemical Society, Houston, Texas.

Kosugi, K., S. Katsura, M. Katsuyama, and T. Mizuyama (2006), Water flow processes in weathered granitic bedrock and their effects on runoff generation in a small headwater catchment, *Water Resources Research, 42,* W02414, doi:10.1029/2005WR004275.

Lasaga, A.C. (1984), Chemical kinetics of water-rock interactions, *Journal of Geophysical Research, 89*(B6), 4009-4025.

Likens, G.E. and D.C. Buso (2006), Variation in streamwater chemistry throughout the Hubbard Brook Valley, *Biogeochemistry, 78,* 1-30.

Lipman, P.W. and W.C. McIntosh (2008), Eruptive and noneruptive calderas, northeastern San Juan Mountains, Colorado: where did the ignimbrites come from?, *GSA Bulletin, 120* (7/8), 771-795, doi:10.1130/B26330.1.

Liu, F., M.W. Williams, and N. Caine (2004), Source waters and flow paths in an alpine catchment, Colorado Front Range, United States, *Water Resources Research, 40,* W09401, doi:10.1029/2004WR003076.

Liu, F., R.C. Bales, M.H. Conklin, and M.E. Conrad (2008), Streamflow generation from snowmelt in semi-arid, seasonally snow-covered, forested catchments, Valles Caldera, New Mexico, *Water Resources Research, 44,* W12443, doi:10.1029/2007WR006728.

Manga, M. (2001), Using springs to study groundwater flow and active geologic processes, *Annual Review of Earth and Planetary Sciences, 29,* 201-228.

McCrea, J.M. (1950), On the isotopic chemistry of carbonates and a paleotemperature scale, *The Journal of Chemical Physics, **19***(6)**,** 849-857.

Millot, R., J. Gaillardet, B. Dupré, and C.J. Allègre (2002), The global control of silicate weathering rates and the coupling with physical erosion: new insights from rivers of the Canadian Shield, *Earth and Planetary Science Letters, 196,* 83-98.

Nelson, S.T., and D. Dettman (2001), Improving hydrogen isotope ratio measurements for on-line chromium reduction systems, *Rapid Communications in Mass Spectrometry. 15,* 2301-2306.

Newman, B.D., A.R. Campbell, D.I. Norman, and D.B. Ringelberg (1997), A model for microbially induced precipitation of vadose-zone calcites in fractures at Los Alamos, New Mexico, USA, *Geochimica et Cosmochimica Acta, 61*(9), 1783-1792.

Pacheco, F.A.L. and C.H. Van der Weijden (2002), Mineral weathering rates calculated from spring water data: A case study in an area with intensive agriculture, the Morais Massif, northeast Portugal, *Applied Geochemistry, 17,* 583-603.

Pacheco, F.A.L. and A.M.P. Alencoão (2006), Role of fractures in weathering of solid rocks: narrowing the gap between laboratory and field weathering rates, *Journal of Hydrology, 316,* 248-265, doi:10.1016/j.jhydrol.2005.05.003.

Pearson, F.J., Jr. (1965), Use of C-13/C-12 ratios to correct radiocarbon ages of material initially diluted by limestone, in *Radiocarbon and Tritium Dating, Proceedings of the Sixth International Conference on Radiocarbon,* Pullman Washington, 357-366.

Pearson, F.J., Jr. and B.B. Henshaw (1970), Sources of dissolved carbonate species in groundwater and their effects on carbon-14 dating, in *Isotope Hydrology 1970,* International Atomic Energy Agency, Vienna, 271-285.

Plummer, L.N., E.C. Prestemon, and D.L. Parkhurst (1994), An interactive code (NETPATH) for modeling NET geochemical reactions along a flow PATH. Version 2.0: Reston, Virginia, *U.S. Geological Survey Water-Resources Investigations Report 94-4169,* 130 pp.

Rad, S.D., C.J. Allégre, and P. Louvat (2007), Hidden erosion on volcanic islands, *Earth and Planetary Science Letters, 262,* 109-124, doi.10.1016/j.epsl.2007.07.019.

Rademacher, L.K., J.F. Clark, G.B. Hudson, D.C. Erman, and N.A. Erman (2001), Chemical evolution of shallow groundwater as recorded by springs, Sagehen Basin, Nevada County, California, *Chemical Geology, 179,* 37-51.

Rademacher, J.K., J.F. Clark, D.W. Clow, and G.B. Hudson (2005), Old groundwater influence on stream hydrochemistry and catchment response times in a small Sierra Nevada catchment: Sagehen Creek, California, *Water Resources Research, 41,* W02004, doi:10.1029/2003WR002805.

Reheis, M.C. and R. Kihl (1995), Dust deposition in southern Nevada and California, 1984-1989: Relations to climate, source area, and source lithology, *Journal of Geophysical Research, 100*(D5), 8893-8918.

Reheis, M.C., J.R. Budahn, and P.J. Lamothe (2002), Geochemical evidence for diversity of dust sources in the southwestern United States, *Geochimica et Cosomochimica Acta, 66*(9), 1569-1587.

Steven, T.A. and P.W. Lipman (1976), Calderas of the San Juan Volcanic Field, southwestern Colorado, in U.S. Dept. of the Interior, USGS Geological Survey Professional Paper 958, 35 pp.

Szynkiewicz, A., M.O. Jedrysek, and M. Kurasiewicz (2006), Carbon isotope effects during precipitation of barium carbonate: Implications for environmental studies, *Environmental Chemistry Letters, 4,* 29-35.

Tóth, J. (1999), Groundwater as a geologic agent: An overview of the causes, processes, and manifestations, *Hydrogeology Journal, 7,* 1-14.

Velbel, M.A. (1995), Interaction of ecosystem processes and weathering processes, in *Solute Modeling in Catchment Systems,* edited by S.T. Trudgill, 486 pp., John Wiley & Sons, Chichester, NY.

Velbel, M.A. and J.R. Price (2007), Solute geochemical mass-balances and mineral weathering rates in small watersheds: Methodology, recent advances, and future directions, *Applied Geochemistry, 22,* 1682-1700, doi:10.1016/j.apgeochem.2007.03.029.

Vogel, J.C. and D. Ehhalt (1963), The use of carbon isotopes in groundwater studies, in *Radioisotopes in Hydrology,* International Atomic Energy Agency, Vienna, 383-395.

Vogel, J.C. (1967), Investigation of groundwater flow with radiocarbon, in *Isotopes in Hydrology,* International Atomic Energy Agency, Vienna, 355-368.

Vogel, J.C. (1970), Carbon-14 dating of groundwater, in *Isotope Hydrology 1970,* International Atomic Energy Agency, Vienna, 235-237.

West, A.J., M.J. Bickle, R. Collins, and J. Brasington (2002), Small-catchment perspective on Himalayan weathering fluxes, *Geology, 30*(4), 355-358.

West, A.J., A. Galy, and M. Bickle (2005), Tectonic and climatic controls on silicate weathering, *Earth and Planetary Science Letters, 235,* 211-228, doi:10.1016/j.epsl.2005.03.020.

White, A.F. and S.L. Brantley (2003) The effect of time on the weathering of silicate minerals: Why do weathering rates differ in the laboratory and field?, *Chemical Geology, 202,* 479-506, doi:10.106/j.chemgeo.2003.03.001.

White, A.F. (2005), Natural weathering rates of silicate minerals, in *Treatise on Geochemistry Volume 5: Surface and Ground Water, Weathering, and Soils,* edited by J.I. Drever, series editors: H.D. Holland and K.K. Turekian, 36 pp., Elsevier, Oxford, UK.

White, A.F. (2008), Quantitative approaches to characterizing natural chemical weathering rates, in *Kinetics of Water-Rock Interaction*, edited by S.L. Brantley, J.D. Kubicki, and A.F. White, 75 pp., Springer, New York, NY.

White, A.F., M.S. Schulz, D.A. Stonestrom, D.V. Vivit, J. Fitzpatrick, T.D. Bullen, K. Maher, and A.E. Blum (2009), Chemical weathering of a marine terrace chronosequence, Santa Cruz, California. Part II: Solute profiles, gradients and the comparisons of contemporary and long-term weathering rates, *Geochimica et Cosmochimica Acta, 73,* doi:10.1016/j.gca.2009.01.029.

Zhu, C. (2005), In situ feldspar dissolution rates in an aquifer, *Geochimica et Cosmochimica Acta, 69,* doi:10.1016/j.gca.2004.09.005

Chapter 6 Long Residence-Time Groundwater, Dynamic Storage, and the Effect on the Streamflow Responses from Large Watersheds to Climate Change[5]

Residence time studies performed at small catchment scales less than 100 km^2 indicate that residence times of streamflow are relatively young, on the order of days to years, and that residence times do not correlate with basin area[1,2]. Instead, they suggest that residence times are controlled primarily by runoff processes associated with hillslope-scale flowpaths and the subsequent mixing of these hillslope responses in the stream network. Hillslope-scale runoff processes are typically limited in storage and if these previous conceptual models are true, then the streamflow response to changes in climatic forcing will be relatively rapid[3]. Unfortunately, these concepts have not been tested at larger watershed scales where large-scale groundwater flowpaths may be critical components of streamflow. Here, we present streamflow ages calculated using the results from endmember mixing analysis coupled with a geochemical chronometer calibrated to the kinetics of weathering reactions in a large (1700 km^2) watershed in the southern Rocky Mountains of Colorado. Our data show that streamflow ages are much older than currently published and are strongly correlated with drainage area. This is a consequence of increasing contributions from long residence-time, geochemically evolved groundwater to streamflow. We conclude that residence times in large watersheds may not be similar to those observed at smaller scales because there are processes responsible for streamflow generation at large scales that may not be

[5] **Frisbee, M.D., F.M. Phillips, A.R. Campbell, and F. Liu (2010), Long residence time groundwater and its effect on apparent ages of streamflow in a large watershed, originally formatted for submission to *Nature Geoscience,* not submitted – awaiting residence time distributions from watershed hydrogeologic model.**

operative at the smaller hillslope scale. These findings indicates that the streamflow response from some large watersheds may be buffered[4], at least initially, against changes in climatic forcing associated with climate change[5,6,7].

Residence times of streamflow can be used to make inferences about the relationship between flowpath distributions and streamflow generation processes within a watershed. Streamflow generation processes at the hillslope and small catchment scale have been well documented in the literature[8] and the majority of residence time studies have also been completed at these small scales[9]. One of the goals of these studies is to derive relationships between residence times and hydrological process behavior at the small scale in hopes of extending that information to larger scales[10]. The relationship between residence times and catchment area, for example, has been investigated at the small catchment scale and the results from these studies indicate that residence times are not correlated with catchment area[1,2]. These studies also indicate that residence times are very young, on the order of days to years and perhaps a decade[2,9]. However, there is contradictory evidence that indicates that chemical constituents may be temporally persistent in watersheds[11,12]. This discrepancy ultimately limits our ability to predict how streamflow generation from large watersheds will respond to climate change. Residence times are directly related to flowpath distributions which are, in turn, related to storage and transmissivity characteristics of the hydrologic system. Response times, a measure of the time-scales for an aquifer to respond to changes in recharge and discharge, are also primarily controlled by storage and transmissivity characteristics of the aquifer[13]. Therefore, streamflow from watersheds exhibiting short residence times and quick response times will respond rapidly to changes in meteoric forcing associated with

climate change while the reverse may hold true for watersheds where long residence-time waters sustain streamflow[3,4].

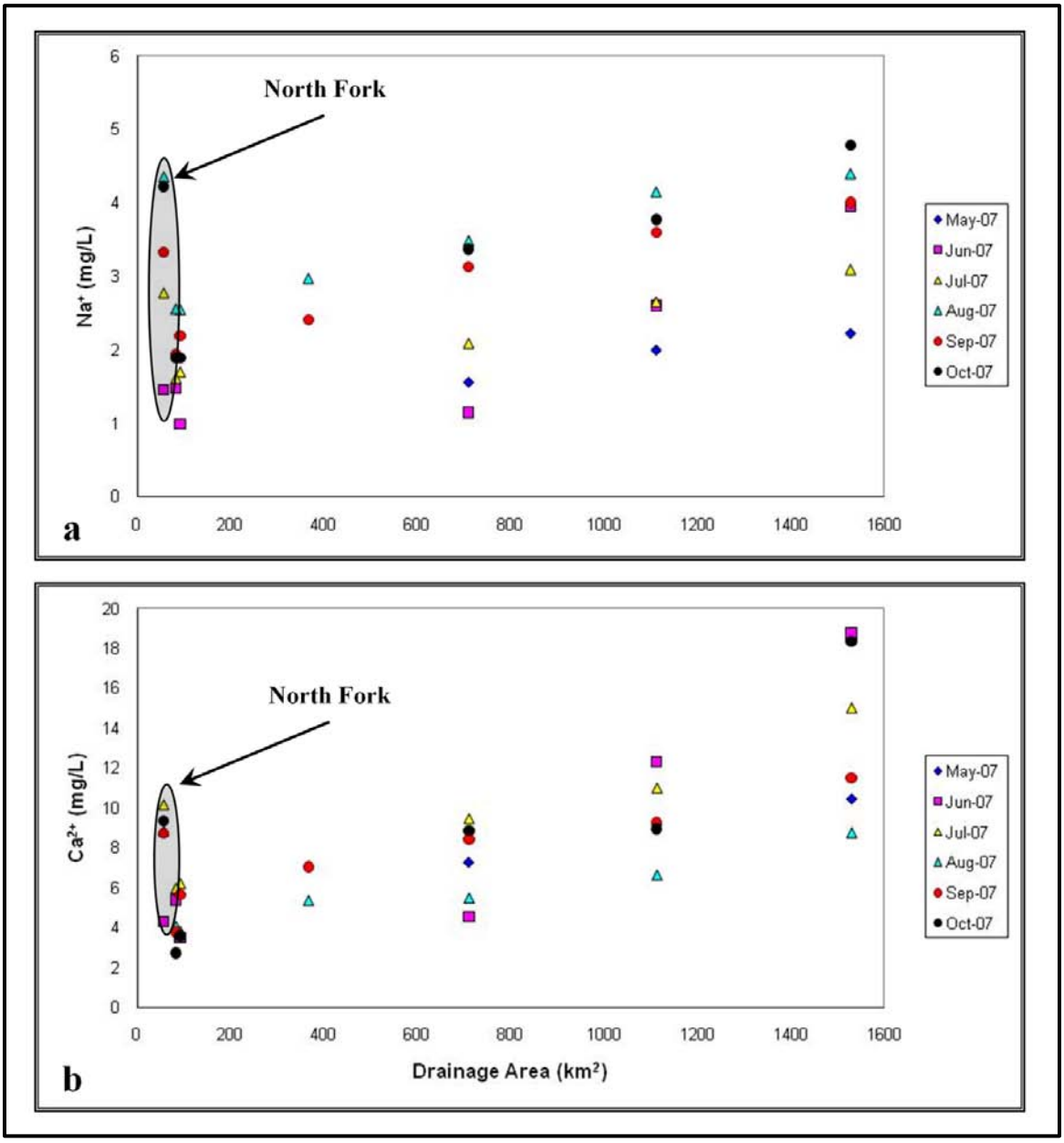

Figure 6.1: Trends in Na^+ and Ca^{2+} with accumulated subwatershed area. Note the development of linear trends in stream chemistry as drainage area increases.

Here, we explore the impact of contributions from long residence-time groundwater on streamflow ages at the large watershed scale using the kinetic rates

responsible for the geochemical evolution of water in a watershed as an indicator of residence time. In this study, we observed linear increases in concentrations of chemical constituents in streamflow as accumulated drainage area increased in the Saguache Creek watershed (1700 km^2) located in the San Juan Mountains of southern Colorado (Figure 6.1). One headwater subwatershed exhibited anomalous chemistry (North Fork in Figure 6.1) and this is probably due to the influence of a conveyance ditch that supplies water to the stream in the upper regions of the subwatershed. Subsequent research found that contributions from geochemically evolved groundwater were necessary to generate the linear trends[14]. In comparison, the surface and shallow-subsurface flowpaths associated with hillslope-scale runoff mechanisms will not provide sufficient geochemical evolution of water to account for these linear trends. In fact, these linear trends were distinctly different than the convergent trends observed in catchments where the aggregation of hillslope runoff processes was thought to be important[15,16] (see convergent behavior in Figure 6.2c as compared to linear trends in Figure 6.2f). These chemical trends represent two different conceptual models of streamflow generation. It is important to draw a distinction between these conceptual models in order to illustrate the effect that the underlying mechanisms of these opposing conceptual models have on residence times of streamflow and future streamflow response to climate change.

One model is essentially two-dimensional and treats streamflow generation at the large watershed scale as the aggregation of runoff responses from individual hillslopes, primarily with surface and shallow subsurface flowpaths (Figure 6.2a)[10,15,16]. Due to the relatively rapid nature of transport through these short flowpaths (Figure 6.2b), the runoff reaching the stream will not be geochemically evolved[17]. The geochemically young

runoff from these hillslope responses become increasingly mixed in the stream network and as scale increases, a median chemical concentration emerges that represents the mixing of geochemically unevolved waters (Figure 6.2c). Furthermore, since hillslope runoff processes are both spatially and temporally heterogeneous[10], there will be substantial variability in the extent of geochemical evolution between hillslopes. More importantly, this conceptual model has very limited storage. The rapidity of the transmission of climate change signals through the hydrologic system can be described using aquifer response times which are again primarily influenced by the specific storage and transmissivity of the aquifer[13]. Thus, if this conceptual model holds, then we would expect to see poor correlations between drainage area and residence times, yet rapid responses to changes in meteoric forcing associated with climate change.

Alternatively, a fully three-dimensional conceptual model treats streamflow generation at the large watershed scale as being controlled by a distribution of large-scale groundwater flowpaths[18,19] as well as surface and shallow subsurface flowpaths (Figure 6.2d). This conceptual model has lots of storage due to the fully 3D representation of the watershed. Streamflow will receive inputs of water representing a distribution of flowpaths ranging from recent, geochemically unevolved water to very old, geochemically evolved water (Figure 6.2e). As scale increases, the stream will receive contributions from longer groundwater flowpaths that are transporting increasingly older[19] and more geochemically evolved waters[17]. This will generate increasing concentrations of chemical constituents in streamflow as scale increases (Figure 6.2f). Therefore, if this conceptual model holds, we would expect to see strong correlations

between drainage area and residence times and a moderated response to changes in meteoric forcing associated with climate change.

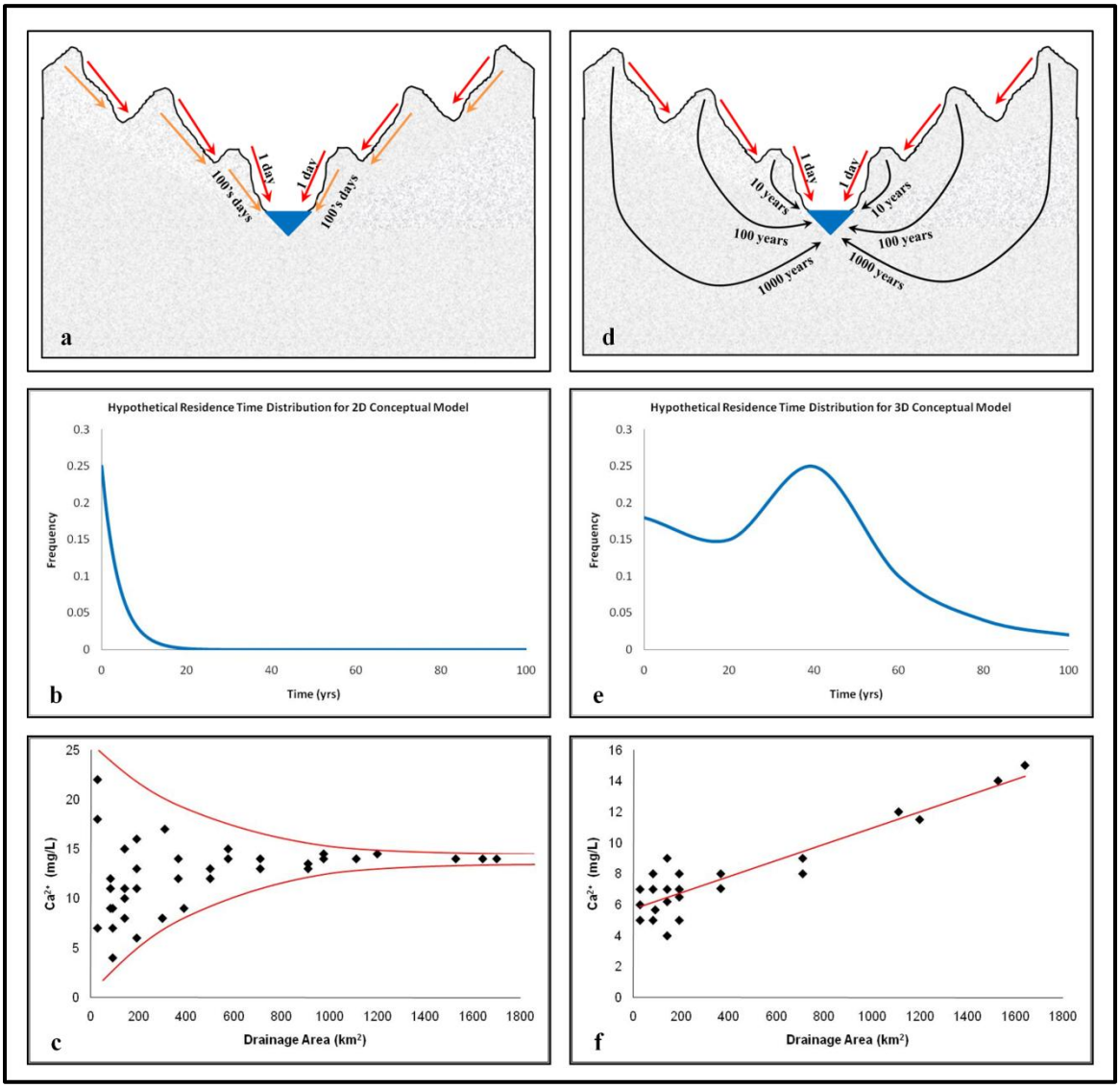

Figure 6.2: Conceptual models for streamflow generation at large watershed scales. The conceptual model for the network-mixing conceptual model is on the left including: a) Schematic representation showing that water from surface and shallow subsurface flowpaths are primary components of streamflow, b) Travel time distribution showing dependence on short flowpaths, and c) Trends in streamflow chemistry indicative of mixing processes with increasing watershed scale. The conceptual model for the 3D catchment-mixing conceptual model is on the right including: d) Schematic representation showing that water from surface and shallow subsurface flowpaths as well as deep groundwater flowpaths are primary components of streamflow, e) Travel time distribution showing increased contributions from longer flowpaths, and f) Trends in

streamflow chemistry indicative of geochemical evolution with increasing watershed scale.

We used endmember mixing analysis (EMMA)[20,21,22] on a four year dataset of chemical and stable isotope compositions in streamflow to quantify the processes responsible for the linear increases in stream chemistry with increasing scale. We used observations of vertical hydraulic gradients measured in mini-piezometers[23] installed in streambeds to quantify temporal and spatial variations of groundwater discharge to streamflow. Our results indicated that contributions from large-scale groundwater flowpaths were necessary to generate the linear increases in stream chemistry[14]. In fact, contributions from groundwater increased as drainage area increased (Figure 6.3a) suggesting that the linear structure in streamflow chemistry observed as drainage area increased (Figure 6.1) was attributed to the increasing contributions from groundwater. Support for this conclusion was provided by the observation that vertical hydraulic gradients measured in mini-piezometers also increased with increasing accumulated drainage area (Figure 6.3b)[14]. These findings provided support for the 3D conceptual model. In fact, runoff processes were operative at the large watershed scale that were not always operative at the hillslope scale. If these groundwater contributions are primary controls on streamflow generation at larger watershed scales, then it follows that they may also affect the relationship between residence times of streamflow and drainage area and more importantly, the magnitude of the residence times in streamflow and response time of streamflow to changes in meteoric forcing.

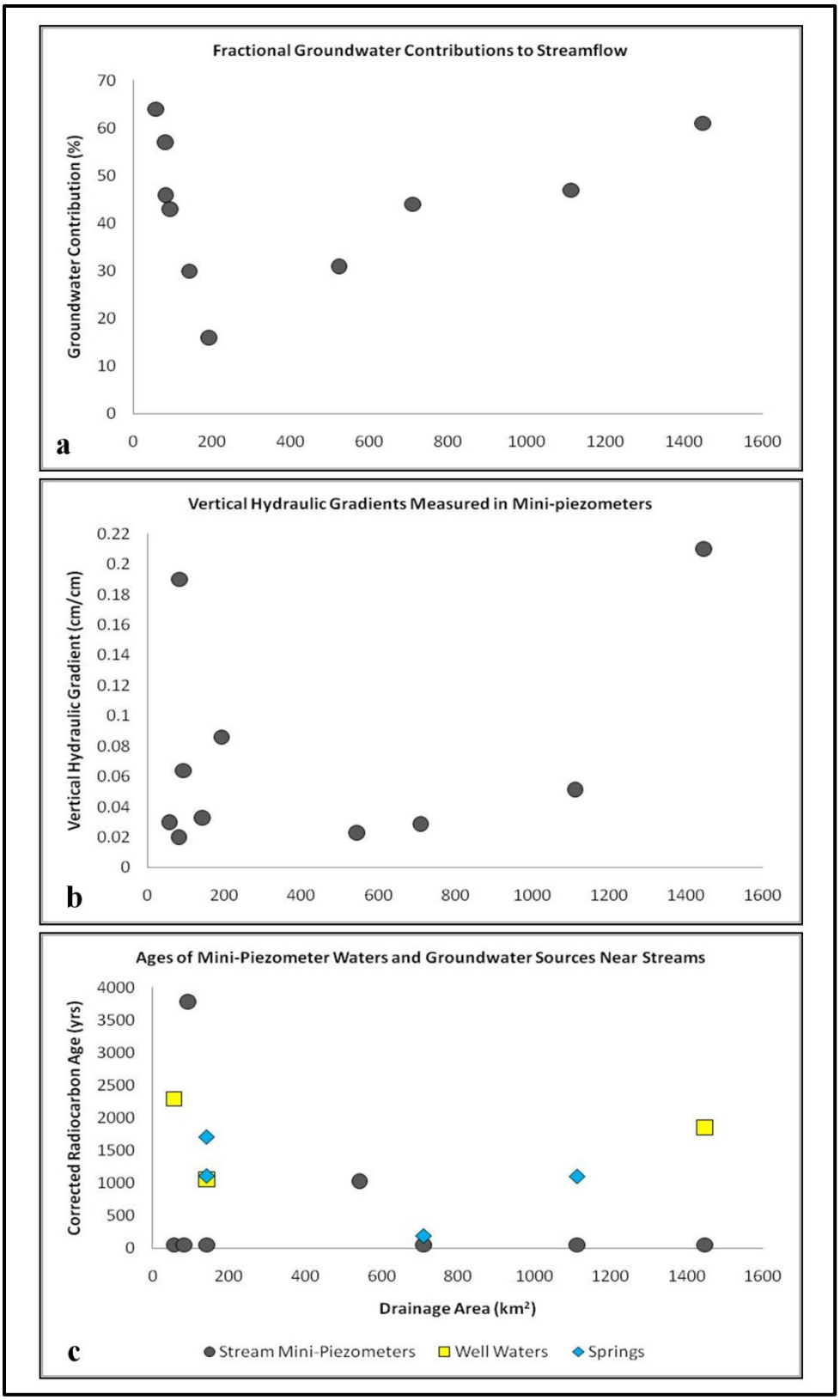
Fractional Groundwater Contributions to Streamflow
Groundwater Contribution (%)
70
60
50
40
30
20
10
0
0
200
400
600
800
1000
1200
1400
1600
a
Vertical Hydraulic Gradients Measured in Mini-piezometers
Vertical Hydraulic Gradient (cm/cm)
0.22
0.2
0.18
0.16
0.14
0.12
0.1
0.08
0.06
0.04
0.02
0
0
200
400
600
800
1000
1200
1400
1600
b
Ages of Mini-Piezometer Waters and Groundwater Sources Near Streams
Corrected Radiocarbon Age (yrs)
4000
3500
3000
2500
2000
1500
1000
500
0
0
200
400
600
800
1000
1200
1400
1600
Drainage Area (km²)
c
Stream Mini-Piezometers
Well Waters
Springs

Figure 6.3: a) Fractional groundwater contributions to streamflow during September 2008, b) Vertical hydraulic gradients measured in mini-piezometers installed in streambeds during September 2008. Note the similarity between a and b beyond a scale of 300 km2, and c) Corrected radiocarbon ages of groundwater discharging to stream measured in mini-piezometers are shown as black filled circles. Yellow squares represent the ages of groundwater samples taken from wells located within 500 m of Saguache Creek and blue diamonds represent the ages of spring waters located within 500m of Saguache Creek. The placement of the groundwater and spring water sampling sites in the figure coincides with stream sampling sites. The squares and diamonds show that older groundwater is discharging near the stream sampling sites.

Initially, we attempted to address this question by directly sampling the groundwater that was discharging to the stream using mini-piezometers installed in streambeds[23]. We collected waters samples from the mini-piezometers and subjected those samples to radiocarbon dating. Old ages were observed in some mini-piezometer waters but the remaining waters exhibited a trend toward modern (young) ages with increasing scale (Figure 6.3c). The chemical composition of the mini-piezometer waters were, however, very similar to the chemistries of waters sampled from local groundwater wells. We attribute the young ages to isotopic exchange processes that occur in the hyporheic zone when groundwater that is flowing toward the stream mixes with water in the hyporheic zone. The hyporheic zone is a zone of enhanced communication between the surface water environment and subsurface stream sediments where mixing can occur between the two on very short time-scales[24,25]. Waters that have been flowing at the Earth's surface are in equilibrium with atmospheric carbon and have high percent-modern carbon (pmC) values. The chemical composition of the water in the stream and the water in the hyporheic zone may, in some cases, be very similar due to the relatively rapid mixing processes between the two waters. For example, at the time of sampling, the groundwater component accounted for 31 to 61 percent of streamflow generation and

the chemical compositions of the stream and hyporheic waters both contained an evolved geochemical signature. Groundwater, on the other hand, is not in equilibrium with modern atmospheric carbon and instead reflects the radiometric decay of carbon. As a consequence, groundwater has much lower pmC values. Groundwater also has a more geochemically evolved chemical composition due to enhanced rock/water interactions in the groundwater flow system. When groundwater flows toward the stream, it mixes with hyporheic water. During this mixing process, the chemical compositions of groundwater and hyporheic water also become mixed. Solute mixing is a linear process and in general, the chemical signature of the mixed water will reflect the addition of the older, more geochemically evolved groundwater. At the same time, the older carbon in groundwater will mix with young carbon in the hyporheic water. The calculation of the age of mixed waters is non-linear. Thus, this will have an opposite effect and the mixed water will be biased toward younger carbon ages. Thus, the mixing process effectively resets the radiocarbon clock of the discharging groundwater once it mixes in the hyporheic zone. Older ages of groundwater were, however, observed in wells and springs located within 500 m of the sampling sites on Saguache Creek providing evidence that older groundwater was discharging near the streams (Figure 6.3c). The groundwater wells were terminated in bedrock at a maximum depth of approximately 55 m indicating that the wells were not sourcing old, isolated groundwater systems. This evidence provided an explanation for the evolved geochemical signature of the mini-piezometers and implied that the streams were in fact receiving contributions from a water source that had undergone enhanced geochemical evolution.

Previous residence time studies at the catchment scale were performed using the stable isotope convolution integral method[1,2,26]. In the forward model, an input function representing a time series of the stable isotopic composition of meteoric inputs is convolved with a network response function that describes the flowpath distribution in the catchment to determine the output time series of the stable isotopic composition in the stream[26]. However, the flowpath distribution is not known *a priori* so we solve the convolution integral for the unknown flowpath distribution. This is essentially a linear model and as a consequence, the output residence times will not differ significantly from the temporal span of the input function[27]. In order to avoid the problems associated with radiocarbon reset in the hyporheic zone and the limitations imposed by the stable isotope convolution method, we chose an alternative approach to estimate the apparent ages of streamflow by creating a geochemical chronometer[12,14,28]. We coupled the results from EMMA with kinetic rates of weathering reactions responsible for the geochemical evolution of water in the watershed to calculate the apparent age of streamflow. Using the results of EMMA, we separated streamflow into the components responsible for streamflow generation at successive sampling sites located on Saguache Creek (Figure 6.4a). Once the components of streamflow were identified, we could estimate the length of time (proxy for age) necessary for the component to obtain its unique geochemical composition using solute weathering release curves (Figure 6.4b). The apparent age of streamflow is then found by adding the ages of the individual components that comprise streamflow (Figure 6.4c).

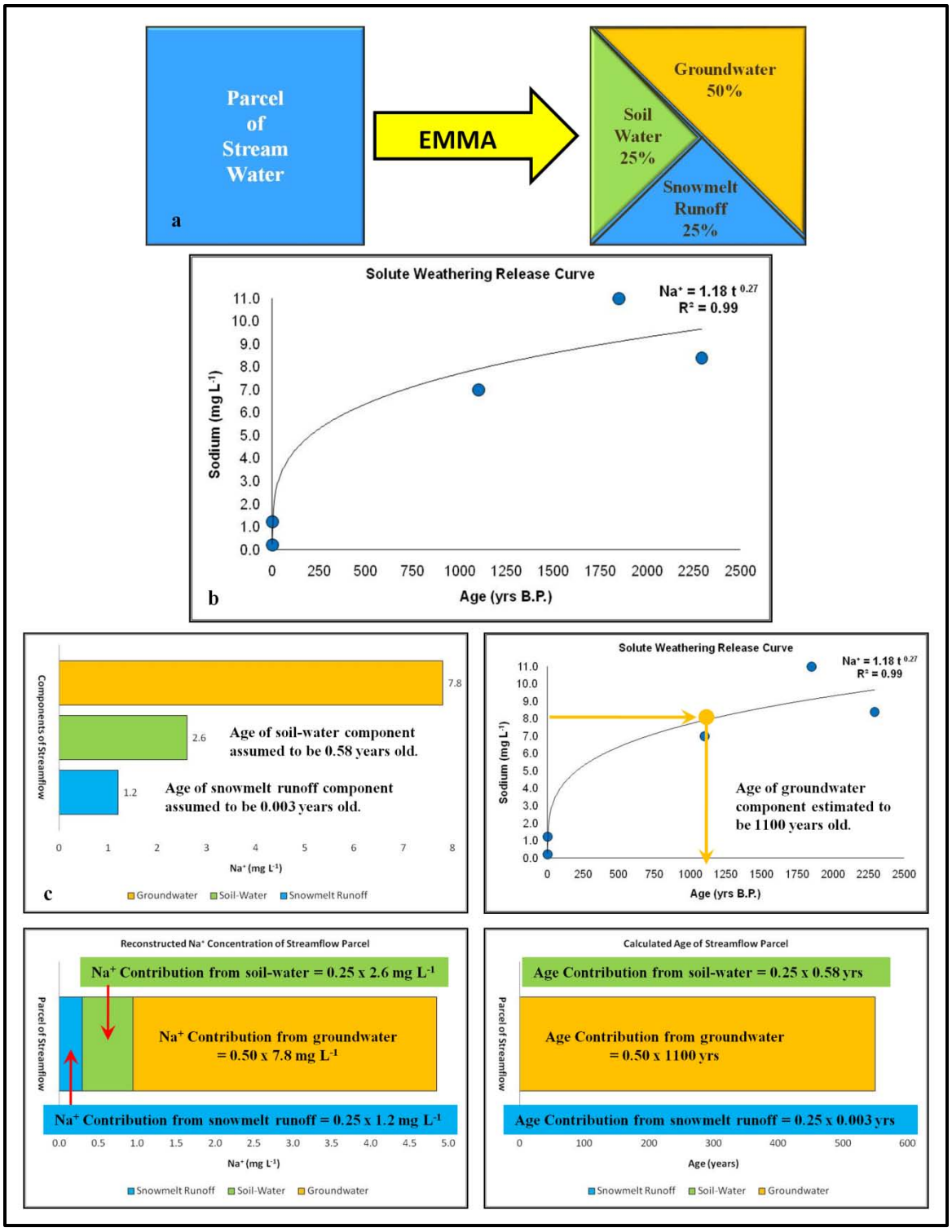

Figure 6.4: Schematic representation of the coupled approach used to calculate apparent ages of streamflow. a) Solute weathering release curve for sodium, b) Schematic representation of a parcel of stream water separated using EMMA into the components responsible for streamflow generation, and c) Calculation of apparent ages of streamflow.

The trends and magnitudes of apparent ages of streamflow calculated using the geochemical approach are very striking. First, the apparent ages in streamflow do increase with increasing drainage area (Figure 6.5) as proposed in the 3D conceptual model (Figure 6.2d). This finding illustrates the effect that contributions from long residence-time groundwater have on streamflow ages. If streamflow generation was controlled by rapid runoff processes (Figure 6.2a), then streamflow ages would be much younger (Figure 6.2b). Second and most important, apparent ages of streamflow are much older than currently published (Figure 6.5). In fact, the apparent ages of streamflow in small drainages ranging from 56 to 200 km^2 ranged from 140 to 1720 years. This is much larger than residence times currently published from studies conducted at similar small scales[1,2]. In comparison, the apparent age of streamflow was 5800 years at the largest accumulated drainage area monitored in Saguache Creek (1450 km^2). In reality, these are mean ages of streamflow that represent the integrated average age of a distribution of travel-times. Travel-time distributions were calculated for the average streamflow ages using gamma distributions with α equal to 0.5. This approach is consistent with previously published research[11]. The resulting distributions are shown in Figure 6.6. These distributions show that streamflow may consist of waters from different sources having residence times that vary from very young waters having residence times on the order of days or weeks to very old waters having residence times on the order of a million years. These findings support the 3D conceptual model and the increased storage associated with that conceptual model implies that streamflow from this watershed may be initially more resistant to changes in meteoric forcing associated with climate change.

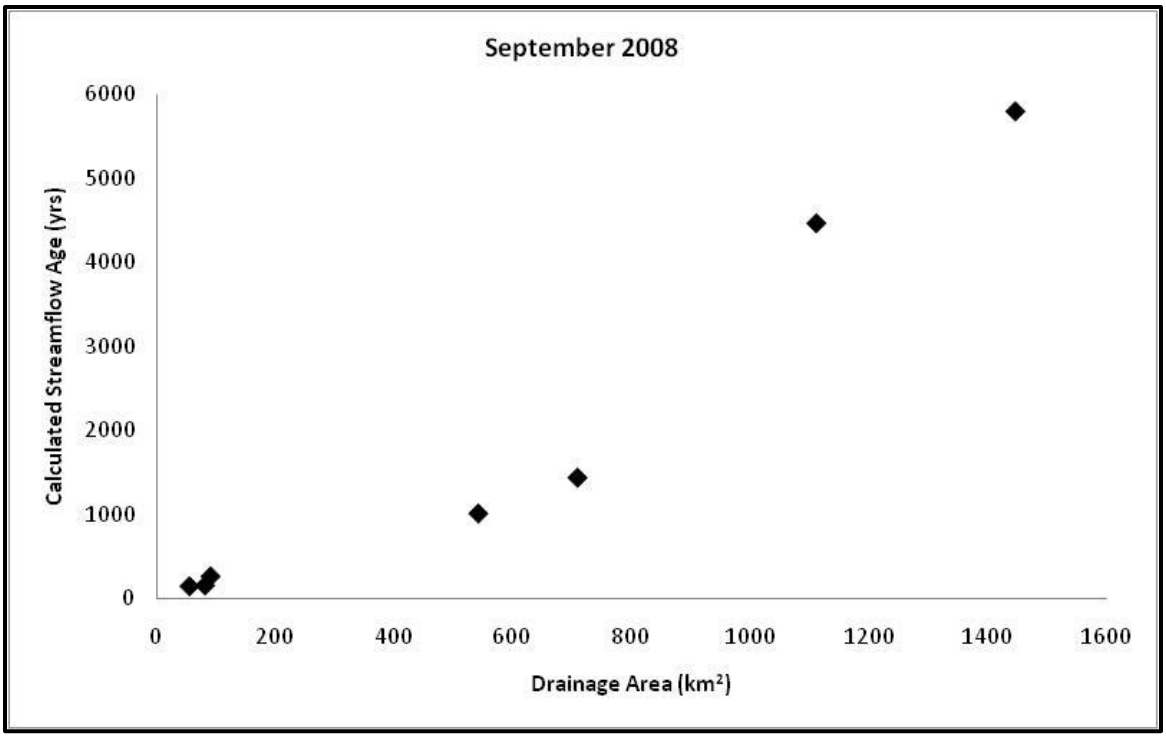

Figure 6.5: Apparent mean ages of streamflow calculated using the geochemical chronometer approach.

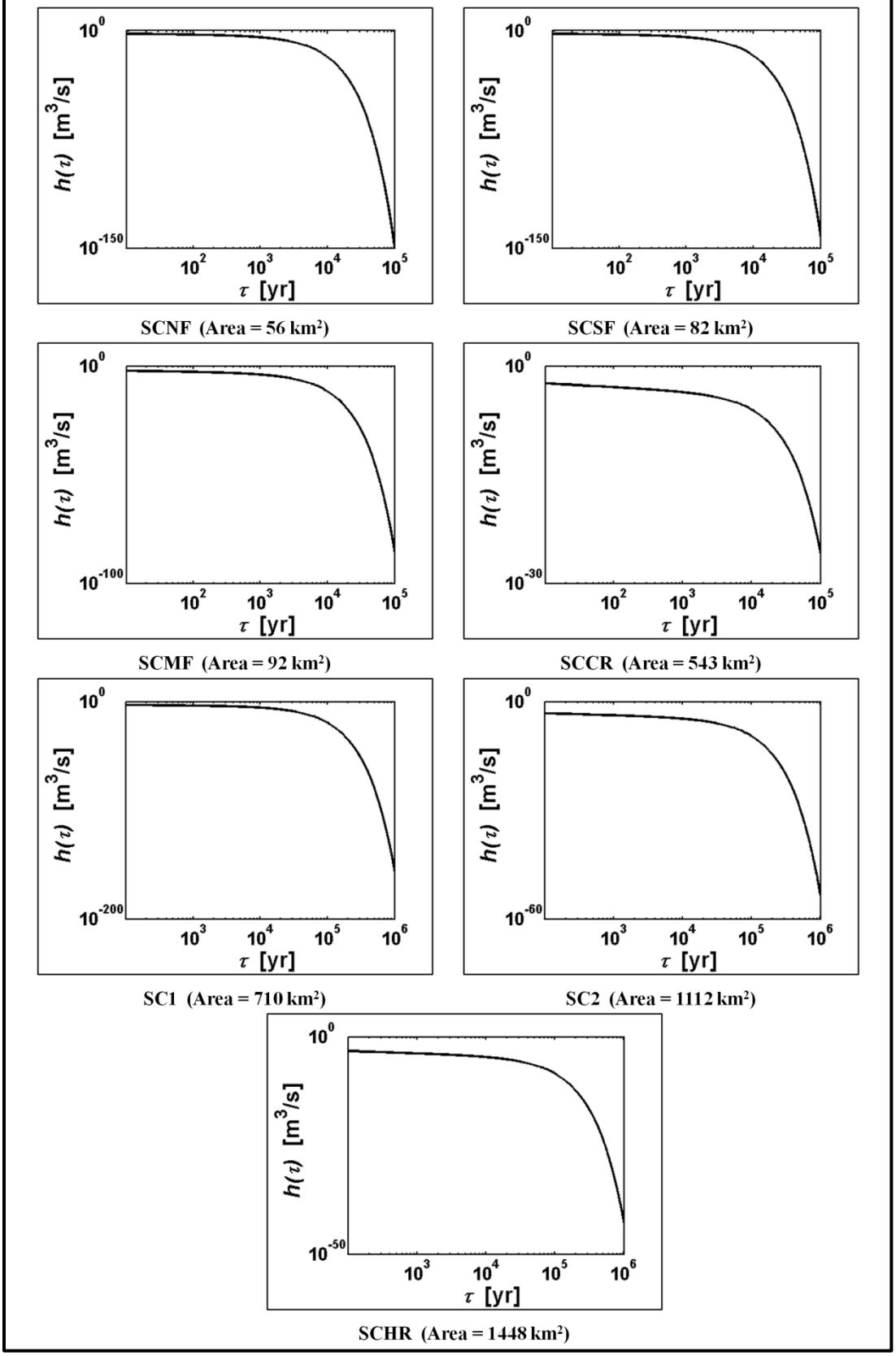
h(t) [m3/s]
τ [yr]
SCNF (Area = 56 km2)
SCSF (Area = 82 km2)
SCMF (Area = 92 km2)
SCCR (Area = 543 km2)
SC1 (Area = 710 km2)
SC2 (Area = 1112 km2)
SCHR (Area = 1448 km2)

Figure 6.6: Hypothetical travel-time distributions for the stream sampling sites based on the gamma distributions presented in previous research[11]. These distributions were calculated based upon the mean streamflow ages displayed in Figure 6.5. Drainage areas are provided here for direct comparison to drainage areas in Figure 6.5.

The uncertainty of the geochemical chronometer was assessed using two different approaches. First, we assessed the uncertainty of the source partitioning provided by the EMMA code by creating numerous samples from an "artificial" stream-water composed of known components and known contributions of each component in each sample (See Chapter 4, Section 4.4.6). The EMMA code successfully identified the three components of streamflow for the hypothetical stream-water and successfully predicted the contributions of each component in each sample. There was no variability between the actual contributions and the predicted contributions. Second, we assessed the uncertainty in the ages of the groundwater component determined using the solute weathering release curves. The overall maximum variability of sodium concentrations in water samples was calculated by comparing the sodium concentrations in samples against the sodium concentrations in duplicate samples. The maximum variability was found to be ± 0.1 mg L^{-1}. All measured sodium concentrations in well waters were adjusted to ± 0.1 mg L^{-1} and two additional solute weathering release curves were generated that bracket the original solute weathering release curve (solid black line in Figure 6.7). The positive variability curve is represented by the '+ 0.1 mg/L' series and bold, dashed green line in Figure 6.7. The negative variability curve is represented by the '- 0.1 mg/L' series and bold, dotted blue line in Figure 6.7. Due to the nature of the power trendlines, these curves intersect near 8.0 mg L^{-1}. Therefore, we plot the absolute range in uncertainty (bold, purple line in Figure 6.7) as a function of sodium concentration and this range may

be exaggerated due to the divergent behavior of the negative variability trendline. The grey box encloses the total range in sodium concentrations observed in well waters that were used to recreate streamflow age. The uncertainty in the age of the groundwater component ranges from 150 years at 9.0 mg L^{-1} to 3800 years at 14.0 mg L^{-1}. While this range in uncertainty seems drastic, there is evidence that supports the old ages of the groundwater components. Although the data are sparse, contours of radiocarbon ages in the upper confined portion of the San Luis Valley aquifer where it intersects the lower reaches of the Saguache Creek watershed may range from 5000 to 10,000 years old[29]. Our geochemical chronometer estimated groundwater ages ranging from 3000 to 9000 years in the lower reaches of Saguache Creek. If groundwater from the upper confined unit[29] is discharged to the lower reaches of Saguache Creek, then the apparent ages of streamflow that we calculate are realistic.

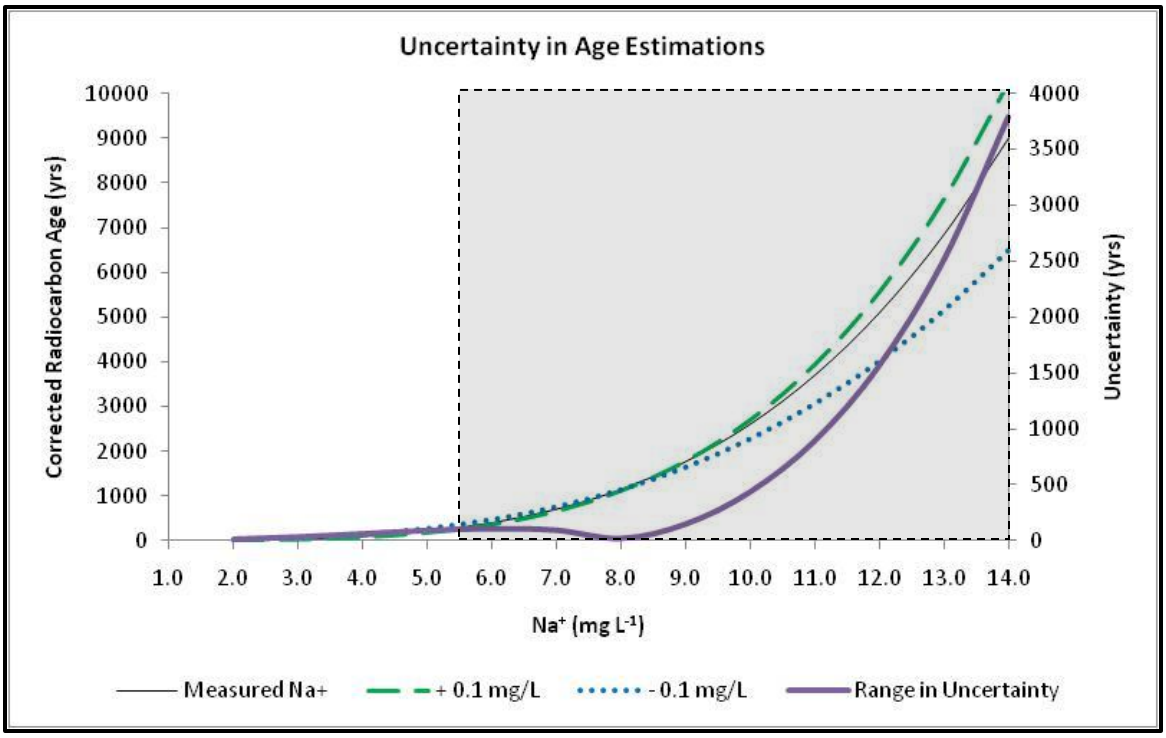

Figure 6.7: Uncertainty in estimation of age of the groundwater component in streamflow. The original solute weathering release curve for sodium is represented by the solid, black line. The bold, dashed green line represents the solute weathering release curve for sodium concentration + 0.1 mg L^{-1} variability and the bold, dotted blue line represents the sodium concentration – 0.1 mg L^{-1}. The bold, purple line represents the uncertainty for each sodium concentration (secondary y-axis) and the grey box encloses the range of sodium concentrations observed in well waters used to recreate streamflow age.

While this is only an initial attempt to address these discrepancies, the implications of these findings are profound. These findings have implications for our conceptual models of how the streamflow response from large watersheds will be affected by climate change. If, for example, the response times of streamflow from large watersheds are short, on the order of days to years, then streamflow will respond rapidly to changes in climatic forcing. However, the reverse may hold true for watersheds where response times are long and long residence-time groundwater is an important component of streamflow generation. This study supports the latter scenario and suggests that the

streamflow response from large watersheds may be buffered, at least initially, against changes in climatic forcing. The long-term streamflow response, however, cannot be accurately predicted if residence times are not accurate. The conceptual models described in this study require further testing to see if these streamflow generation mechanisms and residence times are similar in other large watersheds under different climatic regimes, geographical locations, and geological settings.

6.1: Methods:

6.1.1: End-Member Mixing Analysis:

A description of end-member mixing analysis is provided in Chapter 4, Section 4.3.1.

6.1.2: Diagnostic Tools of Mixing Models:

Diagnostic tools of mixing models are described in Chapter 4, Section 4.3.2.

6.1.3: Selection of Endmembers:

The selection of endmembers is described in Chapter 4, Section 4.3.3.

6.1.4: Measurement of Vertical Hydraulic Gradients:

The technique used to measure vertical hydraulic gradients is described in Chapter 4, Section 4.3.4.

6.1.5: Creation of Solute Weathering Release Curves:

The technique used to create solute weathering release curves is described in Chapter 5, Section 5.4.6.

6.2: Author Contributions:

M.D.F. designed the research plan, conducted field work to collect water samples, analyzed and interpreted the data, and wrote the paper. F.M.P. secured the financial support for this study and participated in the analysis and interpretation of the data and contributed to the writing of this paper. A.R.C. provided support on the stable isotope analysis and participated in the analysis and interpretation of the data. F.L. provided the coding and support for EMMA and provided assistance in the interpretation of the EMMA results.

6.3: Additional Information:

The authors declare no competing financial interests. Reprints and permissions information is available online at http://npg.nature.com/reprintsandpermissions. Correspondence and requests for materials should be addressed to M.D.F.

6.4: References:

1. McGlynn, B.L., McDonnell, J.J., Stewart, M., & Siebert, J. On the relationship between catchment scale and streamwater residence time. *Hydrol. Process.* **17,** 175-181, doi:10.1002/hyp.5085 (2003).

2. McGuire, K.J. et al. The role of topography on catchment-scale water residence time. *Wat. Resour. Res.* **41,** W05002, doi:10.1029/2004WR003657 (2005).

3. Tague, C. et al. Deep groundwater mediates streamflow response to climate warming in the Oregon Cascades. *Climatic Change.* **86,** 189-210, doi:10.1007/s10584-007-9294-8 (2008).

4. Maxwell, R.M. & Kollet, S.J. Interdependence of groundwater dynamics and land-energy feedbacks under climate change. *Nature Geosci.* **1,** 665-669, doi:10.1038/ngeo315 (2008).

5. Mote, P.W., Hamlet, A.F., Clark, M.P. & Lettenmaier, D.P. Declining mountain snowpack in western North America. *B. Am. Meteorol. Soc*. 39-49, doi:10.1175/BAMS-86-1-39 (2005).

6. Seager, R. et al. Model projections of an imminent transition to a more arid climate in southwestern North America. *Science*. **316,** 1181-1184, doi:10.1126/science.1139601 (2007).

7. Service, R.F. As the West goes dry. *Science*. **303,** 1124-1127 (2004).

8. Beven, K. *Benchmark Papers in Hydrology: Streamflow Generation Processes.* (International Association of Hydrological Sciences, Oxfordshire, UK, 2006).

9. McGuire, K.J. & McDonnell, J.J. A review and evaluation of catchment transit time modeling. *J. Hydrol.* **330,** 543-563, doi:10.1016/j.hydrol.2006.04.020 (2006).

10. Sivapalan, M. Process complexity at hillslope scale, process simplicity at the watershed scale: is there a connection? *Hydrol. Process.* **17,** 1037-1041, doi:10.1002/hyp.5109 (2003).

11. Kirchner, J.W., Feng, X., and Neal, C. Fractal stream chemistry and its implications for contaminant transport in catchments. *Nature,* **403,** 524-527 (2000).

12. Rademacher, L.K., Clark, J.F., Clow, D.C. & Hudson, G.B. Old groundwater influence on stream hydrochemistry and catchment response times in a small Sierra Nevada catchment: Sagehen Creek, California. *Wat. Resourc. Res.* **41,** W02004, doi:10.1029/2003WR002805 (2005).

13. Erskine, A.D. & Papaioannou, A. The use of aquifer response rate in the assessment of groundwater resources. *J. Hydrol.* **202,** 373-391 (1997).

14. Frisbee, M.D. Streamflow Generation Processes and Residence Times in a Large, Mountainous Watershed in the Southern Rocky Mountains of Colorado, USA. Ph.D. Dissertation, Dept. of Earth and Environmental Science, New Mexico Tech, Socorro, NM, USA (2010).

15. Shaman, J., Stieglitz, M., & Burns, D. Are big basins just the sum of small catchments? *Hydrol. Process.* **18,** 3195-3206, doi:10.1002/hyp-5739 (2004).

16. Uchida, T., Asano, Y., Onda, Y., & Miyata, S. Are headwaters just the sum of small hillslopes? *Hydrol. Process.* **19,** 3251-3261, doi:10.1002/hyp-6004 (2005).

17. Bricker, O.P. & Jones, B.F. Main factors affecting the composition of natural waters, in *Trace Elements in Natural Waters.* edited by B. Salbu and E. Steinnes. (CRC Press, Boca Raton, FL, 1995).

18. Tóth J. A theoretical analysis of groundwater flow in small drainage basins. *J. Geophys. Res.* **67,** 4812-4975 (1963).

19. Cardenas, M.B. Potential contribution of topography-driven regional groundwater flow to fractal stream chemistry: Residence time distribution analysis of Tóth flow. *Geophys. Res. Lett.* **34,** L05403, doi:10.1029/GL029126 (2007).

20. Christophersen, N., & Hooper, R.P. Multivariate analysis of stream water chemical data: The use of principal components analysis for the end-member mixing problem. *Wat. Resourc. Res.* **28** (1), 99-107 (1992).

21. Hooper, R.P. Diagnostic tools for mixing models of stream water chemistry. *Wat. Resourc. Res.* **39** (3), 1055, doi:10.1029/2002WR001528 (2003).

22. Liu, F., Bales, R.C., Conklin, M.H., & Conrad, M.E. Streamflow generation from snowmelt in semi-arid, seasonally snow-covered, forested catchments, Valles Caldera, New Mexico. *Wat. Resourc. Res.* **44,** W12443, doi:10.1029/2007WR006728 (2008).

23. Baxter, C., Hauer, F.R., & Woessner, W.W. Measuring groundwater-stream water exchange: New techniques for installing minipiezometers and estimating hydraulic conductivity. *T. Am. Fish. Soc.* **132,** 493-502 (2003).

24. Harvey, J.W. & Bencala, K.E. The effect of streambed topography on surface-subsurface water exchange in mountain catchments. *Wat. Resourc. Res.* **29**(1)**,** 89-98 (1993).

25. Haggerty, R., Wondzell, S.M., & Johnson, M.A. Power-law residence time distribution in the hyporheic zone of a 2nd-order mountain stream. *Geophys. Res. Lett.* **29,** 1640, doi:10.1029/2002GL014743 (2002).

26. Maloszewski, P., & Zuber, A. Determining the Turnover Time of Groundwater Systems with the Aid of Environmental Tracers. *J. Hydrol.* **57,** 207-231 (1982).

27. Botter, G., Bertuzzo, E., & Rinaldo, A. Transport in the hydrologic response: Travel time distributions, soil moisture dynamics, and the old water paradox. *Wat. Resourc. Res.* **46,** W03514, doi:10.1029/2009WR008371 (2010).

28. Rademacher, L.K. et al. Chemical evolution of shallow groundwater as recorded by springs, Sagehen Basin; Nevada County, California. *Wat. Resourc. Res.* **179,** 37-51 (2001).

29. Mayo, A.L., Davey, A., & Christiansen, D. Groundwater flow patterns in the San Luis Valley, Colorado, USA revisited: An evaluation of solute and isotopic data. *Hydrogeol. J.* **15,** 383-408, doi:10.1007/s10040-006-0079-3 (2007).

Chapter 7 Conclusions and Recommendations

7.1: Epilogue:

For this dissertation, I investigate large-scale groundwater flowpaths in a large (1700 km^2) watershed and the role of these groundwater flowpaths on streamflow generation processes, streamflow chemistry, bedrock weathering reactions, and apparent ages of streamflow. In the early part of this study (Chapters 2 and 3), I evaluated a modified passive capillary sampler, M-PCAPS, that was designed to collect samples of infiltrating meltwater during the snowmelt season in remote, seasonally inaccessible watersheds. This methodology was an improvement over previously employed methods used to quantify the geochemical and stable isotopic composition of the soil-meltwater endmember. In Chapter 4, I propose and test two conceptual models of streamflow generation at the large watershed scale against four years of chemistry and stable isotope observations in streamflow and potential components of streamflow. In this chapter, I employ endmember mixing analysis (EMMA) and observations of vertical hydraulic gradients measured in mini-piezometers installed in streambeds to quantify the role of large-scale groundwater in streamflow generation at the large watershed scale. In Chapter 5, I propose and test two conceptual models of springflow generation against four years of chemistry and stable isotope observations in springflow and potential components of springflow. I employ EMMA to determine if the groundwater component of springflow is variable and to what extent this variability affects solute weathering release curves based on springflow data. I develop a geochemical chronometer based on solute weathering release curves that can be used to estimate the kinetic age of the groundwater component of streams and springs. In Chapter 6, I return to the conceptual

models of streamflow generation proposed in Chapter 3 and discuss the impact of these conceptual models on the streamflow response of large watersheds to changes in meteoric forcing associated with climate change. I test these conceptual models by coupling the EMMA results from streamflow separations with the geochemical chronometer approach to estimate apparent ages of streamflow.

7.2: Synthesis and Recommendations:

Streamflow generation processes and residence times at the large watershed scale are poorly understood. In comparison, the hydrologic literature contains a wealth of information from studies of streamflow generation processes and residence times at the hillslope and small catchment scale. However, few of these studies attempt to scale their findings to larger scales. This is not an easy task since hillslope runoff processes tend to be temporally and spatially very heterogeneous and highly complex while hydrologic behaviors at the larger watershed scale tend to be structured and perhaps, simplistic. To further complicate matters, there has been very little effort to actually measure and quantify the mechanisms responsible for streamflow generation at the large watershed scale. For watershed hydrologists, this is a complicated problem especially since there is an increasing urgency to understand streamflow generation processes at larger watershed scales given the recent concerns over climate change and its impact on regional and global water resources. This study fills and addresses this gap in our understanding by examining the processes responsible for streamflow generation at the large watershed scale and discussing the implications of these findings with respect to climate change.

7.2.1: M-PCAPS Methodology

The M-PCAPS methodology is a simple and robust method to collect samples of infiltrating meltwater or rainfall. The wicking process does not fractionate water and if the wicks are thoroughly cleaned, the geochemical signature of the infiltrating meltwater will also be preserved. The M-PCAPS design provided improvements over the methods presented in *Earman et al.* [2003]. Our design provided information on the geochemical evolution of infiltrating meltwater with depth, soil-water fluxes, and subsurface runoff processes that would have otherwise been difficult to quantify empirically or by using surface proxies. While our design methodology is suitable for the thin, rocky soils often encountered in alpine settings, alternative approaches such as those documented in *Gee et al.* [2002, 2003] will provide temporal time-series of soil fluxes in deep soils. I recommend its deployment in thin soils or in seasonally inaccessible regions where conditions may prohibit intensive maintenance or reliance upon an electrical source. This method is inexpensive, robust, and easily deployed.

7.2.2: Streamflow Generation Processes:

In this portion of the study, I used EMMA results and measurements of vertical hydraulic gradient to test two conceptual models of streamflow generation at the large watershed scale. One conceptual model is essentially two-dimensional and treats streamflow generation at the large watershed scale as the aggregation of runoff responses from individual hillslopes, primarily surface and shallow subsurface flowpaths [*Sivapalan,* 2003]. Alternatively, a fully three-dimensional conceptual model treats streamflow generation at the large watershed scale as being controlled by a distribution of large-scale groundwater flowpaths [*Tóth,* 1963] as well as surface and shallow subsurface

flowpaths. Since contributions from basin-scale groundwater are so critical in distinguishing between these two conceptual models, I was interested in answering the following question. What is the role of groundwater in streamflow generation in the Saguache Creek watershed and do groundwater contributions in streamflow become structured with increasing scale? I used the results from EMMA and measurements of vertical hydraulic gradients to quantify the role of groundwater in streamflow across multiple scales in the Saguache Creek watershed.

The major findings of this portion of the study were that groundwater contributions were important components of streamflow generation at all scales and more importantly, that groundwater contributions did increase with increasing scale from accumulated drainage areas greater than 300 km^2. This finding was also supported by measurements of VHG which indicated that VHG increased with increasing scale from accumulated drainage areas greater than 300 km^2. When considered together, these findings support the 3D catchment-mixing conceptual model over the network-mixing conceptual model in this large, alpine watershed.

The implications of these findings are that large-scale groundwater contributions are dominant controls on streamflow generation and on trends in streamflow chemistry across multiple scales in this large watershed. Furthermore, the structure of groundwater contributions in streamflow has important implications for our perception of apparent ages in streamflow. These old, persistent contributions from groundwater are likely responsible for the tailing observed in residence time distributions in watersheds. I assert that, at least in the Saguache Creek watershed, groundwater contributions are the framework for the geochemical signal observed in streamflow across multiple scales and

that hillslope-scale runoff processes superimpose noise on that signal. My findings cast doubt on the hillslope aggregation concepts for scaling runoff processes to larger watershed scales at least in the Saguache Creek watershed.

For future work, there are two major things that need to be investigated further. Two trends were apparent in the plot of chemical constituents against increasing accumulated drainage area. Groundwater contributions were highly variable in drainage areas less than 300 km^2; however, groundwater contributions increased linearly with increasing scale beyond this critical area. It is recommended that additional effort be spent in quantifying the processes responsible the emergence of the linear increasing trend at approximately 300 km^2 and in quantifying the mechanisms responsible for the variability in small drainages. Is this emerging trend due to the presence of the La Garita caldera wall that is also located in the approximate vicinity? If so, how does this feature affect the development and connectivity of groundwater flowpaths between the headwaters and downstream stretches of Saguache Creek? If this geologic feature were not present, would the linear trends in streamflow observed beyond 300 km^2 develop at a much smaller scale, perhaps in the headwater streams themselves? These questions could be answered within a hydrogeologic modeling framework for the watershed.

The impact of hyporheic waters on streamflow chemistry and more importantly, on the chemistry of waters sampled in the mini-piezometers was not quantified in this study but deserves future attention. Most studies indicate relatively quick exchange rates between water flowing in the stream and water in the hyporheic zone [*Harvey and Bencala*, 1993; *Haggerty et al.*, 2002]. If this is true, then we would expect that mixing processes in the hyporheic zone would not add significant age to the stream. This may

not be true for chemistry. Future work will investigate the impact of hyporheic waters on discharging groundwater to the stream.

7.2.3: Solute Weathering Release Curves:

In this portion of the study, I investigated how temporal variability in the groundwater component of springflow generation affects solute weathering release curves by testing two conceptual models of springflow generation against our spring chemistry observations. In one conceptual model, springflow is generated only by groundwater and as a consequence, the chemistry observed in springflow will represent only the solutes released by chemical weathering reactions involving groundwater flow. Alternatively, in the second conceptual model, springflow is integrative and is composed of different components representing different water sources. Consequently, the groundwater component in springflow may not be temporally consistent and the chemistry observed in springflow will represent solutes released by possibly many different chemical weathering reactions. In order to quantify the temporal variability of the groundwater component in springflow, I employed endmember mixing analysis (EMMA) using 4 years of springflow chemistry and stable isotope data from the Saguache Creek watershed. My goal in conducting this research was to answer the following questions. Is the groundwater component in springflow generation temporally variable and if so, how does this variability affect solute weathering release curves?

The major finding of this study was that groundwater was a significant component of springflow generation in all springs analyzed in this study; yet, no spring was composed of 100 percent groundwater. The groundwater component ranged from 8 to 98 percent of springflow overall. Groundwater contributions varied with elevation. In

general, high elevation springs exhibited the most temporal variability in the groundwater component. Lower elevation springs typically exhibited more temporally stable groundwater components. All these factors illustrate the integrative nature of springflow even those springs that emerge from local bedrock. It also illustrates the need for caution in the analysis of springflow chemistry especially when it is assumed to be representative of local groundwater.

The implication of this variability is that, in all cases, the calculated weathering release from corrected springflow was lower than that from the wells. Springs are integrative and it cannot be assumed that springs sample similar geochemical evolutionary pathways in the groundwater flow system. As a result of this complex integrative behavior, the weathering release curves for uncorrected springflow will overpredict the solute release from bedrock as compared to corrected springflow. In fact, the weathering release curves for uncorrected springflow will overpredict Si by 50 percent, Ca^{2+} by 10 percent, Mg^{2+} by 51 percent, Na^{+} by 7 percent, and K^{+} by 32 percent. As a consequence, estimates of solute release from bedrock weathering based on uncorrected springflow will be too large.

For future work, further quantification on the variability of the groundwater endmember in springflow generation from other watersheds with different lithologies and climatic forcings is needed in order to provide more accurate constraints on bedrock weathering rates in groundwater flow systems. We also need to improve the methodologies used to calculate the contributing area for springs. This is a complex problem where a well-defined catchment area may not be possible in all situations. It,

nonetheless, limits our ability to estimate weathering rates and is, perhaps best suited for a combined tracer and hydrogeologic modeling approach in future work.

7.2.4: Apparent Ages of Streamflow:

In this final portion of the study, I pulled together the results of the previous two chapters to illustrate the larger implications of our findings. I calculated streamflow ages using the results from the endmember mixing analysis performed in Chapter 3 and coupled those results with a geochemical chronometer calibrated to the kinetics of weathering reactions and presented in Chapter 4.

The major findings of this study indicate that the apparent ages in streamflow do increase with increasing drainage area as proposed in the 3D conceptual model. Second and most important, apparent ages of streamflow are much older than currently published [*McGlynn et al.*, 2003; *McGuire et al.*, 2005] and the apparent ages of streamflow in small drainages ranging from 56 to 200 km^2 ranged from 140 to 1720 years. The apparent age of streamflow was 5800 years at the largest accumulated drainage area monitored in Saguache Creek.

The implication of these findings is that streamflow sustained by long residence time groundwater may be initially more resistant to changes in meteoric forcing associated with climate change. This will not be true for streamflow that is sustained by a distribution of surface and shallow subsurface flowpaths. In that case, we would expect streamflow to respond quickly to changes in meteoric forcing associated with climate change.

Future work will be completed in the form of a fully 3D hydrogeologic model of the watershed. Residence time distributions will be calculated for each stream sampling

location in order to provide support for the findings described in Chapter 6, in particular Figure 6.6. Future work is recommended to investigate other environmental tracers or sampling methodologies that will allow successful direct sampling of the groundwater discharging to the streams. Perhaps it would be useful to install deeper piezometers or a nest of piezometers installed at different depths below the streambed at selected stream sites. These could be instrumented with temperature sensors. Thus, there would be observations of temperature with depth, ages with depth, and perhaps chemistry with depth. These depth profiles would be extremely useful in rigorously testing these and other alternative conceptual models.

7.3: References:

Earman, S., A.R. Campbell, F.M. Phillips, and B.D. Newman (2006), Isotopic exchange between snow and atmospheric water vapor: Estimation of the snowmelt component of groundwater recharge in the southwestern United States, *Journal of Geophysical Research, 111,* D09302, doi:10.1029/2005JD006470.

Gee, G.W., A.L. Ward, T.G. Caldwell, and J.C. Ritter (2002), A vadose zone water fluxmeter with divergence control, *Water Resources Research, 38,* doi:10.1029/2001WR000816.

Gee, G.W., Z.F. Zhang, and A.L. Ward (2003), A modified vadose zone fluxmeter with solution collection capability, *Vadose Zone Journal, 2,* 627-632.

Harvey, J.W., and K.E. Bencala (1993), The effect of streambed topography on surface-subsurface water exchange in mountain catchments, *Water Resources Research, **29***(1)**,** 89-98.

Haggerty, R., S.M. Wondzell, and M.A. Johnson (2002), Power-law residence time distribution in the hyporheic zone of a 2nd-order mountain stream, *Geophysical Research Letters, **29,*** 1640, doi:10.1029/2002GL014743.

McGlynn, B.L., J.J. McDonnell, M. Stewart, and J. Siebert (2003), On the relationship between catchment scale and streamwater residence time, *Hydrological Processes, 17,* 175-181, doi:10.1002/hyp.5085.

McGuire, K.J., J.J. McDonnell, M. Weiler, C. Kendall, B.L. McGlynn, J.M. Welker, and J. Siebert (2005), The role of topography on catchment-scale water residence time, *Water Resources Research, 41,* W05002, doi:10.1029/2004WR003657.

Sivapalan, M. (2003), Process complexity at hillslope scale, process simplicity at the watershed scale: is there a connection?, *Hydrological Processes, 17,* 1037-1041, doi:10.1002/hyp.5109.

Tóth J. (1963), A theoretical analysis of groundwater flow in small drainage basins, *Journal of Geophysical Research, 67,* 4812-4975.